THE GEOLOGY, GEOCHEMISTRY AND GEOCHRONOLOGY OF THE ATNARPA IGNEOUS COMPLEX, S.E. ARUNTA INLIER, NORTHERN AUSTRALIA: IMPLICATIONS FOR EARLY TO MIDDLE PROTEROZOIC TECTONISM AND CRUSTAL EVOLUTION

BY

Jian-xin Zhao

Department of Geology and Geophysics,
The University of Adelaide,
Australia

April, 1989

A thesis submitted to the University of Adelaide
in partial fulfilment of the requirements for
the degree of Master of Science

awarded 16.8.89

This thesis contains no material which has been accepted for the award of any other degree or diploma in any Institution and, to the best of my knowledge and belief, contains no copies or paraphrases of material previously published or written by other people, except where due references are made in the text of this thesis.

DATED 25-4-1989 SIGNED _____

CONTENTS

LIST OF APPENDICES

LIST OF PLATES Page in front

LIST OF TABLES Page in front

LIST OF FIGURES

ABSTRACT

The study area is dominated by the Atnarpa Igneous Complex (AIC), which is associated with a basement supracrustal assemblage and juxtaposed with a cover sequence of the Amadeus Basin. Systematic field, petrographic, geochemical, U-Pb and Rb-Sr isotopic and geochronological studies were focused on the Atnarpa Igneous Complex principally in the Atnarpa area, which have put some constraints on the nature of the geochemical and tectonic evolution of Proterozoic crust in the SE Arunta Inlier.

Three major rock units, namely, the Atnarpa Calc-alkaline Suite (ACAS), the Atnarpa Granitic Batholith (AGB) and the Atnarpa Tonalite-Basalt Suite (ATBS), are recognised to be sequentially emplaced during the early to middle Proterozoic time.

The Atnarpa Calc-alkaline Suite (ACAS) is considered to be a typical high-level calc-alkaline suite with some transitional trondhjemitic affinities in its felsic differentiates. Its genesis is formulated in terms of high-level fractional crystallization from a parental magma with high oxygen and water fugacities. The parental magma is considered to be mantle-derived, being related to oceanic crust subduction under the continental margin. Its crystallization age is dated by U-Pb zircon isotopics at 1879±11/10 Ma. This is the oldest U-Pb zircon age so far known in the Arunta Inlier.

The Atnarpa Granitic Batholith (AGB) is composed of the pre-collisional Atnarpa Older Tonalite (AOT) and Leucogranite (AOLG) and minor syn-collisional Atnarpa Muscovite Granite (AMG). The AOLG yields a U-Pb zircon age of 1873±11/10 Ma and the AOT, 1863±33/27 Ma (Sando 1987). The AOT & AOLG are characteristic of low K_2O, Rb, REE, Th, Rb/Sr and inferred $^{87}Sr/^{86}Sr$ initial ratios and high Na_2O, MgO, Fe_2O_{3tot}, Sr, Ba, Sc, and Ni, which is quite distinctive from the Barramundi Association of similar ages (Wyborn 1988; Wyborn and Page 1983). The AOT and AOLG are interpreted as being derived by crystal fractionation from one parental magma. The parental magma is considered to be generated by both partial melting and assimilation of a mafic underplate with a short crustal pre-history due to the addition of heat and material from the ascending less-silicieous mantle-derived calc-alkaline magma.

The AMG is geochemically unrelated to the AOT & AOLG. It, however, shows

geochemical affinities to the syn-collision peraluminous S-type granite of Harris et al. (1986), and is considered to be derived from anatexis of a sedimentary source within supracrustal levels owing to a subduction initiated marginal collison similar to the Cordilleran type.

The Atnarpa Tonalite-Basalt Suite (ATBS) is a bimodal high-level suite with geochemistry, including strongly fractionated REE pattern with HREE depletion in the Atnarpa Younger tonalite (AYT), similar to the ubiquitous Archean tonalitic-basaltic bimodal suites. The AYT is dated at 1751±12 Ma, which marks the second magmatic event in this area. Its calculated $^{87}Sr/^{86}Sr$ initial ratio at 1751 Ma is 0.7017. The ATBS is considered to be formed in response to the opening and closure of a marginal or back-arc basin.

Tectonically, whilst the orogenesis of most of the northern Australian Proterozoic terrains has been interpreted to be essentially ensialic and rift-related without the involvement of oceanic crust subduction (Etheridge et al. 1987), the SE margin of the Arunta Inlier is considered to represent a continental margin during the early to mid Proterozoic, analogous to the Cordilleran Orogenic Belt. The study area has undergone two episodes of subduction-related magmatism, probably in response to episodic change in subduction rate or the crustal formation events to the south of the Arunta Inlier, as indicated by the Sm/Nd data from the Musgrave Inlier (McCulloch 1987). The first episode (1860 - 1880 Ma) was contemporaneous to the wide-spread Barramundi Association (Etheridge 1987) and the second episode (e.g. 1751 Ma), to the magmatism in the Entia Dome, Harts Range area (Cooper et al. 1988) as well as other places in the northern Australian Proterozoic terrains (Page 1988). The upper mantle under the SE margin of the Arunta Inlier must have experienced multi-stage differentiation and depletion in order to account for the unusually high positive initial ε_{Nd} values for the AIC and very low Sr initial ratio in the AYT (0.7017).

Rb/Sr isotopic data of whole rocks and micas indicate that the study area has subsequently suffered from several episodic thermal- deformational events. These include: (1). 1670 Ma old event of regional deformation and amphibolite facies metamorphism; (2). fast cooling from 500°C to below 320°C during 1512 - 1469 Ma; (3). substantial crustal uplift at around 1000 Ma probably in response to the subsidence of the Amadeus Basin and (4). the Palaeozoic Alice Springs Orogeny.

ACKNOWLEDGEMENT

This project was suggested and supervised by Dr John Cooper whose guidance in various aspects was greatly appreciated. I extend my thanks to John and his wife Joyce, Prof. Larry Frakes and his wife Esther for their heartfelt care and help which made our life in Adelaide really unforgettable.

I specially acknowledge Drs Shen-su Sun and Puquan Ding for many incisive discussions and kind-hearted encouragement.

I also wish to express my appreciation to the following members of the technical staff for their invaluable assistance: David Bruce, Geoff Trevelyan, Phil McDuie, John Stanley, Rick Barrett, Evert Bleys, John Willoughby, Wayne Mussared and Sherry Proferes.

I thank my home government, especially the Chinese Embassy, for nominating me as a sponsored, overseas student. I am grateful to the Embassy for my living allowance, and to AIDAB for payment of my Overseas Student Charge, under the China-Australia Technical Cooperation Program.

Last, but by no means least, to my wife Fang (Faye), thank you for your affections and encouragement, for your dedicative assistance in many aspects, particularly for colouring all the copies of the geological map of the study area and almost half of the computer keyboard work.

CHAPTER ONE: INTRODUCTION

1.1 LOCATION OF THE STUDY AREA

The study area is located within the Anarpa Igneous Complex, SE margin of the Arunta Inlier of northern Australia (Fig. 1-1 & 2). The main mapping area, approximately 30 square kilometres in size, is situated around the Atnarpa Homestead, 90 km ENE Alice Springs. Localities of field work also include Arltunga, White Range, Marmalade Dam, Tommy's Gap, and Star Creek areas and the area south of the Atnarpa Range (Fig. 1-3). Most samples were collected from the mapped area. Others were taken from the Marmalade Dam and Giles Creek areas (Appendix 2).

1.2 PREVIOUS INVESTIGATIONS

Detailed regional geological investigations of the Arunta Inlier, including systematic mapping, have been undertaken by BMR workers since the 1960's (e.g. Shaw & Stewart 1975; Shaw et al. 1979,1982,1984; Stewart et al. 1984). The Arltunga Nappe Complex, where the study area is located, was investigated in detail by Stewart (1971a,b), Forman (1971), Forman et al. (1967) and Shaw et al. (1971). These indicated the presence of a complexly folded and faulted, so-called "mobile belt" in which a stratigraphy could not be unravelled but from which a classification of "Divisons" and "Tectonic Zones" emerged.

Isotopic studies, mainly Rb-Sr, ^{40}Ar-^{39}Ar and K-Ar work, undertaken by Cooper et al. (1971), Stewart (1971a), Armstrong and Stewart (1975), Iyer et al. (1976), Allen & Stubbs (1982) and Black et al. (1983), provide some geochronological information for the study area. These generally recorded mid-Proterozoic formation ages with mineral updating in the mid Palaeozoic.

An honour's project carried out by Sando (1987) in the Tommy's Gap area is also related to this study.

Recently a large scale, structural, geochemical and isotopic constraints (e.g. Ding & James 1985; James & Ding 1988; Foden et al. 1988; Etheridge et al. 1987; McCulloch 1987) have been put on the tectonic and crustal evolution of the Arunta Inlier.

All these works will be further reviewed in the relevant chapters later on.

1.3 AIMS OF THIS STUDY

1. To produce a geological map on the scale of about 1:12,500 of the study area (see enclosure);

2. to investigate the field relations, petrography, geochemistry and geochronology of a variety of lithologies within the study area, with the emphasis on the Atnarpa Igneous Complex;

3. To make a synthesis of the tectonic evolution of the southeastern Arunta Inlier during the early to middle Proterozoic using petrological, geochemical, isotopic and temporal constraints.

1.4 METHODS IN THIS STUDY

1. Field reconnaissance on a larger area followed by detailed mapping on foot within the Atnarpa area using colour aerial photographs (about 1:25,000 in scale), enlarged to 1:12,500 in scale;

2. Microscopic determination of some 150 thin sections and polished thin sections;

3. Geochemical analyses of major and trace elements on 97 samples representative of the main lithologies in the study area;

4. REE analysis by isotopic dilution method on 10 selected samples;

5. Isotopic dating including U-Pb analyses of zircon and sphene, Rb-Sr analyses of WR and mica.

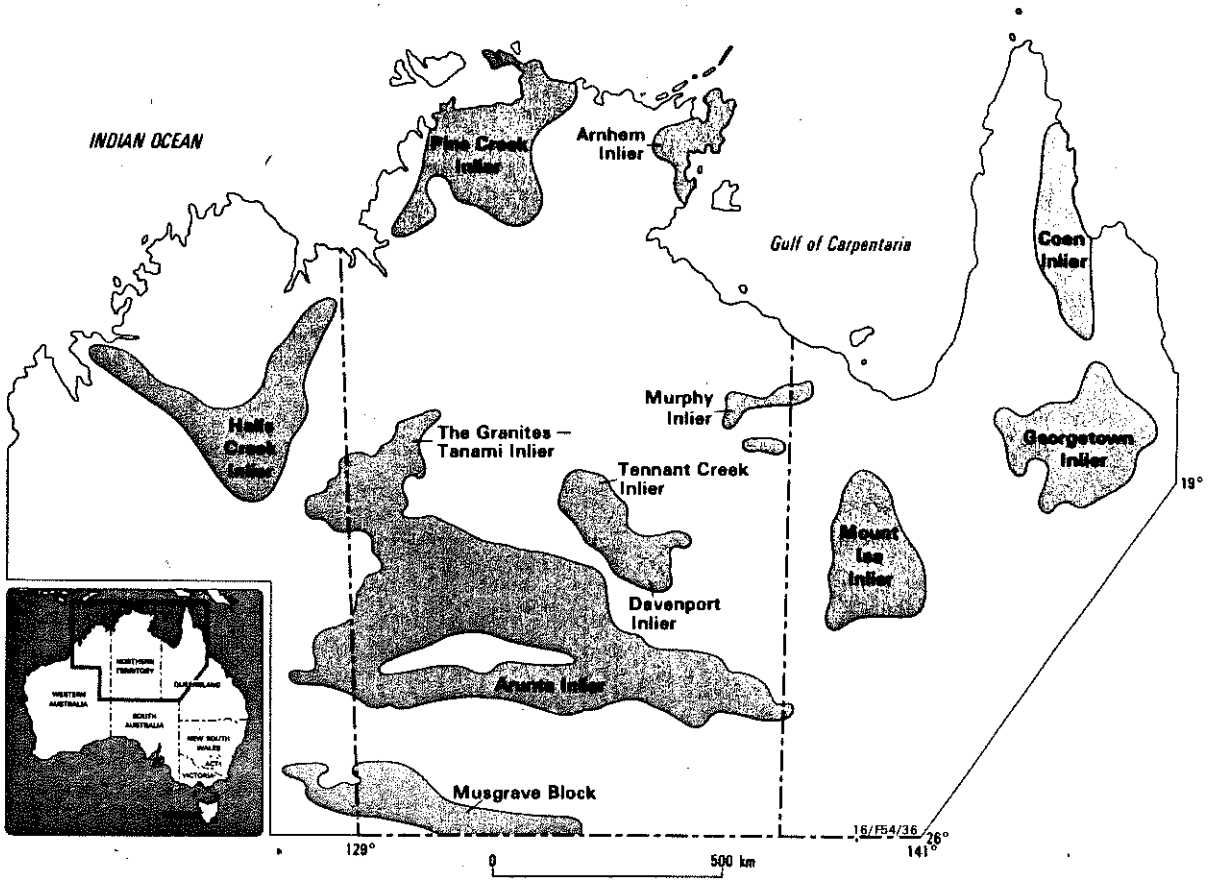

Fig. 1-1. Location of the Arunta Inlier and other Proterozoic terrains of northern Australia (after Wyborn & Page 1983).

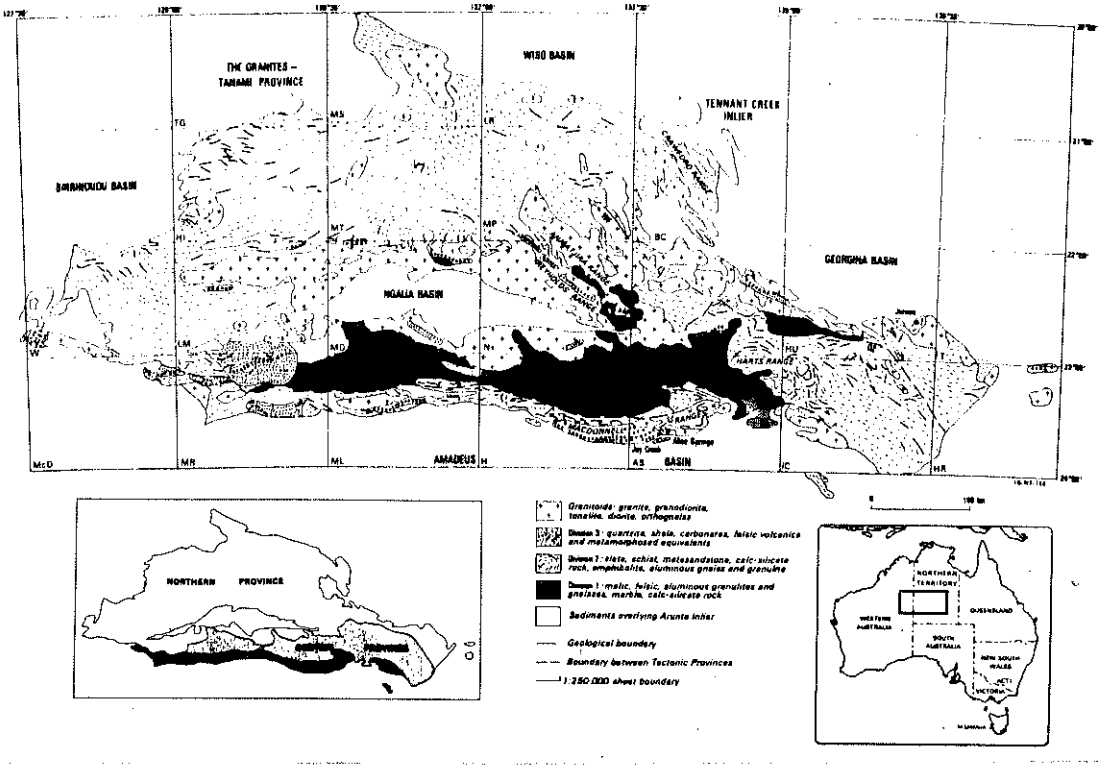

Fig. 1-2. Geological map of the Arunta Inlier showing major stratigraphic divisions and and tectonic provinces of Stewart et al. (1984). The Atnarpa Igneous Complex is coloured in red.

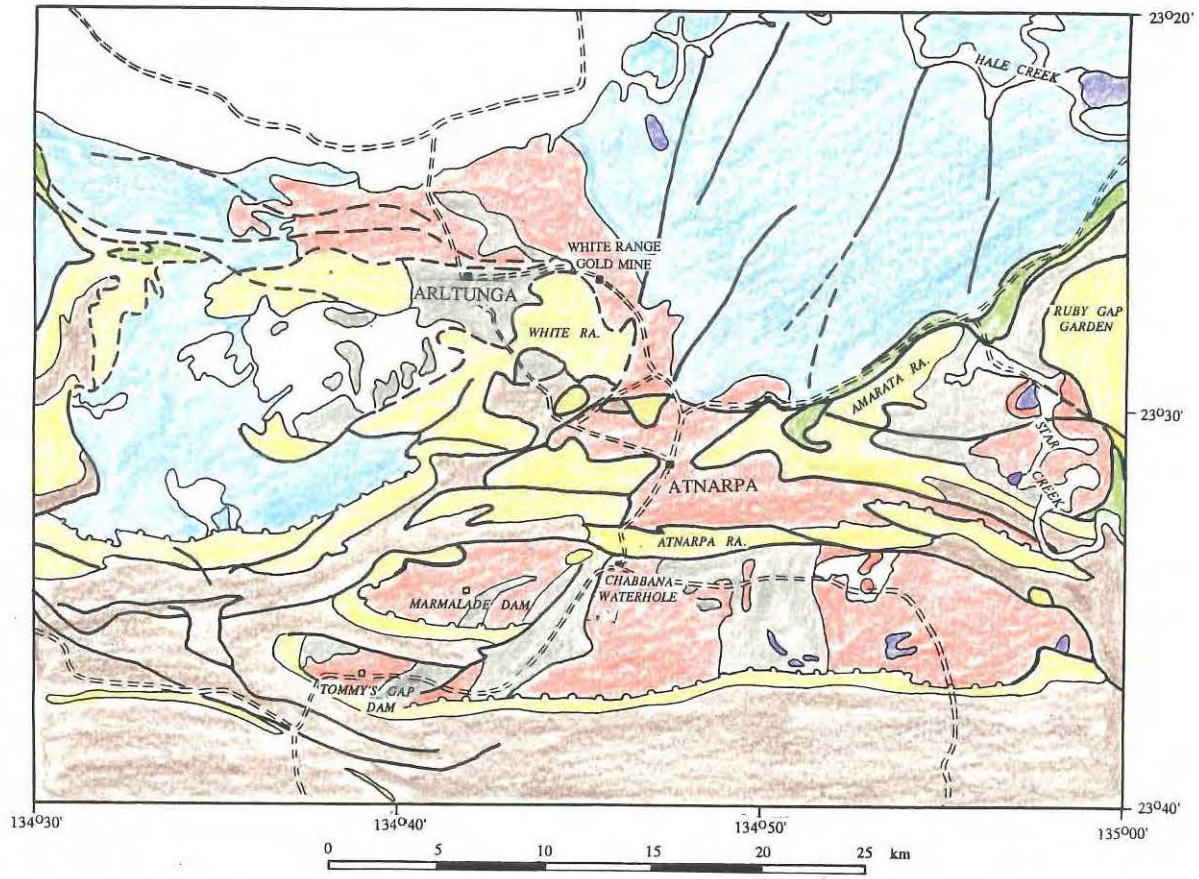

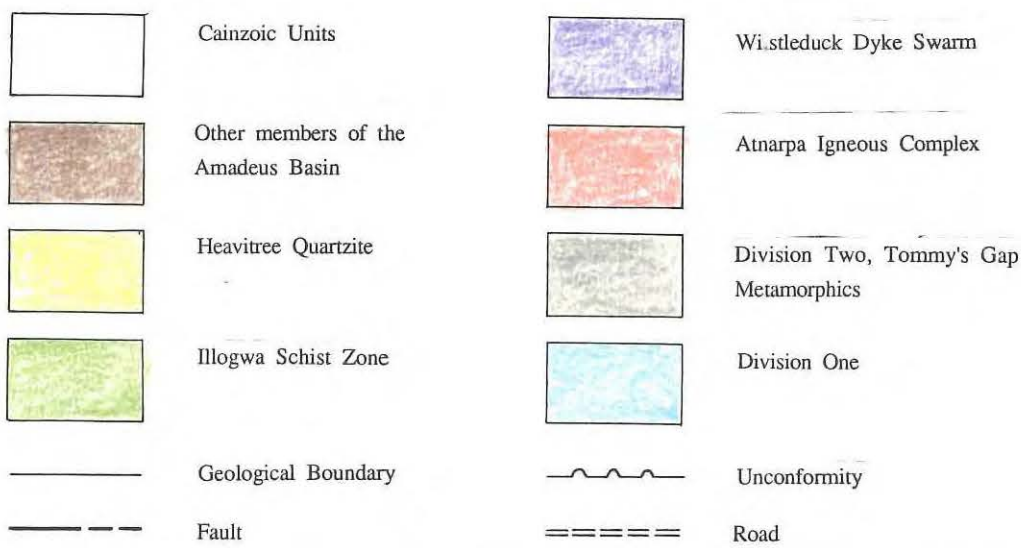

Fig. 1-3: Geological sketch map of the Atnarpa Igneous Complex and associated lithologies of the Arunta basement and Amadeus Basin cover. Simplified after the BMR 1:250,000 Geological Series, Alice Springs Sheet (1983).

CHAPTER TWO: GENERAL GEOLOGY

2.1 REGIONAL GEOLOGY

The study area is located at the SE margin of Arunta Inlier, central Australia, i.e. the boundary between the Arunta Inlier and Amadeus Basin. From comparative lithological studies (Stewart et al. 1984), the Arunta Inlier has been subdivided into three broad stratigraphic groups of early to mid-Proterozoic age. They are: Division One, a series of mafic and felsic granulites with some amphibolite grade gneisses; Division Two, a more widespread association with basal quartzofeldspathic gneisses and amphibolites, overlain by pelitic metasediments and amphibolites; and Division Three, the youngest and least extensive group consisting of primarily quartz rich metasediments. This is associated with a variety of igneous complexes of different ages (Stewart et al. 1984).

Shaw et al. (1984) have also divided the Arunta Inlier into three major tectonic provinces (Northern, Central and Southern), on the basis of different lithological, structural and metamorphic characteristics. As a result, the Division-Province concept of the BMR has been proposed to explain the geological history of the Arunta Inlier in terms of a complex, Proterozoic, ensialic, mobile belt model (Shaw et al.1984).

Later, Etheridge et al. (1987) proposed an extentional rifting model, which involves an assumed Archean protolith being subsequently sandwiched between an underlying Early Proterozoic mantle-derived underplate and an overlying Early to Middle Proterozoic upper crust. This upper crust (turbidites and granitic batholiths) is considered to be derived from both reworked Archean protolith and partial melting of the mafic underplate.

Recently, Ding and James (1985) and James and Ding (1988) have used their detailed mapping in the Harts Range area, to propose a multi- extension-compression model to explain the evolutionary mechanism for the older Strangways Orogenic Belt and the younger Harts Range Orogenic Belt being juxtaposed by a thick subhorizontal detachment zone.

The Amadeus Basin is a unit of Central Australian Platformal Cover where a thick sequence of platformal type sediments were deposited during late Proterozoic to Palaeozoic time (Plumb 1979).

Ding et al. (in prep.) are making a detailed study of the tectonic relationship between the

Arunta Inlier and Amadeus Basin on the SE margin of Arunta Inlier. The work will place further new restrictions on the deformation events of that area.

2.2 LITHOLOGIES OF THE STUDY AREA

2.2.1 CLASSIFICATION AND TERMINOLOGY

Both the basement assemblages of Arunta Inlier and cover sequences of Amadeus Basin are recognised within the study area. Their present juxtaposition is interpreted as being the result of the event which produced the Arltunga Nappe Complex which is currently considered to have formed in the Carboniferous Alice Springs Orogeny. The basement assemblages are mainly igneous rocks, herein termed the Atnarpa Igneous Complex, which are entangled with some supracrustals of Division One of Stewart et al. (1984). The cover sequence here includes only the basal units of the Amadeus Basin sequence, i.e. the Heavitree Quartzite and the Bitter Springs Formation. This study focuses on the basement assemblages, especially the Atnarpa Igneous Complex. The following is a list of rock types classified on the basis of field relations, petrography, geochemistry and geochronology within the study area:

1. Atnarpa Igneous Complex (AIC)
    (1). Atnarpa Calc-alkaline Suite (ACAS) (~1879 Ma)
        1). Fine-grained Amphibolite &/or Hornblende Gneiss
            A. Basaltic Type
            B. Microdioritic Type
        2). Medium to Coarse-grained Amphibolite and Hornblende Gneiss
            A. Mafic Member
                a. Cumulates
                b. Differentiates
            B. Felsic Member
                a. Meta-diorite
                b. Meta-quartz Diorite
                c. Meta-plagiogranite

(2). Atnarpa Granitic Batholith (AGB)

1). Atnarpa Older Tonalites (AOT)(~1863 Ma, Sandø 1987)

2). Atnarpa Older Leucogranites (AOLG) (~1873 Ma)

3). Atnarpa Muscovite Granite (AMG)

(3). Atnarpa Tonalite-Basalt Suite (ATBS)(~1751 Ma)

1). Atnarpa Younger Tonalite (AYT)

2). Atnarpa Younger Basaltic Amphibolite (AYBA)

3). minor Dioritic Porphyrite

2. Basement Supracrustal Assemblage (BSA)

(1). Quartzofeldspathic Gneiss

(2). Calc-silicate

(3). Schistose Amphibolite

(4). Mylonite and Tectonite

(5). Others such as Biotite Gneiss, Biotite Quartz Schist, Metapelite, Muscovite Gneiss and Muscovite Quartz Schist.

3. Cover Sequence of the Amadeus Basin.

Notes:

(1). It is common for using terms such as "pre-, syn-" and "post- tectonic" or "orogenic" to describe groups of igneous rocks. However, this leads to two problems: 1). The meaning of the term "orogeny" is quite confusing; 2). In a poly-deformed and metamorphosed Precambrian terrain, rock fabrics may not always be a reliable indicator. Therefore, the author prefers to use the words "older" and "younger" to distinguish the rock types in the study area because, in this instance, isotope ages appear to be more reliable.

(2). Most of the basement rocks in the study area are extensively metamorphosed and names such as "amphibolite" and "gneiss", are appropriate. However, for the purpose of recording identified igneous parentage, the igneous terminology prefixed by "meta-" is used. This discrimination is based on field relations and the relics of igneous features discerned in the thin sections.

2.2.2 ATNARPA CALC-ALKALINE SUITE (ACAS)

On the basis of field observations, petrography and geochemistry, the term Atnarpa Calc-alkaline Suite (ACAS) is proposed to represent an genetically related igneous assemblage, which ranges from mafic to felsic compositions, and intrusive to volcanic types. The rocks are characterized by the occurrence of numerous small offshoots, layers and boudins, and the close coexistence with basement supracrustal rocks.

The ACAS is located within the eastern part of the area, which was previously mapped as tonalite, granodiorite and calc-silicate by BMR workers on the 1:100,000 Geological Map Series, Arltunga-Harts Range Region Sheet (BMR, 1984). However, these rocks are found to be different from the true tonalite and granodiorite in many aspects, including field relations, mineral assemblage and geochemistry. Field reconnaissance also indicates the so-called diorites on the south side of Atnarpa Range and in the Tommy's Gap area as well as the so-called Tommy's Gap Metamorphics (BMR, 1983, 1984) are actually similar to the ACAS.

The coarse-grained ACAS generally consists of a mafic member and a felsic member, with the latter crosscutting the former (Plates 2-1.1 & 1.2). The most mafic types in the mafic member are cumulate meta-pyroxenite and meta-melagabbro. The cumulate texture can be seen in hand specimen, e.g. cumulas mineral hornblende megacrystals (usually metamorphosed from clinopyroxene), some up to 2cm in size, are surrounded by the intercumulas gabbroic liquidus phase. Some such megacrystals are enlongated along and wrapped by the foliation fabric. Clear cumulative bands are are locally developed by compositional and textural variations (e.g. Plate 2-1.3). However, the main types in the mafic member are the massive to foliated metagabbro to metadiorite which is dominated by amphibole and plagioclase. Most mafic members are compositionally and texturally transitional into one another. Differentiation within bands on variable scales can be recognised locally, but, in general, they crosscut the strongly foliated amphibolites and other supracrustals (e.g. Plate 2-1.4).

The rock types in the felsic member of coarse-grained ACAS range from metadiorite, through quartz diorite to plagiogranite. The compositional change is controlled by the contents of felsic minerals. As with the mafic member, amphibole is the main dark mineral. This contrasts with the true tonalite and granodiorite where biotite is the main dark mineral. In addition, the felsic member also crosscut foliated basement supracrustals.

The fine-grained basaltic amphibolite, black in colour, is either transitional to or crosscut by the coarse-grained types. Some outcrops look quite massive but close observation reveals foliations that are well defined. Coarse-grained ACAS is sometimes interlayered with the AGB. Here minor fine-grained basaltic amphibolite veinlets or finer layers are recognized in the mafic layers (e.g. Plate 2-2.6).

The fine-grained microdioritic amphibolite or hornblende gneiss usually coexists with the basement supercrustals and the ACAS. It is grey in colour and displays slight to strong foliation. It is crosscut by both coarse-grained felsic and mafic members (e.g. Plate 2-1.1). Plagioclase porphroblasts are very obvious within the contact zone. These are probably formed by thermal recrystallization during magma intrusion. Undissolved xenoliths are also found in the coarse-grained quartz diorite of the ACAS.

Similar crosscutting relations between the felsic member and mafic member were observed in Tommy's Gap and Star Creek areas (e.g. Plates 2-1.5 & 1.6).

2.2.3 ATNARPA GRANITIC BATHOLITH

The AGB occurs as composite stocks/batholith and covers about 60% of the mapped basement area. It can be generally grouped into older leucogranites (AOLG), older tonalites (AOT), and minor peraluminous muscovite granite (AMG) on the basis of deformational fabric, mineral composition, geochemistry and geochronology.

(1). *ATNARPA OLDER LEUCOGRANITES (AOLG)*

The leucogranites have suffered different deformation at different locations. Generally they can be roughly grouped into massive, foliated and mylonitised types. In the shear zones, they are seriously mylonitised and even sliced (e.g. Plate 2-2.4). Field observations indicate that leucogranites on the west are more massive but those on the east, more deformed and sheared. The leucogranites on the east display a well-defined lineation trending N to NNE. This fabric variation is probably consistent with the presence of the thrusts and shear zones (see enclosed map).

Texturally the leucogranites consist of a medium to coarse grained major phase and a fine to medium grained minor phase. The coarse-grained phase ranges from mainly pink to white in colour. The pink colour is probably due to different proportion of K-feldspar present. The

fine-grained phase is always pink-coloured. The fine-grained phase normally crosscuts the coarse-grained phase as dykes. But locally these two phases may be transitional. Pods of fine-grained massive type are found in the AYT. It is not clear whether they are older inclusions or younger sheets.

The leucogranites appear to be younger than the ACAS as a small number of xenoliths or rafts of the ACAS and BSA have been recognised within them (e.g. Plate 2-2.1; also see enclosed map). However in other places, they are transitional into the ACAS and BSA and are here characterized by an increasing amount of felsic gneiss, pegmatite, aplite and large outcrops of the ACAS. In the transitional zone, the leucogranite becomes indistinguishable from quartzofeldspathic gneiss. This is probably because of the intense deformation that has substantially destroyed their age relations.

(2). *ATNARPA OLDER TONALITES (AOT)*

The AOT in the AGB has a higher colour index and higher amount of plagioclase and biotite than the AOLG. Obviously some varieties with more pink K-feldspar are composionally transitional to granodiorite. By comparison, the tonalite in the Tommy's Gap area is essentially the same as the tonalite at Atnarpa and Marmalade Dam. In the less deformed Marmalade Dam area, two phases of AOT are recognised, of which, a medium -grained, massive, dyke-like minor phase crosscuts a coarse-grained, slightly foliated major phase. The minor phase is characterised by spheroidal weathering. Abundant xenoliths of the ACAS and BSA, e.g. basaltic amphibolite, cumulates, calc-silicate, muscovite schist, are present. Local contact metamorphism between xenoliths and the AOT can be observed. Numerous plagioclase porphyroblasts occur in the basaltic amphibolite. However, some obviously younger dioritic porphyrite and dolerite dykes crosscut the granodiorites.

The relative age relationship between AOT and AOLG is not clear in the field because of intensive fracturing and weathering. A few fine-grained granitic dykes which crosscut the granodiorites, may provide a clue. A similar situation was observed in the Tommy's Gap area.

Pb and Zn mineralization occurs on the western edge of the map along the contact of the AOT with the cover assemblage of carbonates, black shale and quartzite.

(3). *ATNARPA MUSCOVITE GRANITE (AMG)*

The AMG is only a small rock body exposed close to the major thrust or the extension of the Illogwa Schist Zone (see BMR Australian 1:250,000 Geological Series, Alice Springs & Illogwa Creek Sheets, 1983). This schist zone has been interpreted as one of the major thrusts in the Arltunga Nappe Complex. Foliation and N-NNE trending lineation are well defined. Grainsize of the AMG is variable but it is roughly zoned, with a white coloured, coarse grained muscovite-rich type being surrounded by a pink coloured, generally fine grained muscovite-poor type which usually occurs at a higher level. Both types are crosscut by aplite and pegmatite veins.

Generally, the presence of muscovite is a characteristic feature of the AMG.

2.2.4 ATNARPA TONALITE-BASALT SUITE (ATBS)

This term is proposed because the AYT and AYBA show close coexistence. The AYBA occurred as numerous rafts and xenoliths in the AYT. Crosscutting relations are very clear (e.g. Plate 2-2.1 & 2.1). Field observation indicates about 10% of the mapped AYT area is actually occupied by the AYBA. Field and petrographic evidence also suggest the minor dioritic porphyrite dykes may be also associated with the AYT and AYBA.

(1). *ATNARPA YOUNGER TONALITE (AYT)*

The AYT is a distinct rock type in this area. The rocks are white- coloured, massive and composed of plagioclase and biotite. Its intrusive age relative to the AGB was not observed in the field. However, the outcrops are very fresh and blocky with only weak deformation and, most importantly, the shear zone which has seriously influenced the leucogranites, seems to have little effect on it (Plate 2-2.4 & 2.5). In addition to AYBA, other types of xenoliths include muscovite schist, metapelite, basement quartzite(?) and dioritic porphyrite. This xenolith assemblage seems to be uncommon in other older rock bodies. Both tonalite and xenoliths are locally altered, which produced epidotization, greisenization and iron mineralization, which suggests restricted circulation of late stage or subsequent solutions.

(2). *AYBA*

The AYBA is massive to slightly foliated, black in colour, occurring as blocks, rafts, or

xenoliths in the AYT. They are crosscut by the AYT with networks of tonalitic veins (Plate 2-2.1). Epidotisation and iron mineralization are observed in the contact zone (e.g. Plate 2-2.3).

The AYBA, associated with dioritic porphyrite, is also found crosscutting the AGB as dykes.

(3). *DIORITE PORPHYRITE*

Dioritic porphyrite is present as dykes in other granitic rocks. Variable amounts of hornblende and plagioclase porphyroclasts can be clearly recognised. In the AYT, it appears to be present as xenoliths where hornblende has been replaced by actinolite as a result of contact metamorphism. Therefore, it is considered to represent the early phase of the AYT or the later phase of the AYBA.

In the field, it was mistakely considered to be baked ACAS. However, petrographic observation indicates it is quite distinctive from the metadiorite in the ACAS (see Chapter Three).

2.2.5 BASEMENT SUPRACRUSTAL ASSEMBLAGE (BSA)

The BSA includes foliated quartzofeldspathic gneiss, calc-silicate, strongly foliated schistose amphibolites, chlorite-actinolite schist, biotite gneiss, muscovite gneiss, biotite quartz schist, muscovite quartz schist, and metapelite. These components are interlayered with each other and coexist with, but are subordinate to the ACAS. They are therefore difficult to differentiate from the ACAS and to map out individually. The proportion of rock types is variable at different locations but quartzofeldspathic gneiss seems to be dominant. In some localities, quartz-rich quartzofeldspathic gneiss underwent spheroidal weathering and is very hard, which looks like quartzite in the field. The calc-silicate composition is variable with colour ranging from brown, yellow, light green to dark green. They appear to be a mixture of metamorphosed impure calcareous sediments. It is generally difficult to distinguish schistose amphibolite from the amphibolite in the ACAS. In the field, schistose amphibolite was indeed found to be interlayered with calc-silicate and to be crosscut by the mafic members of the ACAS. In addition, the chlorite-actinolite schist is probably altered schistose amphibolite.

Deformation is strong in the BSA with the development of a well-defined foliation and lineation. The intensity of lineation generally increases in the vicinity of the thrusts.

2.2.6 COVER SEQUENCE

Only the basal units of the Upper Proterozoic Amadeus Basin are exposed in the study area. They are the Heavitree Quartzite and carbonate-rich Gillen Member of the Bitter Springs Formation. The metamorphism grade is generally much lower than that in the basement.

2.2.7 SUMMARY

The study area is divided into two broad lithological units, the Arunta basement and the lowermost units of the Amadeus Basin cover. The supracrustal assemblage in the basement is intruded by a high-level to volcanic ACAS and followed by the emplacements of first the AGB and then the ATBS at a later stage.

2.3 METAMORPHISM OF THE STUDY AREA

Regional metamorphic grade in the study area reaches approximately amphibolite facies and is featured by the extensive coexistence of a green amphibole-plagioclase assemblage, mainly in the ACAS. Most of the clinopyroxene in the mafic members of the ACAS has been replaced by metamorphic amphibole. Replacement of hornblende and plagioclase by an actinolite-epidote-sphene-chlorite assemblage represents subsequent retrograde metamorphism.

However, a search has failed to reveal suitable metamorphic minerals for any quantitative estimation of the P-T conditions involved. The metamorphic conditions for amphibolite facies rocks in the Southern Province adjacent to the AIC have been estimated at 500--600°C and 3--5 kb (Shaw et al. 1984). These estimates may be suitable for the metamorphism in the study area.

Thrusting in this area has caused local retrograde metamorphism to green schist facies. This has caused considerable mylonitization. However, it is unknown if the retrograde mineral assemblage can be directly linked to this particular event.

Contact metamorphism and hydrothermal alteration have occurred locally but the metamorphic grade has been masked by later regional retrograde metamorphism.

The overall lower metamorphic grade indicates the rocks in the study area were buried at much shallower depths than those in the Strangways and Harts Ranges areas (Ding & James 1985).

2.4 STRUCTURE OUTLINE

It is difficult to investigate the early deformational history of the study area, especially within the basement, owing to the intensive overprinting of the later stage Arltunga Nappe movement, and strong weathering in key locations.

Generally the deformations of the study area can be assessed as two groups: those only in the basement and those in both the basement and the cover.

The earlier basement structure is dominated by the NE-SW oriented foliation which is defined in all the basement rocks. The foliation is defined by the enlongation and flattening of granular minerals such as feldspar and quartz and alignment of prismatic and flaky minerals such as mica. However, it is unknown how many generations of foliation occurred in the study area. Two major generations of foliation which transect at various angles can be locally observed both in outcrops and in thin sections. In addition, a similar orientation of foliation has been recognised on the south side of the Atnarpa Range, and in the Marmalade Dam and Tommy's Gap areas.

A disturbed but generally N-S trending brittle shear zone has affected most of the basement in the study area (e.g. Plate 2-2.4). This shear zone also shows drag folding along the mapped younger thrust as indicated in the enclosed map (see enclosure). It may predates the AYT as field observation indicates that the massive tonalite has a sharp contact with the "sliced" schists, which are mainly retrogressive granitic mylonite (Plate 3-3.7). However, despite this apparent age relationship, the sharp contact can also be explained as a kind of "augen structure" on a mega-scale because different rock types may have different resistence to deformation. Another phenomenon is that a strongly foliated NE-SW trending muscovite quartz schist is found as rafts in the younger tonalite. In one thin section, the NE trending foliation has been obviously folded and a second foliation (EW trending) along the fold axial plane has developed (Plate 3-4.1). Another thin section displays a typical S-C tectonite in which the muscovite and quartz ribbons have a major orientation transected by a minor orientation due to shearing movements (Plate 3-4.2). Overall, these observations demonstrate that brittle thrusting and dynamic metamorphism may have occurred in the Precambrian. This combined with the coexistence between the high-level AYT and deep-seated AOT-AOLG suggests a significant pre-AYT crustal uplift may have occurred.

Nevertheless, the existence of pre-AYT, post-AGB & ACAS sedimentation, deformation

and metamorphism and crustal uplift is ambiguous. The much clearer magmatic texture and much less deformation in the AYT than in the ACAS and AGB and the distinctive xenolith assemblage in the AYT (absent in the ACAS, AGB and BSA) may suggest such a case.

The deformation which involves both basement and cover is characterized by the thrusts and folds of the Arltunga Nappe Complex. This has produced a horizon of mylonitized shear zone (the Illogwa Schist/Shear Zone) and penetrative fabric, especially lineation, overprinted on the nearby basement rocks (up to 1 km away). An interesting feature is that whilst the foliation in the basement varies considerably, the lineation in it is always oriented to N to NNE (0--10 degree) (see enclosed map). This is in accordance with the alignment by the movement of the broadly E-W trending thrusts. Drag and sheath folds were developed in the basement interlayers near the thrust, in which the angle (less than 25 degree) and direction (from N to S) of thrusting is clearly indicated (Plates 2-2.7 & 2.8). This ductile deformation at the root of the thrust is also quite different from the older brittle shear zone. It must be the result of substantial regional loading. In addition, the NE-SW normal faults may syn-date or post-date this thrusting event.

The banded structure, i.e. members of mafic and felsic gneisses interlayered on a cm to m scale, or called lit-par-lit style, which is a dominant feature in the Harts Ranges (e.g. Foden et al. 1988; Ding & James 1985), is only locally present in the study area (e.g. Plate 2-2.6). It is also confined to places close to the shear zones. Instead, individual igneous rock bodies are more blocky and their boundaries are generally defined. This also shows that the Atnarpa Igneous Complex formed at a depth shallower than the Harts Range sequences.

PLATE 2-1 FIELD PHOTOGRAPHS

1. The fine grained microdioritic hornblende gneiss of the ACAS is crosscut and captured by the quartz diorite of the ACAS.

Locality: P1.1

2. The mafic member of the ACAS is crosscut by the felsic member (probably the quartz diorite) in the ACAS.

Locality: P1.2

3. The inhomogenous appearance of the ACAS rocks is due to a change in the composition and grainsize which is indicative of differentiation.

Locality: P1.3

4. Cumulate metagabbro or pyroxenite of the ACAS intruding the biotite gneiss of the BSA.

Locality: P1.4

5. A cross cutting relationship between the felsic and mafic members of the ACAS occurs in Tommy's Gap area.

Locality: P1.5.

6. Similar crosscutting relationship to that in the ACAS occurs in the Star Creek area about 20 km east of the Atnarpa Station.

Locality: P1.6.

7. A xenolith of the ACAS in the AOLG.

Locality: P1.7.

8. A fine-grained basaltic amphibolite of the ACAS is crosscut by a granite, probably the AOLG.

Locality: P1.8

1

2

3

4

5

6

7

8

PLATE 2-2 FIELD PHOTOGRAPHS

1. An AYBA xenolith is crosscut by the AYT as network veins.

Locality: P2.1.

2. An AYBA xenolith is crosscut by the AYT. Both of the them are deformed and foliated.

Locality: P2.2.

3. The metamorphosed contact zone between the AYT host rock and the AYBA xenolith. The yellow-coloured weathered surface is indicative of the occurrence of sulfide minerals, probably present as a result of contact metamorphism. Iron mineralization were also observed around this locality. T=tonalite; X=xenolith of the AYBA; Z=contact zone.

Locality: P2.3.

4. The undeformed AYT shows a sharp contact with the sliced retro- gressive granitic mylonite in the older shear zone.

Locality: P2.4.

5. A closer observation of the relationship similar to that in 4 (a location very close to P2.4).

Locality: P2.5.

6. The metagabbro of the ACAS is locally interlayered with the AOLG (the pink-coloured layer) in a lit-par-lit style. The black layer in the metagabbro is the fine-grained basaltic amphibolite of the ACAS.

Locality: P2.6.

7. A drag fold developed in the interlayered Arunta basement rocks in the vicinity of the thrust (the Illogwa Shear Zone). The arrow points to the direction of thrusting movement. In the field, this drag fold looks like a cross-section of a sheath fold.

Locality: P2.7.

8. Z-shaped drag folds in the vicinity of the thrust (the Illogwa Shear Zone). Arunta basement rocks are interlayered with Heavitree quartzite of the Amadeus Basin due to thrusting movement. Q= Heavitree Quartzite.

Locality: P2.8.

1

2

3

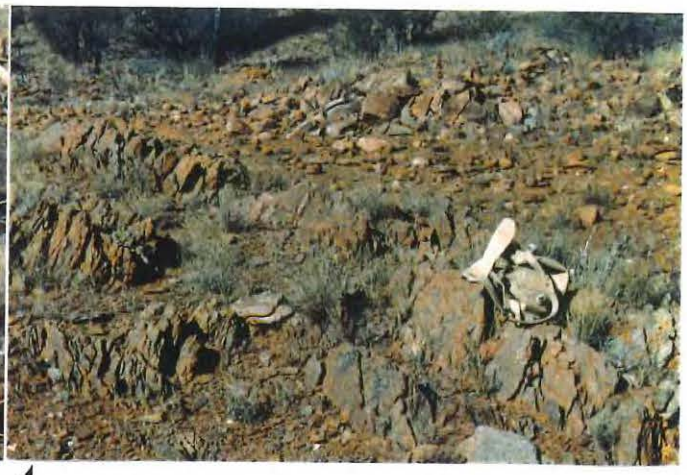

4

5

6

7

8

CHAPTER THREE: PETROGRAPHY

3.1 INTRODUCTION

The petrographic analysis of some 150 thin and polished thin sections was undertaken in order to describe in detail a representative selection of the lithologies of the Arunta basement in the study area.

Where appropriate an attempt was made to see through the intensive metamorphism for traces of original magmatic character. For example, features such as zoning in feldspar are considered to represent magmatic texture, especially if supported by field evidence, although it is recognised that this property can be caused by metamorphism in some circumstances. In addition, it is assumed that, if both fine and coarse-grained amphibolites coexist, it is highly probable that they were derived from two texturally distinct precursors, e.g. volcanics and intrusives, respectively, rather than from one precursor with different degrees of metamorphism.

3.2 PETROGRAPHY OF THE ATNARPA CALC-ALKALINE SUITE (ACAS)

The ACAS is defined to be an association of a variety of igneous rock types, which are apparently genetically related. Broadly it can be subdivided into a coarser-grained type and a finer -grained type, and further subdivided into mafic members and felsic members, respectively.

3.2.1 MAFIC MEMBERS OF THE COARSER-GRAINED TYPE

Two types of rocks are recognised in the coarse-grained mafic members:

1). Cumulates, which compositionally range from metapyroxenite, meta-melanogabbro to meta-gabbroic anorthosite.

2). Differentiates, including metagabbro to metadiorite and their amphibolite equivalents. Some cumulates containing intercumulas phases may be transitional to this type.

3.2.1.1 *CUMULATE*

Cumulate metagabbro is mainly composed of relict clinopyroxene and hornblende (40--70%), plagioclase (30--55%). In some samples, intercumulas quartz and accessory zircon are

recognised. Secondary minerals include actinolite, sphene, apatite, epidote, chlorite, and zoisite. The clinopyroxene is a Ca-rich type, but definitely not pigeonite, as the (+)2V (optical axial angle) is greater than 40°. No orthopyroxene and olivine have been identified. The grainsize is variable but mainly medium to coarse. A cumulative origin is supported by the following evidence: (1). An ophitic texture is obvious in the porphyritic massive samples. Here the granular pyroxene crystals fill in the intergranular triangular spaces defined by long prismatic subhedral to euhedral plagioclase crystals or they enclose and engulf plagioclase (Plate 3-1.1). (2). Poikolitic texture is another important feature, i.e. hornblende poikiloblasts, or relict pyroxene phenocrysts, encloses primary euhedral plagioclase. In the mafic mineral-rich samples, the hornblende poikiloblasts, up to 5mm in size, compose about 50% of the rock. (3). Dark and light minerals concentrate separately to form local anorthositic and pyroxenitic segregates (Plate 3-1.2). (4). Microcline is present as an intercumulas phase following the intergranular space defined by subhedral relict pyroxene phenocrysts in a metapyroxenite sample (Plate 3-1.3). Here the pyroxene crystallized earlier than the plagioclase. (5). Plagioclase displays higher than normal interference colours in the less altered samples. Optical microscopic determination indicates it contains a high An content up to 78%. This occurrence is also consistent with a cumulative origin. (6). In addition, plagioclase and its pseudomorphs are quite often subhedral to euhedral and zoning is seen to be well developed in the less altered crystals.

Clear metamorphic features are imposed on the mafic rocks by a combination of regional deformation and metamorphism. Clinopyroxene is normally replaced by green hornblende and fibrous actinolite either along cleavages and cracks or around the grain boundaries (Plates 3-1.1 to 4). Pyroxene-hornblende mosaics are quite obvious, the two minerals being distinguished by different extinction angles, different interference colours and different crystal shapes (Plates 3-1.3 & 4). Pyroxene relicts look dirty owing to alteration and magnetite exsolution along cleavages and cracks. Pseudomorphs are preserved where pyroxene has been intensively replaced by hornblende. They occurs as dirty cores with typical cleavages within the metamorphic hornblende.

Plagioclase is commonly altered to saussurite, zoisite, and sericite associated with some epidote. Pseudomorphic outlines remain even if plagioclase has suffered intensive alteration.

The abundant metamorphic hornblende can be divided into two types, namely, poikiloblastic and prismatic (e.g. Plate 3-1.3 & 4). The former displays ragged boundaries, with sphene and

epidote replacement along cleavages and cracks, and contains a number of inclusions such as plagioclase, prismatic hornblende, quartz, apatite and sphene crystalloblasts. Pyroxene relicts and pseudomorphs are still visible in such poikiloblasts. The finer prismatic hornblende usually displays straight margins and is almost inclusion free. However less intensive sphene replacement is also present. Apatite idioblasts, some up to 0.5mm in size, are present within hornblende and intergranular spaces. Another unusual phenomenon is the occasional presence of zircon in the samples with ophitic texture.

The intensity of metamorphism and hornblendization parallels the degree of deformation. In foliated samples, the foliation is well defined by the enlongation of plagioclase and alignment of prismatic hornblende (Plate 3-1.4).

The gabbroic anorthosite consists mainly of plagioclase (70--95%), clinopyroxene and hornblende (5--20%) and secondary sphene and epidote, with a grainsize about 0.5--5mm. Slight foliation is visible in both hand specimens and thin sections. Plagioclase crystals are very fresh and most of them are subhedral to euhedral. The An content is very high, up to 80% by optical microscopic determination. Zoning is well developed in some crystals with An content ranging from 69--79% from margin to core. Pyroxene is partly replaced by hornblende and obvious relicts are present (Plate 3-1.5). Primary magmatic hornblende can not be positively identified by a petrographic method.

3.2.1.2 *DIFFERENTIATES*

It is difficult to distinguish differentiates from cumulates owing to transitional features. However, the following points are a useful guide. In differentiates: (1). Plagioclase is much more Ab rich, e.g. An=43%; (2).Quartz is more abundant; (3). Less pyroxene relicts have been identified and at least some hornblende is originally magmatic; (4). A trace amount of biotite is recognised in the relatively felsic types. (5). Accessory minerals such as zircon, monazite, rutile, sphene, apatite (mostly metamorphic) are commonly present (e.g. Plate 3-1.6 & 7). e.g., sample 87173 contains abundant euhedral zircons, with the longest up to 0.2mm in length. About 2% of sphene crystalloblasts, the biggest up to 2mm in size, is also present. The enrichment of zircon in such a rock type seems to be too early to fit in a fractionation trend. (6). Little of the cumulate texture described above is recognized in the differentiates. However a normal magmatic feature

such as subhedral and zoned plagioclase is rather extensively preserved. (7). Both euhedral and irregular types of opaques, probably magnetite and/or ilmenite, show enrichment in some differentiations (e.g. Plate 3-2.1). The earlier crystallization of such minerals may have effectively precluded the enrichment of iron and titanium in the later stages.

3.2.2 FELSIC MEMBERS OF THE COARSER-GRAINED TYPE

This group of rocks is mainly composed of hornblende, plagioclase (An<43%) and quartz. The grainsize is variable, mainly medium to coarse. It can be subdivided into metadiorite, meta-quartz diorite and metaplagiogranite on the basis of quartz content and the proportion of An in plagioclase (e.g. Plate 3-1.8, 2.2 to 2.4). Quartz diorite seems to be the dominant phase. A minor amount of biotite may occur in the quartz diorite. Microcline, perthite and granophyric quartz may be present in the plagiogranite, but they are quite insignificant. No obvious enrichment of K-feldspar and mica with increasing quartz can be observed. Accessory and secondary minerals in this group of rocks include zircon, sphene, apatite, monazite, rutile, epidode, zoisite, sericite, and chlorite. Zircon and sphene may be enriched in the quartz diorite.

Separate descriptions are unnecessary for the three types of felsic members as they possess similar petrographic features. The following is a list of their major characteristics.

1). Diorite is the most mafic type in this member. It is distinguished from the mafic member as it crosscutts the latter. Compositionally it is transitional to quartz diorite. Grainsize is variable and seems to be related to fractionation. Quartz is only a minor phase in this type. Zircon is present as well-preserved euhedral crystals (e.g. Plate 3-1.8). Most of the plagioclase in the diorite is partially altered to sericite. However, a few euhedral grains display saussuritized pseudomorphs, and may be from an An-richer cumulas phase.

2). Only a few magmatic features can be discerned in thin sections of the felsic member. Some euhedral to suhedral plagioclase crystals display visible zones. Alteration of plagioclase is stronger to the inner zones, which leads to dirty cores (Plate 3-2.2). The plagiogranite contains granophyric quartz and a trace amount of irregular microcline, which infill the intergranular spaces, and exhibits typical granophyric texture (e.g. Plate 3-2.4).

3). Many zircons are present in quartz diorite, which is consistent with a Zr enrichment, differentiation trend. For example, about 8 zircon grains (50--300 micrometre long) were identified

in only one hornblende mosaic. Most zircons are short and prismatic in shape. Some long prismatic and irregularly shaped types are also found. Zoning can be recognised in some grains by variable interference colours. Most zircons are present as inclusions in hornblende and cause pleochroic halos. A few are present in plagioclase and intergranular spaces.

4). Metamorphic characteristics are much more common than magmatic ones. Most rocks are deformed to some extent. This is observed in thin sections by granulation of crystals, especially quartz, undulose extinction and rupture zones in quartz, grain orientation defining foliations, bending of twin lamellae, cross-lamellae deformation twinning in plagioclase, kink-bands in biotite, and the mylonitization and the presence of augen structures in some samples. Recrystallization is commonly present along the grain boundaries and rupture zones. Triple-point junction, sutured and irregular grain boundaries are also indicative of recrystallization. Replacement and alteration of minerals such as the epidote group, sphene, apatite, chlorite and sericite is extensive. Sphene alteration is the most spectacular. Both larger irregular sphene crystalloblasts and smaller diamond-shaped iodioblasts are present (e.g. Plates 3-2.3 & 4). These occur either along the cleavage and cracks in hornblende or follow the intergranular spaces.

5). Hornblende is the major dark mineral. It shows light brown to dark green pleochroism. Several generations can be recognised. The poikiloblastic type is irregular in shape, and contains numerous inclusions such as crystalline to paracrystalline quartz grains, prismatic hornblende, sphene, epidote, plagioclase, zircon and apatite. The prismatic type is finer in size, contains fewer inclusions and is aligned to particular foliations. The third type occurs as fine crystalline to paracrystalline grains, which sit in the intergranular spaces or around the boundaries of courser hornblende grains. These may result from recrystallization of granulated fragments.

6). Fine grained, microdioritic, amphibolite inclusions are observed both in hand specimen and thin section of quartz diorite. They are foliated in a plane parallel to that in the host quartz diorite, indicating that the deformation must postdate quartz dioritic intrusion. This further supports the suggestion that these two rock types are genetically related.

3.2.3 FINE-GRAINED AMPHIBOLITES

The fine-grained amphibolites in the ACAS are grouped into two types, basaltic and microdioritic, after their aparent volcanic precursors, e.g. basalt and andesite, respectively.

3.2.3.1 *BASALTIC-TYPE AMPHIBOLITE*

The basaltic-type amphibolite (e.g. Plate 3-2.5), which is mainly foliated fine grained (grainsize<1mm), and composed of fine crystalline to paracrystalline green hornblende, plagioclase, quartz, biotite, accessary zircon and secondary minerals such as epidote, sphene, sericite and magnetite. The hornblende is prismatic or diamond-shaped, and is interlocked with altered to fresh plagioclase and a few quartz grains. A well-developed foliation is defined by the prismatic hornblende crystals and a slight enlongation of plagioclase. Poikoloblastic epidote, which replaces hornblende and plagioclase and is intergrown with sphene, displays little re-alignment by the deformation. This indicates that epidote growth must postdate the amphibolitic metamorphism and deformation. A felsic vein which crosscuts the rock, generally parallel to but locally transecting the foliation, is also not affected by the deformation. In addition, broad deformation lamellae, perpendicular to the foliation, are displayed by the systematic change of interference colours in hornblende along the direction of foliation. The same phenomenon, as well as undulose extinction in quartz, exists in the felsic vein. This suggests that a subsequent deformation, which postdates the felsic vein, has occurred.

3.2.3.2 *MICRODIORITIC-TYPE AMPHIBOLITE*

This rock type contains more feldspar but less hornblende than the basaltic type. As it is deformed, it could be called a fine-grained hornblende gneiss if its igneous parentage was not understood.

Generally two types of microdioritic amphibolite are recognised, i.e. even-grained and porphyroblastic.

The porphyroblastic type (e.g. Plate 3-2.7) is confined to the contact between the coarser-grained ACAS and the even-grained microdioritic-type. Plagioclase porphyroblast aggregates compose about 10--15% of the rock apparently formed during the intrusion of the coarser-grained ACAS. The enlongation of these porphyroblasts define a clear foliation.

The even-grained types (e.g. Plate 3-2.6) are composed of plagioclase (50--60%), hornblende (20--30%), quartz (5%$\pm$), opaques (1--2%), sphene (1--2%) and minor epidote, chlorite, and sericite. Some zircon grains are also recognised. The grainsize is normally less than

1mm. Plagioclase is granular, subhedral to anhedral, and has undergone only slight sericite alteration. Hornblende is prismatic to granular and displays light brown to dark green pleochroism. it is usually altered to epidote, chlorite and sphene. Quartz is also granular and follows the irregular intergranular spaces. It generally exhibits undulose extinction. Two types of sphene, larger porphyroblasts (0.5mm) and smaller idioblasts (0.1mm), are identified. Both euhedral and irregular-shaped opaques are also present. Sutured grain boundaries and triple-point junctions are generally well developed. In the foliated samples, foliation is clearly defined by the enlongation of granular minerals and the alignment of prismatic hornblende, sphene and chlorite.

3.2.4 SUMMARY

1). The ACAS contains a variety of rocks, with precursors probably ranging from volcanics to intrusives, and cumulates to differentiates. These are related through initial fractional crystallization of clinopyroxene+plagioclase and later precipitation of hornblende, plagioclase and magnetite.

2). The close coexistence of coarse-grained ACAS and fine-grained ACAS, combined with characteristic features such as ophitic texture in some mafic cumulate metagabbro, and the occurrence of minor anorthosite, suggests a high-level emplacement.

3). The general absence or only minor presence of biotite and K-feldspar in the felsic differentiates suggests a rather distinctive fractionation trend similar to the trondhjemitic trend (Arth et al. 1978).

4). Petrographic features indicate that the intrusion of the ACAS predates the major deformation and extensive amphibolite facies metamorphism.

5). Mafic minerals, especially clinopyroxene, have substantially changed during metamorphism but some magmatic features have been preserved in the plagioclase. This reflects that mafic minerals and feldspar have different sensitivity to hydration of amphibolitic metamorphic fluid.

3.3 PETROGRAPHY OF THE ATNARPA GRANITIC BATHOLITH (AGB)

As described in Chaper Two, the AGB can be subdivided into three groups: older leucogranites (AOLG), older tonalites (AOT), and minor muscovite granite (AMG).

3.3.1 ATNARPA OLDER LEUCOGRANITE (AOLG)

The AOLG is composed of alkali-feldspar (microcline and perthite) and acidic plagioclase (60--70%), quartz (25--35%), biotite and some muscovite (0--3%) and accessory and secondary minerals including sphene, zircon, opaques, monazite, rutile, epidote, zoisite, sericite and chlorite. The proportion of alkali-feldspar to plagioclase is variable. Generally the finer grained phase is richer in alkali-feldspar than the coarser grained phase and therefore most of it is true granite. The coarser grained phase ranges from adamellite to granodiorite in modal composition.

Banded and mylonitised samples have feldspars which occur as augens with strong boundary granulation and enlongation. Quartz is completely granulated and ribboned and appears as paracrystalline to leaf-like grains, which show undulose extinction. Dark minerals have been fragmented to form veinlets along grain boundaries. A network of sericite veinlets is also present.

Some primary textures can be observed in the less deformed to massive samples, e.g. 1). alkali-feldspar encloses plagioclase and 2). plagioclase displays zoning and sericite alteration which becomes more intensive towards the dirty cores (Plate 3-3.4). Large bent biotite flakes are present. Some are partly altered to epidote, chlorite, and muscovite. Some deformation, such as granulation, bending of cleavages and kink-bands, has also occurred in the more massive types. However, quartz shows sutured boundaries instead of being ribboned.

The AOLG contains zircons which are present as inclusions in biotite. Zoning is well developed in some euhedral grains, which is indicative of a magmatic origin (e.g. Plate 3-3.3). The sodium phase in perthite is irregularly shaped and quite dirty. Some of it even crosscuts twin lamellae, indicating a metasomatic rather than exsolution origin. Occasionally this veinlet-like phase transects plagioclase, producing local albitization. A sphene porphyroblast, with a core filled with altered minerals and associated with apatite inclusions, manifests a metamorpic origin.

3.3.2 ATNARPA OLDER TONLAITE (AOT)

The AOT in the Atnarpa area is composed of acidic plagioclase and some K-feldspar (70%), quartz (15%), biotite (10%), opaques (2%) and accessory and secondary minerals such as zircon, apatite, rutile, monazite, allanite, epidote, chlorite and sericite. About 30% of the minerals in the rock have been granulated (e.g. Plate 3-2.8). Quartz is completely granulated and displays

undulose extinction and has sutured boundaries. K-feldspar and acidic plagioclase poikilitic megacrystals (5mm) show granophyric intergrowth with numerous quartz patches. Other inclusions in these megacrystals can also be observed. One K-feldspar megacrystal contains a plagioclase inclusion that has granulated and rounded boundaries. Deformation lamellae are developed in some of these megacrystals. K-feldspar usually displays no twins and has lower interference colours from which they can be readily distinguished from polysynthetically twinned plagioclase. Two types of biotite are observed, i.e., a minor amount of larger flakes and numerous finer laths. They normally infill intergranular and granulated spaces or replace feldspars. Locally finer laths may be aligned. Replacement by chlorite and epidote is common. Dark brown coloured pleochroic halos, caused by zircon inclusions, are very obvious. Opaques, possibly magnetite, can be classified into two types, earlier euhedral to subhedral crystals (0.1--0.5mm) and later irregular aggregates. The euhedral type always contains fluid inclusions. The irregularly-shaped type shows intergrowth with biotite laths which may be locally aligned. Numerous zircons, mostly prismatic, some fragmented, are present. Growth zones are well developed in some grains. A few prismatic grains show replacement by paracrystalline epidote groups and felsic minerals. Apatite crystalloblasts (0.5mm) replaced an earlier phase of biotite but were then replaced by later phases of biotite and epidote.

Two phases of AOT were recognised in the Marmalade Dam area. The coarse-grained phase contains less or little K-feldspar but a certain amount of hornblende and is therefore more mafic. The deformation is less significant and magmatic features, such as granitic texture and zoning in plagioclase, are clearly preserved (Plate 3-3.1). Biotite crystalls are larger and more flaky and contain numerous inclusions such as sphene, zircon, epidote and apatite. Some replacement along cleavages is also observed. It is interesting to note that some zircon grains display clear older cores with younger overgrowths. The finer grained phase is more evolved, containing some microcline but no hornblende. Abundant zircon and sphene are also present.

The AOT in the Tommy's Gap area is compositionally similar to that in the Atnarpa and Marmalade Dam areas, containing plagioclase, K-feldspar, biotite, numerous zircon, opaques, sphene, and allanite. Some euhedral allanite grains display typical oscillatory zones (Sando 1987; this study), indicative of fractional crystallization. However, a zoned zircon inclusion within the allanite has some characteristics of inheritance. Again, deformation of the AOT in Tommy's Gap

area is weaker than that in the Atnarpa area.

3.3.3 ATNARPA MUSCOVITE GRANITE (AMG)

Petrographically the AMG consists of microcline, perthite, sodium plagioclase (albite--oligoclase), quartz, muscovite, cassiterite(?), epidote and sericite, with the texture ranging from equigranular to megacrystic. The enrichment of muscovite in this rock type is the most characteristic feature (e.g. Plate 3-3.6). Garnet, tourmaline (?) and zircon are present in the pinkish even-grained type of the outer zone (e.g. Plate 3-3.5). Most of the body is deformed, being strongly foliated and mylonitized. Some of the rarer less deformed rocks show recognizable granitic textures consistent with a magmatic origin, e.g. subhedral sodium plagioclase is interlocked with anhedral or irregular K-feldspar and quartz. Sodium plagioclase and other inclusions are obviously present in K-feldspar phenocrysts in the megacrystic types. Few overgrowths on and replacement of the phenocrysts have been observed. Some biotite is present in the outer zone types, but it generally appears to have altered to muscovite. Primary muscovite is usually set in the intergranular spaces of other minerals. Most of it is strongly deformed, as shown by bending of cleavage, undulose extinction and kink-bands. This indicates the muscovite formation predates the major foliation. Garnet is also flattened and enlongated by the foliation.

The rocks are slightly altered by post magmatic hydrothermal fluids. Sericite is the most common alteration product. It occurs along cleavages, cracks and boundaries of the feldspars, and on the margins of muscovite. Some sericite veinlets crosscut muscovite crystals which further emphasizes that the muscovite formed earlier. Phyllic alteration is present as network veinlets in strongly deformed specimens. Some alteration of epidote and zoisite is also observed. Generally the amount of alteration and recrystallization is related to the degree of deformation. The highly deformed rocks contain minerals which have been granulated, enlongated, twisted, ribboned and recrystallized and crosscut with phyllic alteration.

3.3.4 SUMMARY

This petrographic study indicates that there is a constant compositional variation trend from the early phase of the AOT to the later phase of the AOLG. This includes: 1). Hornblende is only present in the most mafic phase of the AOT; 2). General decrease in biotite content. It tends to

concentrate in the AOT and early coarse-grained phase of AOLG. 3). The proportion of plagioclase to alkali-felspar tends to decrease, e.g. alkali-feldspar is absent in the hornblende-bearing AOT and present in its later phase and it becomes predominant over plagioclase in the later phase of the AOLG. Such a general variation could be due to a fractional crystallization process, and this is further supported by the occurrence of magmatically zoned zircons and allanite, especially the oscillatory type.

The AMG is a distinctive rock type. Although it is similar to the later phase of the AOLG in some mineral compositions, such as alkali-feldspar, it is distinctive from the AOLG in the enrichment of muscovite, the presence of garnet and tourmaline (?) and magmatic zoning of the rock body.

3.4 PETROGRAPHY OF THE ATNARPA TONALITE-BASALT SUITE (ATBS)

As mentioned in the last Chapter, the ATBS is somewhat a bimodal high-level suite including the AYT, the AYBA and minor dioritic to andesitic porphyrite.

3.4.1 ATNARPA YOUNGER TONALITE (AYT)

The AYT can be texturally subdivided into a porphyritic type and a massive type (e.g. Plates 3-4.4 & 5). Both types are slightly foliated.

In the porphyritic type, porphyroclasts (45%) include plagioclase (andesine, up to 43% of An content) and biotite. The groundmass (55%) is composed of felsic paracrystals, biotite and opaques. Although recrystallization occurs, a blastopilotaxitic texture is still discernable (e.g. Plates 3-4.3 & 4). In the massive type, the major minerals are plagioclase (andesine--oligoclase) (70%), quartz (10--20%) and biotite (5--15%). Accessory and secondary minerals in both types are zircon, apatite, opaques, monazite, rutile, epidote, muscovite, sericite, and chlorite.

Typical magmatic features are well developed in the AYT. e.g. plagioclase is normally euhedral to subhedral and prismatic. Zoning is well preserved, especially the oscillatory zones, which is unequivocally of magmatic origin (Plate 3-4.3). An anorthoclase porphyroclast (1 cm) has been identified and it shows granophyric intergrowth with quartz. It contains straight twin lamellae which are quite different from cross-hatched twins typical of microcline. Phenocrysts of anorthoclase suggest that the AYT formed at a very high level and high temperature. In addition, a

crossing Karlsbad-albite twin with cross extinction is also observed in the cross section of a plagioclase crystal. The blastopilotaxitic texture mentioned above is also a typical magmatic feature.

Biotite, with grainsize up to 5 mm, is very fresh in the younger tonalite (e.g. Plate 3-4.5). Nevertheless, two types, i.e. larger flakes and finer laths, are readily recognised. The finer laths may result from recrystallization of the granulated margins of the larger flakes. Quartz is present as granulated aggregates with sutured boundaries, and usually displays undulose extinction.

Accessory zircon is less common and usually smaller in grainsize than that from AOT. Some crystals are also present as inclusions in biotite and cause pleochroic halos. Little sphene was observed, suggesting a lower Ti content. Epidote and sericite are the most common secondary minerals.

Deformation has caused granulation in most grains, and has produced bending and kink-bands in biotite. However it appears to be less intense than that in the other igneous rocks.

Contact metamorphism between xenoliths and tonalite has resulted in skarnization, greisenization and iron-mineralization. The xenolith assemblage includes massive amphibolite, muscovite schist, metapelite, quartzofeldpathic gneiss, quartzite and even conglomerate quartzite.

3.4.2 ATNARPA YOUNGER BASALTIC AMPHIBOLITE (AYBA)

The AYBA is composed of actinolitic hornblende, plagioclase, opaques and minor quartz. Secondary minerals include epidote, sphene, chlorite and sericite. Magma heating by the AYT may cause local quartzofeldspathic enrichment such as the presence of more quartz, microcline and biotite. Magnetite is also enriched in the samples from the contact zone. However, the major difference between the basaltic amphibolite in the ACAS and the AYBA lies in the obvious magmatic features preserved in the AYBA (e.g. Plate 3-4.7). (1). Clear blasto-ophitic textures were observed in the less altered massive AYBA inclusions, i.e. the long prismatic plagioclase formed triangular framework. But no pyroxene relict was identified due to hydration processes during subsequent amphibolite grade metamorphism. (2). Some AYBA samples display a porphyroblastic texture. The porpyroblasts are composed of plagioclase pseudomorphs and a few hornblende aggregates. This feature can be identified in hand specimen, as white-coloured spots. A similar occurrence was observed in the massive fine-grained amphibolite in the Tommy's Gap area, where it crosscuts the AOT (Sando 1987). All such phenomena are generally absent in the

completely recrystallized basaltic amphibolite in the ACAS (e.g. Plate 3-2.5).

3.4.3 MINOR DIORITIC PORPHYRITE

This minor type is compositionally dioritic or andesitic, being present either as dykes in the AGB (e.g. Plate 3-4.8) or as xenoliths in younger tonalite (e.g. Plate 3-4.6). A spectacular porphyritic texture is present in both hand specimens and thin sections. The phenocrysts are composed of green hornblende, well-zoned plagioclase (including oscillatory zoning) and some opaques, which are all euhedral in shape (Plate 3-4.6). The groundmass is mainly felsic paracrystallites with a pilotaxitic texture. The grain size and concentration of the phenocrysts are variable so that the rock mineralogy ranges from porphyrite to diorite over very short distances. This minor diorite is obviously different from the metadiorite in the ACAS as shown by its clear magmatic texture (Plate 3-4.8). Xenoliths present in the AYT suffer from intensive actinolitization, sericitization and recrystallization. However, some well-preserved zones in plagioclase indicate that they are originally magmatic.

3.4.4 SUMMARY

Petrographical study has demonstrated that primary magmatic features are well-preserved in the ATAS, which indicates it is quite different from other older igneous rocks in the Atnarpa area.

All these magmatic features suggest that the ATBS was formed at a very high level. Its coexistence with the AGB, especially the crosscutting relations, may be the result of a crustal uplift and subsequent erosion period predating the emplacement of the ATBS.

The distinctive xenolith assemblage in the AYT, which is generally absent in the ACAS and AGB, suggests a basinal sedimentation may have occurred during the time interval between the formation of the older AIC (the ACAS and AGB) and the emplacement of the ATBS.

3.5 BASEMENT SUPERCRUSTAL ASSEMBLAGE (BSA)

The BSA is subordinate to the igneous complex, and therefore it is difficult to establish a complete sequence for the BSA. Petrographical analysis combined with field observation indicates that the BSA is composed of quartzofeldspathic gneiss, calc-silicate, schistose amphibolite, biotite gneiss, muscovite gneiss, muscovite schist, metapelite and mylonites.

The quartzofeldspathic gneiss contains K-feldspar (perthite and microcline) and plagioclase (45--80%), quartz (15--50%), biotite, muscovite, and accessory and secondary minerals. Some samples contain garnet and zircon (e.g. Plate 3-3.7). The grainsize is variable but mostly fine. Both K-feldspar-rich and plagioclase-rich types are recognised but the former is dominant. The quartz-rich variety is very hard. It was initially called quartzite in the field. This variable composition indicates at least some of it may be paragneiss. However the plagioclase-rich type may be derived from igneous precursors. Foliations are well-defined by the alignment of mica and enlongation of granular minerals. A granoblastic texture, with sutured boundary and three-point jointing at 120 degree, is well developed.

Biotite gneiss (87056) is mainly composed of plagioclase, quartz, biotite, minor microcline and some accessory muscovite and opaques. It is crosscut by mafic cumulate (e.g. Plate 2-1.4). The alignment of biotite and enlongation of granular minerals defines a clear foliation. Some plagioclase porphyroblasts display zoning in their rectangular cores which are margined by an irregular, recrystallised phase. These cores suggest a magmatic origin.

Calc-silicate is composed of quartz (70--5%), carbonate (0--70%), actinolite-tremolite (0--25%), epidote group (10--20%), minor sphene and perthite. Compositionally it ranges from impure marble to impure quartzite. A foliation is defined by quartz ribbons and the alignment of especially epidote and actinolite, as well as the other minerals.

The muscovite gneiss contains quartz, muscovite and minor feldspar. A foliation is well defined. The muscovite is very fresh and almost inclusion-free (photo).

Muscovite schist is found both in the shear zone and as rafts in the AYT. It consists essentially of muscovite, quartz and minor garnet. The garnet is also cracked and enlongated along the foliation. As described in Chapter Two, one sample is a typical SB tectonite, whilst the other records two generations of foliations (Plates 3-4.1 & 2). Its occurrence as xenoliths in the AYT has been used to argue for crustal uplift and dynamic metamorphism early in the Precambrian.

Metapelite is also found as xenoliths in the AYT and it consists mainly of paracrystalline felsic minerals and mica.

Strongly foliated amphibolite is found to be closely associated with calc-silicate. It is crosscut by the the mafic members of the ACAS. A strongly foliated chlorite actinolite schist, identified in the thin section, is considered to be the alteration product of such an amphibolite.

PLATE 3-1: PHOTOMICROGRAPHS

1. Cumulate metagabbro of the ACAS (87176). The ophitic texture is clearly defined by prismatic plagioclase crystals. On the upper margin and upper left corner, clinopyroxene grains are partially replaced by hornblende. On the upper right corner, a prismatic plagioclase crystal is engulfed by hornblende. Crossed nicols.
2. Cumulate metagabbro of the ACAS (87174). Granular plagioclase (An=70-80%) and clinopyroxene concentrate separately to form local anorthositic and pyroxenitic seggregates. Triple junctions defined by plagioclase indicate equilibrium recrystallization. Some clinopyroxene grains have been replaced by diamond-shaped hornblende. Cross nicols.
3. Cumulate pyroxenite of the ACAS (88086). Intercumulas microcline infills the marginal space defined by a relict euhedral clinopyroxene phenocryst, which has been partially replaced by hornblende and further altered to epidote. Crossed nicols.
4. Cumulate metagabbro of the ACAS (87174). Clinopyroxene grains are typically replaced or corroded by hornblende. Smaller prismatic or diamond-shaped hornblende grains are aligned along the foliation. Crossed nicols.
5. Gabbroic anorthosite of the ACAS (88049). Relict clinopyroxene, being irregularly shaped, infills the intergranular spaces defined by subhedral plagioclase (An=70-80%). Clinopyroxene has been substantially replaced by hornblende. Crossed nicols.
6. Mafic differentiate (metagabbro?) of the ACAS (87173). Prismatic hornblende grains cluster around a hornblende poikiloblast, which encloses a plagioclase aggregate and is replaced by sphene along cleavages. A zircon grain is included by the marginal prismatic hornblende. Triple junctions are well developed in the plagioclase aggregate. Crossed nicols.
7. Mafic differentiate (meta- melanodiorite?) of the ACAS (87038). Plagioclase has been pseudomorphosed by saussurite. Apatite crystalloblasts set in the hornblende aggregate. Intergranular quartz shows granophric extinction, which may be an intercumulas phase or result from metamorphism. Plane polarised light.
8. Metadiorite of the felsic member, the ACAS (87103). A representative sample. Hornblende contains numerous exsolution phases, probably sphene. Plagioclase is slightly altered to sericite. A zircon grain is set in plagioclase. Crossed nicols.

Symbols: hb=hornblende; PL=plagioclase; Q=quartz; sp=sphene; Ep= epidote; mc=microcline; Zr=zircon.

Bar=1mm

Sample localities are shown in Appendix-2.

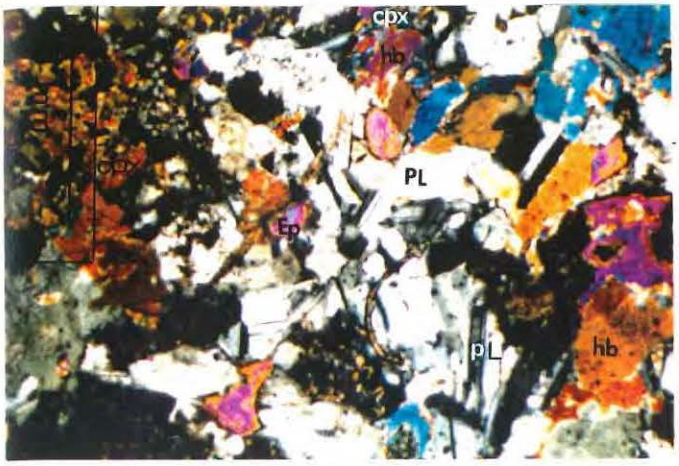
cpx
hb
PL
ep
pL
hb

1

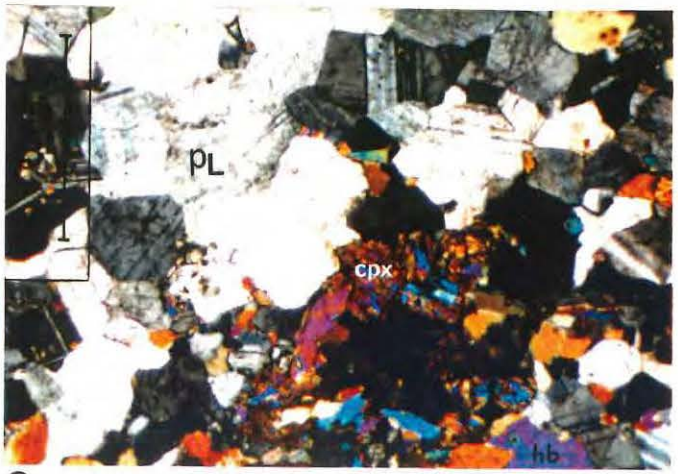
pL
cpx
hb

2

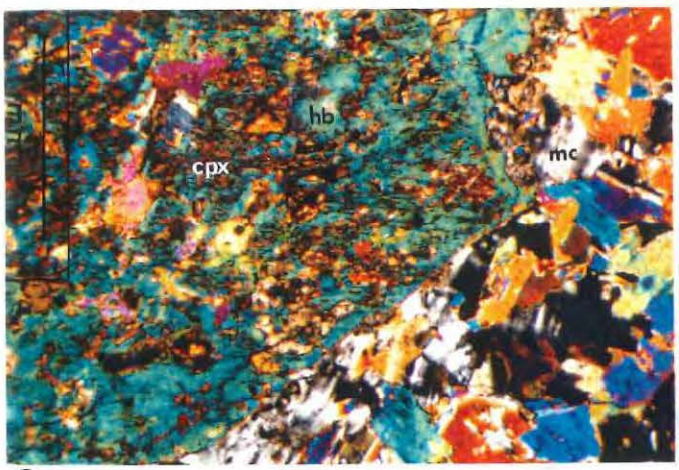
hb
cpx
mc

3

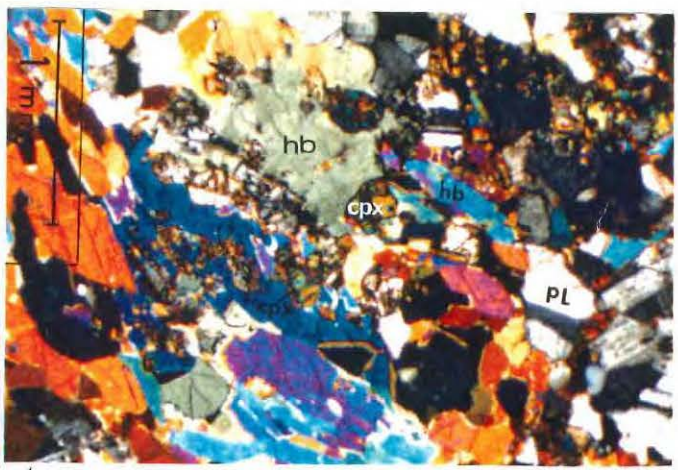
1 mm
hb
cpx
hb
PL

4

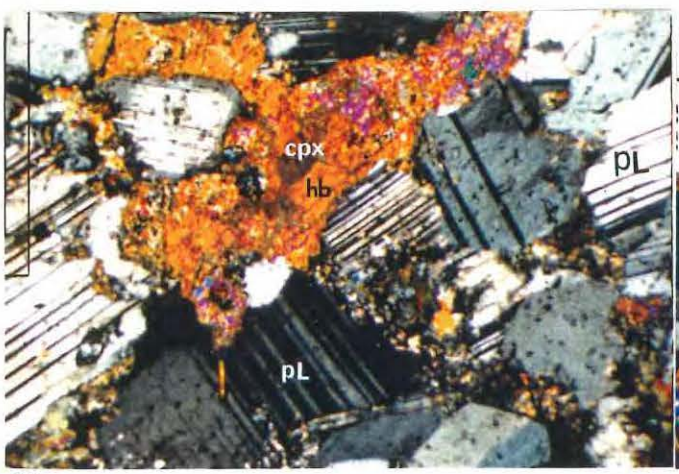
cpx
hb
pL
pL

5

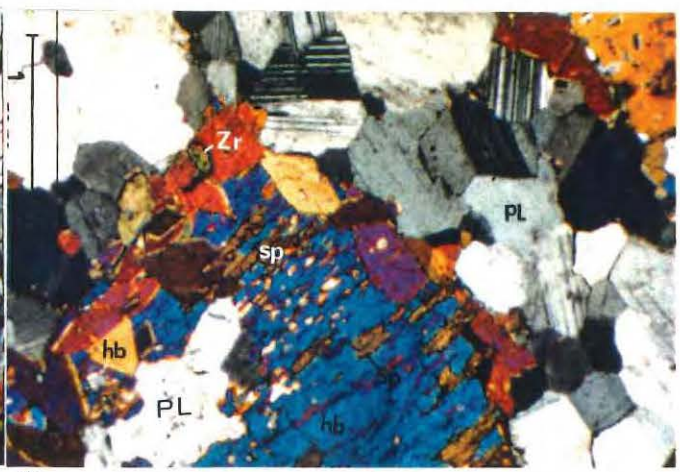
Zr
PL
sp
hb
PL
hb

6

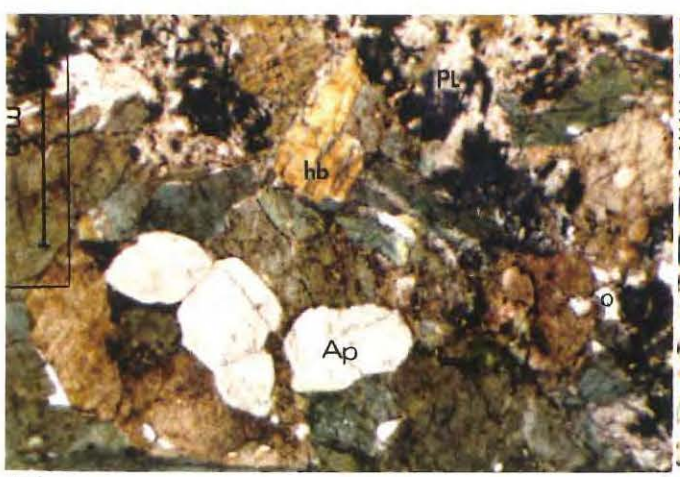
PL
hb
Ap

7

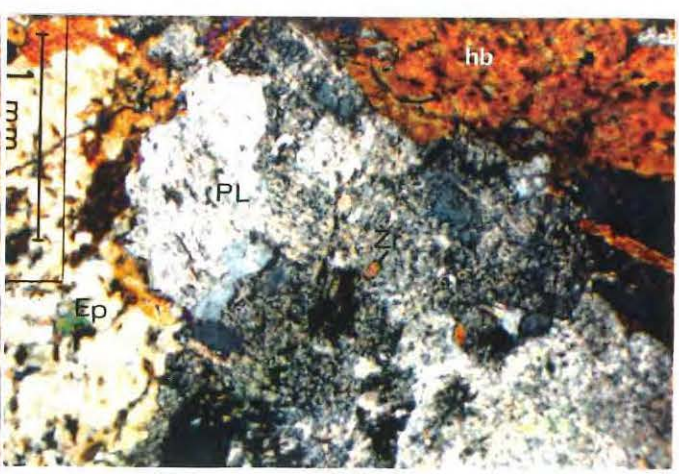
1 mm
hb
PL
Ep

8

PLATE 3-2: PHOTOMICROGRAPHS

1. Mafic differentiate of the ACAS (87143). Notably the high content of the opaque mineral, probably magnetite, is indicative of a high oxygen fogacity in the magma. Crossed nicols.
2. Meta- quartz diorite of the ACAS (87064). Notably the short prismatic plagioclase grains are well zoned and show stronger alteration in the cores. Crossed nicols.
3. Typical meta quartz diorite of the ACAS (87122). Crossed nicols.
4. Meta plagiogranite of the ACAS (87121). The sample is strongly foliated. However, it is still clear that the granophyric quartz shows consistent extinction positions. The white coloured part is at about 45° position. The grey coloured part is close to the extinction position. The black coloured part is at the extinction position, which also displays an undulose extinction feature. Hornblende is replaced by sphene and epidote. Another major mineral is plagioclase. It is notable that neither biotite nor K feldspar is present. Crossed nicols.
5. Fine-grained basaltic amphibolite of the ACAS (87058). The foliation is well defined by the alignment of prismatic hornblende. The upper right corner is an undeformed felsic vein. This sample is quite different from Plate 3 4.1, the metabasalt of the AYBA. Crossed nicols.
6. Fine grained microdioritic hornblende gneiss of the ACAS (87127). More quartz and plagioclase are present. The foliation is well defined by alignment of hornblende and flattening of quartz and plagioclase (only slightly). Notably again, no K feldspar or biotite is present. Crossed nicols.
7. Fine grained microdioritic hornblende gneiss of the ACAS (87064F). A xenolith in 87064, the quartz diorite. The porphyritic plagioclase aggregates are well developed due to recrystallization during the emplacement of the meta quartz diorite (87064). Triple junctions and sutured grain boundaries are also clearly present. The foliation is still visible. Crossed nicols.
8. Tonalite of the AOT (88031). Sample has been strongly granulated and altered by chloritie and sericite. A zircon grain is present. Crossed nicols.

Symbols: mt=magnetite; gQ=granophyric quartz; Bi=biotite; chl=chlorite. Other symbols the same as in Plate 3 1.

Bar= 1 mm.

Sample localities are shown in Appendix 2.

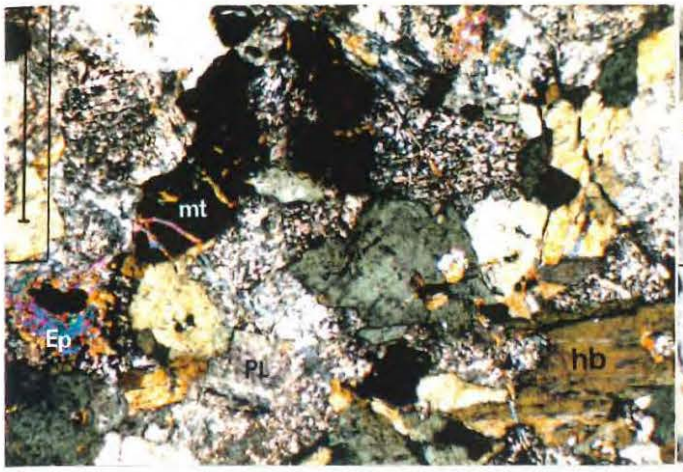
mt
Ep
PL
hb

1

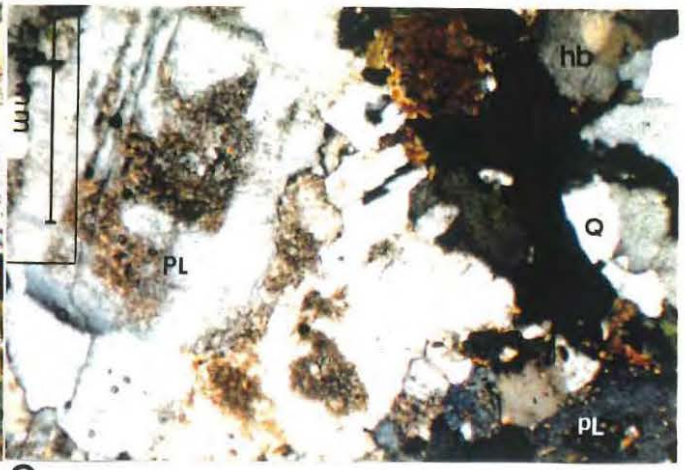
hb
Q
PL
PL

2

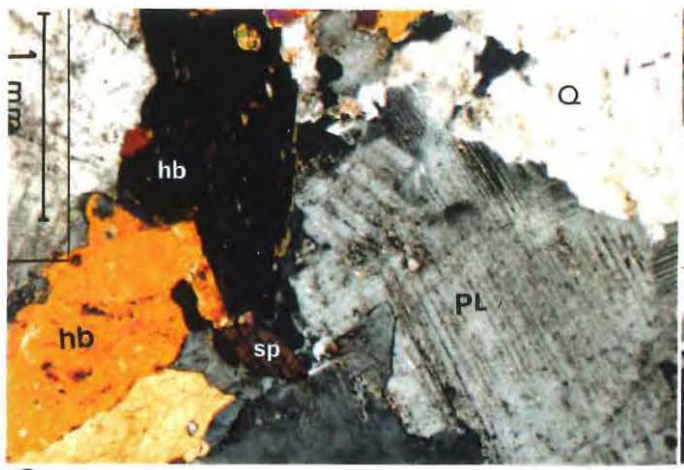
1 mm
Q
hb
hb
sp
PL

3

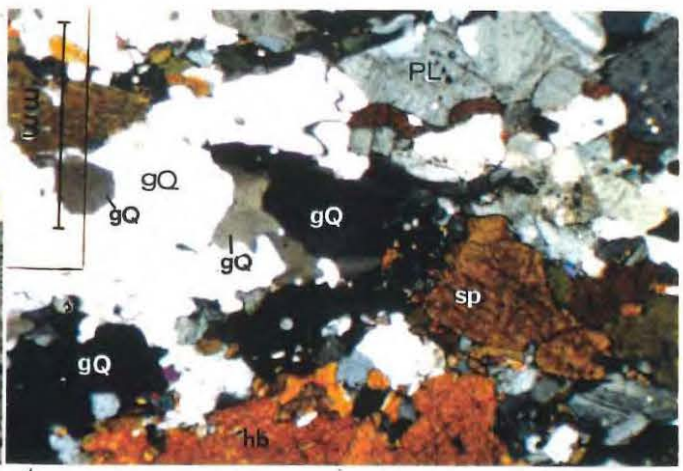
PL
gQ
gQ
gQ
gQ
sp
gQ
hb

4

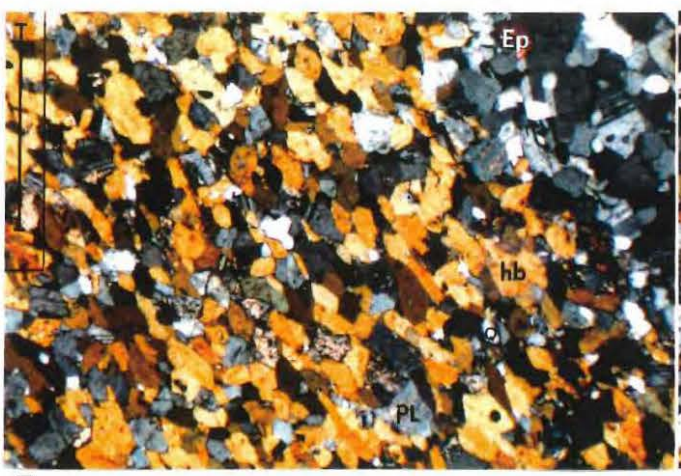
Ep
hb
Q
PL

5

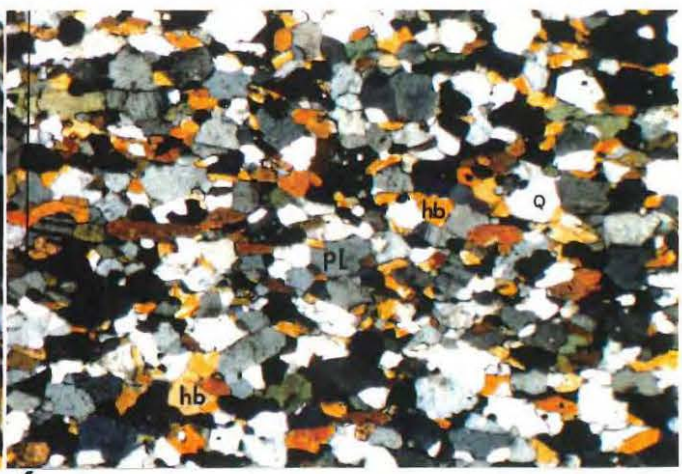
hb
Q
PL
hb

6

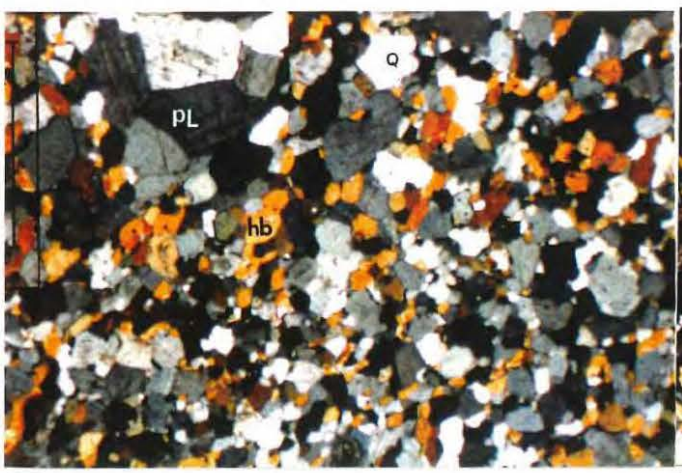
Q
PL
hb

7

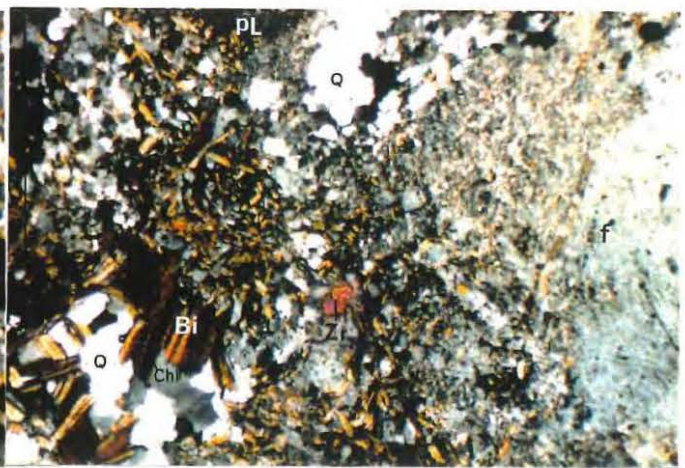
PL
Q
f
Bi
Q
Chl

8

PLATE 3-3: PHOTOMICROGRAPHS

1. Tonalite of the AOT from the Marmalade Dam (88087). It is composed of subhedral plagioclase, hornblende, biotite and quartz. A zoned plagioclase crystal is at the upper left corner. Crossed nicols.

2. Foliated leucogranite of the AOLG (87106). Quartz is granulated and ribboned. Crossed nicols.

3. Massive biotite granite of the AOLG (88111). A zoned zircon grain is enclosed by biotite. Crossed nicols.

4. Massive biotite granite of the AOLG (88111). Biotite is granulated and replaced by muscovite. Feldspar is altered to sericite. Subhedral plagioclase is increasingly altered towards the core, which is indicative of compositional zoning. Crossed nicols.

5. Mylonitised garnet-bearing muscovite granite of the AMG. Quartz and muscovite have been ribboned along the foliation. Garnet is also enlongated along the foliation. Crossed nicols.

6. Muscovite granite of the AMG. Kink-bands are well developed in the muscovite and sodium plagioclase grains. Sericite veinlets represent the main alteration. Crossed nicols.

7. Garnet-bearing quartzofeldspathic gneiss of the BSA (87034). Quartz has been ribboned. An augen structure is defined by twisted garnet and feldspar megacrystals. Crossed nicols.

8. Foliated muscovite gneiss (87052). The foliation is defined by the alignment of muscovite and enlongation of quartz and feldspar. Crossed nicols.

Symbols: muc = muscovite; Ga = garnet; f = feldspar. Others are the same as in Plates 3-1 & 2.

The bars, except for No.3, are equal to 1 mm. The bar in No.3 equals 0.25 mm.

Sample localities are shown in Appendix-2.

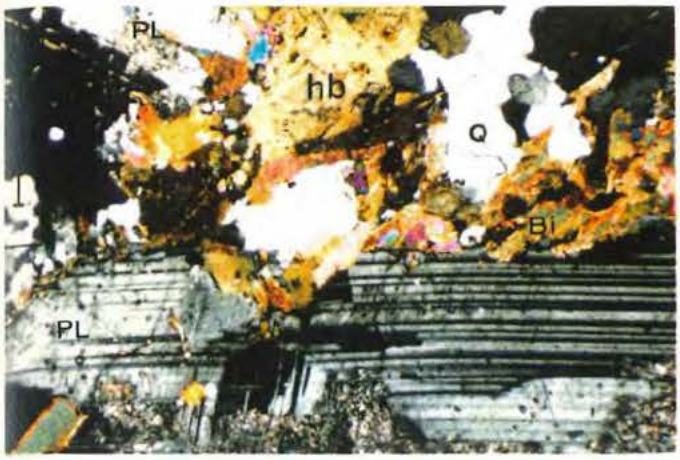
PL
hb
Q
Bi
PL

1

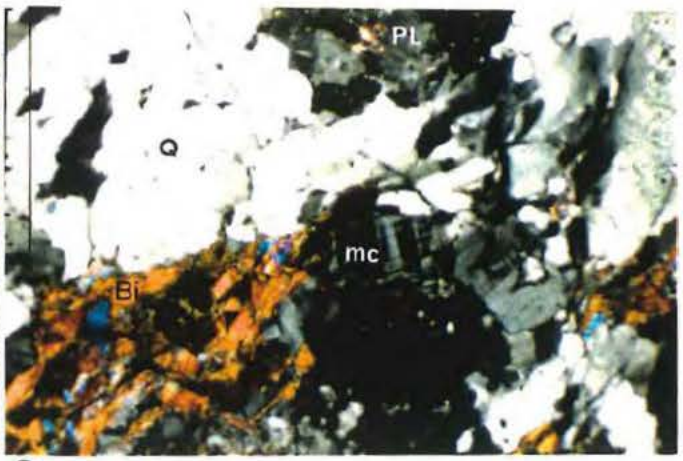
PL
Q
mc
Bi

2

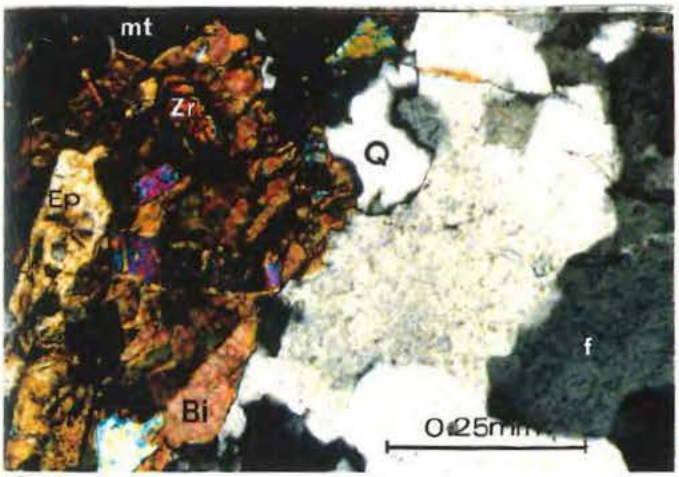
mt
Zr
Q
Ep
f
Bi
0.25mm

3

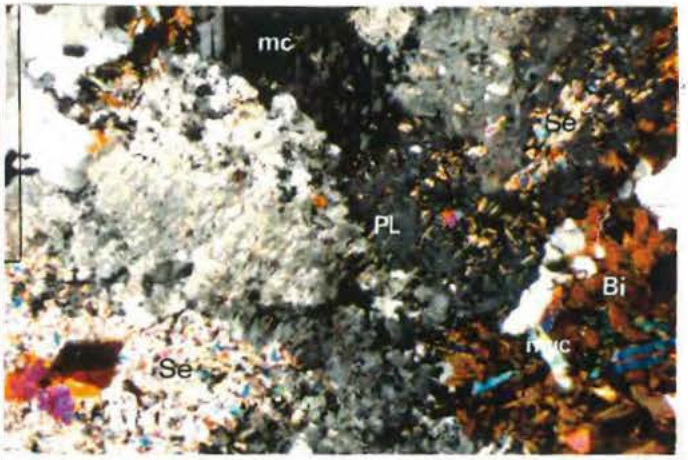
mc
Se
PL
Bi
Se

4

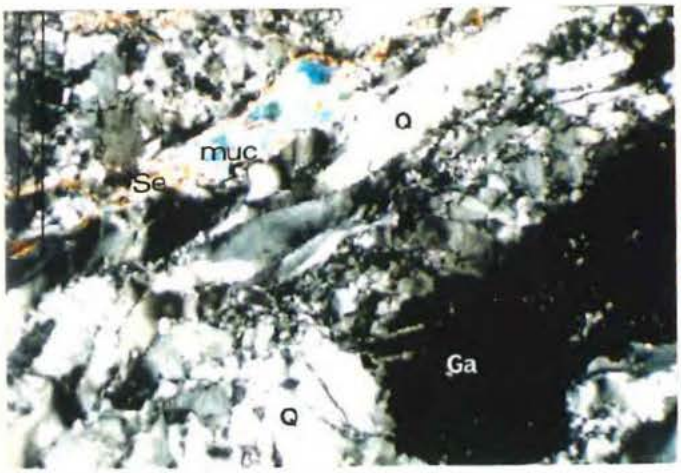
Q
muc
Se
Ga
Q

5

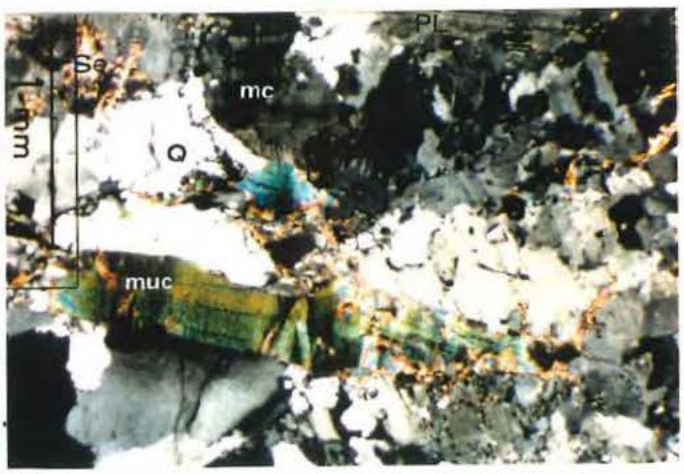
PL
Se
mc
Q
muc

6

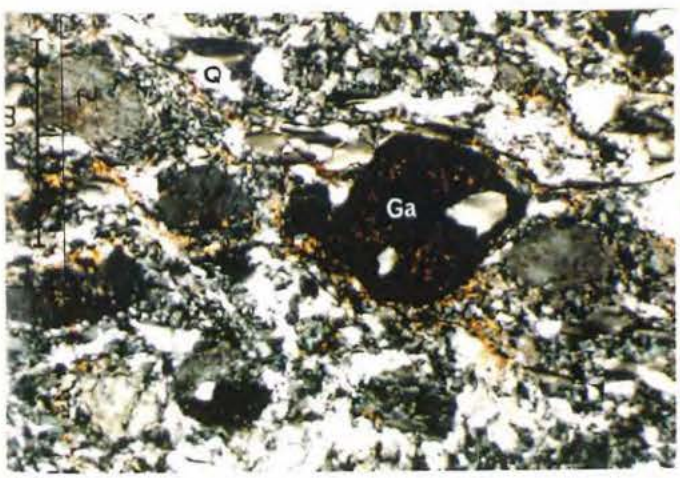
Q
Ga

7

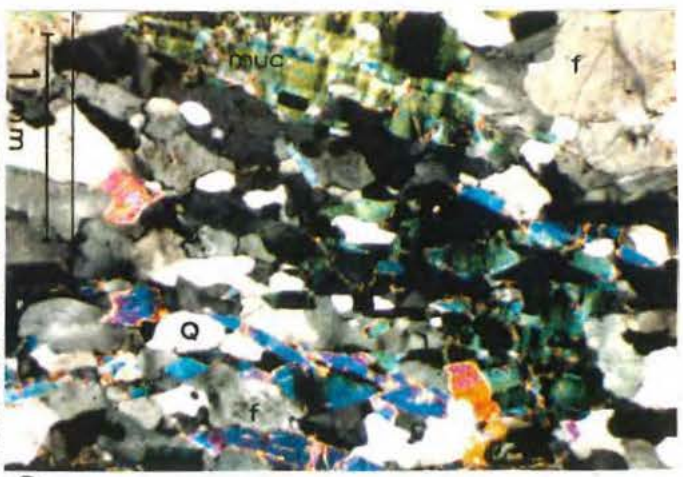
muc
f
Q
f

8

PLATE 3-4: PHTOTMICROGRAPHS

1. Muscovite schist (87071). A xenolith in the AYT. Two generations of foliations are developed. S_1 is developed by the alignment of muscovite and quartz. S_2 is defined by the deformation lamelae in the muscovite grains, nearly perpendicular to S_1. Crossed nicols.

2. Garnet-bearing muscovite schist (87070). A xenolith of the AYT. A typical S-C tectonite. Crossed nicols.

3. Porphyritic tonalite of the AYT (88110). Oscillatory zoning is perfectly developed in a euhedral plagioclase phenocryst. The matrix is felsic and blastopilotaxitic texture is visible in this thin section. Crossed nicols.

4. Porphyritic tonalite of the AYT (88110). A general view. Crossed nicols.

5. Massive even-grained tonalite of the AYT (87107). A biotite grain is twisted, granulated and altered to epidote along grain boundary. The euhedral to subhedral plagioclase is zoned. Crossed nicols.

6. Dioritic porphyrite or andesite (?) of the ATBA (87081). This ccurrs as xenoliths in the AYT. An euhedral plagioclase phenocryst displays typical oscillatory zones. Hornblende phenocrysts are also present. The pilotaxitic texture is still visible in the felsic matrix. Crossed nicols.

7. Porphyritic diorite of the ATBA (88008D). A dioritic texture is defined by euhedral to subhedral prismatic plagioclase which forms triangular framework. Crossed nicols.

8. Metabasalt (or dolerite) of the AYBA (88008B). Ophtical texture is still clearly defined by prismatic plagioclase. Dark mineral is mainly actinolite, which may be derived from pyroxene. Crossed nicols.

Symbols the same as in previous plates.

Sample localities are shown in Appendix-2.

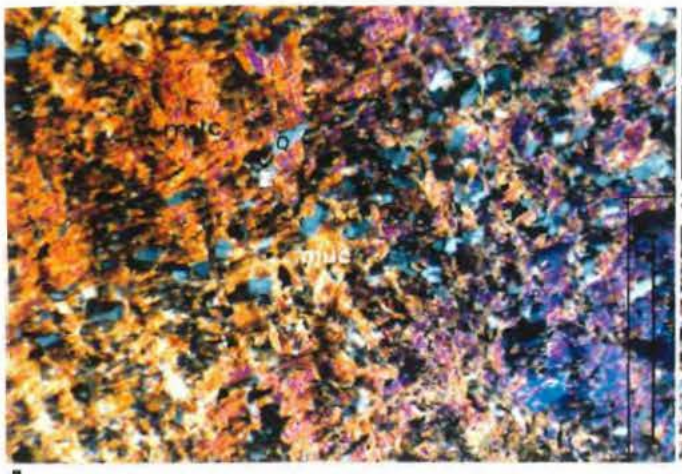

1

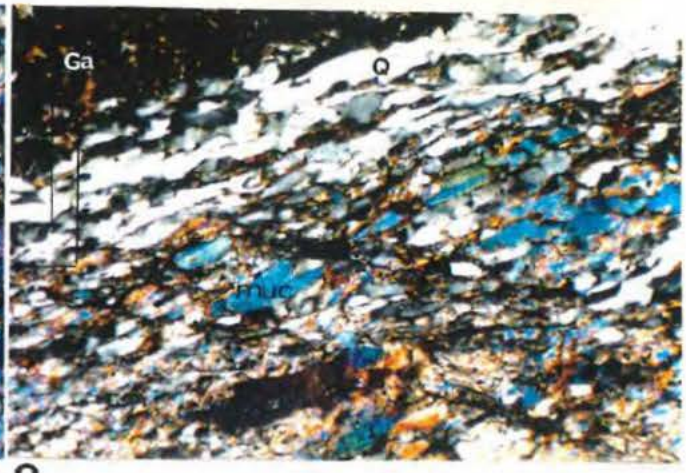

2

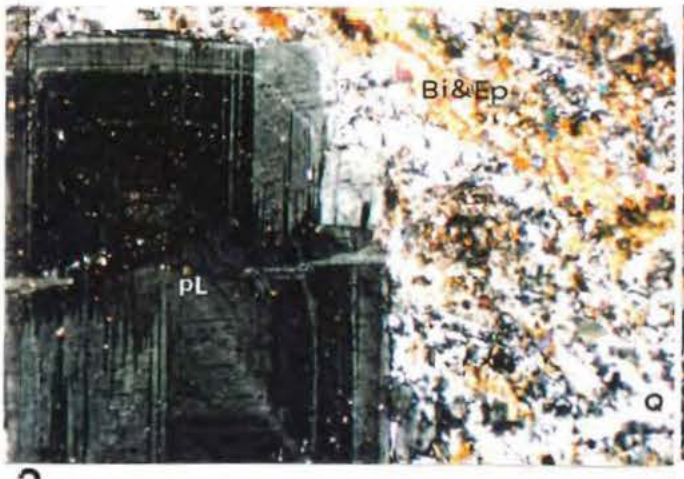

3

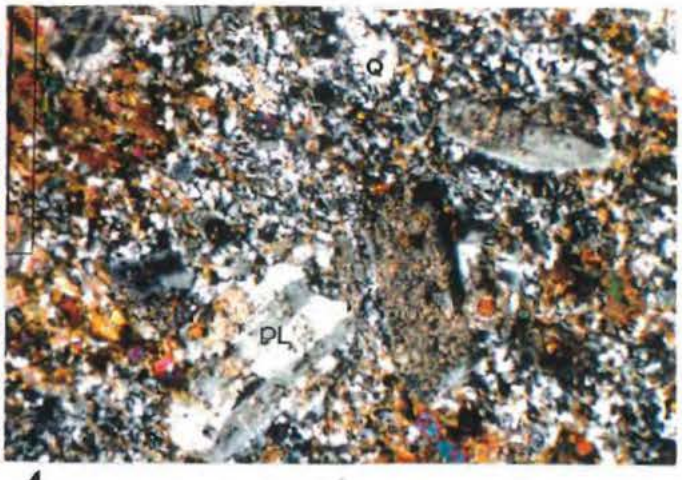

4

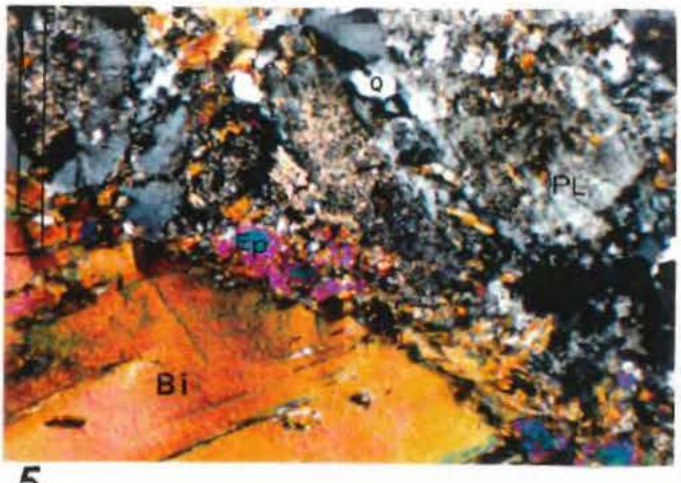

5

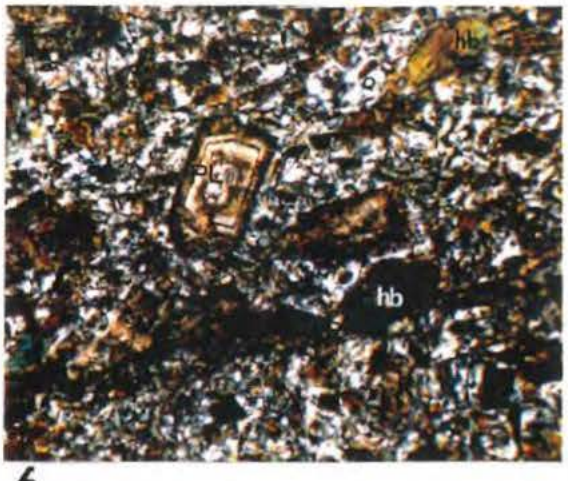

6

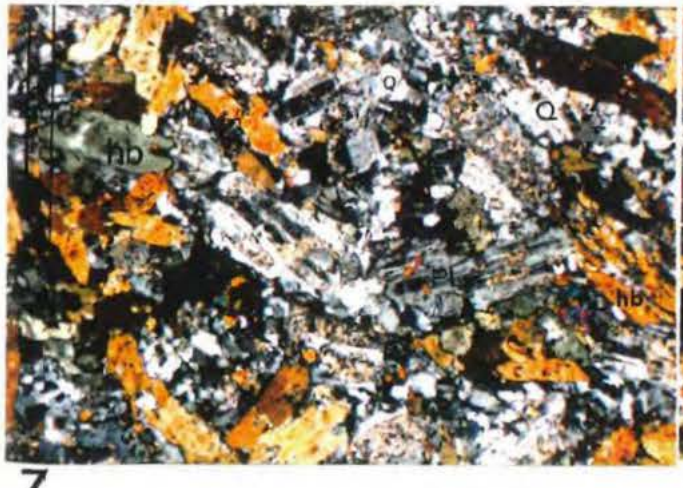

7

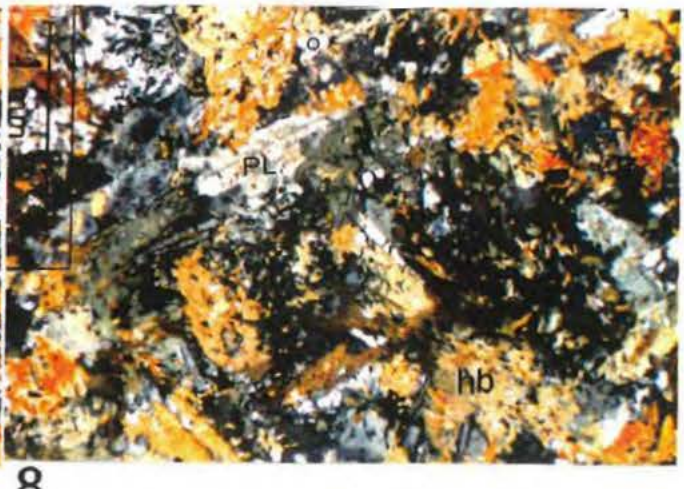

8

CHAPTER FOUR: GEOCHEMISTRY

4.1 INTRODUCTION

Major and trace element whole rock data for the 97 samples analysed are presented in Appendix-3 and 10 REE results in Appendix-4. Data of Sando (1987) for the AOT from the Tommy's Gap area are listed in Appendix-5. Analytical procedures are outlined in Appendix-1.

The sampling was undertaken with emphasis on the coarse-grained (intrusive) ACAS, AGB and the AYT. Fewer samples were taken from the fine-grained basaltic amphibolites of the ACAS and ATBS.

4.2 GEOCHEMISTRY OF THE ACAS

4.2.1 INTRODUCTION

In this section, the main geochemical features of the members of the ACAS are briefly described. The significance of these observations is discussed in detail as a whole.

It is common to employ MgO as an abscissa for other elements to reflect fractionation trends in mafic rocks which have only a limited SiO_2 range. The Harker diagrams are more useful for rock assemblages with wide SiO_2 ranges. However, the D.I. of Thornton and Tuttle (1960) has an advantage over both MgO and SiO_2 in that it can assist in showing differentiation trends for both types of rocks mentioned above. As the ACAS consists of both of such rock types, the D.I. is conveyed as an abscissa for other elements. The strong positive correlation between SiO_2 and D.I. indicates that the D.I. is suitable to represent SiO_2 as an indicator (Fig.4-1A).

4.2.2 GEOCHEMICAL FEATURES OF THE CUMULATE

Although a compositional hiatus exists, cumulate metapyroxenite, metagabbro and anorthosite show significant correlation of most major and trace elements with D.I. (Fig.4-1). Their plots are well separated from those of the differentiates. The values of D.I. combined with the major and trace element trends indicate that the anorthosites are later stage cumulates than the metagabbros. This is because the earlier precipitated phases are normally more mafic or calcic and therefore the earlier stage cumulates have more negative D.I. values.

When compared with their mafic differentiates, the cumulate metagabbros are characterised by very negative D.I. values, lower SiO_2 (47.14--51.49%), Al_2O_3 (9.35--16.55%), Fe_2O_{3tot} (6.04--9.23%), Na_2O (0.77--2.18%), FeO*/(FeO*+MgO) and TiO_2; and higher MgO (9.71--13.91%), CaO (12.07--15.59%), CaO/Al_2O_3, Cr, Ni and Sc (e.g. Fig.4-1). The high Cr (up to 2798ppm) and Ni (up to 258ppm) are strong evidence for a cumulate origin.

The cumulate anorthosites are characterized by extremely high Al_2O_3 (24.74--27.91%). CaO, Sr, Pb are also the highest among all the ACAS samples. However, they are obviously low in SiO_2, TiO_2, MnO, Fe_2O_{3tot}, MgO, Na_2O, P_2O_5, FeO*/(FeO*+MgO), CaO/Al_2O_3, Cr,Ni,Sc,Zn,Nb,V,Y and REE if compared with other mafic members (Fig.4-1 & Appendix-3A).

Cumulate metagabbro 88016D was analysed for REE. The result shows that it has a fractionated pattern with $(Ce/Yb)_N$=12.1, slight negative Eu anomaly, low Sr content and low absolute REE content (58.9ppm) (Fig.4-5 & Appendix-4).

4.2.3 GEOCHEMICAL FEATURES OF THE DIFFERENTIATES

The differentiates display a continuous compositional variation ranging from gabbro, through diorite, quartz diorite to plagiogranite with regard to SiO_2 content (about 49 - 78%) and D.I. value (-8 to 21) (see Fig.4-1 and Appendix-3A).

Overall, they are characterised by rather low TiO_2 (0.09--0.78%), Y (4.7--30ppm) and Nb (0.8--6.8ppm). Rb/Sr ratios are generally less than 0.1 and mostly less than 0.05 and K/Rb ratios range from 200--600 (Fig.4-1 & 2; Appendix-3A).

On the elements versus D.I. plots, MgO,Fe_2O_{3tot}, CaO, MnO, CaO/Al_2O_3, Cr,Ni,Sc,Cu and V decrease with increasing D.I.. TiO_2, Al_2O_3, Na_2O,Ga and Zr increase initially but decrease during the later stages. Feo*/(FeO*+MgO) and Nb increase slightly. K_2O, Rb, Sr and Ba show a random variation. No increase in K_2O contents, K/Rb and Rb/Sr ratios with increasing SiO_2 has been observed.

REE patterns of diorite sample 88014 and quartz diorite sample 87064 are almost parallel except for Dy, Er and Yb where they transect (Fig.4-5). Their $(Ce/Yb)_N$ ratios range from 9.7--17.1. They are also parallel to that of sample 88016D but the absolute REE contents are higher (Appendix-4). Generally, these three patterns show a very slight but visible negative Eu anomaly.

Fig. 4-1. Selected diagrams (A-P) of major, trace elements and ratios against Differentiation Index (D.I.) for the Atnarpa Calc-alkaline Suite. Solid lines with arrows indicate differentiation trends. Cumulate plots are indicated by broken lines which do not represent differentiation trends.

SYMBOLS

- Cumulate Anorthosite
- Cumulate metagabbro & Metapyroxenite
- Mafic Differentiate
- Felsic Differentiate

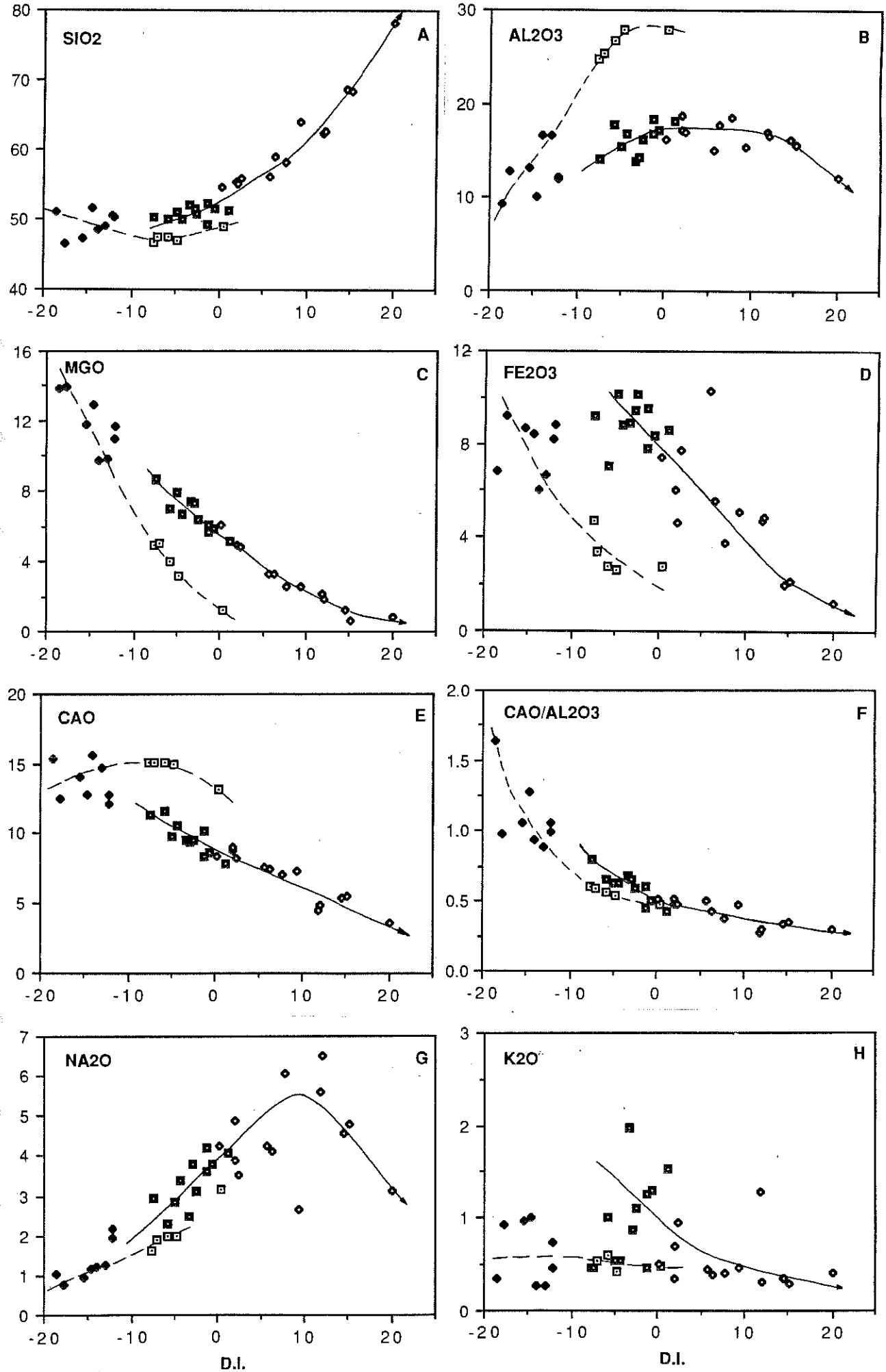

Fig. 4-1

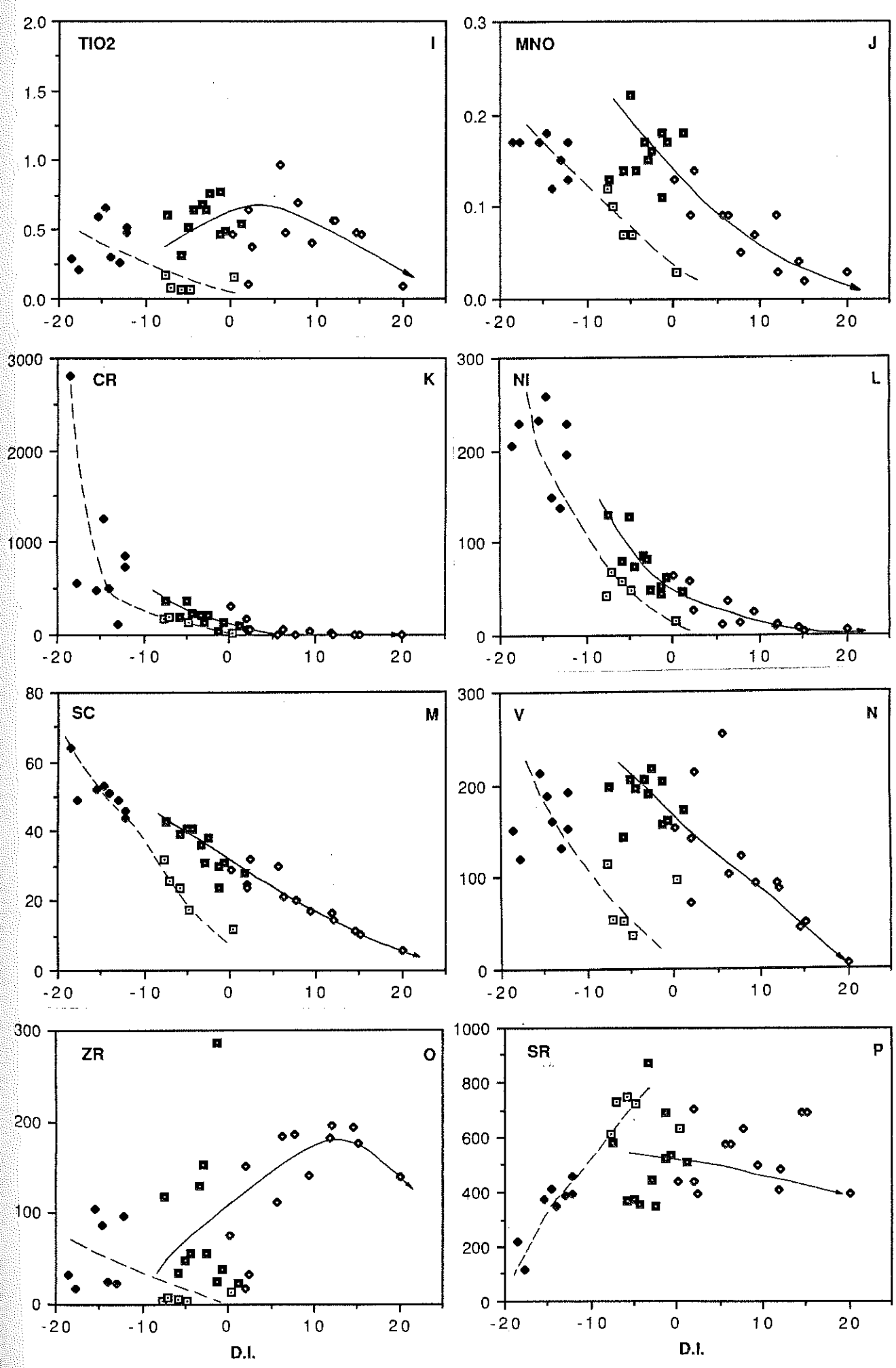

Fig. 4-1

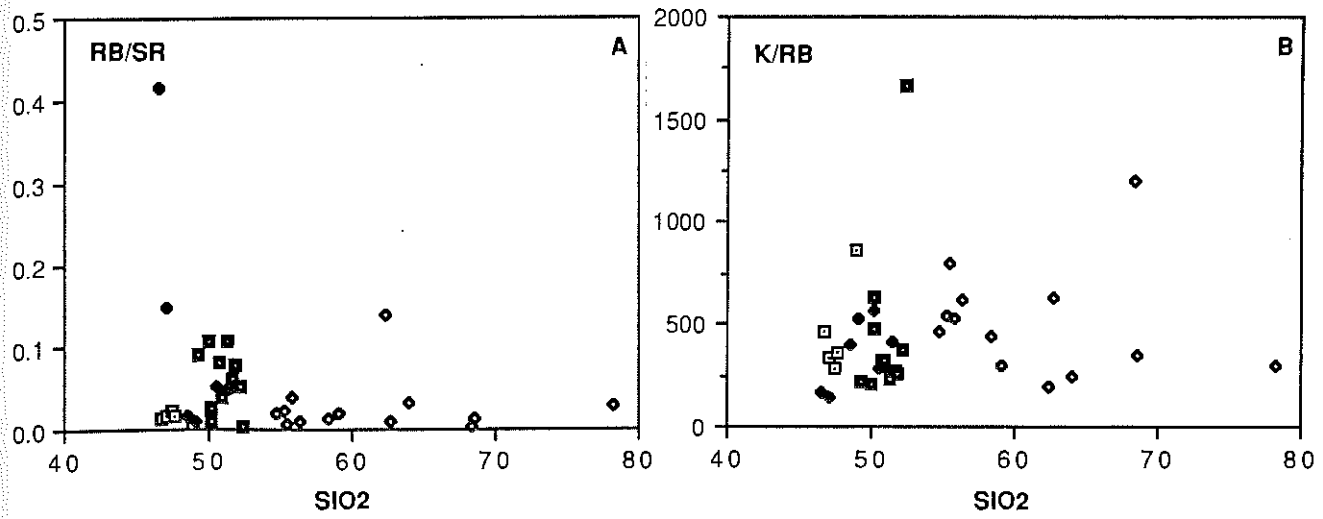

Fig. 4-2. Rb-Sr and K/Rb ratios against SiO2 diagrams for the Atnarpa Calc-alkaline Suite. Symbols as for Fig. 4-1.

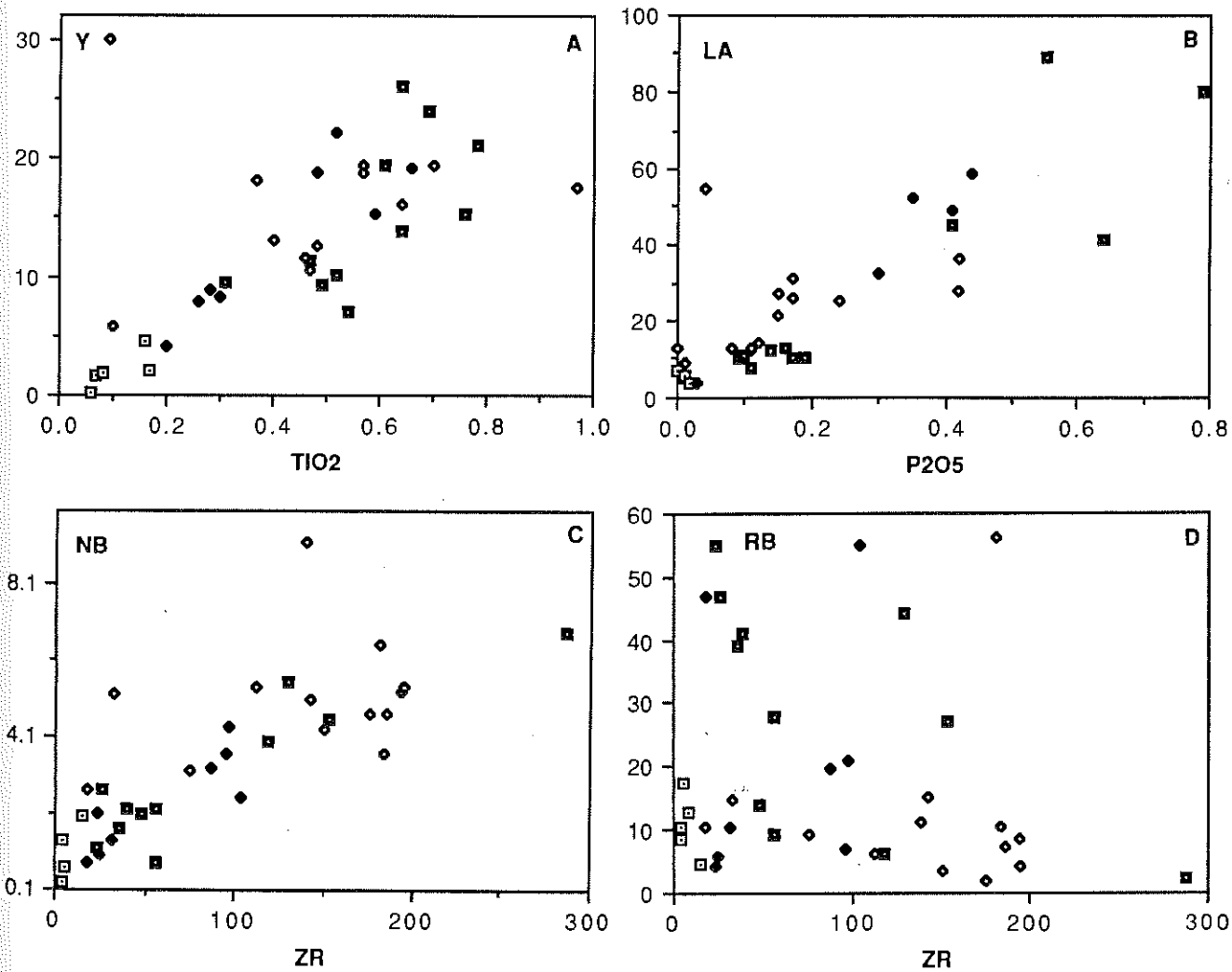

Fig. 4-3. Selected incompatible trace element variation diagrams for the Atnarpa Calc-alkaline Suite. Symbols as for Fig. 4-1.

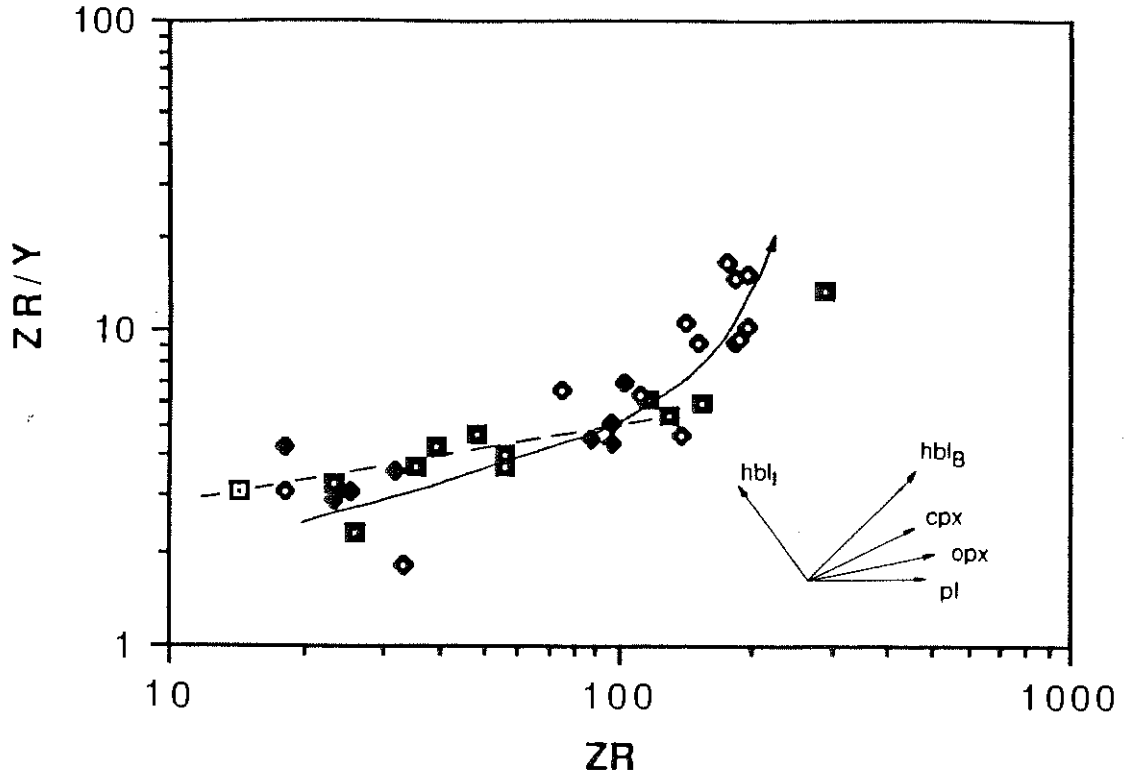

Fig. 4-4. Zr/Y vs Zr variation diagram for the Atnarpa Calc-alkaline Suite. Mineral vectors are based on the mineral-liquid distribution coefficients for Zr, Y of Pearce and Norry (1979). hbl=hornblende, cpx=clinopyroxene, opx=orthopyroxene, pl=plagioclase, I=intermediate, B=basic. Plot symbols as for Fig. 4-1.

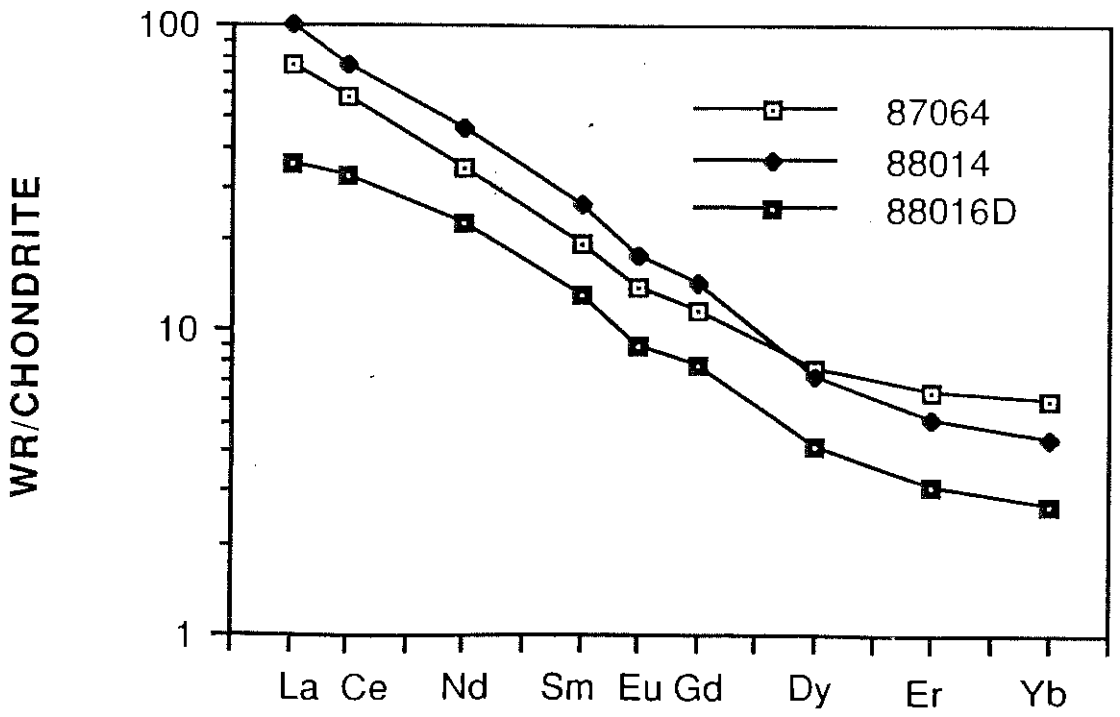

Fig. 4-5. Chondrite-normalized REE patterns for the representative samples of the ACAS.

4.2.4 GEOCHEMICAL FEATURES OF THE FINE-GRAINED AMPHIBOLITE

Only one sample of microdioritic type was analysed. It is compositionally andesitic, with higher Fe_2O_{3tot} and TiO_2 relative to its coarse-grained equivalent (Appendix-3A).

Its HYG-element abundances normalized to primordial mantle are quite similar to the coarse-grained metadiorite (88014) and meta- quartz diorite (87064).

4.2.5 DISCUSSION

4.2.5.1 *ELEMENT MOBILITY AND WALL-ROCK CONTAMINATION*

Petrographical evidence indicate that the ACAS rocks have undergone amphibolite grade metamorphism. Field observations show that they occur as numerous small rock bodies which leads to a high surface-area to volume ratio as discussed by Foden et al. (1988). These two factors should provide great opportunity for wall-rock contamination and element mobility.

On Fig.4-3, linear correlation among Zr,TiO_2, Y, Nb and P_2O_5 indicates these elements are essentially immobile during metamorphism and alteration. However for LIL element such as K,RB,Sr and Ba, element-pair correlations are disturbed probably by preferential trace element mobility and redistribution of these element during metamorphic processes. Sample 87142 with K_2O and Ba levels up to 1.97% and 2229 ppm, respectively, is a case of subsequent enrichment in these two elements. However, the strong correlations of many other major and trace elements with the D.I. and SiO_2 also indicate that many of the magmatic features have been well preserved.

Some well-elvoved samples such as 88019-2 may have suffered from wall-rock contamination as indicated by an extremely high SiO_2 content (up to 78%) and an inhomogeneous appearance in the field and hand specimen. The diagrams Y-TiO_2, La-P_2O_5, Nb-Zr indicate that a contaminant with high REE,Y,Nb and SiO_2 but insignificant TiO_2 and P_2O_5 may have been involved. An alkali-rich fluid, which contains high REE,Y,Nb,Si in the form of F^- and Cl^- complexes may have been the carrier (Chatterjee and Strong 1985).

Rollinson and Windley (1980) have argued for selective elemental depletion during metamorphism of some Archean granulites (tonalite-trondhjemite suite). The Atnarpa data provide no evidence to support that the depletion in K and Rb for the ACAS is due to metamorphism. For instance: (1). Most of the ACAS have K/Rb ratios ranging from 200 to 600 (Fig.4-2B). But K/Rb

ratios in the depleted Archean granulites are much higher, with mean values of 1900 and 1180, respectively. (2). Metamorphism in the ACAS only reaches amphibolite facies grade. It is lower than the dehydrated granulite which may have undergone the removal of granitic partial melts (Fyfe 1973). (3). Tarney and Windley (1977) suggested that the LIL elements could be removed by a CO_2-rich fluid, but no CO_2-rich, e.g. carbonate alteration has been observed in the ACAS. Therefore, it is considered that the amphibolite grade metamorphism in the ACAS only caused some local redistribution of the LIL elements and that the selective depletion in Rb and K is the property of the primary magma.

4.2.5.2 *PETROGENESIS OF THE ACAS*

The following questions need to be answered: (1). Are the rocks in the ACAS genetically related and how did they form? (2). What is the relationship between the fine-grained amphibolites and the coarse-grained amphibolites? (3). What is the derivation of the primary magma(s)? This discussion will focus on the first question.

4.2.5.2.1 *Consideration of alternatives to crystal fractionation*

Many models have been proposed for the genesis of a rock association like the ACAS. These includes restite-controlled partial melting (White & Chappell 1977; Compston & Chappell 1979), hybridisation and magma mixing (Eichelberger 1978; De Paolo 1981), progressive partial melting (Green & Ringwood 1968; Ringwood 1974; Emmermann 1977) and crystal fractionation (e.g. Arth et al. 1978).

The restite-controlled partial melting model, a process of varying degrees of unmixing of residual solid from intersitial melt, seems inappropriate for the ACAS because of the presence of cumulates, the curved element variation diagrams (both Harker type and D.I. type) and great compositional variation in minerals such as plagioclase (An 20--80).

The hybridisation model, i.e., assimilation of solid mafic material by granitic liquid, has been used to explain variations for calc-alkaline magmas (Eichelberger 1978). As it is virtually similar to the restite-unmixing model, this model is unsuitable for the ACAS for the same reasons.

The progressive partial melting model allows segregation, extraction and upward intrusion of successively less silicic magma batches from a common source region, resulting in a spectrum

of rock compositions. This model may be able to explain some element variations but fails for the reverse intrusive sequence in the ACAS.

By comparison, the fractional crystallization model, a process of early crystallized solid phases, partially or completely separating from intersitial melts in an evolutionary trend, can explain most of the features mentioned above.

4.2.5.2.2 *Fractional crystallization of the ACAS*

Petrographic evidence in the last Chapter has indicated that the ACAS is dominated by high-level fractionation of clinopyroxene and plagioclase which is followed in the later stages by the precipitation of a hornblende+plagioclase+magnetite assemblage. The change would occur when the increasing water and oxgen fugacities and decreasing temperature reach critical limits. In this Chapter, here geochemical evidence will formulate the same conclusion.

(1). Major and trace element compositions of the cumulate metagabbro and metapyroxenite are consistent with the petrographic evidence that they represent magmatic cumulates. They are high in MgO, Cr,Ni and Sc but low in $Fe_2O_{3tot.}$ and Na_2O, especially some exceptionally high in Cr and Ni, indicating these rocks do not correspond to reasonable liquid composition. The meta-anorthosites are exceptionally high in Al_2O_3, CaO and Sr, Pb but low in most of other elements, notably Ti, P_2O_5, Nb, Zr and REE (except Eu), also strongly suggesting a cumulate origin.

(2). On the elements against D.I. diagrams, cumulate and differentiate trends are clearly separated. The cumulates follow a linear evolution trend for most major elements, consistent with clinopyroxene and plagioclase as major cumulated phases in them. A dramatic decrease in MgO, Fe_2O_{3tot}, CaO/Al_2O_3 and increase in Al_2O_3 in the middle stages support a precipitation of clinopyroxene+plagioclase assemblage with plagioclase becoming increasingly dominant in the later stages. A substantial drop in Cr,Ni,Sc also supports the early precipitation of clinopyroxene. These element variations are probably because earlier formed cumulates contain clinopyroxene with higher Mg# and plagioclase with higher An%, and because clinopyroxene:plagioclase ratios may vary in cumulates formed in different stages. Metacumulates with variable amount of trapped residual liquid could also account for these variations.

(3). The continuous, well-correlated evolutionary trends for the differentiates are also typical

of crystal fractionation. For the mafic differentiates, MgO and CaO contents varies widely without significant increase in SiO_2 level, indicating a fractionation dominated by removal of clinopyroxene+plagioclase assemblage with similar bulk SiO_2 level to that in the melt. The decrease in CaO and CaO/Al_2O_3 and increase in Na_2O in the middle stage differentiates (e.g. diorites and quartz diorites) demonstrate a progressive precipitation of calcic plagioclase. In addition, the downward slope for MgO, Fe_2O_{3tot} and upward slope for FeO*/(FeO*+MgO) indicate that some amount of mafic minerals may be involved during the middle to later stage fractionation. It is more likely that the precipitation of hornblende, a mineral normally with less SiO_2 content than clinopyroxene, could, in combination with plagioclase, causes the increase in SiO_2 level for the residual liquid. This process may lead to Na_2O and Al_2O_3 contents reaching a peak at the transition to acidic stage. In the acidic stage, crystallization of quartz, a mineral with dilution effect, becomes significant in the differentiates, which reduces the Na_2O and Al_2O_3 contents.

(4). The constant K/Rb (Fig.4-2) and random K_2O behaviour relative to Na_2O (Fig.4-1) in most ACAS rocks exclude biotite and K-feldspar from consideration as major fractional phases.

(5). The geochemical variation of Al_2O_3 vs CaO for the Entia amphibolite and Huckitta tonalite and granodiorite has been modelled by Foden et al. (1988) as due to such a fractionation process that starts from fractionating cpx+amph:plag(4:1) followed by the removal of increasing amount of plagioclase ($\pm$biotite) and ended at precipitating plagioclase and amphibolite at a ratio 4:1. The ACAS rocks plot on the similar trend to that of the Entia rocks except for the minor anorthosite which plots on the upper right hand corner (see Fig.6-1). A similar fractionation process may have occurred on the ACAS.

(6). Major element variation trends may not be able to discriminate hornblende from pyroxene as fractionating phases. However, it is readily reflected by HFS elements. It has been demonstrated that hornblende has higher distribution coefficients for Ti,Zr,Y and Nb than clinopyroxene. They are even higher in the hornblende crystallized from an intermediate liquid (Pearce & Norry 1979). Accordingly, the fractionation trend of the differentiates on logZr/Y--logZr (Fig.4-4, the solid line with arrow) clearly indicates that early stage fractionation dominated by clinopyroxene and plagioclase is substituted by hornblende and plagioclase in the later stage. Similar conclusions can be made from logY--logZr and $logTiO_2$--logZr diagrams. On

the logTiO_2--logZr, it is shown that both hornblende and magnetite fractionation may occur in the later stages. These features are quite similar to the fractionation trends modelled for some calc-alkaline suite by Pearce and Norry (1979).

The cumulates follow a somewhat linear trend on Fig. 4-4 (the broken line. Some anorthosites with Zr<10ppm are not plotted), which is consistent with the fact that these observed cumulates are dominated by clinopyroxene+plagioclase assemblage. Similar features are present in other diagrams mentioned above.

(7). Similarly, the lower Ti/V ratios of both cumulates and differentiates are consistent with a higher oxygen fugacity in the primary magma and the trend defined by the felsic differentiates (see Fig.4-20) is considered to be due to the precipitation of magnetite and/or hornblende in an increasing fO_2 environment (Shervais 1982).

(8). Fractionation of clinopyroxene, a mineral with partition coefficients for REE less than 1 and higher for HREE than LREE (Whalen 1985) could, in combination with plagioclase, enrich all REE in the residual liquid. This explanation accounts for the similar REE patterns of cumulate 88016D and differentiate 88014 but low toal REE content of the cumulate (Fig.4-5). However, REE pattern of sample 87064, the quartz diorite, seems not consistent with the fractionation of hornblende during the later stage. Normally fractionation of hornblende will lead to the residual liquid having a REE pattern characterised by prolonged depletion in HREE and positive Eu anomaly such as in the calc-alkaline-trondhjemitic suite of the Southwest Finland (Arth et al. 1978). But HREEs in 87064 (SiO_2=62.71%) are slightly higher than those in the more mafic differentiate 88014 (SiO_2=55.48%). This pattern may be partially due to the enrichment of zircon, a HREE-extremely enriched phase, in sample 87064 and the change of bulk distribution coefficients of major precipitating phases upon cooling. The predominant fractionation of plagioclase over hornblende, a phase with distribution coefficient less than 1 but higher for LREE than HREE, may preclude the depletion of REE, especially for HREE and the development of positive Eu anomaly in the residual liquid. Therefore, the precipitation of a combination of plagioclase and hornblende with plagioclase fractionation becoming increasingly dominant, and the continuing enrichment of Zr in the residual liquid may produce a residual liquid with a REE pattern like 88064. However, it cannot be ruled out that the felsic and mafic members in the ACAS may be derived from different parental magmas or different pulses of magma emplacement from

one fractionally layered magma chamber in depth.

(9). The accessory minerals such as apatite, zircon, sphene, monazite and ilmenite are very effective REE carriers and therefore the involvement of such minerals during partial melting and fractionation processes may have significant influence on the REE patterns (e.g. Green 1981; Watson & Hanson 1984; Sawka et al. 1984). Here for the ACAS, the positive correlations of LREE, Y with Zr,TiO_2, P_2O_5 (e.g. Fig.4-3) indicate a combination of such accessory minerals must have been involved in the fractionation process, especially for the REE-enriched metagabbros such as 87142, 87173, 88017 and 88018 (see Appendix-3A). However, the early precipitation of such minerals is not consistent with a normal fractionation trend (e.g. Fig.4-1O). Thus this phenomenon may be caused by unusual thermodynamic conditions or perhaps by the addition of an external contaminant.

The second possibility seems unreasonable as it is difficult to explain why the contaminant has so selectively effected the REE and HFS elements without apparently disturbing other element patterns.

However, the first possibility seems to be more feasible. Watson and Hanson (1985) reported that Zr saturation is a function of temperature and composition. In a liquid of fixed composition, it is highly dependent on the temperature. The early precipitation of zircon could be due to a sudden drop in temperature. This could happen if small magma volumes intruded from depth into high-level ensialic crust. The occurrence of the ACAS as small numerous rock bodies intruding the BSA suggests an opportunity of rapid cooling during emplacement. Similar explanation could also account for the early precipitation of other accessory minerals such as apatite and sphene.

Such a lowering of pressure as well as temperature could also cause the precipitation of anorthosite observed as local bands. Any further pressure drop due to local rock fracturing would further enhance such anorthosite fractionation.

In conclusion, major, trace and REE element characteristics have demonstrated that the ACAS, at least the coarse-grained intrusive types, are related by a high-level, in situ, fractional crystallization. This is dominated by clinopyroxene+plagioclase (±hornblende) during the early stages and subsequently followed by the removal of plagioclase+ hornblende+magnetite (or ilmenite) during the later stages, due to increasing water and oxygen fugacities along with

fractionation trend.

Exceptional precipitation of some REE-enriched accessory minerals during the early stage is probably caused by a sudden drop in temperature and pressure in small magma volumes, which have been rapidly transported to the upper crust. The precipitation of minor anorthosite is also considered to be initiated in this process.

4.2.5.3 *CALC-ALKALINE AFFINITIES OF THE ACAS*

Many suggestions have been proposed for element variation diagrams as discriminants of tectonic settings (e.g. Pearce and Cann 1973; Irvine and Baragar 1971; Miyashiro and Shido 1975; Shervais 1982; Meschede 1986). However, such discrimination was mainly formulated for Phanerozoic rocks and tectonic settings. Their usefulness when applied to Proterozoic rocks has yet to be demonstrated. In addition, many such diagrams are formulated only for volcanic rocks. As intrusive rocks were usually fractionated and coexist with cumulates, the applicability of these diagrams for them is further suspect. Therefore, care must be taken when using them. However, if the ACAS shows consistent features on a variety of diagrams, its geochemical affinities may be reflecting useful tectonic information. In addition, geochemical variations in many volcanic suites have been attributed to fractionation processes in depth (e.g. Pearce and Norry 1979). Any such volcanic rocks with phenocrysts are in essence geochemically transitional to cumulates. This indicates discrimination diagrams formulated from volcanic rocks should theoretically apply to intrusives.

The AFM diagram of Irvine and Baragar (1971) and Feo*/MgO--SiO_2 diagram of Miyashiro and Shido (1975) are suitable for both volcanics and intrusives with a wide range of SiO_2 contents. The ACAS follows a typical calc-alkaline trend on the AFM diagram (e.g. Fig. 4-17). Most of the ACAS samples plot into the calc-alkaline field on the FeO*/MgO--SiO_2 diagram. In addtion, almost all of the ACAS plots fall into the subalkaline field on the SiO_2-alkalis discrimination diagram of Irvine and Baragar (1971) (Fig. 4-18).

Similarly, on the Ti-V diagram of Shervais (1982), the mafic rocks of the ACAS plot into the field of arc basalts which suggests a high oxygen fugacity in the parental magma. The felsic rocks of the ACAS follow a typical calc-alkaline trend due to precipitation of magnetite and/or hornblende (Fig. 4-20).

Fig. 4-17. The ACAS follows a typical calc-alkaline trend on the AFM discrimination of Irvine and Baragar (1971). Symbols: cross=felsic differentiate, empty box =mafic differentiate, filled triangle=cumulate metagabbro & metapyroxenite. Cumulate anorthosite plots have been omitted.

Fig. 4-18. The ACAS samples are plotted into the subalkaline field (including calc-alkaline and tholeiitic) on the alkalis versus SiO_2 discrimination diagram of Irvine and Baragar (1971). x= cumulate anorthosite. Other symbols as for Fig. 4-17.

Fig. 4-19. The ACAS shows strong depletion in K & follows somewhat trondjemitic trend on the Na-K-Ca discrimination diagram of Barker & Arth (1976). Symbols as for Fig. 4-18.

Fig. 4-20. The ACAS follows a calc-alkaline trend on the Ti-V discrimination diagram of Shervais (1982). Symbols as for Fig. 4-1.

Fig. 4-21. The mafic samples are plotted into the field of calc-alkaline basalt on the Zr-Ti-Y discrimination diagram of Pearce & Cann (1973).
Symbols as for Fig. 4-17.

Fig. 4-22. The mafic ACAS plots fall into the field of calc-alkaline basalt on Zr-Ti discrimination of Pearce & Cann (1973). Symbols as for Fig. 4-17.

Fig. 4-23. The mafic ACAS plots fall into the field of calc-alkaline basalt on the MnO-TiO_2-P_2O_5 discrimination diagram of Mullen (1983). Symbols as for Fig. 4-17.

Fig. 4-24. The ACAS samples are plotted into the field of volcanic arc basalt on the Zr-Nb-Y discrimination diagram of Meschede (1986). Symbols as for Fig. 4-17.

Key: A=alkaline, SA=subalkaline, CA=calc-alkaline, TH=tholeiitic, CAB=calc-alkaline basalt, IAT=island-arc tholeiite, LKT=low-K tholeiite, OIT=oceanic island tholeiite, OIA=oceanic island alkaline basalt, MORB=mid-oceanic ridge basalt, P=primordial, N= normal, VAB=volcanic arc basalt, WPA=within plate alkaline basalt, WPT=within plate tholeiite.

Fig. 4-17

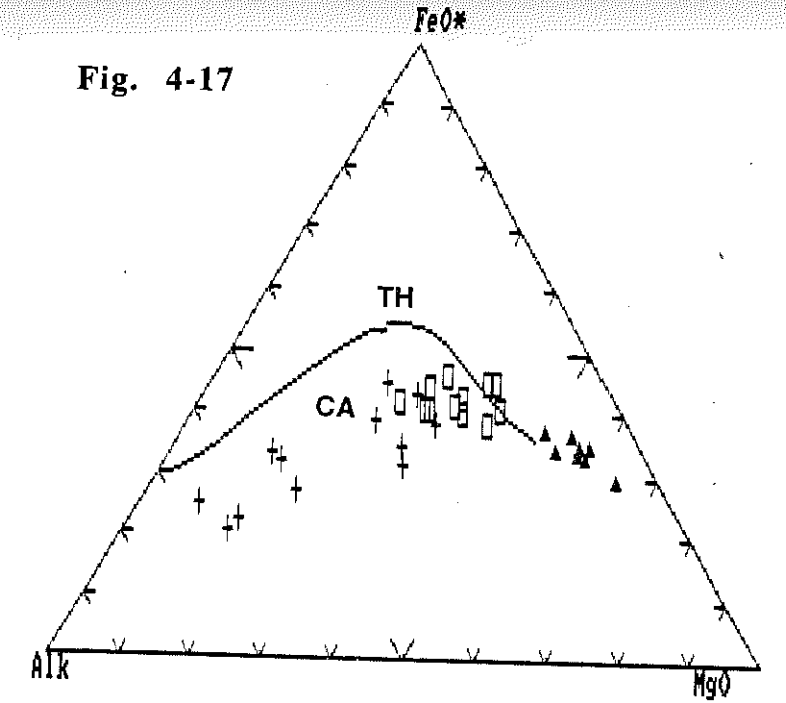

Fig. 4-18

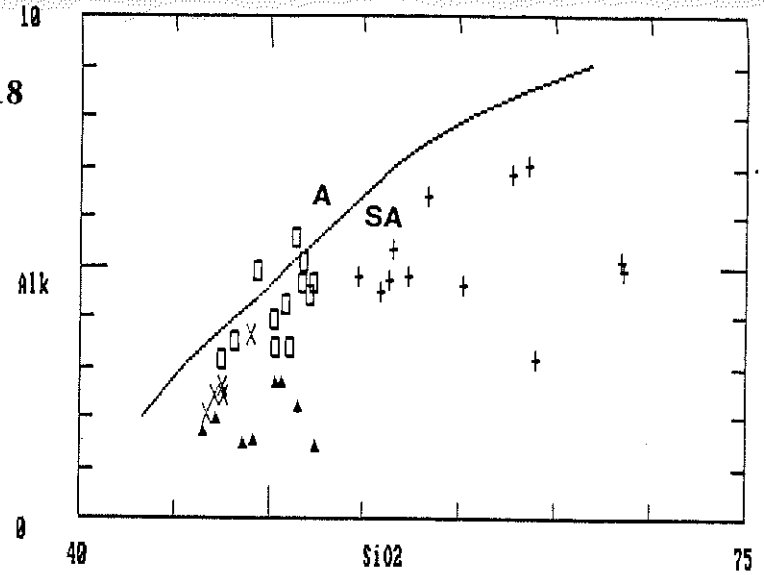

Fig. 4-19

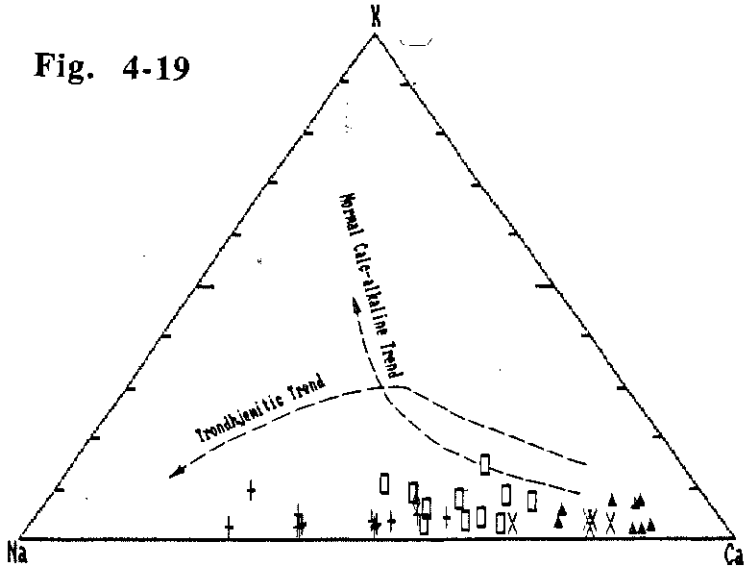

Fig. 4-20

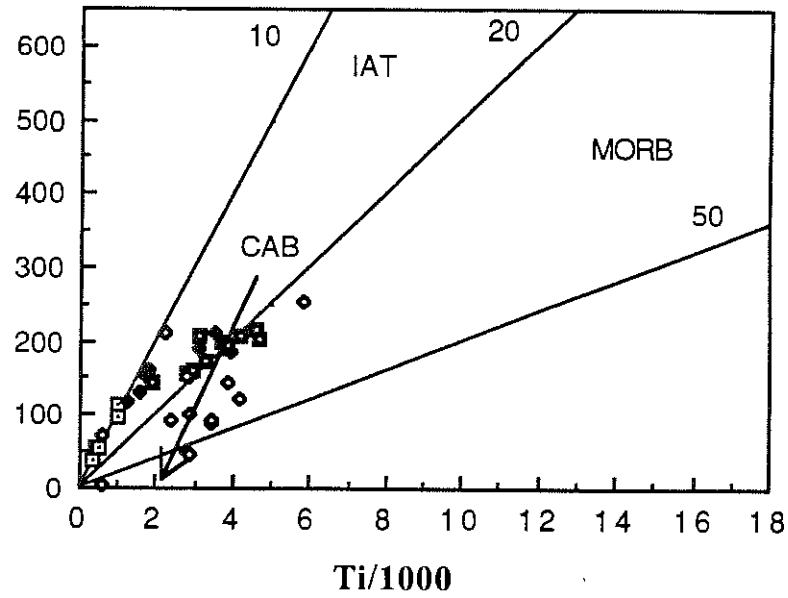

Fig. 4-21

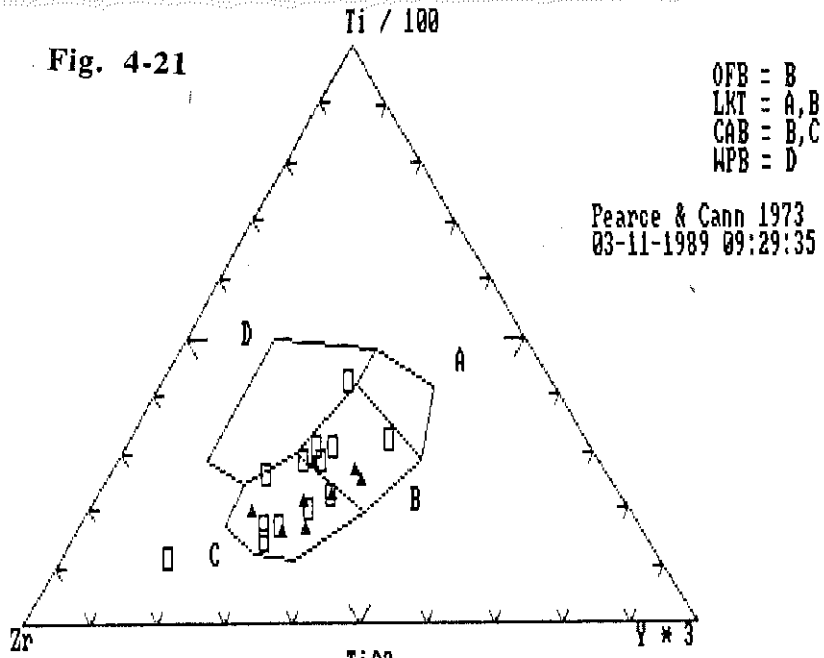

Fig. 4-22

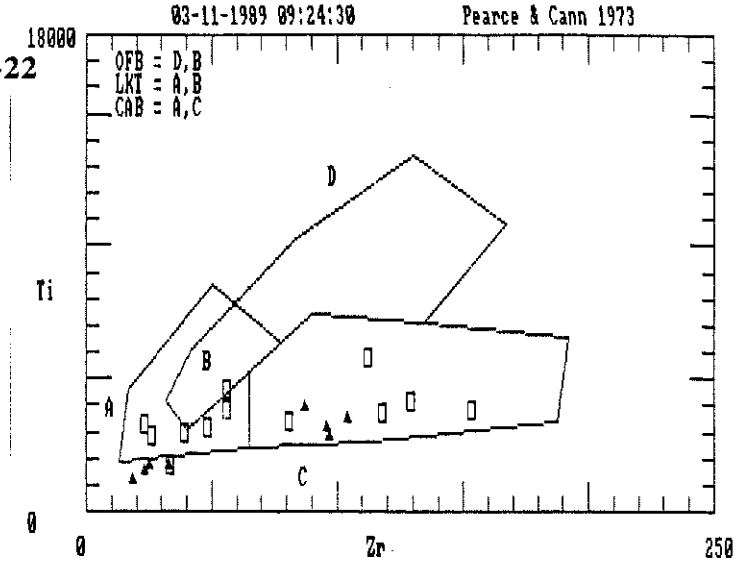

Fig. 4-23

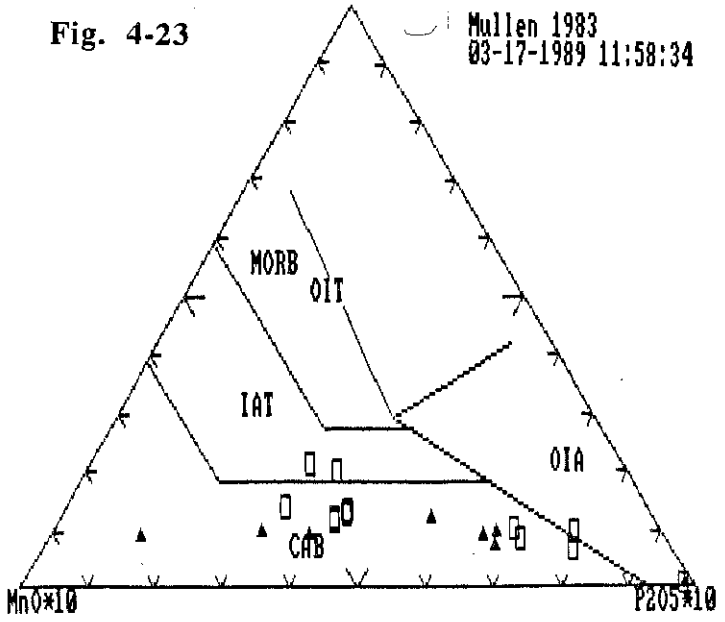

Fig. 4-24

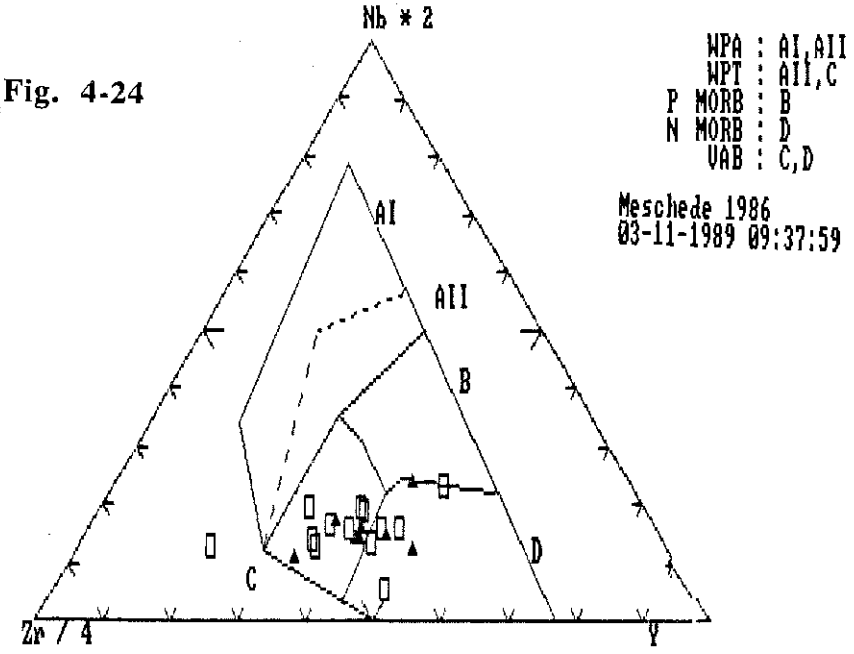

Some other diagrams, such as Zr--TiO_2, Zr--Ti--Y of Pearce and Cann (1973), MnO--TiO_2--P_2O_5 of Mullen (1983), Zr--Nb--Y of Meschede (1986) were formulated from analyses of basaltic rocks taken from different tectonic settings. These trace elements are considered to be immobile during metamorphism and often better reflect the primary features. To minimise the effect of fractionation, only the mafic rocks of the ACAS have been used. As the ACAS is considered to range from a high-level intrusion to volcanics, these diagrams may be applicable. Indeed, most of the mafic rocks of the ACAS plot in the calc-alkaline field defined in each diagram (Fig.4-21,22,23,24). Some anomalies may be caused by fractionation. e.g., one sample (87173) plotted very close to Zr corner on the Zr--Ti--Y diagram. This is believed to be due to local precipitation of zircon.

In addition, Barker and Arth (1976) have used normative Ab--Q--Or and Na--K--Ca diagrams to discriminate Na-enriched but K-depleted, trondhjemitic trends from common calc-alkaline trends. In these diagrams, the ACAS plots are quite distinctive, showing extreme depletion in K and generally follow the trondhjemitic trend (fig.4-19).

In conclusion, the ACAS is a complete calc-alkaline suite with its felsic differentiates showing transition to the trondhjemitic trend of Barker and Arth (1976).

4.3 GEOCHEMISTRY OF THE AGB

4.3.1 INTRODUCTION

In this section, the AGB is divided into two genetic groups which will be discussed separately. Most analyses are those from the mapped area. Two AOLG and one AOT analyses are from Marmalade Dam. Seven AOT analyses are taken from Sando (1987) (see Appendix-5). In addition, two analyses on an apparently younger granitic dyke (unaffected by the older shear zone) and an aplite respectively have been presented for comparison (Appendix-3C).

4.3.2 GEOCHEMICAL FEATURES OF THE AOLG AND AOT

The following features can be deduced from the analyses:

(1). Normal linear to curved trends for most elements, such as TiO_2, Al_2O_3, MgO, $Fe_2O_{3tot.}$,MnO,CaO,P_2O_5, Ni,Sc,V,Sr,Ga, and Zn, occur on Harker diagrams (Fig.4-6),

indicating an evolution trends through the rock types tonalite--coarse-grained granite--fine grained granite. But Na_2O, K_2O, Rb, Ba are relatively scattered. Zr,Nb,Y display a somewhat unusual enrichment away from the evolutionary trends.

(2). A compositional hiatus exists between 68--72% SiO_2 content.

(3). Overall, the rocks are characterised by low K_2O/Na_2O (most less than 1), Rb (<100ppm) and Rb/Sr (generally < 0.5), high Ca,Sr,Ba and increasing trends for K/Rb, Rb/Sr ratios.

(4). The AOT, with SiO_2 ranging from 62 to 68%, is rich in CaO (3--5%), Fe_2O_{3tot} (4--6%), MgO (1--3%), Cr,Ni,Sc and V.

(5). The AOLG has SiO_2 ranging from 72 to 78%. The fine grained phase shows depletion in TiO_2, Al_2O_3, Fe_2O_{3tot}, MgO, CaO, MnO, P_2O_5, V, Zr, REE, Sc, Ni, Ga, Sr and Zn but enrichment in Rb and Pb and increasing Rb/Sr and K/Rb ratios compared with the coarse-grained phase. The fine-grained phase also has a relatively higher SiO_2 content (see Fig.4-6).

(6). REE patterns for the AOT and AOLG are characterised by (Fig.4-12 & Appendix-4):

1). $(Ce/Yb)_N$ ranging from 7.19 to 12.85;

2). a slight negative Eu anomaly and Yb enrichment;

3). with increasing SiO_2, $(Ce/Yb)_N$ firstly increases and then drops; the total REE content initially falls and then rises; the negative Eu anomaly continuously increases.

4.3.3. GEOCHEMICAL FEATURES OF THE AMG

10 analyses of the AMG have a narrow range of fairly high SiO_2 contents (74-76%). When plotted on the Harker diagrams, distintive geochemical features are revealed. e.g., TiO_2, Fe_2O_{3tot}, MgO, CaO, P_2O_5, REE, V, Sc, Zr, Sr and Ba are significantly low, and Al_2O_3, K_2O, K_2O+Na_2O, Rb, Ga, Y, Nb, Pb,Zn, K_2O/Na_2O, Rb/Sr and Rb/Zr are significantly high , when compared with the AOLG analyses with same SiO_2 contents (see Fig.4-6, the solid-line cycle). The high Rb, Rb/Sr, Rb/Zr, K_2O/Na_2O, K_2O, Ga and Pb are most obvious (e.g. Fig.4-6J,K,P & T; Fig.4-8). Most molar $Al_2O_3/(CaO+Na_2O+K_2O)$ values are >1.1. This result, combined with higher K_2O/Na_2O ratios and normative corundum >1%, is consistent with S-type granites under

the classification of Chappell and White (1974).

In addition, samples of the AMG display strong interelement correlation (Fig.4-9). Among them, the negative correlation of Y with Zr is quite distinct from the trends in the AOLG and AOT. The lower K/Rb ratio and dramatic increase in Rb, Rb/Sr are also quite distinctive.

The AMG is chemically zoned. The pink-coloured, fine-grained outer type (e.g. 88089,88099) has higher Zr, TiO_2, V, REE, Sr and Ba and lower Rb/Sr, Y than the white-coloured, coarse-grained inner type (e.g. 88090).

One sample (88090) from the AMG exhibits a peculiar V-shaped REE pattern and strong depletion in total REE (Fig.4-13). It can now be predicted from the negative Y--Zr and positive Ce-Zr correlations that the less-evolved samples with higher Zr contents (e.g. 88099) will have a normal down-slope REE pattern and also be richer in total REE than the more evolved samples (e.g. 88090).

4.3.4 DISCUSSION

4.3.4.1 *METAMORPHISM, CHEMICAL MOBILITY AND EXPLANATION OF Na/K AND K/Rb RATIOS*

It has been demonstrated that the AIC has undergone amphibolite grade metamorphism. Therefore some LIL elements may possibly be mobile under this condition. They are further suspect if they display somewhat irregular trends on the Harker diagrams (e.g. Fig.4-6E,F,K).

Therefore, it is reasonable to question whether the higher Na/K ratio, lower Rb content and increasing trend for K/Rb ratios are inherited magmatic features or metamorphic overprints.

The possibility of metamorphic overprint, especially the involvement of large scale transportation of these elements, seems to be unlikely for the following reasons: (1). Crustal sources cannot provide a fluid with high Na/K ratios, because the supracrustal quartzofeldspathic gneiss nearby mainly has high K_2O/Na_2O as indicated by petrographic evidence. (2). K, Rb depletion may occur in granulite where it is caused by dehydration or removal of partial melts during granulite grade metamorphism. The metamorphism in Atnarpa is a hydration process. Large transportation of the LIL elements out of system seems to be less likely. (3). The albitization, a process of sodium metasomatism (e.g. Xu Keqin et al. 1984), is only of minor significance and

cannot account for such high Na_2O values in the AOT & AOLG.

The second possibility, i.e. the inheritage of the primary magma, is more reasonable. In such a case, metamorphism only cause internal redistribution in Na_2O and K_2O and have not substantially changed the bulk Na/K ratio. The albitisation and sericitisation may be caused such a process.

High and increasing K/Rb ratio found in the Archean tonalitic-trondhjemitic gneisses of the Scourie Complex has been described by Rollinson and Windley (1980) as due to relative depletion of Rb against K_2O during granulite metamorphism. Following the previous arguement (see 4.2.5.1), an increase in K/Rb ratios with SiO_2 in the AOT & AOLG cannot be attributed to the subsequent metamorphism. This is because: (1). K/Rb ratios in most of the Atnarpa granitic rocks plot withins the 200--600 range. This is considered to be normal for crustal rocks (Rollinson and Windley 1980); (2). No apparent partial melting such as migmitization, which is indicative of removal of a K-rich partial melt, has been observed. (3). No carbonate alteration indicative of a CO_2-rich fluid, which tends to remove K and Rb (Tarney & Windley 1977), occurs in the AGB; (4). Alteration and metamorphism cannot account for the good correlation between K/Rb ratios and SiO_2 content. Accordingly, the K/Rb trend and low Rb content are considered to be magmatic features rather than metamorphic overprint.

In addition, it is unlikely that the somewhat irregular trends for Zr, Nb and Y on Harker diagrams for the AOLG and AOT are due to metamorphic disturbance because the HFS elements are normally immobile during metamorphism (eg. Sivell and Foden 1988). The HFS elements are less mobile than LIL elements such Sr. But Sr still displays a linear trend and show no evidence of disturbance by metamorphism. A reasonable explanation for these behaviors will be made in the following text.

Another problem is that some of the Na-rich AOLG and AOT are peraluminous. However, as reviewed by Pitcher (1987), the peraluminity is a fundamental problem. It can be generated by a number of diverse mechanisms (Clarke 1981; Halliday et al. 1981), ranging from a particular type of crystal differentiation to deep-level assimilation or anatexis of pelitic materials. For instance, it has been demonstrated that a hornblende extraction during differentiation is capable of producing peraluminous trends in the residual liquid, even in calc-alkaline magmas (Ewthorn et al. 1976; Abbott 1981). Therefore, a peraluminous granite cannot be dogmatically grouped into S-type

Fig. 4-6. Harker diagrams (A--T) for the Atnarpa Older Tonalite, Atnarpa Older Leucogranite and Atnarpa Muscovite Granite. Solid-line balloons outline the AMG plots. Broken-line balloons represent the fields for the Kalkadoon-Ewen-Leichhardt association, a representative member of the Barramundi Association (Wyborn and Page 1983). Dotted-line balloons diaplay the fields of the Barramundi Association as indicated by Wyborn (1988).

Symbols:

+ AOT

◊ Coarse-grained phase of the AOLG

▾ Fine-grained phase of the AOLG

X AMG

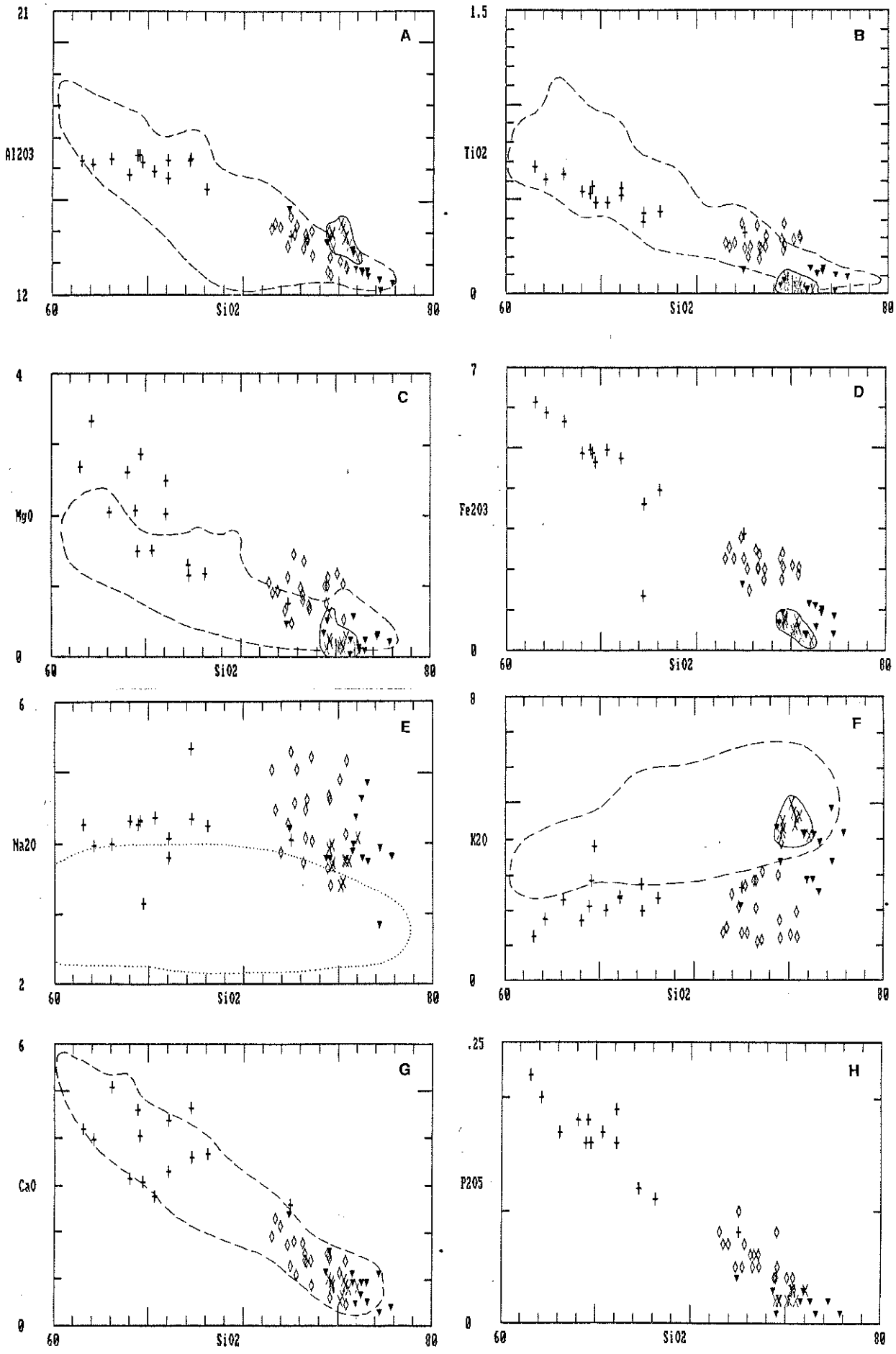
A
21
Al2O3
12
60
SiO2
80
B
1.5
TiO2
0
C
4
MgO
D
7
Fe2O3
E
6
Na2O
2
F
8
K2O
G
CaO
H
.25
P2O5

Fig. 4-6

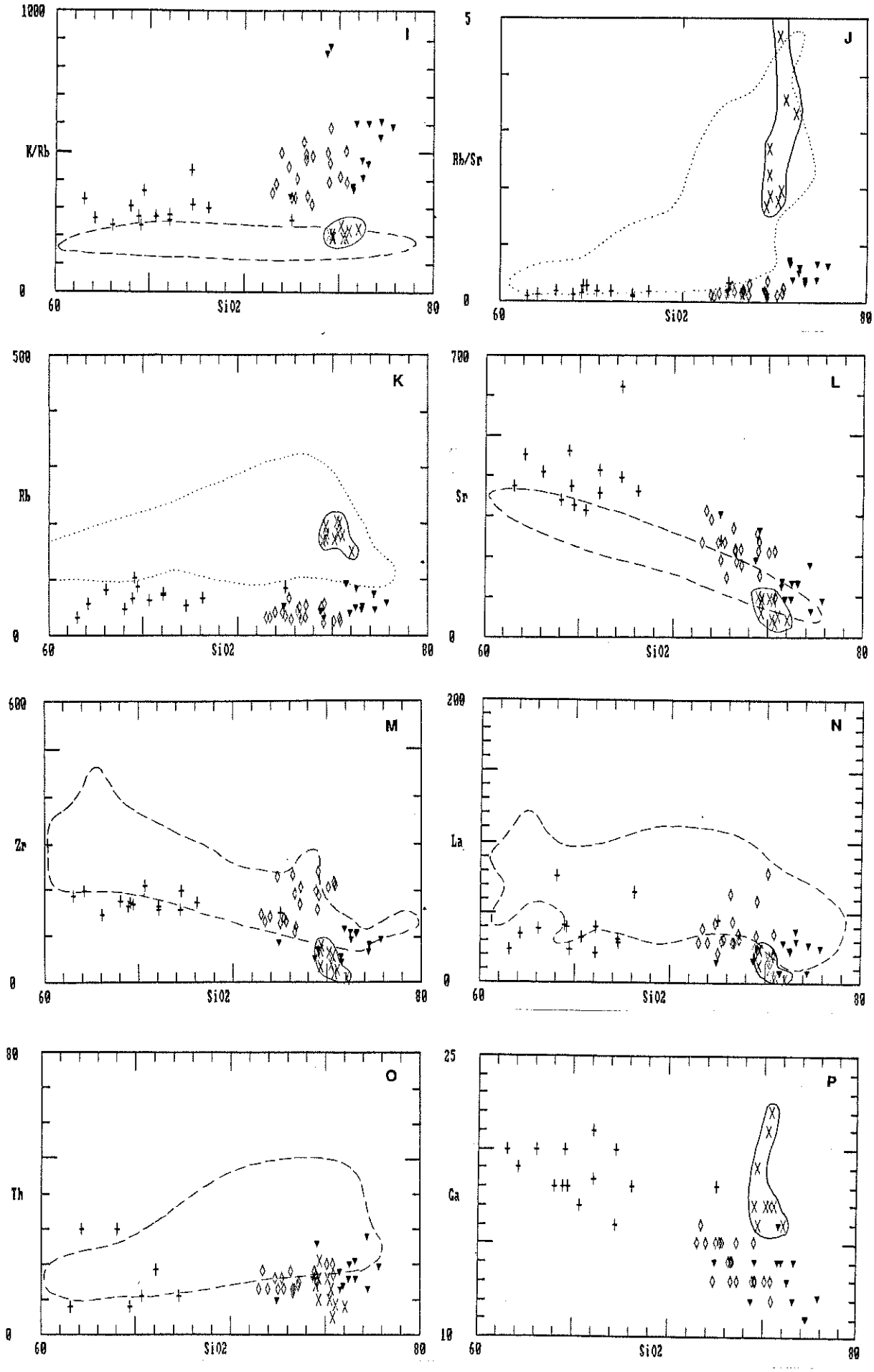
1000
K/Rb
0
60
SiO2
80
I
5
Rb/Sr
0
60
SiO2
80
J
500
Rb
0
60
SiO2
80
K
700
Sr
0
60
SiO2
80
L
600
Zr
0
60
SiO2
80
M
200
La
0
60
SiO2
80
N
80
Th
0
60
SiO2
80
O
25
Ga
10
60
SiO2
80
P

Fig. 4-6

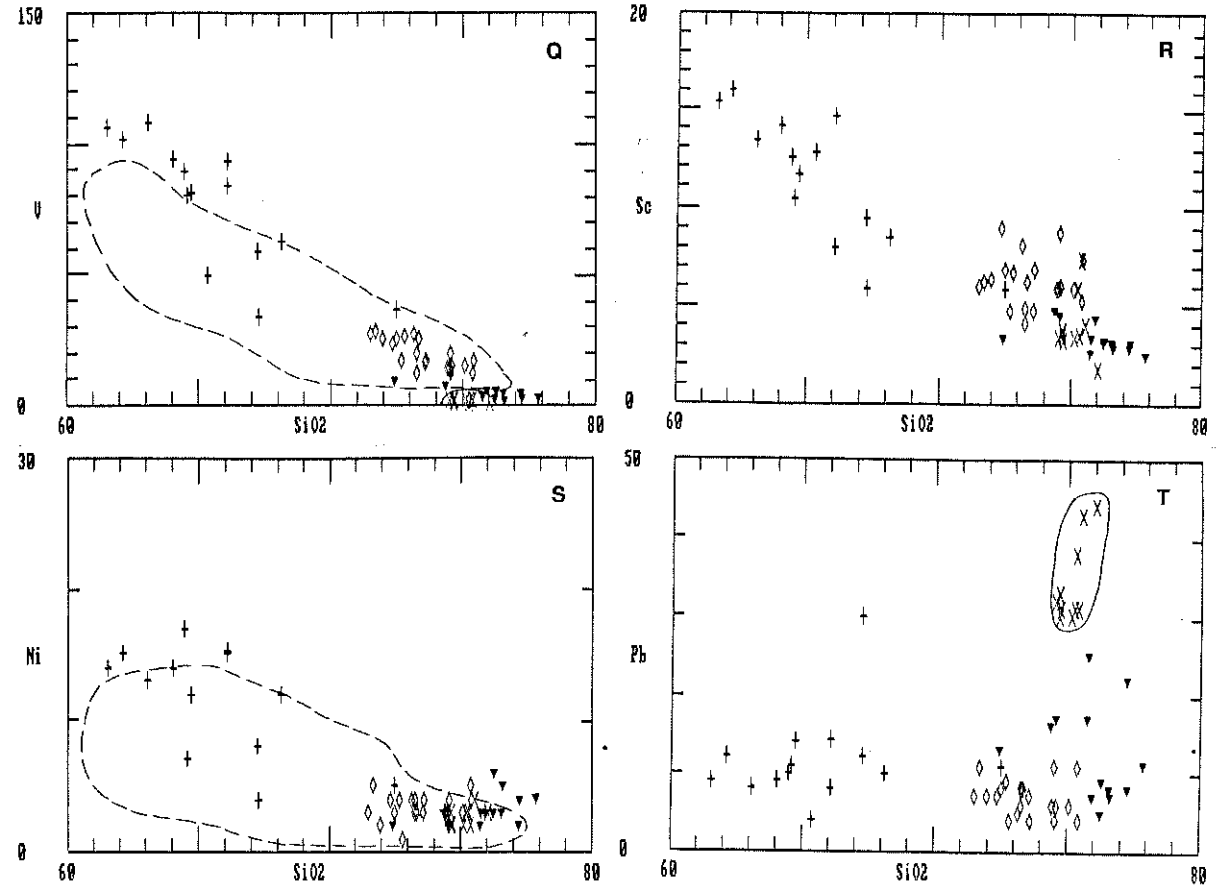

Fig. 4-6

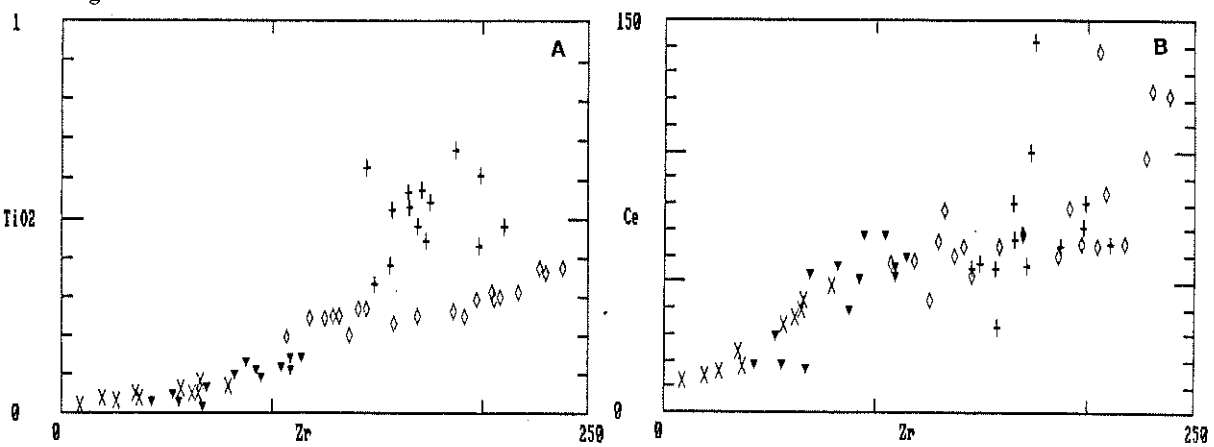

Fig. 4-7. TiO2, Ce vs Zr diagrams for the AOT, AOLG and AMG. Symbols as for Fig. 4-6.

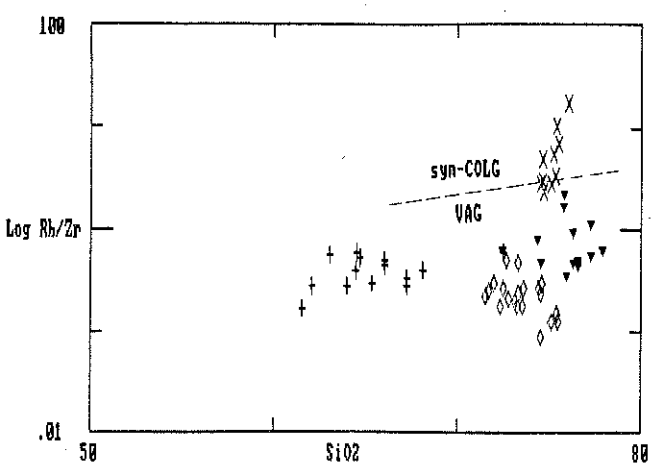

Fig. 4-8. The AOT, AOLG and AMG are plotted on the LogRb/Zr-SiO2 discrimination diagram of Harris et al (1986). The AMG plots fall on the transition to the syn-collisional granite field. Syn -COLG=syn-collisional granite, VAG= volcanic arc granite. Plot symbols as for Fig. 4-6.

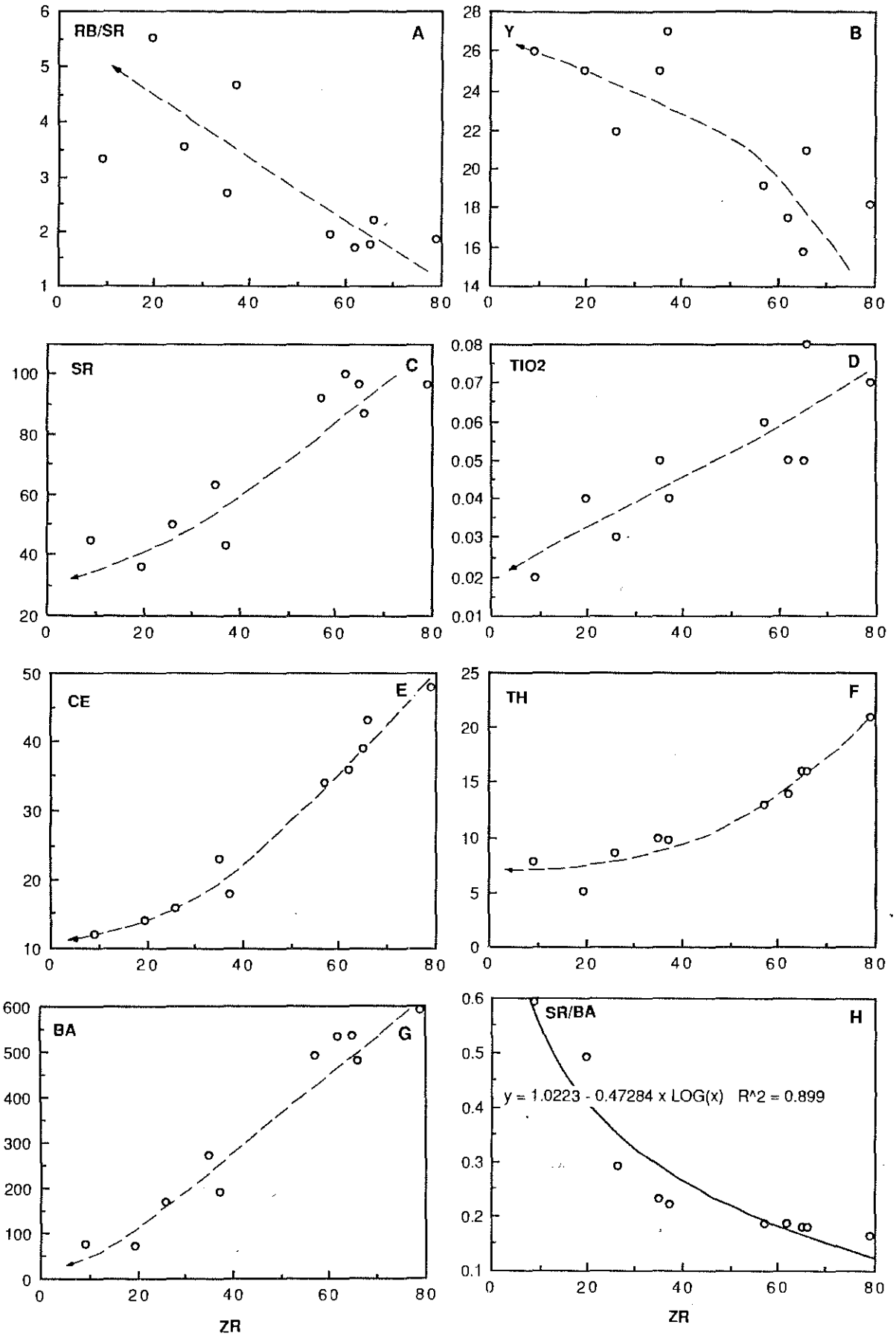

Fig. 4-9. Trace elements and ratios vs Zr diagrams for the AMG. Broken lines with arrows indicate fractionation trends.

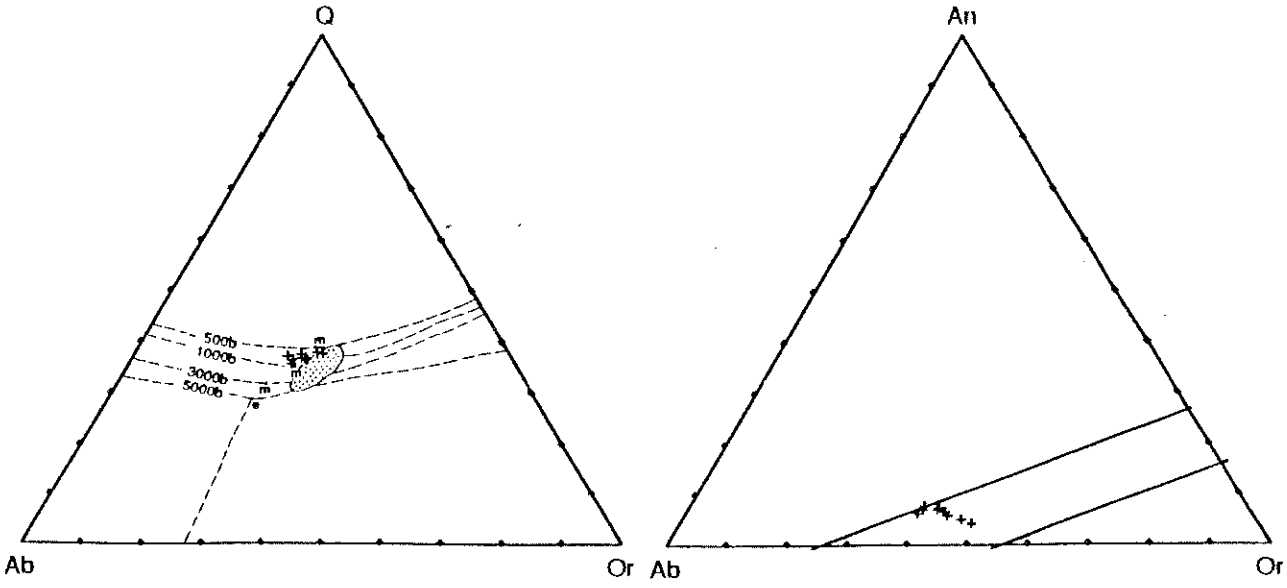

Fig 4-10. The AMG analyses are plotted into the low temperature trough on the normative Q-Ab-Or ternary diagram of Tuttle and Bowen (1958) and An-Ab-Or ternary diagram of Kleeman (1965). m=minimum point, e=eutectic point.

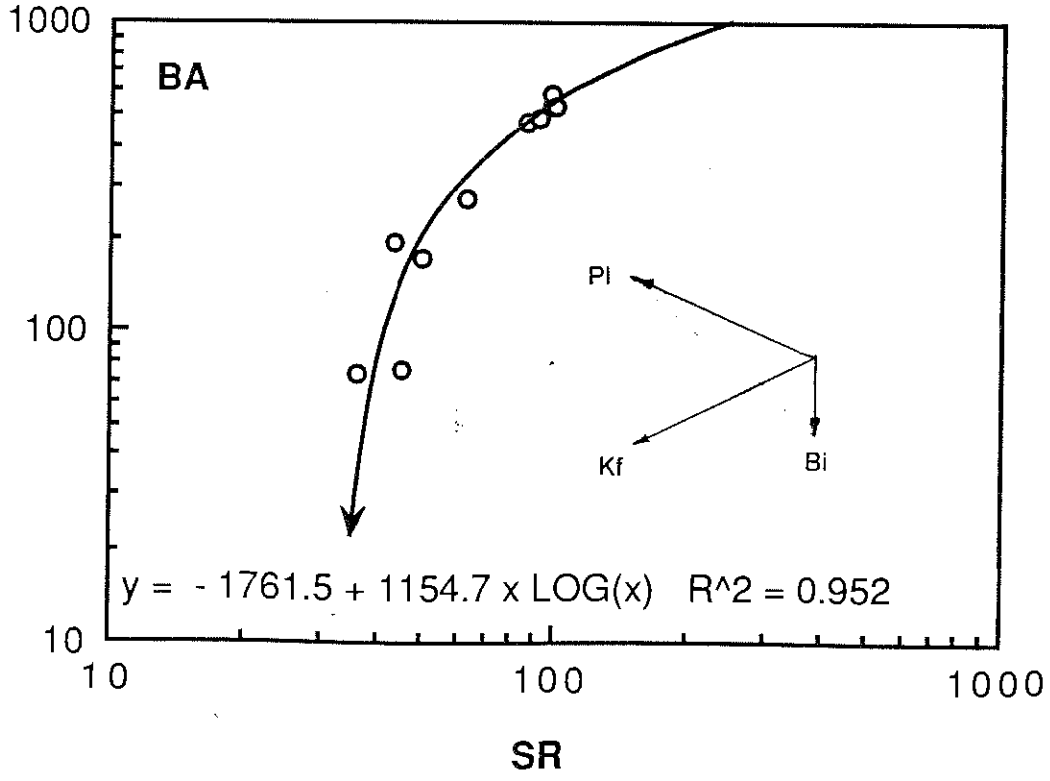

Fig. 4-11. The AMG follows a typical fractionation trend on the logSr - logBa diagram. Mineral vectors after Higgins et al (1985). Pl=plagioclase, Kf=K-feldspar, Bi=biotite.

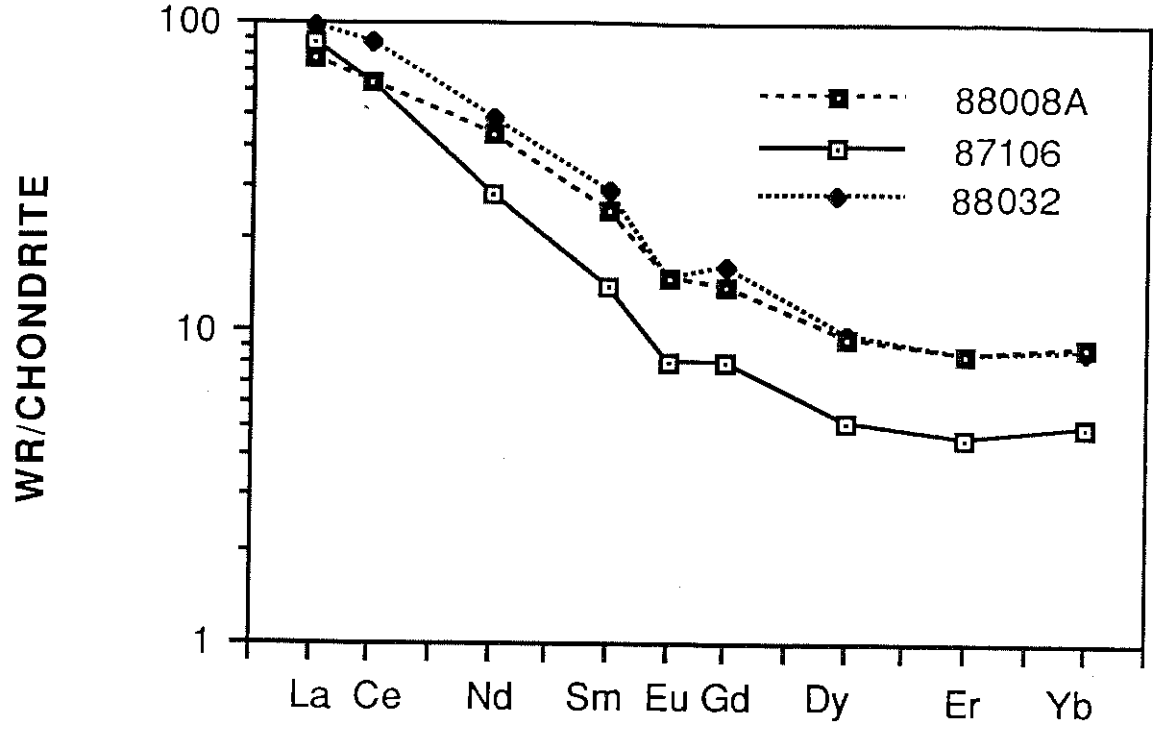

Fig. 4-12. Chondrite-normalized REE patterns for the representative samples of the AOT (88008A) and AOLG (87106, 88032).

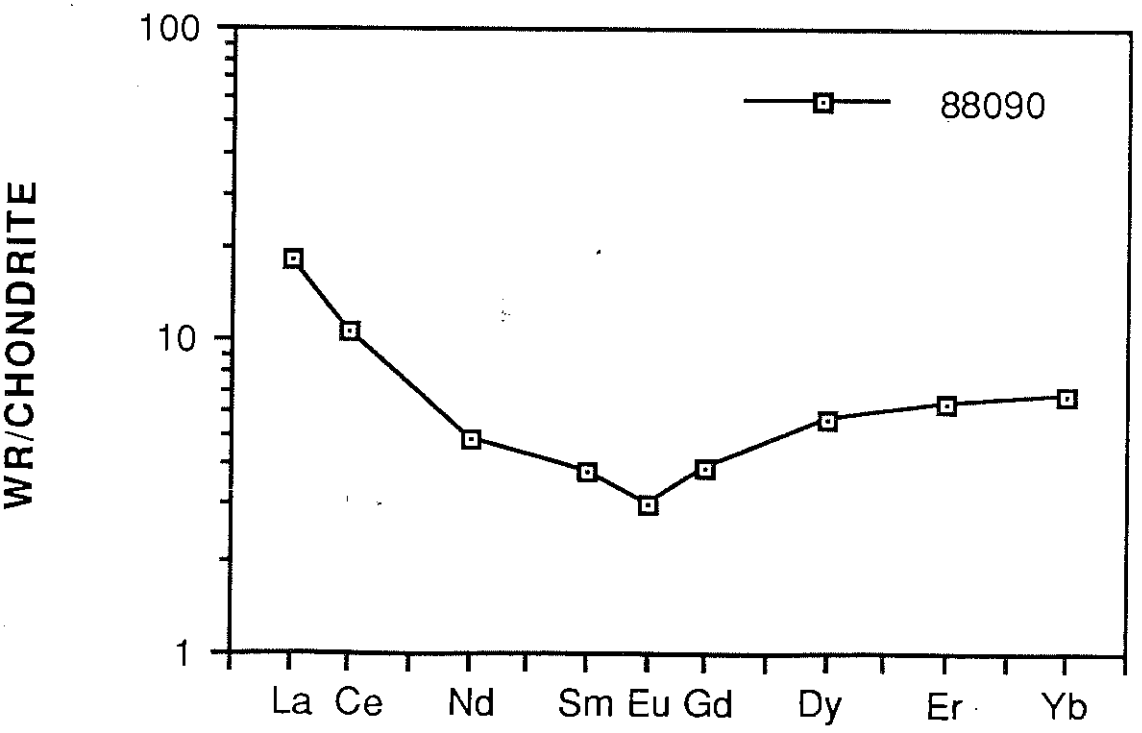

Fig. 4-13. Chondrite-normalized REE pattern for the representative sample of the AMG

granites (White et al. 1986).

4.3.4.2 *PETROGENESIS OF THE AOT AND AOLG*

Obvious field relations and geochemical trends indicate that the two phases of the AOLG are consanguineous, and consistent with a fractionation process, by the crystallization of feldspar and accessory minerals such as zircon, sphene, and apatite.

It is difficult, however, to put constraint on the genetic relationship between the AOT and AOLG although temporal and spatial relations are apparent. This is partly because the field relations and chemistry in the AGB are not as clear as in the ACAS and partly because granites themselves are more problematic (Pitcher 1987).

Currently there are several models which have been set up to explain the genesis of apparent consanguineous suites of granites. They include: (1) crystal differentiation (Wright and Doherty 1970; Arth 1976); (2) magma mixing (Grove et al. 1982; De Paolo 1981); (3) restite-controlled unmixing (Chappell and White 1977); (4) separation of immiscible fluid; (5) thermogravitational diffusion (Hildreth 1979, 1981) and (6) convective fractionation (Spark et al.1984). But the former two models are more generally favoured alternatives. It is certainly beyond the reach of this thesis to review and test on all these models, however the following remarks concerning the relationship between the AOLG and AOT will be made.

Possibility one: It could be radically argued that the AOT & AOLG are genetically unrelated on the basis of the compositional hiatus and the anomalous behavior of Zr on the Zr - SiO_2 diagram (Fig. 4-6M) and different trends on the Zr-TiO2, Zr-P2O5 diagrams (e.g. Fig.4-7A). However, many other geochemical similarity and the well-correlated trends on the Harker diagrams for most of the major and trace elements indicate that this arguement has no solid ground. The anomalies for Zr, Nb, P_2O_5 could be due to local uneven distribution. Insufficient fractionation either by crystal precipitation, or magma convection (Spark et al. 1984) or thermogravitational diffusion (Hildreth 1981) within a siliceous and therefore viscous magma chamber may lead to local uneven distribution for these highly charged elements. In addition, both fractionation and restite unmixing process can produce a compositional hiatus, depending on the degree of unmixing or separating of the two phases (Mortimer 1984).

Possibility two: partial melting or magma mixing or both.

There is not enough evidence to accept or refute discrete partial melting or magma mixing at variable degrees.

Possibility three: restite-unmixing.

Linear or near-linear variations for many elements on the Harker diagrams (see Fig.4-6) are consistent with a restite unmixing model. But these trends can also produced by insufficient separation of crystal from residual liquid during fractionation (Wall et al. 1987; Clarke and Mueche 1985). Furthermore, restite unmixing model may fail to explain the following observations: 1). enhedral, well-zoned plagioclase, allanite (oscillatory zones, see Sando 1987) and zircon in the AOT and AOLG; 2). Increasing K/Rb ratios; 3). geochemical similarity of the AOT-AOLG to the ACAS (see Chapter Seven) and (4). some elements follow curved line trends on the Harker diagrams (e.g. Fig. 4-6A,I & L).

Possibility four: fractionation process.

By comparison, a process dominated by fractionation, either by crystal settling or magma convection, is favoured, although partial melting or mixing models cannot be ruled out. The geochemical evidence that supports a fractionation model are outlined as follows:

(1).Trends for Fe_2O_3,MgO, Ni, Sc suggest early crystallization of ferromagnesian minerals, probably hornblende and biotite. Trends for TiO_2 and V are consistent with either fractionation of hornblende and biotite or precipitaton of magnetite/ilmenite (even sphene). Trend for P_2O_5, and the generally curved trend for Zr are in accord with apatite, zircon fractionation.

2).A fall in CaO, CaO/Na_2O indicates early fractionation of plagioclase. The regular decrease in Sr suggests feldspar fractionation.

3).The curved variation trend for Al_2O_3 probably reflects the change in ratio of ferromagnesian minerals to plagioclase despite the lower An, lower Al_2O_3 content of the later plagioclase.

4).General increase in $Na_2O + K_2O$ is consistent with the enrichment of alkali-feldspars, especially K-feldspar, in the later stage differentiates, e.g. the fine-grained phase of the AOLG.

This may be caused by the removal of relatively more calcic plagioclase and some other mafic minerals during the early stage fractionation.

5).The constant K/Rb ratio has been considered by Wyborn and Page (1983) and Wyborn (1988) to be strong evidence to support a restite unmixing model for the genesis of the Kalkadoon-Ewen-Leichhardt association, Mount Isa Inlier. Therefore, the behavior of K/Rb ratio in the AGB suggests a genetic difference between these two granitic suites of the same age. The present author attributes the increase of K/Rb ratios to earlier precipitation of biotite relative to K-feldspar. The removal of biotite, a mineral with a much greater distribution coefficient for Rb (2.24 in Arth 1976 and 3.3 in Gill 1978) than K-feldspar (0.34 in Arth 1976) would produce a marked decrease in K/Rb value in the residual liquid.

6).The REE patterns in Fig. 4-12 can be interpretated in this way: For SiO_2 range from 62-72%, fractionation is dominated by plagioclase, hornblende and minor biotite, causing an increase in the $(Ce/Yb)_N$ ratio and Eu negative anomaly and total REE depletion (Fig.4-12). For SiO_2 range of 72-76%, the fractionation is dominated by feldspars and biotite, resulting in total REE enrichment, decrease in $(Ce/Yb)_N$ and further increase in negative Eu anomaly. It is likely that some REE-enriched accessory mineral, such as zircon, apatite, allanite or sphene may have also precipitated, which may effectively preclude too much Eu anomaly development.

7).REE pattern for 88008A suggests that hornblende and plagioclase fractionation may have occurred during an even earlier stage.(i.e. $SiO_2 < 62\%$). The Yb enrichment and flatter HRE pattern are considered to be typical of hornblende fractionation (Arth and Barker 1976).

In conclusion, the genesis of the AOLG and AOT is considered to be dominated by fractional crystallization of initially a hornblende + plagioclase assemblage followed by removal of a biotite + feldspar assemblage. These were sometimes accompanied by precipitation of accessory minenals such as apatite, sphene, zircon and allanite. This geochemical conclusion is consistent with petrographic observations.

4.3.4.3 *PETROGENESIS OF THE AMG*

Peraluminous muscovite or alkali feldspar granites like the AMG have been recognised in many places in the world (e.g. Higgins et al. 1985; Mackenzie et al. 1988; Chatterjee and Strong 1985; Xu Keqin et al. 1984) and their origin is still controversial, with suggestions including: 1).

magmatic crystallization (Mackenzie et al. 1988; Webb et al. 1985), 2). intensive post-magmatic metasomatism or hydrothermal alteration (e.g. Higgins et al. 1985), 3). combination of both processes and 4). transformation or granitisation (Xu Keqin et al. 1984).

The AMG is in many aspects analogous to the recently described Tasmanian Lottah Granite (Mackenzie et al. 1988), e.g. both are associated with more voluminous normal granitic intrusions; both share similar mineralogy and geochemistry and both are petrographically and geochemically zoned. From an essentially geochemical study, Higgins et al. (1985) suggested that the Lottah granite formed as a result of metasomatic emanations from the other major intrusions. However, Mackenzie et al. (1988) made use of a combination of petrographic, mineralogical, geochemical, experimental, geochronological and isotopic constraints to argue that the Lottah granite is essentially magmatic and genetically unrelated to the adjacent major granitic intrusion.

By comparison, some features displayed on the Harker diagrams may suggest a kinship between the AOLG and the AMG, i.e. the AMG could possibly be interpreted as the latest phase of the AOLG which subsequently suffered from sub-solidus alteration.

However, such an alteration model cannot explain the following observations:

1). Geochemical zoning in the AMG.

2). The well defined inter-element correlations, especially among Ti,Th,Zr (see Fig.4-9). Zircon, where most of Zr is found, is usually extremely inert, unless being affected by highly alkaline melts (Watson 1979), whilst Ti and Th-bearing phases including ilmenite, sphene, biotite and monazite can be more easily altered. Therefore such strong correlations are usually considered to be due to magmatic process (Webb et al. 1985).

3). Although phyllic alteration fluid can activate the HFS elements such as Zr and Ti and influence the REE patterns (Chatterjee and Strong 1985), petrographic and geochemical evidence indicate that the highest Zr, Ti contents are found in the most intensively deformed and altered outer-zone types (e.g. samples 88089, 88099).

4). It is considered that the younger thrusting event has made little contribution to the geochemical features of the AMG because, muscovite, the major Rb-bearing mineral, predates the major foliation.

Similarly, some phenomena preclude that the AMG is genetically related to the older granites. They include 1). the reverse trends on Y--Zr, K/Rb--SiO_2 diagrams; 2). the significantly

different Rb/Sr and K_2O+Na_2O of the AMG; 3). the occurrence of garnet and tourmaline in the AMG in contrast with the general absence in the AOT and AOLG; 4). the general enrichment of muscovite in the AMG but no such tendence in the AOLG and AOT.

Alternatively, petrographic and chemical zoning, major and trace element variation trends indicate that the AMG may be probably derived by a highly evolved magma or from very low degree partial melting of a crustal composition source. This initial magma must then have fractionally crystallized the minerals feldspar (sodium plagioclase and K-feldspar), biotite, zircon, monazite, apatite, sphene and ilmenite.

In such a process, the megacrystic texture and enrichment of muscovite in the inner zone granites can be attributed to the crystallization of granite melts at low undercooling temperature (Swanson 1977) or the accumulation of a volatile-enriched magma in the roof of the magma chamber (Webb et al. 1985). Experimental studies indicate that the solidus temperature of a granitic melt can be substantially depressed, even as much as to below 600°C at 1kb pressure (Manning & Pichavant 1983) by the enrichment of the elements F, Li, B. Some such enrichment is indicated by the presence of tourmaline. In such a melt, muscovite is a liquidus or near-liquidus phase to the last stage of the crystallization (London 1987). Therefore, it is possible that the melt for the AMG may be derived from low-degree partial melting of a supracrustal source, e.g. the quartzofeldspathic gneiss. The presence of minor garnet in both the AMG and some quartzofeldspathic gneiss may provide a clue to such a relatioship.

The well correlated relations of HFS and REE elements vs Zr plots (e.g. Fig.4-9) are consistent with fractionation of an assemblage containing zircon, sphene, apatite, monazite and biotite. The low concentrations for these elements may be due to strong peraluminity of the magma and the low undercooling temperature (Watson & Harrison 1983, 1984). The reverse correlation of Rb/Sr with Zr also suggests a fractionation of feldspar. Here it is necessary to explain why Zr is chosen as an indicator to such a fractionation trend (e.g. Fig. 4-9). This is because: (1) Zr shows a strongly correlated decrease with increasing SiO_2 over its short range, indicating a Zr-rich mineral such as zircon is involved in fractionation; (2). Relative to SiO_2, Zr has a wide range in concentration and is usually immobile during metamorphism and therefore better reflects primary magma features.

The trends of the AMG plots on the logSr - logBa diagram (Fig.4-11) clearly displays that

the earlier stage fractionation is dominated by K-feldspar+ biotite assemblage but the amount of biotite (and/or muscovite) precipitated increases during the later stages.

Webb et al. (1985) explained the reverse trends for the LREE and HREE (and Y) (e.g. Fig. 4-9B & E) as due to the greater fractionation of feldspar relative to mica combined with effective monazite, sphene and apatite precipitation (Webb et al. 1984). This is consistent with the enrichment of muscovite in the late stage differentiates near the roof of the magma chamber and with the trend on the logSr -logBa diagram.

The AMG compositions plot very close to the minina within 0.5--1.0 kb $P(H_2O)$ range in the system Ab-Q-Or of Tuttle & Bowen (1958). In the system Ab-An-Or, they fall into the low temperature trough of Kleeman (1965) and trends toward the low pressure limiting line (Fig.4-10). These normative features indicate that the AMG may have crystallized from a near 100%-liquid magma derived from low degree partial melting within supracrustal level.

It is interesting to notice that the AMG is geochemically very similar to the syn-collision peraluminous leucogranites recognised by Harris et al. (1986), in that they are highly felsic and peraluminous and have low TiO_2, Zr, REE contents and high Rb/Sr, Rb/Zr ratios. The AMG also falls in the field of syn-collision leucogranites on the Rb/Zr--SiO_2 diagram (Fig.4-8).

4.4 GEOCHEMISTRY OF THE ATBS

4.4.1 GEOCHEMICAL FEATURES OF THE AYT

Six samples cover SiO_2 contents ranging from 58--66% with four of them around 64--65%.

Compared with the AOT of the same SiO_2 contents, the AYT has a characteristically lower TiO_2 (0.2--0.3%), Fe_2O_{3tot} (3--4%), P_2O_5 (0.1%), Zr (71--97ppm), Nb (2.9--4.7ppm), V and Rb/Sr, slightly lower Rb, Sc, Cr, Ga but obviously higher Al_2O_3 (16--19%) and Ni, slightly higher CaO (4--7%), CaO/Na_2O (1.1--1.6%) (e.g. Fig.4-14, Appendix-3).

The AYT has a distinct REE pattern characterised by a strong HREE depletion [$(Ce/Yb)_N$=23.7--32.1], similar to many Archean and Proterozoic high-Al_2O_3 type trondhjemites and tonalites (e.g. Barker & Arth 1976; Arth et al. 1978; Tarney et al. 1979). But no positive Eu anomaly has ever been observed (Fig.4-15).

By comparison, high Al_2O_3, CaO, Ba, Sr (>500ppm) Na_2O/K_2O and low Rb/Sr, TiO_2, Nb

and Y are similar to those found in the Archean tonalites (see Table 4-1).

4.4.2 GEOCHEMICAL FEATURES OF THE AYBA

Only one sample of this type was analysed. It is different from the ACAS in having higher TiO_2, Fe_2O_{3tot}, V and Y and lower Sr for the same SiO_2 content.

It is moderately enriched in LREEs but the HREE pattern is notably flat and unfractionated [$(Ce/Yb)_N$=4.8]. Slight Eu negative anomaly [$(Eu^*/Eu)_N$ =0.84] is present (Fig.4-16).

By comparison, its higher Cr, Ni, Sc, Fe, Mn and lower Sr, Ba, Rb contents appear to resemble the Archean basalts (Condie 1985) (also see Table 4-2). Its HREE pattern is similar to that of MORB (Sun et al. 1979). Actually, it also plots in the MORB field on the Cr--Y diagram (Pearce 1980). However the LREE pattern is more enriched than E-type MORB but similar to the calc-alkaline basalts. The feature of LIL/HFS decoupling seems to resemble the calc-alkaline basalts. if these features are representative, the AYBA is likely to display transitional features among arc-type basalts (e.g. calc-alkaline basalt), MORB-type basalts and Archean basalts.

4.4.3 DISCUSSION

The considerable differences in age (more than 100 Ma) and geochemistry rule out any direct genetical relationship between the AYT and the AGB. However, it has been demonstrated that the AYT shares many similar geochemical features, including REE patterns with many Archaean and Proterozoic trondhjemites and tonalites (Barker & Arth 1976; Arth et al. 1978; Tarney et al. 1979).

As reviewed by Barker (1979), the high-Al_2O_3 type trondhjemitic-tonalitic suite is found mainly in two geologic environments: (1). Archean gray gneiss terrains where it forms a major rock type, often in association with earlier basaltic rocks, to give a compositionally bimodal suite (e.g. Barker & Arth 1976 and McGregor 1979); (2). Along Proterozoic and Palaeozoic continental margins, that apparently are related to subduction or to subsidary back-arc spreading where they are typically accompanied by much greater volumes of the calc-alkaline suite (Arth et al. 1978; Tarney et al. 1979).

The REE patterns of these high-Al_2O_3 trondhjemitic-tonalitic suites have been explained by Arth & Barker (1976) as due to either hornblende-controlled fractionation of hydrous basaltic

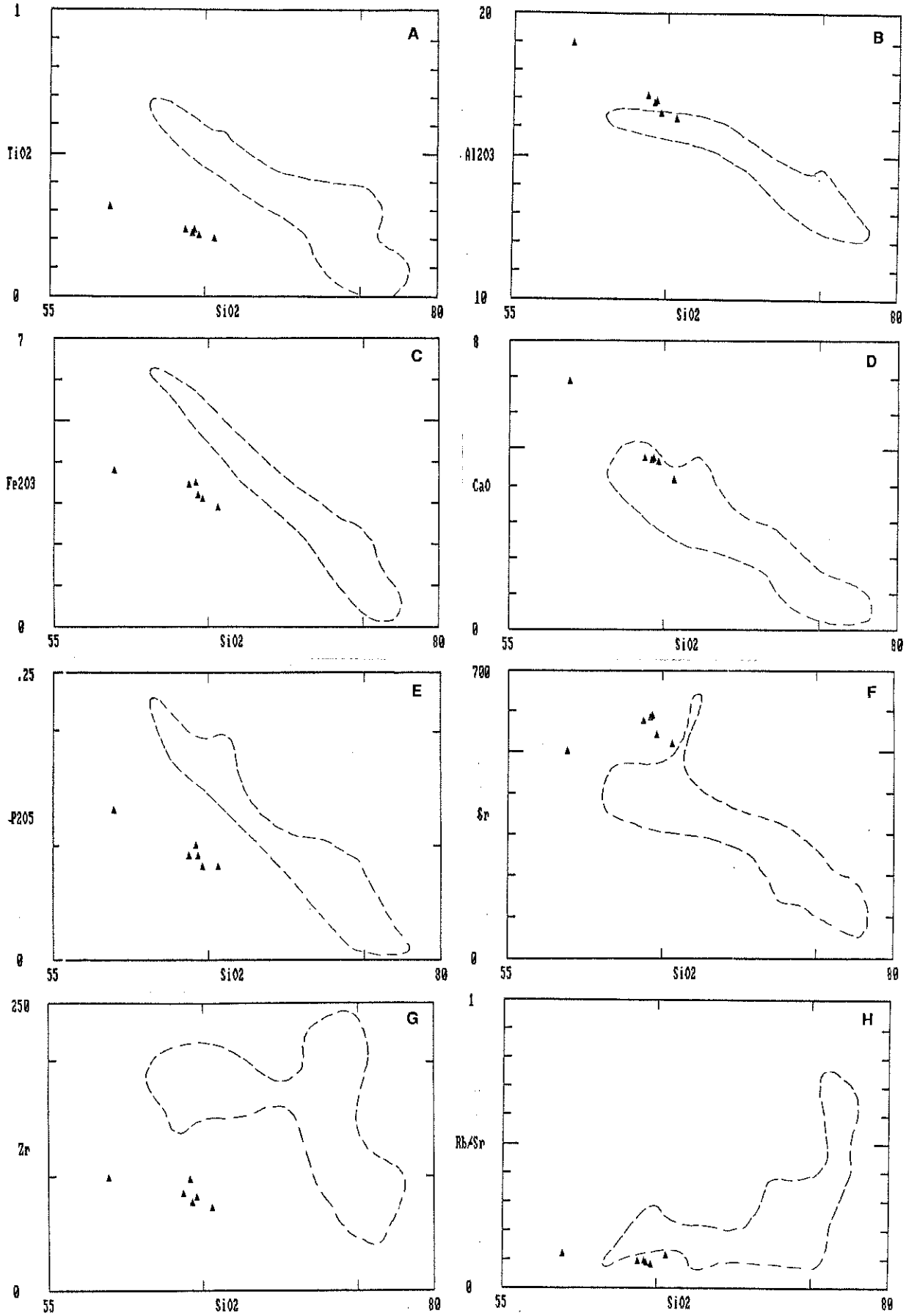

Fig. 4-14. Selected Harker diagrams for the Atnarpa Younger Tonalite. The fields for the AOT and AOLG on each diagrams have been outlined.

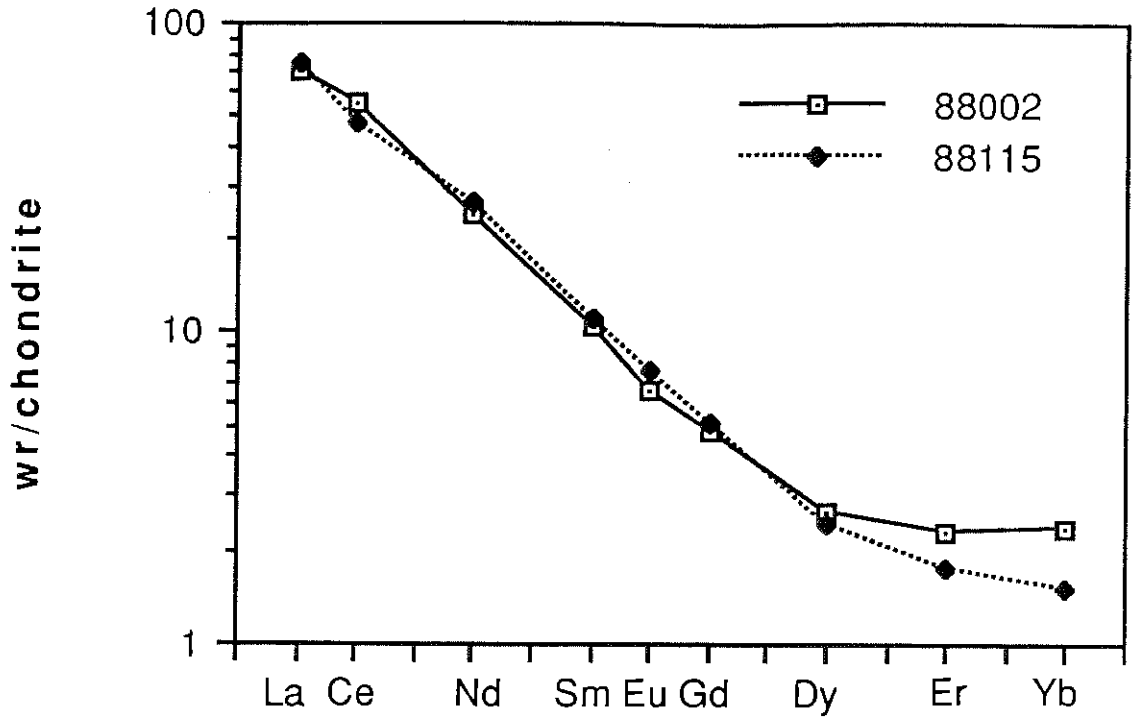

Fig. 4-15. Chondrite-normalized REE patterns for the representative samples of the AYT.

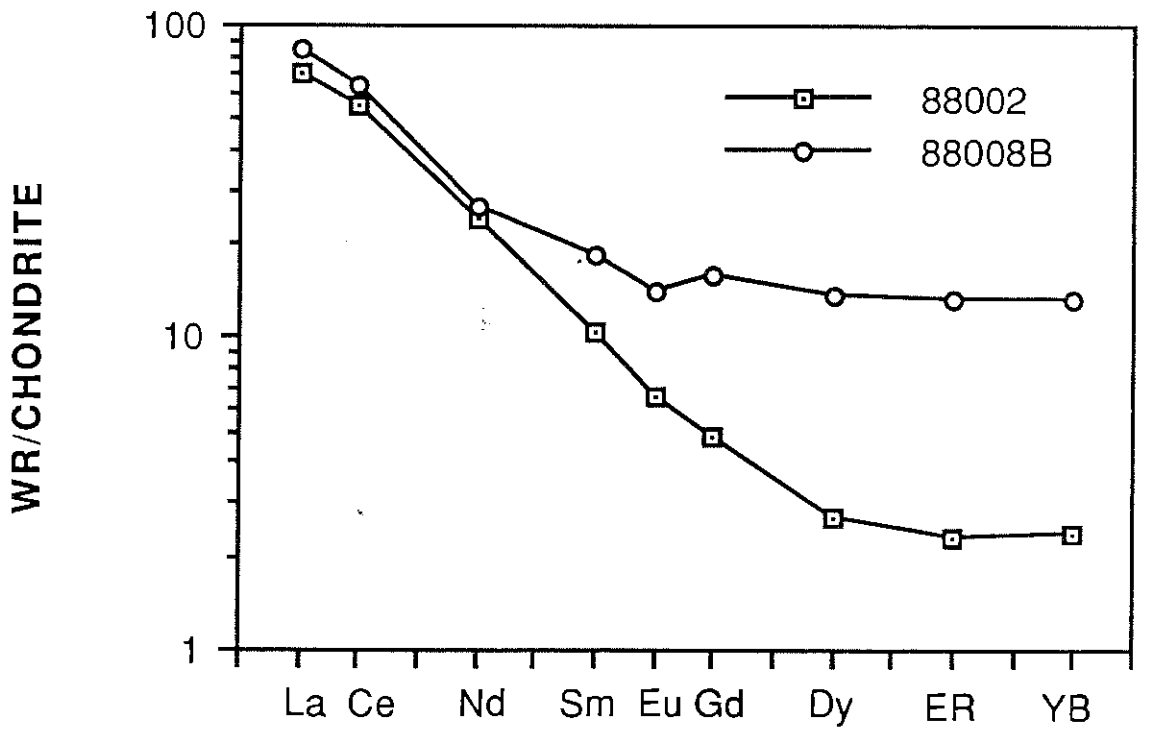

Fig. 4-16. Chondrite-normalized REE pattern for the representative sample of the Atnarpa Younger Basaltic Amphibolite of the ATBS. Sample 88002 of the AYT is plotted for comparison.

Table 4-1

	AT	AYT
Major elements in wt%		
SiO2	66.70	64.48
TiO2	0.34	0.22
Al2O3	16.04	16.71
Fe2O3	1.49	3.21
FeO	1.47	----
MnO	0.04	0.08
MgO	1.44	2.37
CaO	3.18	4.56
Na2O	4.90	3.70
K2O	2.09	2.12
P2O5	0.14	0.09
Trace elements in ppm		
Cr	32	14
Ni	20	17
Rb	74	52
Sr	580	560
Y	7	7.4
Zr	193	82
Nb	6	3.8
Ce	71	47
La	32	25
Pb	22	10
Th	11	9.6
Element ratios		
K/Rb	234	338
Rb/Sr	0.127	0.093
Ba/Rb	9.6	16.6
Ba/Sr	1.2	1.5
Ce/Y	10	6.4
Zr/Nb	32	22

Table 4-2

	ARCHAEAN BASALTS		88008B
	>3.5 b.y.	2.5-3.5 b.y.	
SiO2	51.2	52.0	50.59
TiO2	0.9	0.9	1.00
Al2O3	15.3	15.0	14.69
FeOt	11.0	10.8	11.61
MgO	8.1	8.0	9.04
CaO	10.1	10.0	9.85
Na2O	2.5	2.6	2.64
K2O	0.5	0.3	0.21
MnO	0.2	0.2	0.25
P2O5	0.1	0.1	0.11
Rb	12	11	3.7
Ba	65	130	91
Sr	120	157	172
Zr	72	90	64
Y	20	27	36
Nb	7.5	5	2.5
Th	1.3	1	1.1
La	4.2	4.5	26.02
Sm	1.8	2	3.50
Yb	1.9	1.9	2.75
V	235	249	326
Sc	37	35	52
Cu	66	82	12
Zn	84	80	93
Ni	150	135	117
Cr	460	350	354

Table 4-1: A geochemical comparison between the Archean tonalites and the AYT. The Data in the AYT column are from the average of 5 AYT WR analyses (with -out 88115). The data in the AT column are from an average of 39 Archean grey gneisses, north of Laxford Bridge, Scotland (Tarney et al. 1979).

Table 4-2: A geochemical comparison between the compositions of the AYBA (88008B) and the average compositions of the Archean basalts of Condie (1985).

liquid or partial melting of metabasaltic rocks, in which process garnet and/or hornblende are residual minerals. Tarney et al. (1979) came to a similar conclusion except that they considered the the partial melting of a garnet amphibolite mafic source took place at a significant water pressure in depth. However, Weaver et al. (1979) recognised dacitic residual liquids, with similar geochemical features to the high-Al_2O_3 tonalite, which may be produced by high-level crystal fractionation.

Field observations suggest that the AYT is in close association with the AYBA. Limited geochemical data for the AYBA suggests some similarity to the Archaean basalts although its LREEs are enriched to some degree. An apparent parent-daughter relationship between these two can be accounted for either by partial melting of a deep-seated AYBA equivalent (e.g. underplate?), leaving hornblende and/or garnet in the residue or by fractionation of hornblende and/or garnet at depth. This is supported by their geochemical similarities of lower K,Rb, Rb/Sr, Ti and Nb and higher Zr/Nb (22--26). The field observations show that intermediate rocks, although present, are only of minor significance. Therefore, the ATBS may indicate a bimodal occurrence similar to the Archean basalt-tonalite suite and in this case, the partial melting model may be favoured.

However, both the AYT and the AYBA display some distinct features of their own. The major differences of the AYT from the Archaean tonalites are: (1). no Eu positive anomaly on the REE pattern; (2). stronger depletion in HFS element including Zr, Ti, Nb; (3). lower SiO_2, Na_2O and higher CaO, MgO, $Fe_2O_{3tot.}$.

The lack of Eu positive anomaly can be attributed to a combination of hornblende+ plagioclase fractionation at intermediate depths (Arth 1979) or fractionation of plagioclase at shallower depths during the process of magma upwelling. This is consistent with the presence of the well-zoned euhedral plagioclase phenocrysts in the AYT.

The lower Zr content rules out the possibility that the AYT is derived from fractionation of a mafic melt. Such an evolved melt always has a higher Zr content at the same SiO_2 content. This inference is also consistent with the bimodal occurrence suggested above. Certainly low Zr content can be related to magma composition such as low Ga/Al ratio and high Al_2O_3 (Collins et al. 1982; Price et al. 1983). If it is assumed that the Zr concentration is in equilibrium with the magma melt, a magma temperature of about 750°C is estimated using the experimental data of Watson and Harrison (1984). Such a temperature appears to be too low and inconsistent with the occurrence of

anorthoclase. The better alternative explanations are that the source was depleted in Zr and other HFS element before partial melting, or the low contents of the HFS elements are caused by partial melting dominated by residual hornblende (not garnet). The hornblende also retains HFS elements in addition to the HREE (e.g. Tarney et al. 1979; Pearce and Norry 1979). Residual hornblende also leads to less depletion in HREEs in the partial melt than does the garnet (e.g. Arth and Barker 1976).

The difference of the AYBA from the Archean basalts lies in its enriched REE pattern and even lower Rb/Sr ratios and Rb and Nb content. This may be related to a different tectonic setting such as a subduction-initiated spreading which will be further discussed later on.

The negative Eu anomaly may suggest a minor amount of plagioclase fractionation during the ascent of the magma. This suggestion is consistent with field and petrographic evidence.

In addition, the more mafic features of the AYT compared with the Archean tonalites may result from a higher degree of partial melting in the source region.

4.5 SUMMARY

(1). Geochemical features indicate that the ACAS is a high-level intrusion formed by fractional crystallization of clinopyroxene+ plagioclase (±hornblende) in the early stages, which is followed by precipitation of hornblende+plagioclase+magneitite (or ilmenite) in the later stages. The change occurs because of increasing oxygen and water fugacities in the residual magma as crystallization progresses.

(2). The AOLG and AOT are geochemically characterised by high Na_2O/K_2O, Sr, Ba, Low Rb and Rb/Sr. The more mafic types have high CaO, MgO, Fe_2O_{3tot}, Cr, Ni, Sc and V. They may be related by crystal fractionation of initially plagioclase+hornblende which is followed by precipitation of increasing feldspar+biotite.

(3). The AMG may be geochemically unrelated to the older granites and was formed by fractional crystallization of a minimum-liquid magma (i.e. restite nearly free) which was derived from low degrees of partial melting at a supracrustal level. It is geochemically similar to the Tasmanian Lottah Granite (Mackenzie et al. 1988) and the syn-collisional peraluminous leucogranite defined by Harris et al. (1986).

(4). The AYT has distinct geochemical features such as high Al_2O_3, CaO, MgO, Fe_2O_{3tot},

Sr and Ba and low Zr, Ti, Y and Nb. It also has a fractionated REE pattern, with HREE depletion, which is quite similar to high-Al_2O_3 type Archean tonalites and trondhjemites. Limited geochemical data also suggest some similarity between the AYBA and the Archean basalts. An association of the AYT with the AYBA manifests a bimodal basaltic-tonalitic magmatism typical in the Archean terrains. Some distinction from the Archean suite indicates that the ATBS may be related to slightly different tectonic setting which will be further discussed later on.

CHAPTER FIVE: GEOCHRONOLOGY AND ISOTOPE GEOLOGY

5.1 INTRODUCTION

U-Pb isotope analyses of zircons and sphenes have been made on the quartz diorite of the ACAS, the AOLG and AYT, respectively. Rb-Sr isotope analyses of whole rocks and mica have been carried out on a selection of AMG, AYT, ACAS and BSA samples. The analytical procedures are outlined in the Appendix-1 and the analytical results shown in Table 5-1 and Table 5-2, respectively.

5.2 PREVIOUS ISOTOPIC WORK IN THE ARUNTA INLIER AND THE PURPOSE FOR THIS STUDY

A group of Sm-Nd isochron data for the Division One granulites (both mafic and felsic) from the central Arunta Inlier has revealed an imprecise crust formation age of around 2000 Ma (Black and McCulloch 1984; Windrim and McCulloch 1986). However, McCulloch (1987) considered that the depleted mantle model ages of 2100 - 2200 Ma for some rocks which have been used for defining the "ischrons" were better dates of the crustal formation episode. It was concluded that a process of mantle underplating was involved.

A great number of Rb-Sr isochron analyses have been carried out in Arunta Inlier (see Black et al. 1983; Stewart et al. 1984) with the oldest age result at about 1820±78 Ma (modified using $\lambda_{87Rb}=1.42 \times 10^{-11}yr^{-1}$)(Iyer et al. 1976). However, these ages have a large uncertainty and are difficult to interpret because the Rb-Sr isotopic system can be easily affected by multi-stage metamorphism and deformation (Black et al. 1978,1979). So far, no crystallization ages of igneous rocks have been clearly defined by the Rb-Sr system in the Arunta Inlier. But these works have been interpreted as several deformational and metamorphic events, i.e. Strangways Event (1800- 1750 Ma), Aileron Event (1700 - 1600 Ma), Anmatjira Event (1500 - 1400 Ma), Ormiston Event (1050 - 900 Ma) and Alice Springs Orogeny (400 - 300 Ma) (Black et al. 1983).

Reconnaissance ^{40}Ar-^{39}Ar study undertaken by Allen and Stubbs (1982) also defines isotopic disturbance events without a tectonic framework to fit them into.

Some Rb-Sr whole rock isochron ages for rocks from the Atnarpa Igneous complex have also been reported previously. They are 1651±47 Ma ($I_{Sr}=0.705\pm0.001$) by Black et al. (1983),

1674±50 Ma (I_{Sr}=0.705) by Bennett (in Cooper et al. 1971) and 1683±23 Ma (I_{Sr}=0.705) by Armstrong and Stewart (1975) assuming $\lambda_{87Rb} = 1.42 \times 10^{-11} a^{-1}$. Black et al. (1983) considered the 1651±47 Ma age was either a minimum crystallization age of the AIC or a record of a subsequent deformation or/and metamorphism episode named the Aileron Event. The date by Armstrong and Stewart (I975) was considered as recording intensive progressive regional metamophism of the preexisting basement.

Several Sm-Nd, Rb-Sr and K-Ar isotopic study of minerals have also been undertaken on rocks from Strangways and Harts Ranges as well as the Altunga Nappe Complex (e.g. Windrium and McClulloch 1986; Mortimer et al. 1987; Armstrong and Stewart 1975; Stewart 1971a). The data were used to assess the thermal and deformational history of the Arunta Inlier. e.g., Windrim and McCulloch (1986) suggested that the Arunta Inlier had experienced a prolonged period of isobaric cooling followed by significant uplift at 1,000 Ma. Armstrong and Stewart (1975) concluded that the Arltunga Nappe Complex was formed during the Phanerozoic Alice Springs Orogeny.

By comparison, there are only a few U-Pb isotopic studies in the Arunta Inlier. Some zircon ages have been reported at around 1767-1730 Ma for Entia gneiss, Entia amphibolite and Bruna gneiss in the Harts Ranges Area (Cooper et al. 1988, Mortimer et al. 1987). No data similar to the age of Barramundi Association (e.g. Page 1988) have yet been reported.

Therefore, the reason for this isotopic study, including zircon U-Pb age determinations on three rock units and a few Rb-Sr istopic analyses, are:

(1).To find the oldest igneous rocks in the in the study area and relate them to those elsewhere;

(2).To clarify the crystallization ages of the AIC to assist in understanding the magmatic evolution and crustal growth in the region;

(3).To test the thermal history in the Atnarpa Area;

(4).To further test the degree of the effect of the Alice Springs Orogeny on the basement Arunta Inlier.

5.3 U-Pb ZIRCON GEOCHRONOLOGY FOR THE ACAS

5.3.1 DESCRIPTION

About 30 kg of quartz diorite sample has been collected from the ACAS at locality A (see enclosed map and Appendix-2) where a relatively bigger outcrop occurs here beside Atnarpa Creek and fresher material is available for sampling.

Abundant zircon grains were extracted from the quartz diorite (87064). These are predominantly euhedral to fragmented, glassy and transparent. Euhedral magmatic zoning is well developed but no rounded older cores with overgrowth have been observed. The least magnetic fractions are composed of purple-coloured, glassy, transparent, short prismatic crystals (about 80-90% with L/W ratio=I.5-2.5) and some droplet-shaped and long prismatic grains (10-20%). The most magnetic fractions consist of straw-coloured, short prismatic grains, with some containing opaque inclusions. The inclusion-bearing grains have been removed by hand-picking before dissolution. All the six fractions have been air abraded using the method suggested by Krogh (1982).

5.3.2 RESULTS

Six selected zircon fractions were analysed. The results are displayed in Table 5-1 and Fig.5-1A. Three least magnetic fractions have only a restricted range of low U contents (273-291 ppm) and are only minimally discordant (<10%). The three most-magnetic fractions contain slightly higher U contents (428-499ppm) and are more discordant. The six fractions define a discordia and with an upper intercept age of 1879$\pm$11/10 Ma and lower intercept age of 199$\pm$62 Ma. The high MSWD of 28.37 suggests some minor disturbing influence.

5.3.3 DISCUSSION

This slightly discordant pattern for such a clearly magmatic rock suggests that the upper intercept records the crystallization age and the low intercept an time of episodic partial Pb loss. This simple history for this rock is supported by the excellent negative correlation of U with $^{206}Pb/^{238}U$ apparent age (e.g. Ludwig and Cooper 1984) (Fig. 5-2A). Field evidence indicate that the quartz diorite usually has some microdioritic amphibolite xenoliths. But both petrographic and

geochemical evidence indicate they are comagmatic. Nevertheless, the reasonable ±11 Ma error combined with the near concordant pattern and general absence of older cores still indicate the upper intercept probably represents a crystallization age.

The quartz diorite crosscuts both fine-grained amphibolites and the mafic member of the coarse-grained ACAS. Therefore, the 1879±11/10 Ma date is considered to be a minimum crystallzation age of the ACAS.

5.4 U-Pb ZIRCON AND SPHENE GEOCHRONOLOGY FOR THE AOLG

5.4.1 DESCRIPTION

About 30 kg of foliated leucogranite sample has been collected from the AOLG at locality B (Appendix-2). This is at the intersection of a small creek and recently made private road and the outcrop is reasonably fresh. A well-defined fabric including foliation and lineation can be seen on the outcrop.

Only a small amount of zircon and sphene was obtained from this sample. Most zircon grains are euhedral to fragmented, transparent crystals. The least magnetic fractions are purple-coloured, glassy and short-prismatic. Some of the larger grains are translucent, a condition which is usually caused by cracks. The most magnetic fractions are straw or brown coloured, transparent and normally have opaque inclusion, but some grains are milky or translucent. All the inclusion-bearing grains and most milky grains were handpicked out before dissolution.

Two fractions of brown-coloured, transparent sphene were also separated and analysed.

All fractions were air abraded before dissolution.

5.4.2 RESULTS

The six zircon fractions have variable U contents ranging from 402 ppm for the least magnetic one to 1009 ppm for the most magnetic one. They fall on a discordia with MSWD=13.32 which intercepts with concordia at 1873±11/10 Ma and 273 ± 27 Ma (Fig. 5-1B). Fraction 5c is the point most displaced from the discordia. If the other five points are regressed alone, the MSWD is reduced to 9.27 with little change in intercepts (1872±11 Ma and 265±32 Ma)

The two sphene fractions display a peculiar discordant pattern in plotting above the zircon

discordia (Fig.5-2C). If the lower intercept of the zircon is used, a reference age of 1732 Ma is obtained. The average $^{207}Pb/^{206}Pb$ age of the two sphenes (which is equivalent to a zero age lower intercept) is 1703 Ma.

5.4.3 DISCUSSION

As no apparently inherited zircons have been observed and the U content is well correlated with $^{206}Pb/^{238}U$ apparent ages (Fig 5-2A), the upper intercept of 1873±11/10 Ma is considered to record the crystallization of the older leucogranite. This age is indistinguishable, within experimental error, from that of the quartz diorite.

The position of the two sphene points to the left of the zircon discordia was unexpected. U-Pb analyses of sphene usually fall on the concordia which records either primary crystallization age or a secondary disturbance such as metamorphism (e.g. Tilton & Grunenfelder 1968; Scharer & Krogh 1986; Corfu & Grunsky 1987). Discordant sphene has been reported but is very rare (Tucker et al. 1986/87).

Petrographic evidence indicates that sphene in the AIC is usually secondary and metamorphically replaces hornblende and biotite. For this reason, the 1732 Ma (or 1703 Ma) sphene age may represent the subsequent metamorphism. However, as discussed later on, the younger reported Rb-Sr isochron dates of about 1670 Ma may more reasonably record the extensive amphibolite grade metamorphism. A more likely alternative is that the sphene concentrates are a mixture of primary and secondary sphenes because petrography cannot discriminate the later metamorphic sphenes from any primary cores. Hence, the 1732 Ma (or 1703 Ma) does not represent a geological event.

5.5 U-Pb GEOCHRONOLOGY OF THE AYT

5.5.1 DESCRIPTION

Samples were collected from two very close localities (C and D) (see Appendix-2) along recently made private roads where outcrops are massive and fresh.

Only a little zircon was extracted from the small sample (87001) collected in 1987. This was supplemented by a larger sample collected in 1988. Overall, most zircon grains are euhedral to

fragmented, glassy, transparent and short prismatic (L/W=1.5-2.5). Euhedral zoning is also developed. The least magnetic fractions are predominantly purple-coloured like those in the quartz diorite and granite but not as transparent as those in the later. The transparency decreases with increasing grainsize. Overgrowths with rounded cores can be discerned in some of the largest grains under the binocular microscope. The most magnetic fractions are straw-coloured, more transparent and euhedrally-zoned. Two of the eight fractions from sample 87001 (Zr-1 and 2) and all five fractions from sample 88002 were air abraded.

5.5.2 RESULTS

The analytical results are displayed in Table 5-1 and Fig. 5-1D. All the 13 fractions cover U contents ranging from 429-964 ppm and are more discordant than the zircon fractions from the AOLG and ACAS samples (Fig. 5-1).

They scatter about a discordia line with MSWD=66.82 and calculated intercepts with concordia of 1768±17/16 Ma and 187±47/46 Ma. The rejection of the coarser, non-air abraded fraction 2 (87001) produces a better-fit regressed line with MSWD=40.75 and intercepts at 1762±15/14 Ma and 176±40 Ma. The fractions 3A (87001) and 3A (88002) are also of larger grainsize, and displaced to the right of the discordia. If all three of the above-mentioned fractions are rejected, the remained 10 analyses define a even better discordia with MSWD=19.41 and intercepts of 1751±12 Ma and 158±30/31 Ma.

5.5.3 DISCUSSION

Correlations of U with $^{206}Pb/^{238}U$ age are more scattered for the tonalite than for the quartz diorite and leucogranite (Fig. 5-2B). But the abraded fractions have generally better correlations than the non-abraded ones, indicating that the outer parts of the zircon grains have more disturbed U-Pb isotopic system. However, abraded fractions Zr-1 and Zr-2 of 87001 (more than 50% of material removed by air-abrasion) were subsplit from non-abraded fractions 3A and 4A of 87001, respectively. As can be see from the discordia (Fig.5-1D) and Table 5-1, the abrasion has not significantly reduced the degree of discordance.

Field observations indicate that there are a few undissolved felsic xenoliths (fined-grained ACAS?) exposed in some outcrops. This, combined with the presence of rounded cores in some

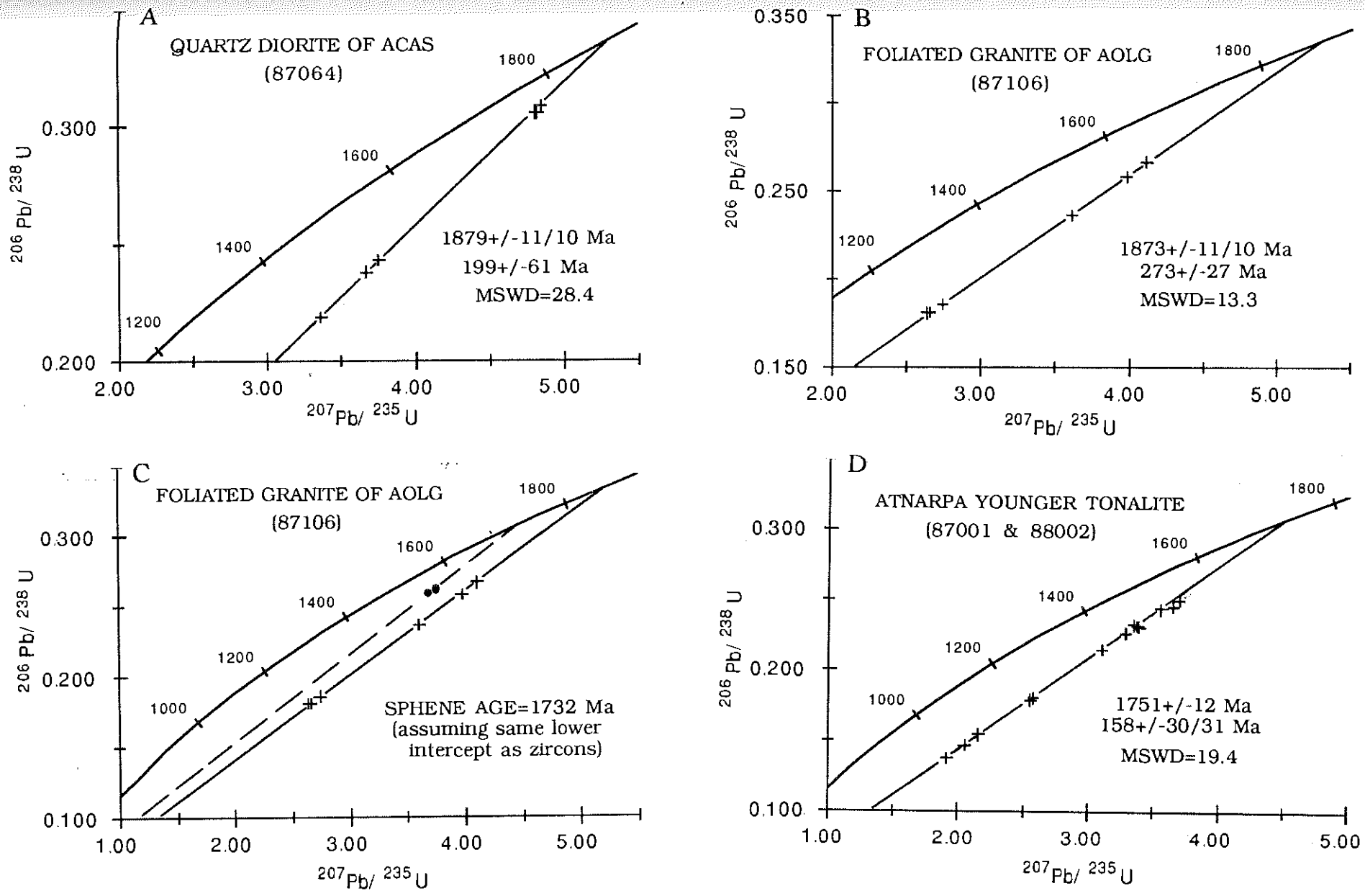

Fig. 5-1. $^{206}Pb/^{238}U$ versus $^{207}Pb/^{235}U$ concordia diagrams for fractions of zircon (+) and sphene (•) from representative samples of the Atnarpa Igneous Complex.

Table 5-1: U-Pb isotopic data from rocks of the Atnarpa Igneous Complex in the Atnarpa area. M and NM mean magmetic and non-magnetic, respectively, and the numbers following are the dip angles of the Frantz separator running at 1.8 amps for zircon and 1.2 amps for sphene. HP=hand-picked. The 206Pb/204Pb ratio is as measured, the other isotopic ratios include radiogenic Pb only.

fraction	Size (microns)	Magnetic response	Weight (mg)	U (ppm)	Pb (ppm)	Atomic ratios					Aparent ages (Ma)		
						206Pb/204Pb	206Pb/208Pb	206Pb/238U	207Pb/235U	207Pb/206Pb	206Pb/238U	207Pb/235U	207Pb/206Pb
Meta- quartz diorite of the ACAS (87064)													
2A	142-105	NM -1	8.95	280	94	4857	6.464	0.30538	4.8248	0.11459	1718	1789	1873
3A	105-75	NM -2.5	9.33	291	97	5015	6.660	0.30538	4.8102	0.11424	1718	1787	1868
4A	75-63	NM -1	8.60	273	91	7970	6.977	0.30853	4.8484	0.11398	1733	1793	1864
4C	75-63	M 1	5.66	499	128	692	4.946	0.21835	3.3608	0.11163	1273	1495	1826
5B	63-53	M 1	6.62	439	114	5784	6.413	0.23778	3.6703	0.11195	1375	1565	1831
6B	53-45	M 1	9.00	428	116	1717	5.841	0.24286	3.7527	0.11207	1402	1583	1833
Foliated granite of the AOLG (87106)													
23A	250-105	NM 1 & HP	2.81	424	110	3033	6.328	0.23630	3.6102	0.11081	1367	1552	1813
4A	105-75	NM 0	6.69	402	118	1047	5.681	0.25808	3.9810	0.11188	1480	1630	1830
5A	75-63	NM -0.5	4.42	387	113	3276	6.522	0.26661	4.1132	0.11189	1524	1657	1830
5C	75-63	M 3.5	5.29	864	169	2861	6.808	0.18064	2.6400	0.10623	1068	1312	1736
6B	63-53	M 3	3.13	799	162	2122	6.661	0.18553	2.7420	0.10719	1097	1340	1752
7B	53-45	M 3	10.08	1009	199	2257	6.725	0.18084	2.6584	0.10663	1072	1317	1743
SPHENE-1	75-105	NM 7	15.14	124	41	242	3.545	0.25807	3.6984	0.10394	1480	1571	1696
SPHENE-2	75-105	M 10	26.63	132	45	306	3.449	0.26090	3.7685	0.10476	1494	1586	1710
Atnarpa Younger Tonalite (87001)													
2	142-105	HP	3.52	429	119	845	5.801	0.24590	3.6527	0.10773	1417	1561	1761
3A	105-75	NM 0.5	9.62	551	140	2288	6.406	0.23097	3.3908	0.10647	1340	1502	1740
4A	75-63	NM 0.5	8.89	639	163	2728	6.243	0.23183	3.3817	0.10579	1344	1500	1728
4B	75-63	M 3.5	3.37	573	115	1242	5.788	0.17891	2.5571	0.10366	1061	1288	1691
5B	63-53	M 3	3.43	908	158	1021	5.595	0.15405	2.1557	0.10149	924	1167	1652
6	53-45	HP	9.11	763	154	1627	5.774	0.18031	2.5750	0.10358	1069	1294	1689
ZR-1	105-75	M0.5, NM1	6.69	565	140	3058	6.567	0.22670	3.2933	0.10536	1317	1479	1721
ZR-2	75-63	M0.5, NM1	5.90	638	150	3291	6.388	0.21496	3.1073	0.10484	1255	1434	1711
Atnarpa Younger Tonalite (88002)													
3A	105-75	NM -0.5	6.70	458	128	1559	5.983	0.25035	3.6977	0.10712	1440	1571	1751
4A	75-63	NM -0.5	7.00	519	133	2309	6.080	0.23266	3.3525	0.10451	1348	1493	1706
4C	75-63	M6, NM7.5	5.26	824	135	1299	5.568	0.14639	2.0513	0.10163	881	1133	1654
5A	63-53	NM -0.5	6.38	507	137	2957	5.942	0.24394	3.5611	0.10588	1407	1541	1730
5C	63-53	M6.5, NM8	6.74	944	146	1150	5.409	0.13731	1.9119	0.10099	829	1085	1642

zircon grains and more scattering on the U-$^{206}Pb/^{238}U$ apparent age diagram, suggests a more complex U-Pb system in the AYT. However, most zircon grains in AYT are uniform, euhedral and display euhedral zones. This suggests magmatic features are predominant. The age may be insignificantly biased by a few grains of older (possibly 1879 Ma) inherited zircons. This is indicated by the consistent bias to older ages in the fractions with larger grainsize. For this reason, fractions 2 & 3A of 87001 and fraction 3A of 88002, which have larger grainsize and cause larger deviations (to older age), are rejected. The age 1751±12 Ma is a better estimate for the crystallization age of the AYT.

5.6 GENERAL DISCUSSION AND SUMMARY ON U-Pb GEOCHRONOLOGY

As has been demonstrated, the AIC falls into two age groups. The ACAS was intruded not later than 1879±11/10 Ma which, is closely followed by the emplacement of the AOLG at 1873±11/10 Ma. The AOT was dated by Sando (1987) at 1863±31 Ma which is indistinginshable within experimental error from the 1873±11/10 Ma age. This 1870-1880 Ma magmatic event is comparable to the early stage of the Barramundi Orogeny as suggested by Etheridge et al. (1987) and Page (1988).

The AYT is substantially younger. It was emplaced at 1751±12 Ma, which is slightly younger than the age of Entia gneiss (1767±2 Ma) but indistinguishable within experimental error from the age of Bruna gneiss (1747±3/2 Ma) in the Harts Range area (Cooper et al. 1988; Mortimer et al. 1987). The 1770-1730 Ma (Cooper et al. 1988) marks the second magmatic event in the southeastern Arunta Inlier.

The 1873 and 1879 Ma ages are the oldest crystallization ages currently known in the Arunta Inlier.

5.6 Rb-Sr GEOCHRONOLOGY

5.6.1 INTRODUCTION

A group of whole rocks and mica Rb-Sr isotopic analyses have been carried out in order to constrain the deformational and thermal history of the eastern Arunta Inlier.

5.6.2 Rb-Sr WR GEOCHRONOLOGY OF THE AMG

An attempt to date the zircon U-Pb age of the AMG has failed because of small yield of zircons and apparently complex history (obviously two generations of zircons) which cannot be analysed on the TSN-206S mass-spectrometer currently available in Adelaide. Therefore, 5 whole rock samples have been analysed for Rb, Sr isotopes.

The analytical results are displayed in Table 5-2 and Fig. 5-3A, C. 5 WR samples cover a good $^{87}Rb/^{86}Sr$ ratio range but scatter about an isochron to produce an imprecise model III age of 1627 ± 164 Ma with $I_{Sr}=0.706\pm0.026$ and MSWD=35.97 ($\lambda_{87Rb}=1.42 \times 10^{-11}$ a^{-1}). Sample 88099 is more strongly sheared and altered. Not surprisingly, it plots farthest away from the isochron (e.g. Etheridge and Cooper 1980). By rejecting this sample, the remainder yields a better fit isochron with MSWD=2.96 and a model II age estimate of 1563 ± 108 Ma with $I_{Sr}=0.720\pm0.016$.

5.6.3 Rb-Sr MICA GEOCHRONOLOGY OF THE AYT, AMG, ACAS & BSA

Four WR-mica pairs from the AYT, the AMG, the metadiorite of the ACAS and muscovite gneiss of the BSA are analysed for Rb-Sr isotopes, respectively. The results and weighted isochron ages are displayed in Table 5-2 and Fig. 5-3B,D.

5.6.4 DISCUSSION

In general, Rb, Sr isotopic systematics are dependent on thermal, chemical and dynamic factors and sampling size or a combination (Etheridge and Cooper 1980; Black et. al 1979; Ovchinnikov et al. 1987; Harrison and McDougall 1980; Hofmann 1979). Orchinnikov et al. (1987) used experimental data to demonstrate that Rb and Sr have very high migrational capacities in geochemical processses owing to low activation energies (about 42 KJ/mole). They also emphasized that this is the main difference of Rb-Sr systematics from K-Ar and U-Pb systematics. Black et al. (1979) indicated that Rb and Sr diffusion is likely to be enhanced by the development of a penetrative schistosity which involving processes such as dislocation generation and migration, grain-boundry sliding migration. This may be further enhanced by high partial pressures of the fluid phase. Etheridge and Cooper (1980) has recognised substantial disturbance on Rb-Sr isochrons by a meteoric fluid in just a low-temperature green-schist grade shear zone.

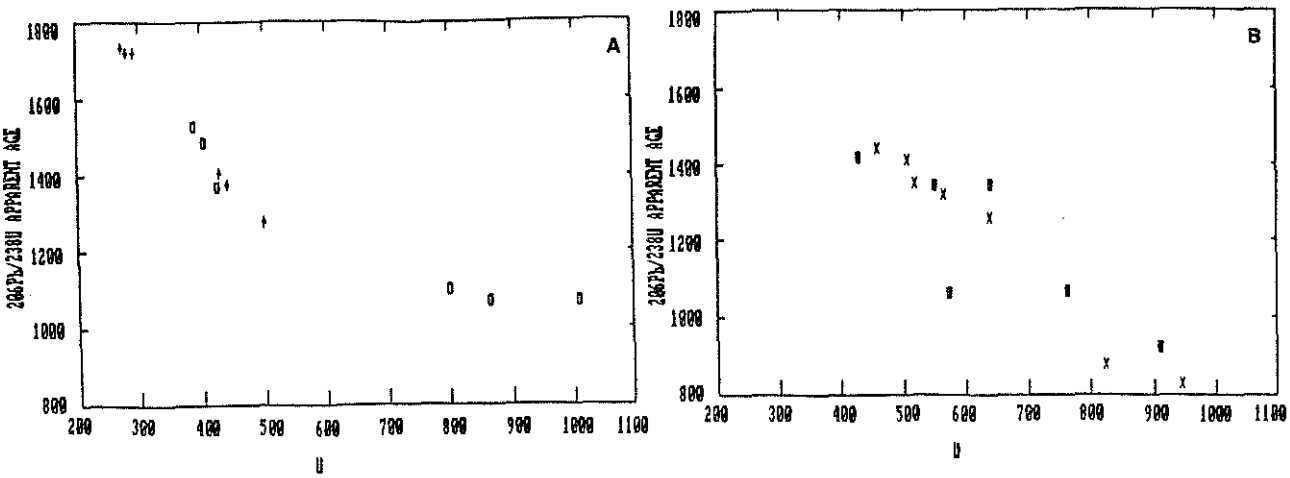

Fig.5-2. (A). $^{206}Pb/^{238}U$ apparent age versus U ppm diagrams for the zircon fractions from ACAS (87064) and the AOLG (87106). Cross= 87064. Empty box=87106. (B).$^{206}Pb/^{238}U$ apparent age versus U ppm diagram for the AYT (87001 & 88002). Filled box=non-air abraded. x=air abraded.

Table 5-2: Rb-Sr isotopic data for samples from the study area

Sample Name	Rb (ppm)	Sr (ppm)	Rb/Sr	87Rb/86Sr	87Sr/86Sr
Muscovite Granite					
88090 WR	163	46	3.54	10.426	0.95500
88093 WR	157	50	2.63	7.754	0.89294
88094 WR	183	34	5.38	15.92	1.07400
88097 WR	185	40	4.61	13.76	1.03015
88099 WR	166	91	1.83	5.354	0.82520
88090 MUSCOVITE	619	8	77.2	327.44	5.45820
Muscovite Gneiss					
87052 WR	48.5	164.6	0.295	0.8542	0.72815
87052 MUSCOVITE	287	32	8.97	27.490	1.30630
Foliated Metadiorite (ACAS)					
87100 WR	26.9	289	0.093	0.2699	0.71072
87100 BIOTITE	163.4	53.9	3.03	8.887	0.84896
AYT					
88002 WR	52.3	551	0.095	0.2749	0.70859
88002 BIOTITE	260	20	12.86	40.280	1.55190

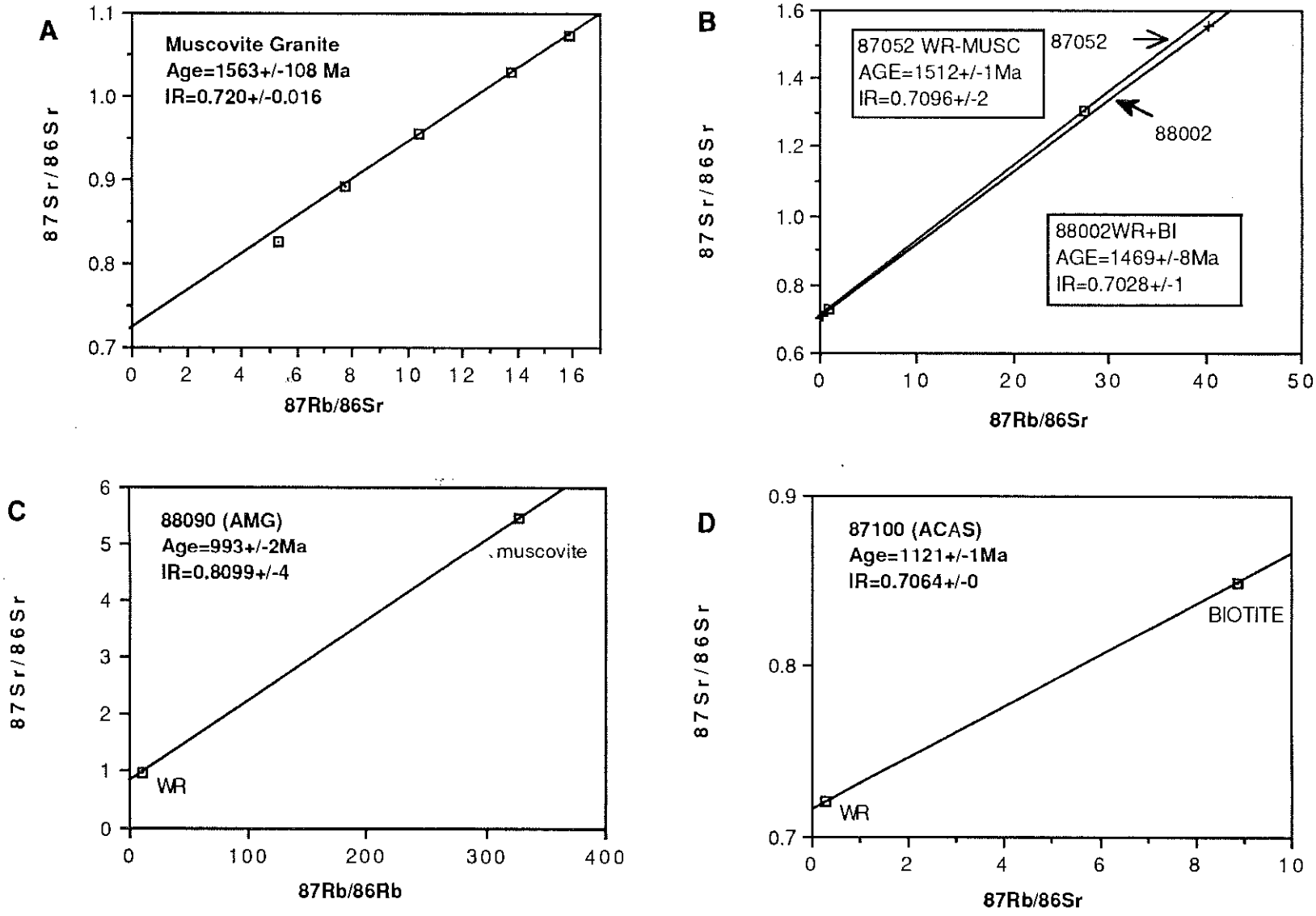

Fig. 5-3. Rb-Sr isochron diagrams for whole rocks and whole rock-mica pairs from the study area.

This, in fact, points to the predominance of geochemical processes over thermal processes in resetting Rb-Sr isotopic systematics. Therefore, Rb-Sr WR isochron ages for magmatic rocks from poly-deformed and metamorphosed terrains which involved all the above mentioned processes, are usually less than the crystallization ages defined by zircon U-Pb systematics (Page 1978; Van Schmus et al. 1987).

Previous Rb-Sr isochron studies on the AIC produced three consistent age results averaged at 1670 Ma (λ_{87Rb}=1.42 x $10^{-11}yr^{-1}$) with $^{87}Sr/^{86}Sr$ initial ratios=0.705 (e.g. Armstrong and Stewart 1975; Bennett in Cooper et al. 1971; Black et al. 1983). This is about 11% younger than our U-Pb zircon ages for the ACAS and AGB. The same phenonmen has been reported by Page (1978) for the low grade metamorphosed Kalkadoon-Leichhardt association from the Mt. Isa Inlier which have similar U-Pb zircon ages to the AOLG & AOT. In contrast, some Rb-Sr isochron ages for the high-grade metamorphosed Archean granulites from Antarctica were reported to be unusually older than the U-Pb zircon ages (e.g. Black et al. 1986). All these observations may be related to the nature of the Rb-Sr isotopic systematics. It may point to the possibility that Rb-Sr isotopic systematics is more easily reset by geochemical processes than thermal factors as discussed in the first paragraph. If it is the case, the 1670 Ma age could be a record to the regional deformation and lower amphibolite facies metamorphism, refered to Black et al. (1983) as the Aileron Event.

The imprecise 1563±108 Ma cannot be distinguished within error from the age of the Aileron Event. The slightly younging and large error suggest the subsequent hydrothermal disturbance probably during the development of the Illogwa Schist/Shear Zone in addition to the effect of the Aileron Event. Therefore, the crystallization age for the AMG must be older than this date.

It is surprising that all the four mica-WR pairs yield Precambrian ages, in contrast with many other Rb-Sr isotopic results which point to Phanerozoic age of the Alice Springs Orogeny (Armstrong and Stewart 1975; Iyer et al. 1976; Mortimer et al. 1987; Windrim and McCulloch 1986). This phenomenon may be related to the fact that the rocks in the study area were buried at shallower depths than those in the Strangways and Harts Ranges where Palaeozoic mica ages were commonly obtained.

Generally, the closing temperatures for muscovite and biotite Rb-Sr isotopic systems are

considered to be about 500°C and 320°C respectively in thermal-factor dominated cooling terrains (e.g. Wagner et al. 1977; Harrison and McDougall 1980). Muscovite grains in the muscovite gneiss are very fresh and almost inclusion and alteration-free (Plate 3-3.8). Therefore, the 1512±1 Ma is explained as the age when the terrain in Atnarpa area cooled to 500°C. Similarly, biotites in the AYT are very fresh and flaky, so the 1469±8 Ma is considered as a date when the terrain cooled to 320°C. Such a large cooling gradient is not consistent with the normal isobaric cooling model as defined by Warren (1983) and Warren and Wyborn (1988) in the northern Strangways Range, although it would not be unusual in other magmatic situations. However, this ages are in accordance with the relatively extentive magmatic event (~1500 Ma) in central Australia recognised by zircon U-Pb isotopic studies (Page 1988; Wyborn et al. 1988) and the metamorphic and deformational event, namely Anmatjira Event (1500--1400 Ma) of Black et al. (1983). This fast cooling event is likely to be caused by either a crustal uplift or reheating of the previously cooled terrain by a thermal-magmatic activity, e.g. at around 1500 Ma (Page 1988; Wyborn et al. 1988). If it was caused by a crustal uplift, a removal of about 7 km thick sequence is needed (assumung geothermal gradient of $25^{o}km^{-1}$).

The biotite age for sample 87100 (1121 Ma), a foliated diorite from the contact between the diorite and quartzofeldspathic gneiss is much younger than the biotite age for the AYT (1469 Ma)(Fig 5-3D). The biotite grains in 87100 are much smaller and brown-coloured and have undergone strong chlorite and epidote alteration. The explanation given by Armstrong and Stewart (1975) for such results is that the Rb-Sr systematics in this biotite was partially reset during a later stage hydrothermal alteration (e.g. during the Alice Springs Orogeny) and the age 1121±1 may be a mixed age and therefore geologically meaningless. Similarly, the 993±2 Ma muscovite age for sample 88090 from the AMG could also be attributed to partial resetting as the AMG has been mylonised and partially altered. These two mica ages are comparable to the Rb-Sr mica ages for the "unaltered basement" within the White Range Nappe dated by Armstrong and Stewart (1975).

However, Windrim and McCulloch (1986) have argued for significant uplift of the Arunta Inlier in the Strangways Range area occurred at about 1000 Ma based on their Rb-Sr isotopic and Al_2SiO_5 barametry data. This arguement supported by ages of between 980 and 1080 Ma for deformational and intrusive events obtained by Allen and Black (1979) and Black et al. (1983). Ding et al. (in prep.) also argue, based on their detailed stratigraphic and structural work, that the

Arltunga Nappe Complex and its major thrust, the Illogwa Schist/Shear Zone was produced during late Precambrian. Shaw et al. (1984) suggested that a metamorphism and deformation took place along the Weldon Tectonic Zone, where the Arltunga Nappe Complex is located, at 1050--900 Ma. This event is named the Ormiston Event by Black et al. (1983), and caused local amphibolite facies metamorphism in the Southern Province. Therefore, it is likely the greenschist alteration in the AIC may have occurred during this event. If it is the case, the ages defined by the altered micas may roughly be attributed to it. It is possible that these consistent arguements may just point to the initiation and development of the Amadeus Basin during that period. A long-lived isobaric cooling model (about 1500 Ma) would make it difficult to understand the formation of this widespread Late Precambrian depositional basin although Warren & Stewart (1988) thought that the effect of the formation of this basin to their isobaric cooling model was negligible.

The previously reported Phanerozoic ages dated by Rb-Sr and K-Ar isotopic systematics of mica and other minerals from the Arltunga Nappe Complex were strictly confined to within the strongly retrograded shear zones, especially within the boundary between the basement rocks and the Amadeus sequence (e.g. Armstrong and Stewart 1975; Stewart 1971a). Field observations by the present author indicated that sample localities 39 and 40 of Armstrong and Stewart (1975) were situated in the area where the rocks (including the tonalites and Heavitree Quartzite) have been strongly sheared and even "sliced". It is from this area that the samples of Armstrong and Stewart (1975) were collected that gave Phanerozoic ages by the Rb-Sr isotopic systematics of their WR-mica pairs. This area is now recognised to be transected by the Illogwa Schist/Shear zone, a division line between the Arunta Basement and Amadeus Basin Cover according to Ding et al. (in Prep.). Two older WR-mica Rb-Sr ages (899 Ma and 1121 Ma assuming $\lambda_{87Rb}=1.39 \times 10^{-11}a^{-1}$) of Armstrong and Stewart (1975) were yielded by the samples they collected from the localities slightly away from the shear zone. Therefore, the extent to which the Alice Springs Orogeny affected rocks in the study area and even the formation history of the Arltunga Nappe Complex must be suspect and needs further investigation.

The WR specimen of the AYT is selected from the same block of rock which yielded the zircon separates. Using the one sample available, the calculated $^{87}Sr/^{86}Sr$ initial ratio at 1751 Ma, the zircon age, is about 0.7017. Petrographic evidence indicate that the AYT has an obvious magmatic texture and the metamorphic overprint is less significant. Therefore, the low initial ratio

may be a reflection of the nature of the primary magma, suggesting either little crustal prehistory or an obvious mantle-derived feature.

The $^{87}Sr/^{86}Sr$ initial ratios of 0.705 yielded from the Rb-Sr isochrons with age averaged at 1670 Ma (Armstrong & Stewart 1975, Black et al. 1983; Cooper et al. 1971) are also very low. Assuming that the regional metamorphism only caused Rb, Sr distribution, then the $^{87}Sr/^{86}Sr$ initial ratio at 1870--1880 Ma crystallization age will be even lower. Warren and McCulloch's Nd isotopic data for the AIC also suggest a strongly depleted mantle source and little crustal prehistory if no REE disturbance has occurred since its formation (Pers. Comm.). The Sr and Nd isotopic data are therefore consistent with each other.

5.7 SUMMARY AND CONCLUSION

The Arunta Inlier in the Atnarpa area has experienced a complex deformational, metamorphic, magmatic and thermal history based on isotopic constraints.

The oldest magmatic event when most of the AIC formed, was dated between 1870--1880 Ma, which is consistent with the early stage of the Barramundi Orogeny in the central Australian Terrains. These dates are the oldest crystallization ages of igneous rocks so far known in the Arunta Inlier.

The AYT was emplaced at 1751±12 Ma, which is only slightly younger than the the crystallization age of the Entia gneiss (1767±2 Ma). This is also comparable to the extensive magmatic event between 1770--1730 Ma recognised in the eastern Arunta Inlier and other Proterzoic terrains (e.g. Cooper et al. 1988; Page 1988).

The subsequent deformation and amphibolite grade metamorphism is dated between 1652--1683 Ma, probably part of the well-documented Aileron Event which occurs extensively in the central Australian terrains.

A fast cooling event occurred between 1512 Ma and 1469 Ma when the temperature dropped from 500°C to below 320°C. This seems in-consistent with the isobaric cooling model of Warren (1983). In contrast, it is likely to be caused by a crustal uplift (up to 7 km) or reheating of the previously cooled terrain by a thermal-magmatic activity, e.g. at about 1500 Ma (Page 1988; Wyborn et al 1988).

The 1100--1000 Ma mica Rb-Sr ages may either record a magmatic, deformational and

hydrothermal event or represent the result of Rb-Sr partial resetting during the Alice Springs Orogeny. The former possibility is broadly consistent with the suggestion of the crustal uplift around 1000 Ma by Windrim and McCulloch (1986), the structural study of Ding et al. (in prep.) and the dates of the local amphibolite grade metamorphic event in the Southern Province (Shaw et al. 1984). It is worthwhile to note that the initiation and development of the Amadeus Basin may occur at around 1000 Ma.

The extent of the effect of the Alice Springs Orogeny on the study area must be suspect as the Phanerozoic mica ages are only confined to the rocks in the strongly sheared and altered schist zones, especially within the boundary between the Arunta basement and Amadeus cover.

All these Precambrian Rb-Sr mica ages suggest that the rocks in the study area was buried at shallower depths than those in the Strangways and Harts Ranges area, where Phanerozoic Rb-Sr mica age were commonly obtained.

Isotopic constraints also indicate that the thermal evolution in the study area is typically episodic, instead of being featured by isobaric cooling as suggested by Warren (1983) and Warren & Wyborn (1988) for the northern Strangways Range.

Low $^{87}Sr/^{86}Sr$ initial ratios for both older AIC and AYT combined with Warren and McCulloch's Nd data demonstrated that the AIC may be directly involved in a depleted mantle source without significant crustal prehistory.

CHAPTER SIX: COMPARATIVE STUDIES

6.1 INTRODUCTION

There are two main hypotheses concerning the tectonic style and the crustal evolution of the central Australia Proterozoic terrains. They are the rift-related, extension-dominated mechanism (e.g. Etheridge et al. 1987) and the subduction-related extension-compression-paired mechanism (e.g. James & Ding 1988; Foden et al. 1988). Both schools have outlined their geochemical constraints which can be analogous to the well-defined Phanerozoic and modern tectonic settings, respectively. This chapter examines the features of the Atnarpa Igneous Complex and its tectonic setting in relation to the above hypotheses.

6.2 GEOCHEMICAL COMPARISON TO THE BARRAMUNDI IGNEOUS ASSOCIATION AND POST-BARRAMUNDI INTRUSIONS

The Barramundi igneous association is dominated by granites and comagmatic volcanics (SiO_2 60--78%). These have been identified in the Halls Creek, Pine Creek, Tennant Creek, Arunta and Mt Isa Inliers with U-Pb zircon ages ranging from 1840--1880 Ma (Wyborn & Page 1983; Etheridge et al. 1987; Page 1988; Wyborn 1988). Geochemically, this areal association is characterised by high K_2O, La, Ce, Rb, Th, U, K_2O/Na_2O, Rb/Sr, and low MgO, CaO, Ni, Cr and low $^{87}Sr/^{86}Sr$ intial ratios (0.703--0.706) (e.g. Wyborn 1988). It only covers the more acidic range on the AFM diagram (Etheridge et al. 1987).

By comparison, most of the AIC rocks share similar U-Pb ages (1873-1879 Ma c.f. 1840-1880 Ma) and low $^{87}Sr/^{86}Sr$ initial ratios with the Barramundi association. However, with regard to many diagnostic geochemical features, the AIC is quite distinctive, e.g.

(1). The AIC covers a SiO_2 range of 46-78%. There is no equivalent in the Barramundi association to the ACAS, which defines a typical and complete calc-alkaline trend on the AFM diagram (Fig.4-17)

(2). The SiO_2 contents of the AOT & AOLG are comparable to the Barramundi association. However, there are many other differences as outlined in Table 6-1 and shown on Fig. 4-6. In general, the AOT and AOLG have lower K_2O, K_20/Na_20, Rb/Sr, Rb, La, Ce, Nd & Th. and higher Na_2O, MgO, Sr, Ba, V, Mn & Sc. The K/Rb ratio increases with increasing SiO_2 instead of

being constant.

(3).Wyborn (1988) has illustrated the I-type granites of different geological ages with a Na_2O vs K_2O diagram. Most Atnarpa granites (i.e. the AOT and coarser-grained AOLG) plot quite close to the field defined by Early Archean and Tertiary granite and quite far away from the "early Proterozoic granites" as decribed by Wyborn (1988) (Fig.6-3).

Some elements of the AMG may be able to be correlated with those of the most evolved Barramundi association. However, the high Ga and Al_2O_3 contents, and the enrichment of Y in the AMG are not comparable.

The post-1820 Ma granites of the Mt. Isa Inlier, as described by Wyborn et al. (1988), are mainly anorogenic I-type intrusions associated with minor S-type microgranite, which are characterised by higher Fe/Mg, TiO_2, Sr, Nb, Y and U than the Barramundi association.

In the Atnarpa area, only the AYT has been identified as a post-1820 Ma felsic rock. Its geochemical features, such as low K/Na, Rb/Sr and $^{87}Sr/^{86}Sr$ initial ratios, low HFS and REE elements as well as strongly fractionated REE patterns, are quite distinct from either Barranundi association or the post-1820 Ma granites as described by the BMR workers.

6.3 COMPARISON WITH THE ORTHOGNEISSES OF THE ENTIA GNEISS COMPLEX, EASTERN ARUNTA INLIER

The orthogneisses of the Entia Complex range from gabbro to true granite. They are represented by Entia massive amphibolite (Sivell & Foden 1988), Huckitta Tonalite Gneiss (HTG), Huckitta Granodiorite Gneiss (HGG) and Inkamulla Granite Gneiss (IGG) (Foden et al., 1988). The massive amphibolite is characteristic of prolonged LIL to HFS decoupling typical in continental margin intrusions (Sivell & Foden, 1988). The tonalite-granodiorite gneiss associated with the massive amphibolite has been formed by crystal fractionation in a manner similar to the orogenic granitoids in the modern Cordileran belts (Foden et al., 1988).

The AIC shows a great similarity with the orthogneisses of the Entia Complex, such as similar rock assemblages, ranging from metapyroxenite to true granite. Among them, the ACAS is petrographically and chemically analogous to the association of Entia amphibolite, HTG and HGG. For instance, amphibolites in both associations show prolonged decoupling between the LIL and HFS elements, such as consistent depletion in Zr, Nb, Ti & Y relative to REE and high La/Nb,

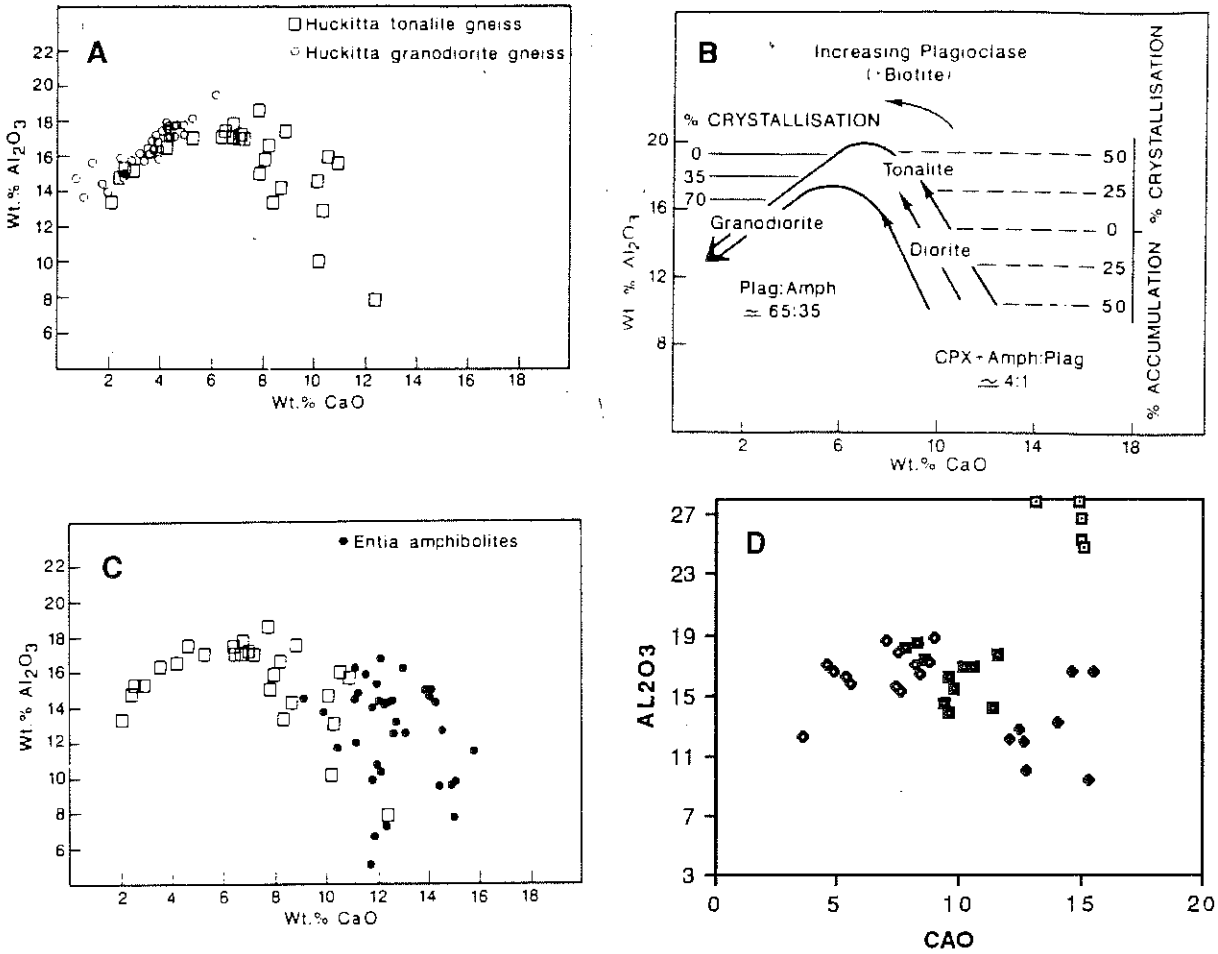

Fig. 6-1 (A), (B) & (C). Al_2O_3 - CaO variation diagrams and a postulated fractionation process for the Entia rocks of Foden et al (1988). (D). Al_2O_3 -CaO variation diagram for the ACAS for comparison with the Entia rocks. Symbols as for Fig. 4-1.

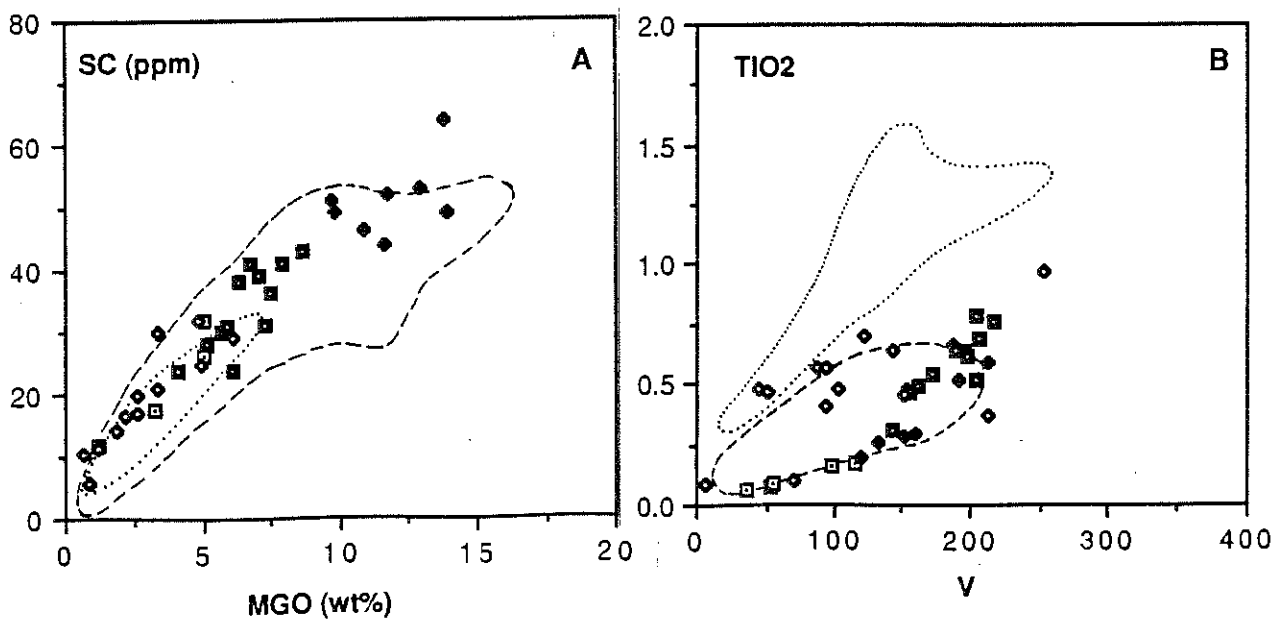

Fig. 6-2. Selected element variation diagrams for the ACAS. Dotted-line balloons outline the fields for the Moruya Batholith from the eastern Lachlan Fold Belt (Griffin et al 1978). Broken-line balloons represent the field for the Huckitta Tonalite of the Entia Gneiss, eastern Arunta Inlier (Foden et al 1988). Symbols as for Fig 4-1.

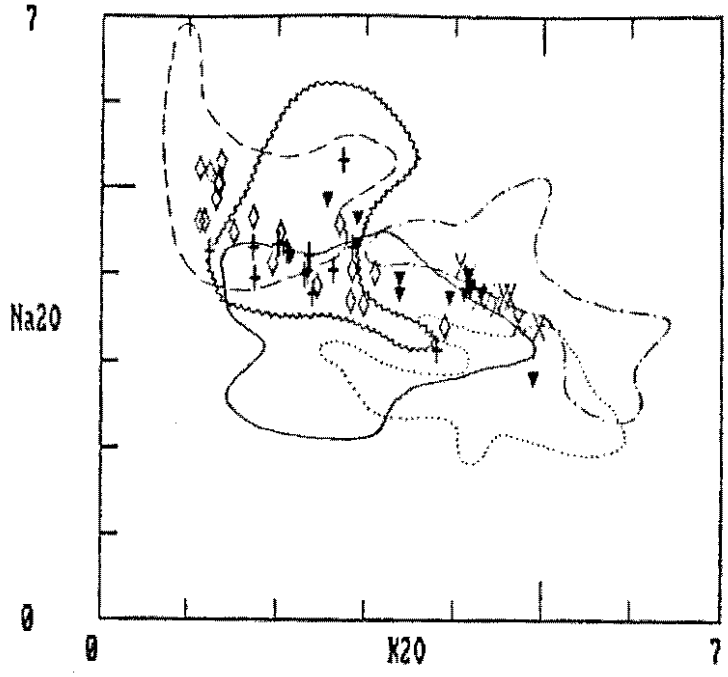

Fig. 6-3. K2O-Na2O variation diagram for the Atnarpa Granitic Batholith. Balloons confine the fields for granitoids occurred in different geological times as summerised by Wyborn (1988). Most of the AGB plots (i.e. the cross & empty diamond types) fall into the fields of the Early Archean and Tertiary granites but far away from the Early Proterozoic granites field of Wyborn (1988). Plot symbols as for Fig. 4-6.

Key:
- — — — — Early Archean granite field
- —·—·—·— Late Archean granite field
- ..... Early Proterozoic granite field of Wyborn (1988)
- ——— Palaeozoic granite field
- ~~~~~ Tertiary granite field

Table 6-1 Geochemical comparison between the Atnarpa granites (the AOT & AOLG) and the Barramundi Association (represented by the Kalkadoon-Ewen-Leichardt Association. Data from Wyborn & Page (1983) and Wyborn (1988)).

	Atnarpa Granites (AOT & AOLG)	Barramundi Association
K2O	1--5%	3--6%
Na2O	>3%	<3%
MgO	0--3.5%	0--2%
Rb	most <100ppm	most >100ppm
Sr	higher	lower
Ba	higher	lower
Zr	lower	higher
La	most <50ppm	most >50ppm
Th	5--25ppm	5--45ppm
Sc	higher	lower
K2O/Na2O	most <1	most >1
Rb/Sr	generally <0.5	generally >0.5
K/Rb	200-600, increase with SiO2 content	100--300, constant

K/Nb ratios. Both associations share similar variation trends or ranges for MgO, CaO, Ti, V, Sc, Rb, Sr, Al_2O_3, CaO (e.g. Fig. 6-1 & 2).

Foden et al. (1988) have noted similarities in the major and trace element variations between the Entia granitoids and the Moruya Batholith in the Lachlan Fold Belt. The later is characterised by a very low Sr initial ratio and a very high Nd initial ratio and therefore has been considered to be similar to M-type or arc-type granitic suites. Similar chemistry can be recognised in the ACAS.

Furthermore, the AGB resembles, to some extent, the HGG and IGG as well as the Lachlan Fold Belt I-type granites of Chappell & White (1982) with regard to MgO-Ni, K_2O-Na_2O and SiO_2-Sr variations (Foden et al. 1988).

However, the AIC is different in some aspects from the Entia orthogneisses. e.g.:

(1). The AIC appears to have formed at a shallower depth than the Entia rocks. This is indicated by:

1). Structurally, the Entia gneiss is deep-seated, resulting in the style of lit-par-lit intrusion. In comparison, the occurrence of the AIC is characterised by more blocky bodies, regardless of being big or small. The lit-par-lit style is only locally present in the Atnarpa area.

2). The metamorphic grade in the Entia area is higher than in the Atnarpa area as indicated by the occurrence of sillimanite and intensive development of migmatite (Foden et al., 1988; Stewart, 1985; Nykiel, 1986).

(2). The ACAS, AOT and AOLG are substantially older than the Entia granites. However, the AYT seems to be identical in age to the Entia granites (Cooper et al., 1988).

(3). There are also some geochemical differences. The Na_2O/K_2O ratio and HFS elements are higher in the AOT and AOLG than in the HGG and IGG. Also, the ACAS shows trondhjemitic fractionation trend during the later stages, which is quite different from the HTG (e.g. Fig. 4-19). Foden et al. (1988) considered that the HTG and HGG were related by crystal fractionation. Such a kinship seems unlikely for the ACAS and AOT.

By comparison, the Alice Springs Granite to the west of the AIC is also characterized by high Na/K, CaO, MgO, Sr and low Rb, Rb/Sr. Some Sm/Nd isotopic data indicate that the Alice Springs Granite was derived from a younger source similar to the AIC (Warren et al., 1988; Warren & McCulloch, Pers. Comm.).

6.4 COMPARISON WITH OTHER SUBDUCTION-RELATED INTRUSIONS

Granitoid of similar age and geochemistry to the AIC have been recognised in Halls Creek Inlier of Western Australia (Ogasawara 1988). The three tonalitic suites which occur in the central part of Halls Creek Inlier are characterised by low K_2O and Rb contents similar to the AOT, AOLG and AYT. The fractionated REE patterns, with HREE depletion, are analogous to the AYT. The younger Bow River granitoid suite in the west of the Halls Creek Inlier has a similar enrichment of K_2O and Rb to the AMG. These granitoids have been considered to be related to the subduction and subsequent collision of the Halls Creek Inlier with the Kimberley Inlier.

By comparison, the ACAS is also petrograpically and geochemically analogous to the Proterozoic calc-alkaline-tronhjemitic gabbro-diorite-tonalite-trondhjemite suite of southwest Finland (Arth et al., 1978). The ACAS shows strong depletion in K and therefore follows a somewhat trondhjemitic trend on the Na-K-Ca discrimination diagram (Fig. 4-19) of Barker and Arth (1976). This property is characteristic of the southwest Finland suite. The different REE patterns in the ACAS may be due to fractionation of assemablages different from those in southwest Finland suite. It appears that there is a dominance of plagioclase removal in the ACAS relative to a dominance of hornblende removal in the southwest Finland suite.

Good anolgues are also found in the Cordilleran belts of western America and the pre-collisional intrusions of the trans-Himalayan Batholith (Honegger et al., 1982). As outlined by Foden et al. (1988), an important factor in this analogy is the association of the tonalite and granodiorite with doiorite and gabbro and the presence of cumulates which are dominated by plagioclase, hornblende and clinopyroxene.

The best analogue in Cordilleran belt is the Peruvian Coastal Batholith (Atherton 1984; Atherton et al. 1983; Pitcher 1984). This has been considered to be mantle derived without significant crustal contamination on the basis of isotopic studies (Atherton et al. 1979). The limited data for the AOT and AOLG show similar ranges and variations of most major and trace elements and norms to the diorite-tonalite-adamellite-granite association of the Santa Rosa superunit in the Coastal Batholith. Notably, the Na_2O content remains high throughout the whole rock types and there are several similarities in the REE patterns. e.g., they both have similar slope, Eu anomaly and Yb enrichment relative to Er, and a similar evolutionary trend (c.f. Atherton 1984). The only

obvious difference lies in the trends for K_2O, Rb and K/Rb. These differences can be attributed to the relatively earlier precipatation of biotite and general absence of clinopyroxene fractionation in the AOT and AOLG.

The granitoid Coastal Batholith is spatially associated with a string of older enlongate high-level gabbroic plutons ranging from ultrabasic rocks to meladiorite (Cobbing et al. 1981). The parent--daughter relationship has been discussed by Pitcher (1984). He considered the parental magmas for the granitoid batholith may be derived from the remelting of an earlier formed underplate of basaltic material. The melting was initiated by a general crustal thickening.

The Peruvian gabbros are more mafic than the ACAS which makes a direct anology difficult. However, similar relationship may still apply to the ACAS and AGB, although not necessarily that of parent to daughter.

In addition, the ACAS can be compared with the pre-collisional plutons of the trans-Himalayan Batholith. They have a similar trend on the AFM diagram, and similar REE patterns (Honegger et al. 1982). The high level features and REE pattern and the assemblage of rock types are also similar to the Aleutian calc-alkaline suite, North America (Perfit et al. 1980) and the Uasilao-Yau Intrusive Complex, New Britain (Whalen, 1985).

However, a comparison with the above-mentioned Phanerozoic calc-alkaline plutons reveals one important difference. The large alkali metals K and Rb usually increase with fractionation trend in the normal calc-alkline suites. But this increase does not exist in the ACAS.

6.5 CONCLUSION

A comparison with rocks in a variety of geological settings indicates:

(1). The AIC shows several important differences from either the Barramundi Association or the post-Barramundi plutons which have been considered by Etheridge et al. (1987) to be related to the closure of ensialic rifts.

(2). The AIC is broadly analogous to the orthogneisses of the Entia Complex but there are differences in age, depth and elemental variation trends of the granitic rocks. The AGB and AYT are likewise similar to a group of granitic suites in the mid-Proterozoic Halls creek Inlier (Ogasawara 1988)

(3). The AOT and AOLG display many similarities to the Peruvian Coastal Batholith

including major, trace and REE element features (Pitcher 1984; Atherton 1984).

(4). The ACAS has a general similarity to both Proterozoic and modern calc-alkaline plutons with regard to rock assemblage, element variations and REE patterns. However, the Na, K and Rb contents are different from those of the Phanerozoic suites. The felsic member of the ACAS, i.e. the late-stage differentiates, display a transition to the trondhjemitic trend, which is analogous to the Southwest Finland suite (Arth et al. 1978).

CHAPTER SEVEN: TECTONIC FRAMEWORK AND CRUSTAL EVOLUTION OF THE SE ARUNTA INLIER

7.1 INTRODUCTION

Recently, more attention has been directed towards the understanding of the Proterozoic lithospheric evolution, with the most significant result being the recognition of a major crust-forming event of global proportions about 1.7 to 2.0 Ga ago (Kroner 1987). However, a vigorous debate centres around the question whether the crust was formed by subduction-related marginal accretion around preexisting crustal nucleii which is analogous to the Phanerozoic plate tectonics (e.g. Hoffman 1980; Condie 1982; Van Schmus et al. 1987; Gorbatscheu and Gaal 1987), or by rift-related mantle underplating where sea floor spreading is short-lived and subduction insignificant (e.g. Kroner 1983; Etheridge et al. 1987). In addition, it has been suggested, mainly on the basis of isotopic constraints, that growth of continental crust in the Archean was dominated by underplating but marginal accretion was the prevailing mechanism after 2.0 Ga (Fletcher et al. 1985; Harris et al. 1987).

In Australia, many workers favour the rift-related non-Uniformitarian model (e.g. Etheridge et al. 1987; Wyborn and Page 1983; Shaw et al. 1984; Wyborn 1988; Page 1988; McCulloch 1987; Wyborn et al. 1988; Warren 1983; Warren and Wyborn 1988; Mortimer 1985). However, some arguements for, or consistent with, subduction-related Uniformitarian tectonism have been made by several other workers in places of either Archean-Proterozoic terrain borders (e.g. Fletcher et al. 1985; Hyne and Gee 1986; Ogasawara 1988) or margins of Proterozoic terrains (James and Ding 1988; Foden et al. 1988; Sivell and Foden 1988).

In the opinion of the non-Uniformitarian school, the early-Proterozoic terrains of north Australia are characterised by: (1). a basin-forming episode within Archean continental crust; (2). contemporaneous mafic underplating; (3). crust-mantle delamination and A-subduction due to heat loss; (4). compressional orogeny and formation of the Barramundi association; (5). long-term (~1500 Ma) isobaric cooling and anorogenic magmatism. This suggestion is supported by: (1). a widespread isochronous orogenic event; (2). the presence of bimodal magmatism and absence of ophiolitic and calc-alkaline suites; (3). uniform geochemistry; (4). anti-clockwise P-T-t path and

post-orogenic isobaric cooling; (5). limited seismic data and (6). analogue to modern tectonics in the African continent.

This tectonic style has been attributed to small-scale mantle convection and is therefore considered to be a short-lived or aborted Wilson cycle (Etheridge et al. 1987) in which the stage of sea-floor spreading and involvement of oceanic lithosphere subduction have been short-cut.

Although it provides the best and most complete explanation on the crust-mantle evolution of the Proterozoic Australia, this model confronts two fundamental difficulties: (1). At least 80% of the Archean continental crust involved was based on inference. Neither zircon data nor Nd isotopic evidence have convincingly proved the existence of the "sandwiched" Archean crust (e.g. McCulloch 1987; Page 1988). (2). The time-span from the initiation of the extensional basin to the formation of the Barramundi Association was estimated to be about 400 Ma (McCulloch 1987). This is two times longer than a normal Wilson cycle (~200 Ma).

Furthermore, recent Nd isotopic studies (McCulloch 1987) indicate that not all of the Australian Proterozoic terrains were formed during the same time (2.1--2.3 Ma). The crustal formation age of the Musgrave Inlier (1770--1890 Ma) to the south of the Arunta Inlier, for example, is substantially younger than the Northern Australian Proterozoic Province but almost identical in age to the two episodes of magmatism in the SE Arunta Inlier. It is interesting to note that the study area may be located just on the border of these two terrains of different ages.

7.2 MAGMA GENESIS OF THE ATNARPA IGNEOUS COMPLEX AND ITS TECTONIC SIGNIFICANCE

The geochemistry and geochronology of the AIC have been discussed in detail in the previous chapters. This section will focus on the natures of individual igneous groups, their magma source and the tectonic significance.

7.2.1 MAGMA GENESIS OF THE ACAS

It has been demonstrated that the ACAS is a typical calc-alkaline suite with some trondhjemitic affinities in its felsic differentiates. Geochemical features indicate that it is formed by high-level fractional crystallization from a parental magma with high oxygen and water fugacities typical of subduction-related magmas (Shervais 1982).

The origin of the parental magma or magmas of a calc-alkaline suite has been discussed by many workers (e.g. Green and Ringwood 1968; Ringwood 1974). The well-accepted opinion is that the parental magma of the calc-alkaline suites is generated by partial melting of suducted oceanic crust or more likely the overlying mantle metasomatised during the dehydration of the subducted oceanic crust (e.g. Tarney and Saunders 1979, for review). Thus, calc-alkaline affinities are considered to be a diagnostic indicator of plate-margin settings.

On the hygromagmatophile-element abundance diagrams (Wood et al. 1979), samples of the ACAS, even including the differentiated felsic members, display evident LIL/HFS element decoupling. Relative to LREE, consistent depletions in Nb, Ti, Y and Zr (for mafic rocks only) are obvious. The La/Nb, Th/Nb ratios are very high (see Appendix-3A). These phenomena have been explained in terms of selective enrichment of LIL and LREE elements in the magma source, i.e. the metasomatised overlying mantle wedge (Tarney et al. 1977). The depletion of HFS elements, typically Nb, is considered to be caused by the source retention of the minor phases such as ilmenite, rutile and sphene which tend to be refractory under hydrous partial melting conditions (Perfit et al. 1980; Tarney and Saunders 1979).

In addition to the above mentioned features, the consistent depletion of K and Rb relative to other LIL elements are also very typical and considered to be primary magma features (see Chapter Four). This may be because the oceanic crust has higher Na/K ratio and lower K, Rb than the continental crust (Chappell and White 1974). Alternatively, K and Rb may have been removed by hydrothermal activity either at the spreading ridge or during the early stage of subduction, before the calc-alkaline magma was generated (Tarney et al. 1979). Low K, Rb, Rb/Sr also indicates that the involvement of a crustal source is less likely.

Partition coefficient data for Nb and Zr for the major precipitating minerals (Pearce and Norry 1979) indicates that the Zr/Nb ratio is less likely to be affected by the fractionation process. This leads to the linear correlation on the Zr--Nb diagram for the ACAS. Therefore, the average value of the Zr/Nb ratios of the ACAS may reflect the nature of the parental magma. Erlank and Kable (1976) used the Zr/Nb ratios to measure the degree of mantle depletion in LIL elements. The average Zr/Nb ratio for the ACAS is about 25, indicating its mantle source has been strongly depleted relative to the chondritic abundance (Zr/Nb=16--18).

7.2.2 COMPARISON BETWEEN THE ACAS AND AOT-AOLG

It is reasonable to ask whether the ACAS and AGB are genetically related. If so, to what degree? A comparison between these two suites is essential for the understanding of the magma genesis of the AOT-AOLG and its tectonic significance.

Obviously, the ACAS and AOT-AOLG cannot be fractionated from one parental magma. This is because: (1). The AOT-AOLG are more voluminous than the ACAS; (2). They do not follow the same fractionation trends. For the same SiO_2 level, the AOT is much richer in MgO, Fe_2O_3, K_2O, K_2O/Na_2O, Rb/Sr, Ni, Sc, V and Nb than the quartz diorite in the ACAS.

However, the AOT-AOLG do share similar geochemistry with the ACAS. For example: (1). The AOT-AOLG are mainly Na rich and have low Rb/Sr and inferred $^{87}Sr/^{86}Sr$ initial ratios. (2). They have similar crystallization ages.

The genetical relations between the ACAS and AOT-AOLG will be discussed in the following section.

7.2.3 MAGMA GENESIS OF THE AOT-AOLG

As indicated, the AOT-AOLG are characterised by low K_2O, Rb, Rb/Sr, REE and Th, and high MgO, Fe_2O_{3tot}, Na_2O, CaO, Sc, Sr and Ba which is distinctive from the Barramundi Association. On the K_2O--Na_2O diagram, the AOT-AOLG samples plot quite close to the Archean and Tertiary granites. It has been previously suggested that the AOT and AOLG are related by crystal fractionation from one parental magma.

The low K, Rb, K/Rb, Rb/Sr and high MgO, CaO, Sc, Sr of this suite rule out any involvement of a clastic sedimentary source. The inferred low $^{87}Sr/^{86}Sr$ initial ratio combined with geochemical similarity to the Archean granites suggests there is little possibility that the AOT-AOLG were derived from partial melting of an Archean crust. In addition, the AOT-AOLG are too felsic to be derived directly from a mantle source (Wyllie 1983).

The Barramundi Association was considered to be derived from partial melting of a fractionated mantle-derived underplate with SiO_2 about 60%. A comparative study has outlined significant geochemical difference between the AOT-AOLG and the Barramundi Association. It follows that the same process may not be suitable for the AOT-AOLG.

However, the parental magma of the Peruvian Coastal Batholith has been interpreted in

terms of the partial melting of the earlier-formed underplate of basaltic material segregated under greatly thinned crust of the back-arc or marginal basin. The remelting of the first-stage source rocks is likely to have been generated from the subducted oceanic crust in response to periods of extra-rapid sea-floor spreading (Pitcher 1984). As the AOT-AOLG shows great geochemical similarity, including major, trace and REE elements and low $^{87}Sr/^{86}Sr$ initial ratios, to the Peruvian Coastal Batholith, a similar process may be suitable for the genesis of the parental magma of the AOT-AOLG. In this case, the mafic underplate may be similar to the magma source of the Barramundi Association, but not necessarily that fractionated. Moreover, in consideration of the age relations and some geochemical similarity between the ACAS and AOT-AOLG, the ascent of the parental magma of the ACAS may be responsible for the initiation of the parental magma of the AOT-AOLG. Both heat and material addition will be necessary to account for the AOT-AOLG magma genesis and geochemical similarity to the ACAS. This model is consistent with the experimental study by Wyllie (1983), i.e. batholith genesis commonly includes a contribution of heat and material from less siliceous magmas generated in subducted oceanic crust and mantle peridotite, as well as granitic components from partial melting of continental crust. This partial melting-mixing model is also similar to the magma genesis of the transitional crust (i.e. plate margins) syntexis-type granite suggested by Xu Keqin et al. (1984).

In conclusion, the parental magma of the AOT and AOLG is considered to be derived from: (1). the partial melting of a chemically less or little fractionated earlier-formed mafic underplate, comparable to the fractionated one which was believed to produce the Barramundi Association (Etheridge et al 1987); and (2). the addition of both heat and material from the mantle-derived less siliceous magma of the ACAS.

7.2.4 MAGMA GENESIS OF THE ATBS

It has been demonstrated that the ATBS closely resembles the Archean bimodal tonalitic-basaltic suite in terms of major, trace and REE geochemistry. A parent-daughter relationship has been discussed in Chapter Four. The discussion here will focus on a tectonic interpretation.

The ATBS displays some distinctions from the Archean suites. In general, both AYBA and AYT show a correlative depletion in HFS elements. The AYBA bears transitional features between

MORB-type basalts and arc-type basalts.

The basalts that form in back-arc or marginal basins are considered to have chemical affinities to both oceanic floor or MORB-type basalts and arc-type basalt (e.g. Saunders et al. 1979; Saunders and Tarney 1979; Holms 1985). These transtional features have been interpreted in terms of addition of a subduction component to the mantle source region (e.g. Tarney et al. 1981). Alternatively, Dupuy and Dostal (1984) attributed the decoupling of HFS/LIL elements in some continental tholeiites to the effect of crustal contamination. But this suggestion fails to explain the low K, Rb, Rb/Sr values in the AYBA.

If the AYBA parental magma was already depleted in HFS elements, it follows that the low contents of HFS elements in the AYT are readily explainable in terms of the partial melting model of Barker and Arth (1976). Also, a higher partial melting may be required to produce the AYT with more mafic features and lower SiO_2 content than the Archean tonalites.

7.2.5 MAGMA GENESIS OF THE AMG

As has been discussed, the AMG is a distinctive rock type showing geochemical affinities to the syn-collisional S-type leucogranites (Harris et al. 1986). It may be derived from anatexis of a sedimentary source at a supracrustal level.

7.3 TECTONIC EVOLUTION OF THE SE ARUNTA INLIER

In the light of Nd isotopic data (McCulloch 1987), the SE Arunta Inlier, including the Atnarpa Igneous Complex, Entia Gneiss Complex and Alice Springs Granite, is likely to represent a continental margin during the early to mid-Proterozoic. A well defined line of magmatic composition change is observed in the Atnarpa Igneous Complex, which extends along the line of Arltunga--Atnarpa--Marmalade Dam--Tommy's Gap. The eastern side of this line is broadly dominated by the high-level ACAS and the western side, by the relatively deep-seated AGB. A regional older brittle shear zone (pre-AYT?) was observed dipping to SEE--SE in the Atnarpa and Marmalade Dam areas. This magmatic polarity is supported by local small scale geophysical data (Dr Burton Murrell of the White Range Gold Mine, Pers. Comm.). The BMR Harts Range-Arltunga 1:100,000 Geological Map also strongly suggests some sort of discontinuity along this line.

Whilst accepting that the ensialic rifting basins were formed within most of the northern Australian Archean protolith as suggested by Etheridge et al. (1987), it is considered that a marginal basin may have formed in the SE Arunta Inlier. This was followed by the accumulation of the BSA including the schistose amphibolite, and mafic underplating (e.g. Wyborn 1988).

During the Barramundi Orogeny, most of the Northern Australian Proterozoic terrains experienced a tectonic compression followed by widespread magmatism with similar geochemical affinities to the Barramundi Igneous Association. However, in the SE margin of the Arunta Inlier, a subduction-related compression and magmatism occurred probably in response of the comtemporaneous crustal formation event to the south of the Arunta Inlier. Either partial melting of the subducted oceanic crust or the partial melting of the metasomatised overlying mantle wedge would produce a calc-alkaline magma. The high-level emplacement of this magma formed the ACAS. Both heat and material addition by the calc-alkaline magma caused partial melting and assimilation of the pre-existing mafic underplate. The resultant magma is responsible for the emplacement of the Na-rich AGB including the AOT and AOLG.

Continuous compression due to an unusually rapid subduction rate eventually led to the closure of the marginal basin and the marginal collision resulted in the anatexis of the supracrustal sedimentary rocks and the formation of syn-collision S-type leucogranite, namely, the AMG. As the occurrence of the AMG is relatively small, it follows that the collision is only a marginal type, typical in the Cordilleran Orogenic Belt (Jones et al. 1986; Dalzeil 1986).

Marginal arc-continental collision may lead to possible crustal uplift and high-level thrusting as indicated by the apparently pre-AYT ductile shear zone and the coexistence between the younger high-level ATBS and the older, relatively deep-seated AOT & AOLG.

After the Barramundi Orogeny, most of the intra-terrain areas in the northern Australia Proterozoic terrains may have been cratonised and followed by anorogenic magmatism (e.g. Etheridge et al. 1987; Wyborn et al. 1988). The terrain margins, however, were still active, which is reflected by the tectono-magmatism in the Harts Range and Atnarpa areas during 1770--1730 Ma (Cooper et al. 1988; this study). In the Atnarpa area, a marginal or back-arc spreading basin was developed (not necessarily developed into oceanic floor) probably in response to episodic subduction movement. The opening and closure of this basin is responsible for the bimodal basaltic-tonalitic magmatism typical in the Archean terrains (e.g. Tarney et al. 1979).

After the bimodal magmatism, the Atnarpa area suffered from several episodic thermal-deformational events, which are broadly comparable to other places in the northern Australian Proterozoic terrains (e.g. Black et al. 1983; Page 1988; Wyborn et al. 1988) and notably correlated with the deformation and metamorphism in the Weldon Tectonic Zone where the Atnarpa Nappe Complex is located (Shaw et al. 1984). This is in contrast with theories of long lived isobaric cooling (Warren 1983).

The first thermal-deformational event is reflected by regional deformation and amphibolite grade metamorphism, referred to Black et al. (1983) as the Aileron Event. Black et al. (1983) considered this event substantially reset the Rb-Sr whole rock systematics at around 1670 Ma.

The second thermal event is recorded by unaltered muscovite and biotite Rb-Sr isotopic systems. It is typified by a fast cooling through 500°C to below 320°C during the period 1512--1469 Ma, probably as a result of crustal uplift (about 7 km) or magmatic reheating of the previously cooled terrain. This may also be due to the fact that the rocks in the study area were buried at shallower depths.

The third thermal event is only poorly-defined by this study but has been demonstrated by Windrim and McCulloch (1986) to be at about 1000 Ma as shown by their internal mineral Rb-Sr isotopic systematics and Al_2SiO_5 barametry. This is considered to involve substantial crustal uplift, probably in response to the subsidence of the Amadeus Basin.

The fouth event is the Phanerozoic Alice Springs Orogeny, recorded in biotite Rb-Sr ages for rocks from the Arltunga Nappe area (Armstrong and Stewart 1975). But its nature and intensity in this area need further investigations.

This tectonic evolution clearly manifested a process of multi-stage mantle depletion. Preliminary Nd isotopic data from the AIC yielded a 1726 Ma model age if assuming initial ε_{Nd} = +6 (Warren and McCulloch, Pers. Comm.). This depleted mantle Sm-Nd model age is unusually younger than the U-Pb zircon crystallization age, which probably means that the assumed initial ε_{Nd} value is incorrect. A higher initial ε_{Nd} is probably required, which may come about if the mantle source reservoir under the SE margin of the Arunta Inlier has suffered from multi-stage extraction and depletion. The multi-stage depletion model will also account for the extremely low $^{87}Sr/^{86}Sr$ intial ratio for the AYT (0.7017).

7.4 CONCLUSION

(1). The study area is composed mainly of the Atnarpa Igneous Complex (AIC), which is accompanied by some Basement Supracrustal Assemblage (BSA) and juxtaposed with a cover sequence of the Amadeus Basin. Several igneous genetical groups have been recognised in the AIC on the basis of field observations, petrograpy, geochemistry, geochronology and isotopic geology. The AIC rocks were intruded during two magmatic episodes, comparable with the widespread 1880--1840 Ma Barramundi Orogeny and the 1770--1730 Ma event in the Harts Range area as well as other places of the north Australian Proterozoic terrains.

(2). The Atnarpa Calc-alkaline Suite (ACAS) is considered to be a typical high-level, calc-alkaline intrusion to volcanics, which shows a transition to a trondhjemitic trend in its felsic differentiates. Its genesis is formulated in terms of high-level fractional crystallization from a parental magma with high oxygen and water fugacities. The parental magma is considered to be mantle-derived, being related to oceanic crust subduction under the continental margin. Its crystallization age was dated by U-Pb zircon isotopics at 1879±11/10 Ma. This is the oldest U-Pb zircon age so far known in the Arunta Inlier.

(3). The Atnarpa Granitic Batholith (AGB) is composed of pre-collisional Atnarpa Older Tonalite (AOT) and Leucogranite (AOLG) and syn-collisional Atnarpa Muscovite Granite (AMG). The AOLG yields a U-Pb zircon age of 1873±11/10 Ma and the AOT, 1863±33/27 Ma (Sando 1987). The AOT-AOLG are characteristic of low K_2O, Rb, REE, Th, Rb/Sr and inferred $^{87}Sr/^{86}Sr$ initial ratios and high Na_2O, MgO, Fe_2O_3, Sr, Ba and Sc, which is quite distinctive from the Barramundi Association of the similar ages (Wyborn 1988; Wyborn and Page 1983) but similar to the Peruvian Coastal Batholith in the Cordilleran Orogenic Belt (Atherton 1984; Pitcher 1984). The AOT & AOLG are interpreted as being derived by crystal fractionation from one parental magma. The parental magma is considered to be generated by both partial melting and assimilation of a mafic underplate, with a short crustal pre-history, due to the addition of heat and material from the ascending, less-silicieous, mantle-derived, calc-alkaline magma.

The AMG is geochemically unrelated to the AOT-AOLG. It, however, shows geochemical affinities to the syn-collision peraluminous S-type granite of Harris et al. (1986), and is considered to be derived from anatexis of a sedimentary source within supracrustal levels.

(4). The Atnarpa Tonalitic-Basaltic Suite (ATBS) is a bimodal, high-level to volcanic suite,

with geochemistry similar to the ubiquitous Archean tonalitic-basaltic bimodal suites. The Atnarpa Younger Tonalite (AYT) was dated at 1751±12 Ma, which marks the second magmatic episode in the study area. Calculated $^{87}Sr/^{86}Sr$ initial ratio at 1751 Ma is 0.7017. The ATBS is considered to be formed in response to the opening and closure of a marginal or back-arc basin.

(5). Tectonically, whilst the orogensis of most of the northern Australian Proterozoic terrains has been interpreted to be essentially ensialic and rift-related without the involvement of oceanic crust subduction (Etheridge et al. 1987), the study area as well as other places of the SE margin of the Arunta Inlier is considered to represent a continental margin during the early to mid-Proterozoic, analogous to the Cordilleran Orogenic Belt. The study area has undergone two episodes of subduction-related magmatism, probably in response to episodic change in subduction rate or the crustal formation events to the south of the Arunta Inlier as indicated by the Sm/Nd data from the Musgrave Inlier (McCulloch 1987). The first magmatic episode is comparable to the Barramundi Igneous Association, and the second, to the magmatism im the Entia Dome, Harts Range area, to the NE of the study area. The upper mantle under the SE margin of the Arunta Inlier must have experienced multi-stage differentiation and depletion in order to account for the unusally high positive initial ε_{Nd} values for the AIC and very low Sr initial ratio in the AYT (0.7017).

(6). Rb/Sr isotopic data of whole rocks and micas indicate that the study area has subsequently suffered from several episodic thermal-deformational events. These include: (1). 1670 Ma old event of regional deformation and amphibolite facies metamorphism, possibly equivalent to the Aileron Event (Black et al. 1983); (2). fast cooling from 500°C to below 320°C during 1512 to 1469 Ma; (3). substantial crustal uplift around 1000 Ma probably in response to the subsidence of the Amadeus Basin and (4). the Carboniferous Alice Springs Orogeny.

7.5 SUGGESTIONS FOR FURTHER INVESTIGATION

(1). Many MORB-like metabasites have been recognised in both Entia Basement and Harts Range Cover (e.g. Sivell 1988; Sivell and Foden 1988), which were considered to be related to a basin-forming episode. However, there is little knowledge about the pre-ACAS history in the Atnarpa area. A search for pre-ACAS MORB-like amphibolite now seems desirable. The schistose amphibolite coexisting with calc-silicate is a likely candidate.

(2). Further Sm/Nd isotopic studies are essential for the AIC.

(3). More geochemical studies need to be carried out on the fine-grained amphibolite within the ACAS.

(4). Further extensive geochemical investigations of the ATBS would be required for a full understanding of the bimodal tonalitic-basaltic magmatism.

(5). U-Pb zircon analysis is required for the AMG, with emphasis on the two generations of zircons. As a S-type granite with a sedimentary source, the inherited zircon grains, which are apparently present in it , may provide useful or even exciting age information about the reworked older crust. This work is in progress.

(6). Some mafic differentiates in the ACAS are unusually enriched in zircon. These zircon grains may be xenocrysts from inclusions of wall rocks captured during magma ascent. If so, they may sampled the "sandwiched" Archaean crust postulated by Etheridge et al. (1987) should it exist. Thus, a suitable U-Pb isotopic study on these zircons, e.g. by the ion probe, could provide exciting results.

(7). The age of the movement of the Arltunga Nappe Complex and its major thrust, the Illogwa Shear Zone and their effect on the geochemistry and isotopics of the Atnarpa Igneous Complex need further investigation.

(8). Further knowledge of pre-AYT, post AOT-AOLG deformation, metamorphism and sedimentation would assist the intepretation of the tectonic evolution.

(9). Preliminary petrographic studies on the rocks taken from the Star Creek area, eastern part of the AIC, reveal some distinction from some rocks in the Atnarpa area. e.g., hornblende is the main dark mineral in the BMR's so-called granodiorite in the Star Creek area (see BMR map, 1984), whereas, biotite is the major dark mineral in the AOT. It is likely that most , if not all, of the igneous rock types, including the "ultramafics", referred to the BMR (1983) as the Wistleduck Dyke Swarm, may represent a genetically-related, zoned, igneous suite with a rock assemblage similar to the ACAS. Many of the age relations outlined in the 1:250,000 map of BMR (1983), which were established on the basis of unreliable Rb-Sr isochron ages, metamorphic grades and deformation features, may be dramatically erratic and need further investigations. At least the *BMR's "younger" "ultramafic Wistleduck Dyke Swarm"* occurred in the Star Creek is crosscut by the *BMR's "older" "granodiorite"*!!

REFERENCES

ABBEY S. 1980. Studies in "standard samples" for use in the general analysis of silicate rocks and minerals; Part 6, 1979 edition of "usuable" values. Geol.Surv.Can.Pap., 80-14:30pp.

ABBOTT R.N. 1981. AFM liquidus projections for granitic magmas, with special reference to hornblende, biotite and garnet. Can. Mineral. 19:103-110.

ALLEN A.R. & BLACK L.P. 1979. The Harry Creek Deformed Zone, a retrograde schist zone of the Arunta Block, Central Australia. J.Geol. Soc.Aust. 26:17-28.

ALLEN A.R. & STUBBS D. 1982. An $^{40}Ar/^{39}Ar$ study of a polymetamorphic complex in the Arunta Block, central Australia. Contrib.Mineral. Petrol. 79:319-332.

ARMSTRONG R.L. AND STEWART A.J. 1975. Rubidium-strontium dates and extraneous argon in the Arltunga Nappe Complex, Northern Territory. J.Geol.Soc.Aust. 22:103-115.

ARTH J.G. 1976. Behaviour of trace elements during magmatic processes--A summary of theoretical models and their applications. J.Res. US Geol.Surv. 4:41-47.

ARTH J.G. 1979. Chapter 3: Some trace elements in trondhjemites - their implications to magma genesis and Palaeotectonic setting. *In:* F. Barker (Editor), Trondhjemites, dacites and related rocks. Development in Petrology 6. Elsevier Scientific Publishing Company. pp123-132.

ARTH J.G. & BARKER F., 1976. REE partitioning between hornblende and dacitic liquid and implications for the genesis of trondhjemitic-tonalitic magmas. Geology,4: 534-536.

ARTH J.G., BARKER F.,PETERMAN Z.E. & FRIEDMAN I. 1978. Geochemistry of the gabbro-diorite-tonalite-trondhjemite suite of the southwest Finland and its implications for the origin of tonalitic and trondhjemitic magmas. J.Petrol., 19:289-316.

ATHERTON M.P., 1984. The coastal batholith of Peru. *In:* R.S. Harman and B.A. Barreiro (Editors), Andean Magmatism. Chemical and Isotopic Constraints. Shiva Geology Series, Cheshire, pp. 168-179.

ATHERTON M.P., McCOUNT W.J., SANDERSON L.M. & TAYLOR W.P. 1979. The geochemical character of the segmented Peruvian Coastal Batholith and associated volcanics. *In:* M.P. Atherton & J. Tarney (Editors), Origin of Granite Batholiths: Geochemical Evidence. pp45-64. Shiva Publishing, Nantwich.

ATHERTON M.P., PITCHER W.S. & WARDEN V. 1983. The Mesozoic marginal basin of central Peru. Nature 305: 303-306.

BAILEY J.C., MORGAN W.R. & BLACK L.P. 1982. Geochemical and isotopic evidence for age, orogenic setting and petrogenesis of the Nychum volcanic association, North Queensland. J.Geol.Soc. Aust. 29:375-393.

BARKER F. 1979. Chapter 1. Trondhjemite: definition, environment and hypothesis of origin. *In:* F. Barker (Editor), Trondhjemites, dacites and related rocks. Development in Petrology 6. Elsevier Scientific Publshing Company. pp1-12.

BARKER F. & ARTH J.G.,1976. Generation of trondhjemitic-tonalitic liquids and Archean bimodal trondhjemite-basalt suites. Geology, 4:596-600.

BLACK L.P. & McCULLOCH M.T., 1984. Sm-Nd ages of the Arunta, Tennank Creek, and Georgetown Inliers of northern Australia. Aust.J.Earth Sci., 31:49-60.

BLACK L.P. & SHERATON J.W. 1986. Late Archaean granulites of the Napier Complex, Enderby Land, Antarctica: a comparison of Rb-Sr, Sm-Nd and U-Pb isotopic systematics in a complex terrain. Precambrian Research 32:343-368.

BLACK L.P., BELL T.H., RUBENACH M.J. & WITHNALL I.W. 1978. The significance of the Rb-Sr tota-rock ages in a multiply deformed and polymetamorphic terrain. In Zartman R.E. (editor). Short papers of the Fourth International Conference, Geochronology, Cosmochronology, Isotope Geology. United States Geological Survey Open File Report 78-701:41-42.

BLACK L.P., BELL T.H., RUBENACH M.J. & WITHNALL I.W. 1979. Geochronology of discrete structural-metamorphic events in a multiply deformed Precambrian terrains. Tectonophysics 54:103-137.

BLACK L.P.,SHAW R.D. & STEWART A.J. 1983. Rb-Sr geochronology of Proterozoic events in the Arunta Inlier, central Australia. BMR J.Aust.Geol.Geophys. 8:129-138.

BLACK L.P. & SHERATON J.W. 1986. Late Archaean granites of the Napier Complex, Enderby Land, Antarctica:a comparison of Rb-Sr, Sm-Nd and U-Pb isotopic systematics in a complex terrain. Precamb.Res. 32: 343-368.

BMR 1983. Australian 1:250,000 Geological Series, Alice Springs and Illogwa Creek Sheets. Second edition.

BMR 1984. Australian 1:100,000 Geological Map Series, Arltunga-Harts Range Sheet. First edition.

CAWTHORN R.G., STRONG D.F. & BROWN P.G. 1976. Origin of corundum-normative intrusive and extrusive magmas. Nature, Lond. 259:102-104.

CHAPPELL B.W. & WHITE A.R.J. 1974. Two contrasting granite types. Pac.Geol. 8:173-174.

CHAPPELL B.W. & WHITE A.J.R. 1982. I- and S- type granites in the lachlan Fold Belt, southeastern Australia. *In:* Geology of Granites and their Metallogenetic Relations. Nanjing, China, pp87-101.

CHATTERJEE A.K. & STRONG D.F. 1985. Review of some chemical and mineralogical characteristics of granitoid rocks hosting Sn,W,U, Mo deposits in Newfoundland and Nova Scotia. *In:* High heat production (HHP) granites, hydrothermal circulation and ore genesis. Edited by: Inst. Mining & Metallurgy, London.

CLARKE D.B. 1981. The mineralogy of peraluminous granites: a review. Can.Mineral. 19:3-17.

CLARKE D.B. & MUECKE G.K. 1985. Review of the petrochemistry and origin of South Mountain batholith and the associated plutons, Nova Scotia Canada. *In:* High heat production (HHP) granites, hydrathermal circulation and orgenesis. Inst.Ming.Metal., London, 41-54.

COBBING E.J., PITCHER W.S., WILSON J.J., BALDAK J.W., TAYLOR W.P., McCOURT W.J. & SNELLING N.J. 1981. The geology of the Western Cordillera of northern Peru. Overseas Mem.Inst.Geol.Sci. No5.

COLLINS W.J., BEAM S.D., WHITE A.J.R. & CHAPPELL B.W., 1982. Nature and origin of A-type granites with particular reference to southeastern Australia. Contrib.Mineral.Petrol. 80:189-200.

COMPSTON W. & CHAPPELL B.W. 1979. Sr-isotope evolution of granitoid source rocks. *In:* M.W. McElhinny (Editor), The Earth: its origin, structure and evolution. Academic Press, London.

CONDIE K.C.,1982. Plate tectonics model for Proterozoic continental accretion in the southwestern United States. Geology, 10:37-42.

CONDIE K.C., 1985. Secular variation in the composition of basalts: an index to mantle evolution. J.Pet. 26:545-563.

COOPER J.A.,MORTIMER G.E. & JAMES P.R. 1988. Rate of Arunta Inlier evolution at the eastern margin of the Entia Dome, central Australia. Precam. Res., 40/41:217-231.

COOPER J.A., WELLS A.T. & NICHOLAS T. 1971. Dating of glauconite from the Ngalia Basin, Northern Territory, Australia. Geol.Soc. Aust.J. 18:97-106.

CORFU F. & GRUNSKY E.C., 1987. Igneous and tectonic evolution of the Batchawana Greenstone Belt, superior Province: a U-Pb zircon and titanite study. J.Geol. 95:87-105.

CUMMING G.L. & RICHARDS J.R. 1975. Ore lead isotope ratios in a continuously changing earth. Earth Plan. Sci. Lett. 28:155-171.

DE PAOLO D.J. 1981. Trace element and isotopic effects of combined wall rock assimilation and fractional crystallization. Earth Plan.Sci.Lett. 53:189-202.

DING P. & JAMES P.R., 1985. Structural evolution of the Harts Range area and its application for the development of the Arunta Block, central Australia. Precam. Res., 27:251-276.

DUPUY C & DOSTAL J. 1984. Trace element geochemistry of some continental tholeiites. Earth Plan.Sci.Lett. 67:61-69.

EICHELBERGER J.C. 1978. Andesitic volcanism and crustal evolution. Nature 275:21-27.

EMMERMANN R. 1977. A petrogenetic model for the origin and evolution of the Hercynian granite series of the Schwarzwald. N.Jb.Miner.Abh. 128:219-253.

ERLANK A.J. & KABLE E.J.D. 1976. The significance of incompatible elements in Mid-Atlantic Ridge basalts from 45°N with particular reference to Zr/Nb. Contrib.Mineral. Petrol. 54:281-291.

ETHERIDGE M.A. & COOPER J.A., 1981. Rb/Sr isotopic and geochemical evolution of a recrystallized shear (mylonite) zone at Broken Hill. Contrib.Mineral.Petrol., 78:74-84.

ETHERIDGE M.A., RUTLAND R.W.R. & WYBORN L.A.I., 1987. Orogenesis and tectonic process in the early to middle Proterozoic of Northern Australia. *In:* A.Kroner (Editor), Proterozoic Lithospheric Evolution. Am.Geophys.Un., Geodynamics Series,17:131-147.

FLETCHER I.R.,WILDE S.A. & ROSMAN K.J.R., 1985. Sm-Nd model ages across the margins of the Archean Yilgarn Block, Western Australia--III. The western margin. Aust.J.Earth Sci., 32:73-82.

FODEN J.D., BUICK I.S. & MORTIMER G.E.,1988. The petrology and geochemistry of granitic gneisses from the east Arunta Inlier, central Australia:implications for Proterozoic

crustal development. Precamb.Res.,40/41:233-259.

FORMAN D.J. 1971. The Arltunga Nappe Complex, MacDonnell Ranges, Northern Territory. BMR Aust. Bull. 18(2):173-182.

FORMAN D.J.,MILLIGAN E.N. & McCARTHY W.R. 1967. Regional geology and structure of the north-eartern margin of the Amadeus Basin, Northern Territory. Rep.BMR Geol. Geophys.Aust., 103.

FYFE W.S. 1973. The granulite facies, partial melting and the Archaean crust. Phil.Trans.R. Soc. Lond. A273:457-461.

GORBATSCHEV R. & GAAL G., 1987. The Precambrian history of the Baltic Shield. *In:* A. Kroner (Editor), Proterozoic Lithospheric Evolution. Am.Geophys.Un., Geodynamics Series, 17:149-160.

GREEN T.H. 1981. Experimental evidence for the role of accessory phases in magma genesis. J.Volcano.Geotherm.Res. 10:405-422.

GREEN T.H. & RINGWOOD A.E. 1968. Genesis of the calc-alkaline igneous rock suite. Contrib.Mineral.Petrol. 18:105-162.

GRIFFIN T.J., WHITE A.J.R. & CHAPPELL B.W. 1978. The Moruya Batholith and geochemical contrasts between the Moruya and Jindabyne suites. J.Geol.Soc.Aust. 25:235-247.

GROVET.L.,GERLACH D.C. & SANDO T.W. 1982. Phase equilibria of calc-alkaline series lavas at Medicine Lake, Northern California:fractionation, assimilation and mixing. contrib. Mineral.Petrol. 80:160-182.

HALLIDAY A.N., STEPHENS W.E. & HARMON R.S. 1981. Isotopic and chemical constraints on the development of peraluminous Caledonian and Acadian granites. Can.Mineral. 19:205-216.

HARISON T.M. & McDOUGALL I. 1980. Investigation of an intrusive contact, northwest Nelson, New Zealand - I. Thermal, chronological and isotopic constraints. Geochim. Cosmochim. Acta 44:1985-2003.

HARRIS N.B.W., HAWKESWORTH C.J., VAN CALSTEREN P. & McDERMOTT, 1987. Evolution of continental crust in southern Africa. Earth Plan.Sci.Lett.,83:85-93.

HARRIS N.B.W., PEARCE J.A. & TINDLE A.G., 1986. Geochemical characteristics of

collision-zone magmatism. *In:* M.P. Coward and A.C. Ries (Editors), Collision Tectonics. Geol.Soc.Spec. Publ., 19:67-81.

HIGGINS N.C., SOLOMON M. & VARNE R. 1985. The genesis of the Blue Tier batholith, northeastern Tasmonia. Lithos 18, 129-149.

HILDRETH W. 1979. The Bishop Tuff: evidence for the origin of compositional zonation in silicic magma chambers. Geol.Soc.Am. Spec.Pap. 180:43-75.

HILDRETH W. 1981. Gradients in silicic magma chambers: implications for lithospheric magmatism. J.Geophys.Res. 86,10153-82.

HOFMANN A.W. 1979. Rb-Sr dating of thin slabs: an imperfect method to determin the age of metamorphism. In E.Jager & J.C. Hunzikerled, Lectures in Isotope Geology. 27-29. Springer-Verlag, Berlin, 329pp.

HOFFMAN P.E.,1980. Wopmay Orogen:A Wilson cycle of the Proterozoic age in the northwest of the Canadian Shield. *In:* D.W. Strangway (Editor), The Continental Crust and its Mineral Deposits. Geological Association of Canada,Spec.Pap.,20:523-549.

HOLM P.E. 1985. The geochemical fingerprints of different tectonomagmatic environments using hygromagmatophile element abundances of tholeiitic basalts and basaltic andesites. Chem.Geol. 51:303-323.

HONNEGER K., DIETRICH V., FRANK W.,GANSSER A., THONI M. & TROMMSDORFF V., 1982. Magmatism and metamorphism in the Ladakh Himalayas (the Indus-Tsangpo suture zone). Earth Plan. Sci. Lett., 60:253-292.

HYNES A. & GEE R.D., 1986. Geological setting and petrochemistry of the Narracoota Volcanics, Capricorn Orogen, Western Australia. Precamb. Res., 31:107-132.

IRVINE T.N. & BARAGAR W.R.A. 1971. A guide to the chemical classification of the common volcanic rocks. Can.J.Earth Sci. 8:523.

IYER S.S., WOODFORD P.J. & WILSON A.F. 1976. Rb-Sr isotopic studies of a polymetamorphic granulite terrain, Strangways Range,central Australia. Lithos 9:211-224.

JAMES P.R. & DING P., 1988. "Caterpillar tectonics" in the Harts Range area:a kinship between two sequential Proterozoic extension-collision orogenic belts within the eastern Arunta Inlier of central Australia. Precam. Res., 40/41:199-216.

KLEEMAN A.W. 1965. The origin of granitic magmas. J.Geol.Soc.Aust. 12, Part I:35-52.

KROGH T.E. 1973. A low-contamination method for hydrathermal decomposition of zircon and extraction of U and Pb for isotopic age determinations. Geochim.Cosmochim.Acta, 37:485-494.

KROGH T.E., 1982. Improved accuracy of U-Pb zircon ages by the creation of more concordant systems using an air abrasion technique. Geochim.Cosmochim.Acta, 46:637-649.

KRONER A., 1983. Proterozoic mobile belts compatible with the plate tectonic concept. Geol.Soc.Am.Mem.,161:59-74.

KRONER A., 1987. Preface and dedication. *In:* A. Kroner (Eiditor), Proterozoic Lithospheric Evolution. Am. Geophys. Un., Geodynamics Series,17.

LUDWIG K.R. 1980. Calculation of uncertainties of U-Pb isotope data. Earth Plan.Sci.Lett. 46:212-220.

LUGWIG K.R. 1983. Plotting and regression programs for isotopic geochemists, for use with HP-86/87 microcomputers. U.S. Geol.Surv. Open.File Rep. 83-849, 94pp.

LUGWIG K.R. & COOPER J.A. 1984. Geochronology of Precambrian granites and associated U-Ti-Th mineralization, north Olary Province, South Australia. Contrib.Mineral.Petrol. 86:298-308.

MACKENZIE D.E., BLACK L.P. & SUN S.S. 1988. Origin of alkali-feldspar granites: an example from the Poimena Granite, northeastern Tasmania, Australia. Geochim. Cosmochim. Acta, in press.

MANNING D.A. & PICHAVANT M. 1983. The role of fluorine and boron in the generation of granitic melts. *In:* M.P. Atherton & C.D. Gribble (Editors) Migmatites, melting and metamorphism. Shiva Publishing Ltd., Cheshire 94-109.

McCULLOCH M.T., 1987. Sm-Nd isotopic constraints on the evolution of Precambrian crust in the Australian continent. *In:* A.Kroner (Editor), Proterozoic Lithospheric Evolution. Am.Geophys.Un., Geodynamics Series,17:115-130.

McGREGOR V.G. 1979. Chapter 6: Archean gray gneisses and origin of the continental crust: evidence from the Godthab region, West Greenland. *In:* F. Barker (Editor), Trondhjemites, dacites and related rocks. Development in Petrology 6. Elsevier Scientific Publishing Company. pp169-204.

MESCHEDE M. 1986. A method of discriminating between different types of mid-ocean ridge

basalts and continental tholeiites with the Nb-Zr-Y diagram. Chem.Geol. 56:207-218.

MIYASHIRO A. & SHIDO F. 1975. Tholeiitic and calc-alkalic series in relation to the behaviours of titanium, vanadium, chromium, and nickel. Am.J.Sci. 275, 265-277.

MORTIMER G.E. 1985. Early to middle Proterozoic granitoids, basaltic dykes and associated layered rocks of S.E. Eyre Peninsula, South Australia. Ph.D thesis, University of Adelaide (unpublished).

MORTIMER G.E.,COOPER J.A. & JAMES P.R. 1987. U-Pb and Rb-Sr geochronology and geological evolution of the Harts Range ruby mine area of the Arunta Inlier, central Australia. Lithos 20:445-467.

MULLEN E.D. 1983. $MnO-TiO_2-P_2O_5$: a minor element environments and its implications for petrogenesis. Earth Plan.Sci.Lett. 62:53-62.

NESBITT R.W. & STANLEY J.L. (Editors) 1980. Compilation of analytical geochemistry reports 1973-1979, Research Report 3. Centre for Precambrian Research, University of Adelaide.

NORRISH K. & HUTTON J.T. 1969. An accurate X-ray spectrographic method for the analysis of a wide range of geologic samples. Geochim. Cosmochim.Acta 33:431-451.

NYKIEL A.J. 1986. The geology, petrology and geochemistry of the area north of Spriggs Creek Bore, western margin of the Entia Dome, Harts range, eastern Arunta Block, Northern Territory. Honours Thesis, University of Adelaide (unpublished).

OGASAWARA M., 1988. Geochemistry of the Early Proterozoic granitoids in the Halls Creek Orogenic Subprovince, northern Austra. Precamb. Res. 40/41:469-486.

OVCHINNIKOV L.N., VORONOVSKIY S.N. & OVCHINNIKOVA L.V. 1986. Isotope geochronology of metamorphic processes. Int.Geol.Rev. 28:584-596.

PAGE R.W. 1978. Response of U-Pb zircon and Rb-Sr total-rock and mineral systems to low-grade regional metamorphism in Proterozoic igneous rocks, Mount Isa, Australia. J.Geol.Soc.Aust. 25:Pt 3, 141-164.

PAGE R.W., 1988. Geochronology of early to middle Proterozoic fold belts in northern Australia:a review. Precamb.Res. 40/41: 1-20.

PAGE R.W. & HANCOCK S.L., 1988. Geochronology of a rapid 1.85--1.86 Ga tectonic transition:Halls Creek Orogen, northern Australia. Precamb.Res. 40/41:447-468.

PEARCE J.A. 1980. Geochemical evidence for the genesis and eruptive setting of lava from Tethyan ophiolites. *In:* A. Panayiotou (Editor), Proceedings, International ophiolite symposium. Cyprus 1979: Nicosia, Cyprus Geol. Surv. pp261-272.

PEARCE J.A. & CANN J.R. 1973. Tectonic setting of basic volcanic rocks. Earth Plan.Sci.Lett. 19:290-300.

PEARCE J.A. & NORRY M.J. 1979. Petrogenetic implications of Ti, Zr,Y, and Nb variations in volcanic rocks. Contrib.Mineral. Petrol. 69:33-47.

PERFIT M.R., BRUECKNER H., LAWRENCE J.R. & KAY R.W. 1980. Trace element and isotopic variations in a zoned pluton and associated volcanic rocks, Unalaska island,Alaska: A model for fractionation in the Aleutian calc-alkaline suite. Contrib. Mineral. Petrol., 73:69-87.

PITCHER W.S. 1984. Panerozoic plutonism in the Peruvian Andes. *In*: R.S.Harmon and B.A.Barreiro (Editors), Andean Magmatism:Chemical and Isotopic Constraints. Shiva Geology Series,pp.152-167.

PITCHER W.S. 1987. Granites and yet more granites forty years on. Geologische Rundschau 76/1:51-79.

PLUMB K.A. 1979. The tectonic evolution of Australia. Eath Sci. Rev., 14:205-249.

PRICE R.C. , BROWN W.M. & WOOLARD C.A. 1983. The geology, geochemistry and origin of late-Silurian high-si igneous rocks of the Upper Murray Valley, NE Victoria. J.Geol. Soc.Aust. 30,443-459.

RINGWOOD A.E. 1974. The petrological evolution of island arc systems. J.Geol.Soc.Lond. 130:183-204.

ROLLINSON H.R. & WINDLEY B.F. 1980. Selective elemental depletion during metamorphism of Archaean granulites, Scourie, NW Scotland. Contrib.Mineral.Petrol. 72:257-263.

SANDO B.G. 1987. The geology, petrology and geochemistry of the Tommys Gap area in the Giles Creek Synform, MacDonnell Ranges, southeastern Arunta Inlier, Northern Territory. Honours Thesis, University of Adelaide (unpublished).

SAUNDERS A.D. & TARNEY J. 1979. Geochemistry of basalts from back-arc spreading centres in East Scotia Sea. Geochim.Cosmochim. Acta 43:555-572.

SAUNDERS A.D., TARNEY J., STERN C. & DALZIEL I.W.D. 1979. Geochemistry of

Mesozoic marginal basin floor igneous rocks from southern Chile. Geol.Soc.Am.Bull. 90:237-258.

SAWKA W.N., CHAPPELL B.W. & NORRISH K., 1984. Light rare earth element zoning in sphene and allanite during granitoid fractionation. Geology, 12:131-134.

SCHARER U., KROGH T.E. & GOWER C.F., 1986. Age and evolution of the Grenville Province in the eastern Labrador from U-Pb systematics in accessory minerals. Contrib.Mineral.Petrol., 94:438-451.

SHAW R.D., LANGWORTHY A.P., OFFE L.A., STEWART A.J., ALLAN A.R., SENIOR B.R. & CLARKE D. , 1979. Geological report on 1:100,000 scale mapping of the Southeastern Arunta Block, Alice Springs 1:250,000 Sheet area, Northern Territory. BMR record 1979/47 (unpbl.).

SHAW R.D., FREEMAN M.J., OFFE L.A. & SENIOR B.R. 1982. Geology of the Illogwa Creek 1:250,000 Sheet area, central Australia - Preliminary data, 1979-80 surveys. BMR Geol.Geophys.Record 1982-83 (unpbl.).

SHAW R.D., STEWART A.J. & BLACK L.P., 1984. The Arunta Inlier: a complex ensialic mobile belt in central Australia. Part 2: tectonic history. Aust.J.Earth Sci.,31:457-484.

SHAW R.D., STEWART A.J., YAN KHAN M. & FUNK J.L. 1971. Progress reports on detailed studies in the Arltunga Nappe Complex, Northern Territory, 1971. BMR, Australia, Record 1971/66.

SHERVAIS J.W. 1982. Ti-V plots and the petrogenesis of modern and ophiolitic lavas. Earth Plan.Sci.Lett. 59:101-118.

SIVELL W.J. 1988. Eastern Arunta orthogneiss suites--implications for a repeated transition from rift to subduction-related magmtism during successive Proterozoic ensialic orogenesis. *In:* Nine Aust.Geol.Conv. Geol.Soc.Aust.Abs., pp370-371.

SIVELL W.J. 1988. Geocheistry of metatholeiites from the Harts Range, central Australia:implications for mantle source heterogeneity a Proterozoic mobile belt. Precamb.Res. 40/41: 261-276.

SIVELL W.J. & FODEN J.D., 1985. Banded amphibolites of the Harts Range metaigneous complex, central Australia: a bimodal basalt-tonalite suite. Precamb.Res., 28:223-252.

SIVELL W.J. & FODEN J.D. 1988. Amphibolites from the Entia Gneiss Complex, eastern

Arunta Inlier:geochemical evidence for a Proterozoic transition from extensional to compressional tectonics. Precamb.Res. 38:235-255.

SPARKS R.S.J., HUPPERT H.E. & TURNER J.S. 1984. The fluid dynamics of evolving magma chambers. Phil.Trans.R.Lond. A310:511-534.

STEWART A.J. 1971a. Potassium-argon dates from the Arltunga Nappe Complex, Northern Territory. J.Geol.Soc.Aust. 17(2):205-211.

STEWART A.J. 1971b. Structural evolution of the White Range Nappe, central Australia. Ph.D thesis, Yale University. University Microfilm Inc. Ann Arbor, Michigan.

STEWART A.J., SHAW R.D. & BLACK L.P., 1984. The Arunta Inlier: a complex ensialic mobile belt in central Australia.Part 1:stratigraphy, correlations and origin. Aust.J.Earth Sci.,31:445-455.

STEWART K.P., 1985. The petrological significance of calc-silicate and associated gneisses, Inkamulla Bore area, Entia Dome, Harts Range, Eastern Arunta Block. Honour's Thesis, the Uinversity of Adelaide (unpbl.).

SUN S.S. & NESBITT R.W. 1978. Petrogenesis of Archean ultrabasic and basic volcanics: evidence from rare earth elements. Contrib.Mineral. Petrol. 65:301-325.

SUN S.S.,NESBITT R.W. & SHARASKIN Y.A.1979. Geochemical characteristics of mid-oceanic ridge basalts. Earth Plan.Sci.Lett. 44:119-138.

SWANSON S.E. 1977. Relation of nucleation and crystal-growth rate to the development and granitic texture. Am.Min. 62:966-978.

TARNEY J. & WINDLEY B.F. 1977. Chemistry, thermal gradients and evolution of the lower continental crust. J.Geol.Soc.Lond. 134:153-172.

TARNEY J. & SAUNDERS A.D. 1979. Trace element constraints on the origin of Cordilleran batholiths. *In*:: M.P. Atherton & J. Tarney (Editors), Origin of Granite Batholiths, Geochemical Evidence. Shiva Publishing Ltd., Cheshire, 90-105.

TARNEY J., SAURDERS A.D. & WEAVER S.D. 1977. Geochemistry of the volcanic arcs and marginal basins of the Scotia are region. *In:* M. Talwani and W.C. Pittman III (Editors), Island Arcs, Deep Sea Trenchews and Back-Arc Basins. Am. Geophys. Union, Maurice Ewing Ser., 1:367-377. Drilling Project 49. U.S. Government Printing Office, Washington. D.C., pp. 657-692.

TARNEY J., WEAVER B. & DRURY S.A. 1979. Geochemistry of Archean Trondhjemitic and tonalitic gneisses from Scotland and East Greenland. *In:* F.Barker (Editor), Trondhjemites, dacites, and relted rocks. Development in Petrology 6. Elsevier Scientific Publishing Company. pp275-299.

TARNEY J., SAUNDERS A.D., MATTEY D.P., WOOD D.A. & MARSH N.G., 1981. Geochemical aspects of back-arc spreading in Scotia Sea and Western Pacific. Phil.Trans.R.Soc.Lond. A300:263-285.

THORNTON C.P. & TUTTLE O.F. 1960. Chemistry of igneous rocks. I. Differentiation Index. Am.J.Sci. 258:664-684.

THORPE R.S. & FRANCIS P.W. 1979. Petrogenic relationships of the volcanic and intrusive rocks of the Andes. *In:* M.P. Artherton & J. Tarney (Editors), Origin of Granite Batholiths, geochemical Evidence. Shiva Publishing Ltd., Cheshire, 65-74.

TILTON G. & GRUNENFELDER M. 1968. Sphene: uranium-lead ages. Science 159, 1458.

TUCKER R.D., RAHEIM A., KROGH T.E. & CORFU F. 1986/87. Uranium-lead zircon and titanite ages from the northern portion of the Western Gneiss Region, south-central Norway. Earth Plan.Sci. Lett., 81:203-211.

TUTTLE O.F. & BOWEN N.L. 1958. Origin of granite in the light of experimental studies in the system $NaAlSi_3O_8$-$KAlSi_3O_8$-SiO_2-H_2O. Geol.Soc.Am.Mem. 74.

VAN SCHMUS W.R., BICKFORD M.E.,LEWRY J.F. & MACDONALD R., 1987. U-Pb geochronology in the Trans-Hudson Orogen, northern Saskatchewan, Canada. Can.J.Earth Sci. 24:407-424.

VAN SCHMUS W.R.; BICKFORD M.E. & ZIETZ I. 1987. Early to middle Proterozoic Provinces in the Central United States. *In:* A.Kroner (Editor), Proterozoic Lithospheric Evolution. Am.Geophys.Un., Geodynamics Series, 17:43-68.

WAGNER G.A., REIMER G.M. & JAGER E. 1977. Cooling ages derived by apatite fission track, mica Rb-Sr and K-Ar dating: uplift and cooling of the central Alps. Memoir Inst. Geol.Mineral., University of Padova, Italy, 30:1-27.

WALL V.J.,CLEMENS J.D. & CLARKE D.B. 1987. Models for granitoid evolution and source compositions. J.Geol. 95:731-749.

WARREN R.G., 1983. Metamorphic and tectonic evolution of granulites, Arunta Block, central

Australia. Nature,305:300-302.

WARREN R.G. & STEWART A.J., 1988. Isobaric cooling of Proterozoic high-temperature metamorphites in the northern Arunta Block, central Australia:implication for tectonic evolution. Precamb.Res. 40/41:175-198.

WARREN R.G., WYBORN L.A.I. & McCULLOCH M.T. 1988. Geochemical studies in the Arunta Block, central Australia. *In:* Nine Aust. Geol.Conv.Geol.Soc.Aust.Abs., p411.

WATSON E.B. & HARRISON T.M. 1984. Accessory minerals and the geochemical evolution of crustal magmatic systems:a summary and prospectus of experimental approaches. Physics Earth.Plan.Int. 35:19-30.

WEAVER S.D., SAUNDERS A.D. & TARNEY J. 1979. A geochemical study of magmatism associated with initial stages of back-arc spreading. Contrib.Mineral.Petrol., 68:151-169.

WEAVER S.D., SAUNDERS A.D., PANKHURST R.J. & TARNEY J 1979. A geochemical study of magmatism associated with the initial stages of back-arc spreading, the Quarternary volcanics of Bransfield Strait, from south Shetland Islands. Contrib.Mineral.Petrol. 68:151-169.

WEBB P.C.,TINDLE A.G.,BARRITT S.D.,BROWN G.C. & MILLER J.F. 1985. Radiothermal granites of the United Kingdom:comparison of fractionation patterns and variation of heat production for selected granites. *In:* High heat production (HHP) granites, hydrothermal circulation and ore genesis. Edited by: Inst. Mining & Metallurgy, London.

WHALEN J.B., 1985. Geochemistry of an island-arc plutonic suite: the Uasilau-Yau Yau Intrusive Complex, New Britain, P.N.G.J. Petrol., 26:603-632.

WHITE A.J.R. & CHAPPELL B.W. 1977. Ultrametamorphism and granitoid genesis. Tectonophys. 43:7-22.

WHITE A.J.R., CLEMENS J.D., HOLLOWAY J.R., SILVER L.T., CHAPPELL B.W. & WALL V.J. 1986. S-type granites and their probable absence in southwestern North America. Geology 14:115-118.

WINDRIM D.P. & McCULLOCH M.T., 1986. Nd ans Sr isotopic systematics of central Australain granulites:chronology of crustal development and constraints on the evolution of lower continental crust. Contrib.Mineral.Petrol.,94:289-303.

WOOD D.A., JORON J. & TREUIL M. 1979. A re-appraisal of the use of trace elements to

classify and discriminate between magma series erupted in different tectonic settings. Earth Plan.Sci.Lett. 45:326-336.

WRIGHT T.L. & DOHERTY P.C. 1970. A linear programming and least sequares computer method for solving petrologic mixing problems. Bull.Geol. Soc.Am. 81:1995-2008.

WYBORN L.A.I., 1988. Petrology,geochemistry and origin of a major Australain 1880-1840 Ma felsic volcano-plutonic suite:a model for intracontinental felsic magma generation. Precamb.Res., 40/41:37-60.

WYBORN L.A.I. & PAGE R.W., 1983. The Proterozoic Kalkadoon and Edwen Batholiths, Mt Isa Inlier, Queensland:source,chemistry, age and metamorphism. BMR J.Aust.Geol.Geophys.,8:53-69.

WYBORN L.A.I., PAGE R.W. & McCULLOCH M.T., 1988. Petrology, geochronology and isotope geochemistry of the post-1820 Ma granite of the Mount Isa Inlier:mechanism for the generation of the Proterozoic anorogenic granites. Precamb. Res. 40/41:509-542.

WYLLIE P.J. 1983. Experimental and thermal constraints on the deep-seated parentage of some granitoid magmas in subduction zones. *In:* M.P. Atherton & C.D. Gribble (Editors), Migmatites, Melting and Metamorphism. Shiva Publishing Ltd., Cheshire 37-51.

XU KEQIN, SUN NAI, WANG DEZI, HU SHOUXI, LIU YINGJUN & JI SHOUYUAN, 1984. Petrogenesis of the granitoids and their metallurgenic relations in South China. *In:* Geology of granites and their metallurgenic relations. Science Press, Beijing, 954pp.

Missing References

Dalzeil IW (1986) Collision and Cordileran Orogenesis: an Andean perspective. In: Coward MP, Ries AC (1981) Collision Tectonics. Geol Soc Spec Publ 19:389-404

Jones DL, Silberbing NJ, Coney PJ (1986) Collision tectonics in the Cordilera of western N. America: examples from Alaska. In: Coward MP, Ries AC (1981) Collision Tectonics. Geol Soc Spec Publ 19:367-387

London D (1987) Internal differentiation of rare-element pegmatites: Effects of boron, phosphorus, and fluorine. Geochim Cosmochim Acta 51:403-420

Sivell W, Rankin P (1983) Arc-tholeiite and ultramafic cumulate, Brook Street Volcanics, west D'Urville Island, New Zealand. New Zealand J Geol Geophys 26:239-257

Watson EB (1979) Zircon saturation in felsic liquids: experimental results and applications to trace element geochemistry. Contrib Mineral Petrol 70:407-419

APPENDIX--1: EXPERIMENTAL TECHNIQUES

(1) ZIRCON & SPHENE U-Pb GEOCHRONOLOGY

Sample selection and preparation

Samples about 20--50 kg in weight were collected from several localities where weathering is minimal for use to separate zircons and sphenes.

These samples were crushed to less than 500μ in grainsize and zircons extracted using conventional Wilfley Table, heavy liquids and electromagnetic techniques. The zircon concentrates were divided first into size and then magnetic fractions.

Zircon fraction selection

The size and magnetic fractions obtained aboved were examined under binocular microscope and further purified by hand-picking to remove any impurities. Grain modifying techniques such as air-abrasion (Krogh 1982) were applied for most of the fractions. Final zircon fractions of 3-10 mg were boiled in aqua regia overnight and rinsed many times in pure water prior to dissolution.

Chemical procedures and isotopic measurement and calculation

The chemical analysis procedures for U and Pb contents and Pb isotopic ratios were adapted from those of Krogh (1973), which include pressure decomposition in teflon bombs followed by spiking and ion exchange column separation. A mixed $^{208}Pb/^{235}U$ spike was used. Blank levels were 1.0 ng of Pb of modern isotopic composition and 0.01ng of U. A modified Thompson TSN 206S mass-spectrometer was used for isotopic ratio measurements. Uncertainties in the $^{206}Pb/^{238}U$ and $^{207}Pb/^{235}U$ ratios are generally 0.3-0.4% at the 95% confidence level. Similarly uncertainties in the $^{207}Pb/^{206}Pb$ ratios are about 0.1%. Concordia-disconcordia analyses were made following Ludwig (1980,1983). Constants utilized in the age calculations are λ_{238U} =

$0.155125 \times 10^{-9}\ a^{-1}$, $\lambda_{235U} = 0.984850 \times 10^{-9} a^{-1}$, $^{238}U/^{235}U = 137.88$. Common lead corrections were made using the isotopic compositions predicted by Cumming and Richards (1975) lead-evolution model.

Sphene

Similar procedures to those for zircons were used for processing sphene fractions. The differences lie in: (1). They were washed using pure acetone instead of aqua regia; (2). They were decomposed in telflon vessels at a lower temperature.

(2) RB-SR GEOCHRONOGY

Sampling of a rock unit for Rb-Sr isotopic analysis is similar to that for WR major and trace element analysis. But for Rb-Sr isochron, a certain outcrop area about $20x20m^2$ was chosen.

WR and mica samples were dissolved in HF-$HClO_4$ and Rb, Sr fractions were collected through conventional ion exchange procedures. Two types of mixed ^{87}Rb-^{84}Sr spikes (one for WR and one for mica) were added to the WR and mica respectively before dissolution. Rb and Sr isotopic ratios were measured using the modified Thompson TSN 206S mass spectrometer. All ratios were corrected for variable mass discrimination by normalizing $^{88}Sr/^{86}Sr$ to 8.3752.

Age and test of significance for Rb-Sr WR isochron are at the 95% confidence limit. The λ_{87Rb} used is $1.42 \times 10^{-11} a^{-1}$.

(3) MAJOR AND TRACE ELEMENT GEOCHEMISTRY

Samples for WR major and trace element analyses were collected from relatively unweathered outcrops. They were crushed in the jaw crusher and about 100g splits were finely powdered (<200 mesh) in the Siebtechnik tungsten carbide mill.

Most major and trace element analyses were determined by the XRF techniques using the

Siemens SRS-1 spectrometer following the method of Norrish and Hutton (1969). Sodium concentrations were analysed on the atomic absorption spectrometer. International Standards and Abbey's (1980) recommented values were used for calibration during trace element determinations.

(4) REE GEOCHEMISTRY

REE analyses were determined by isotope dilution mass spectrometry following the method described in Sun and Nesbitt (1978). The general procedures have been compiled in a single volume of analytical method reports by Nesbitt and Stanley (1980). However, some modification has been made in this study. This includes: (1). Sample sizes used for analyses in this study are about 100-300mg and generally much smaller than that described in the reports of Nesbitt and Stanley (1980); (2). Sample and spike were directly weighed into 30ml teflon bomb and a pressure decomposition at T=200°C was applied for most of the samples, especially the zircon-rich felsic types; (3). REE fractions were collected by passing the sample solution through two cation exchange columns recently calibrated by the present author. The collection positions for these fractions are slightly different; (4). Normally, the REEs are separated into a HREE fraction, a MREE fraction, a Ce fraction free of Nd and a La fraction fraction free of Ce and Ba. But some excellent runs indicate that the La and Ce isotopic ratios can be measured on one fraction without significant interference.

In addition, the two types of spikes used in this study were made by Dr Shen-Su Sun. Their parameters have been listed in the reports of Nesbitt and Stanley (1980).

APPENDIX-2: SAMPLE AND PHOTOGRAPH LOCALITIES

Localities of samples for photomicrographs, WR, REE and isotopic analyses and field photographs are shown in the accompanying map. Solid squares represent localities for field photographs, and solid triangles, localities of samples for zircon U-Pb isotopic analysis. Symbol "x" stands for localities of other types of samples. For legend, refer to the geological map in the enclosure.

A few samples such as 87131, 88056, 88100 to 88113 were collected from transported rock blocks in the lower reach of the Atnarpa Creek in the study area. This sampling was undertaken only after a general understanding of the field relations. Usually much less weathered specimens essential for geochemical analyses can be obtained in this way.

Samples 88046 to 88049 were taken from south of the Atnarpa Range, that is, about 2 km SE of the Chabana Waterhole in the BMR 1:100,000 Geological Map, Harts Range-Arltunga Sheet. Samples 88051 & 88052 were collected at about 25 km on the track from the Atnarpa Station to Tommy's Gap. Samples 88084 to 88087 were taken from the Marmalade Dam area.

SAMPLE AND PHOTOGRAPH LOCALITY MAP

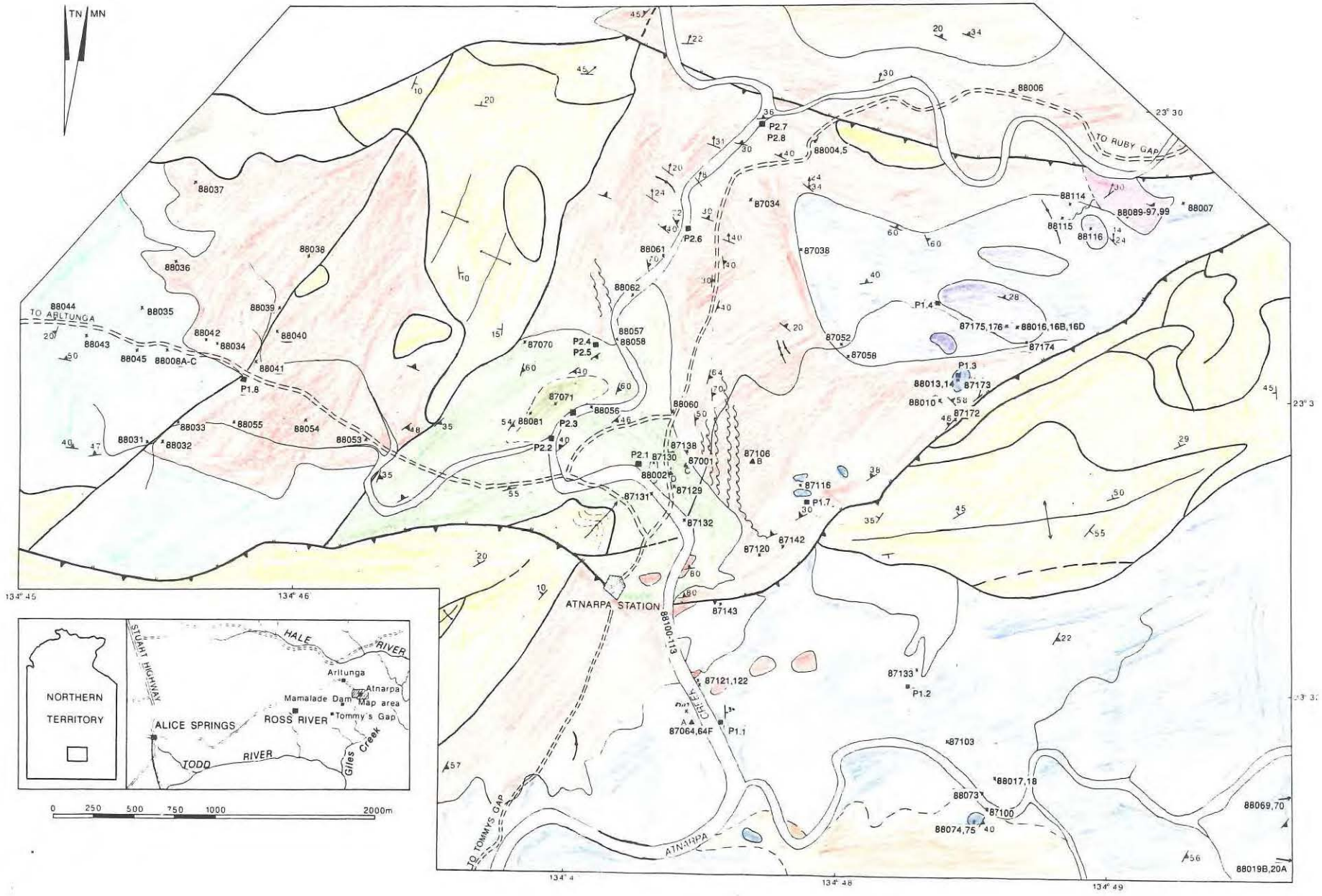

APPENDIX--3: WR MAJOR AND TRACE ELEMENT ANALYTICAL DATA

Note One: Total Fe is expressed as Fe_2O_{3tot}. L.O.I. (loss on ignition) is determined by ignition at 960°C. n.d.: not determined.

Note Two: There are a number of XRF major element analyses which give low "total" values. For testing, 3 analyses with low "totals" and one with normal "total" were repeated by re-fusing the previously fused samples at the same fusion temperature overnight (960°C). The results are listed in the following table. The original values are also outlined for comparison. It can been seen that the values of the repeated analyses for the samples with low "total" values do have in general proportionally increased, except for MgO values, which change dramatically probably due to the "standard" problem (Stanley, personal discussion). However, the "total" values in these repeated analyses are still low but the repeated analysis on the sample with normal "total" value still produces a normal "total" value.

A further attempt to fuse the sample at a higher temperature (e.g. over 1000°C) failed as samples started melting at this temperature.

Through these tests, an inferrence is made that the analyses with low "total" values could be caused by crystalline volatiles such as $(OH)^-$ which might be retained in the samples at the fusion temperature. Therefore, a normalized values (to 100% water free) during data processing for all other analyses with low total values remain reliable.

Sample	88008A		88047		88049		88055	
	original	repeated	original	repeated	original	repeated	original	repeated
SiO2	61.51	61.95	55.30	55.59	48.95	48.93	73.14	72.74
Al2O3	16.27	16.41	18.72	18.84	27.91	27.89	13.43	13.46
Fe2O3t	6.15	6.18	4.61	4.60	2.79	2.79	2.47	2.46
MnO	0.10	0.11	0.09	0.09	0.03	0.04	0.05	0.02
MgO	2.68	2.90	4.42	4.96	1.21	1.47	0.96	0.93
CaO	4.17	4.19	9.04	9.07	13.19	13.17	1.75	1.73
Na2O	4.25	4.25	3.89	3.89	3.16	3.16	3.71	3.71
K2O	1.22	1.18	0.70	0.68	0.48	0.47	2.83	2.82
TiO2	0.67	0.66	0.10	0.10	0.16	0.16	0.36	0.36
P2O5	0.22	0.20	0.00	0.00	0.00	0.00	0.06	0.06
L.O.I.	0.98		1.34		0.97		1.16	
Total	98.22	90.00	98.21	99.16	98.85	99.04	99.92	99.44

Appendix-3A: Major and trace element analytical data for the ACAS. Rock types: 1=cumulate anorthosite; 2=cumulate pyroxenite to gabbro; 3=differentiative gabbro; 4=diorite; 5=quartz diorite to plagiogranite; 6=fine-grained microdiorite

Rock Type	1	1	1	1	1	2	2	2
Sample Name	88007	88049	88050	88051	88052	87174	87175	88176
Major elements (wt%)								
SiO2	47.47	48.95	47.06	46.67	47.57	50.27	48.59	47.14
TiO2	0.07	0.16	0.06	0.17	0.08	0.52	0.30	0.59
Al2O3	26.68	27.91	27.81	24.74	25.35	11.97	16.55	13.25
Fe2O3tot	2.82	2.79	2.65	4.69	3.37	8.86	6.04	8.69
MnO	0.07	0.03	0.07	0.12	0.10	0.13	0.12	0.17
MgO	4.04	1.21	3.24	5.00	5.01	10.96	9.71	11.76
CaO	15.06	13.19	14.94	15.15	15.05	12.71	15.59	14.03
Na2O	1.98	3.16	1.97	1.62	1.91	2.18	1.20	0.97
K2O	0.60	0.48	0.43	0.47	0.54	0.47	0.28	0.96
P2O5	0.01	0.00	0.01	0.01	0.02	0.35	0.09	0.41
L.O.I.	1.12	0.97	1.20	1.05	1.16	1.25	1.62	2.12
Total	99.92	98.85	99.44	99.69	100.16	99.64	100.09	100.09
Trace elements (ppm)								
Cr	199	16	138	178	200	742	501	493
Ni	59	16	49	43	67	196	149	232
Sc	24	12	17.5	32	26	46	51	52
V	53	97	36	114	55	191	160	213
Cu	10	18	6	15	8	43	136	7
Pb	12	9	7	6	9	4	4	4
Zn	32	19	29	43	38	61	41	79
Rb	17.3	4.6	10.6	8.4	12.6	6.9	5.9	55
Ba	244	321	214	101	118	313	139	198
Sr	748	634	724	613	726	458	350	373
Ga	18	20	18	19	17	12	13	12
Nb	0.7	2	1.4	0.3	0	3.7	1	2.5
Zr	5.1	14.4	4.4	3.5	810	96	25	104
Y	1.7	4.6	0.3	2	1.9	22	8.2	15.3
Th	1.1	6.3	1.5	0.6	0.6	11	2	9.5
U	2.9	5.2	2.5	1.9	1.4	3.3	1.9	4.7
La	5	7	5	6	4	52	10	49
Ce	21	20	16	10	16	118	22	94
Nd	1	0	0	1	8	62	11	55

Continued

Rock Type	2	2	2	2	2	3	3	3
Sample Name	88016	88016D	88018	88086	88116	87038	87143	87173
Major elements (wt%)								
SiO2	49.09	51.21	50.59	51.49	46.46	49.98	52.10	52.28
TiO2	0.26	0.28	0.48	0.66	0.20	0.31	0.69	0.78
Al2O3	16.55	9.35	12.13	9.48	12.70	17.71	13.90	16.86
Fe2O3tot	6.65	6.82	8.22	8.41	9.23	7.06	8.93	7.85
MnO	0.15	0.17	0.17	0.18	0.17	0.14	0.17	0.11
MgO	9.84	13.80	11.62	12.91	13.91	7.02	7.48	5.70
CaO	14.66	15.32	12.07	12.75	12.49	11.59	9.58	10.15
Na2O	1.25	1.02	1.93	1.18	0.77	2.30	2.48	4.22
K2O	0.27	0.35	0.73	1.00	0.93	1.00	1.97	0.46
P2O5	0.11	0.09	0.44	0.30	0.03	0.09	0.55	0.64
L.O.I.	1.34	1.74	1.93	1.64	2.38	2.12	1.49	0.76
Total	100.17	100.15	100.31	100.00	99.27	99.32	99.34	99.81
Trace elements (ppm)								
Cr	120	2798	859	1260	565	184	212	30
Ni	138	205	229	258	228	80	85	45
Sc	49	64	44	53	49	39	36	30
V	132	151	153	187	120	143	206	204
Cu	45	28	7	77	47	14	17	6
Pb	4	8	5	4.6	1	7	7	2
Zn	55	59	70	66	64	68	78	35
Rb	4.2	10.5	21	19.9	47	39	44	2.3
Ba	91	509	328	982	205	240	2229	326
Sr	384	219	396	411	113	370	872	689
Ga	13	9	12	11	9	14	13	19
Nb	2.1	1.4	4.4	3.3	0.8	1.7	5.5	6.8
Zr	23	32	97	87	18.2	35	129	287
Y	7.9	8.8	18.7	19.3	4.2	9.4	24	21
Th	1.6	1.4	3.5	5.7	1.6	3	11	3.9
U	3.3	1.6	2.6	4.4	2.1	3.8	5	3.4
La	12	11	59	32	4	10	89	41
Ce	37	29	120	72	11	25	171	94
Nd	16	18	69	42	3	6	76	49

Continued

Rock Type	3	3	3	3	3	3	3	3
Sample Name	88004	88013	88017	88033	88070	88073	88113	88114
Major elements (wt%)								
SiO2	50.80	50.27	51.68	50.98	48.11	50.18	51.32	51.73
TiO2	0.76	0.61	0.64	0.52	0.57	0.64	0.54	0.49
Al2O3	16.28	14.09	14.41	15.49	15.36	16.91	18.19	17.32
Fe2O3tot	10.15	9.24	9.44	10.14	11.16	8.85	8.57	8.34
MnO	0.16	0.13	0.15	0.22	0.22	0.14	0.18	0.17
MgO	6.36	8.62	7.30	7.94	8.97	6.73	5.17	5.91
CaO	9.60	11.35	9.40	9.85	10.14	10.61	7.81	8.65
Na2O	3.12	2.93	3.80	2.86	2.41	3.40	4.06	3.78
K2O	1.10	0.47	0.87	0.54	1.10	0.54	1.52	1.29
P2O5	0.14	0.41	0.79	0.19	0.19	0.10	0.17	0.16
L.O.I.	1.39	1.20	1.42	1.20	1.88	1.14	1.87	1.43
Total	99.86	99.32	99.90	99.93	100.13	99.24	99.40	99.27
Trace elements (ppm)								
Cr	215	366	129	363	21	225	91	144
Ni	49	130	81	127	76	74	46	61
Sc	38	43	31	41	42	41	28	31
V	216	198	189	205	217	195	173	161
Cu	69	12	20	44	10	3	14	22
Pb	4	4	3	4	3	3	4	5
Zn	59	55	58	70	94	48	73	69
Rb	28	6.2	27	14.1	41	9.3	55	41
Ba	226	187	298	359	382	137	277	299
Sr	350	581	442	373	389	357	511	538
Ga	15	14	17	14	18	17	19	19
Nb	0.8	4	4.6	2.1	406	2.2	1.2	2.2
Zr	56	118	153	48	81	56	23	39
Y	15.2	19.5	26	10.2	18.6	13.9	3237	9.2
Th	0.5	6.9	4.9	1.3	0.7	1.6	7	2.2
U	3.8	2.6	2.4	1.2	0.5	3.5	0.6	2.9
La	12	45	80	10	19	11	10	13
Ce	32	114	178	20	66	21	28	33
Nd	11	59	103	9	55	15	11	20

Continued

Rock Type	4	4	4	4	4	4	5	5
Sample Name	87133	88006	88014	88046	87047	88069	87064	87121
Major elements (wt%)								
SiO2	58.34	54.69	55.48	55.88	55.30	59.03	62.71	68.43
TiO2	0.70	0.46	0.64	0.37	0.10	0.48	0.57	0.47
Al2O3	18.54	16.35	17.16	17.07	18.72	17.88	16.61	15.68
Fe2O3tot	3.78	7.44	6.03	7.78	4.61	5.58	4.87	2.13
MnO	0.05	0.13	0.09	0.14	0.09	0.09	0.03	0.02
MgO	2.58	6.10	4.96	4.84	4.42	3.35	1.86	0.65
CaO	7.05	8.43	8.77	8.24	9.04	7.54	4.86	5.54
Na2O	6.03	4.26	4.87	3.54	3.89	4.11	6.51	4.80
K2O	0.40	0.51	0.34	0.94	0.70	0.38	0.31	0.29
P2O5	0.24	0.11	0.42	0.01	0.00	0.12	0.15	0.15
L.O.I.	0.86	1.04	0.68	1.10	1.34	0.88	0.46	0.44
Total	98.57	99.52	99.44	99.91	98.21	99.44	98.94	98.60
Trace elements (ppm)								
Cr	8	301	53	59	170	55	7	0
Ni	13	63	58	27	58	36	11	3
Sc	20	29	25	32	24	21	14.4	10.4
V	122	152	142	213	71	103	88	50
Cu	7	26	7	7	13	4	6	5
Pb	4	7	3	6	5	6	5	5
Zn	30	47	30	56	37	32	16	11
Rb	7.5	9.1	3.5	14.6	10.6	10.6	4.1	2
Ba	193	255	176	182	140	137	257	203
Sr	630	437	706	391	441	573	482	691
Ga	21	17	17	18	14	18	20	17
Nb	4.7	3.2	4.3	5.2	2.7	3.7	5.4	4.7
Zr	186	75	150	33	18	184	195	176
Y	19.4	11.6	16.2	18.1	5.8	12.5	18.7	10.5
Th	5.8	2.8	7.8	4.8	11	2.3	6.1	7.2
U	3.1	1	3.6	2.3	2.8	3.3	2.3	2.4
La	25	13	36	9	13	14	27	21
Ce	48	36	68	14	28	29	49	49
Nd	26	9	35	13	15	18	23	19

Continued

Rock Type	5	5	5	5	6
Sample Name	88010	88019B	88020A	88075	88074
Major elements (wt%)					
SiO2	68.62	78.21	64.00	62.00	56.34
TiO2	0.48	0.09	0.40	0.57	0.97
Al2O3	16.23	12.19	15.57	16.95	15.19
Fe2O3tot	1.98	1.25	5.10	4.72	10.26
MnO	0.04	0.03	0.07	0.09	0.09
MgO	1.22	0.81	2.54	2.19	3.32
CaO	5.38	3.57	7.40	4.54	7.58
Na2O	4.54	3.11	2.67	5.60	4.26
K2O	0.35	0.40	0.46	1.28	0.45
P2O5	0.17	0.04	0.08	0.17	0.42
L.O.I.	0.82	0.47	0.90	1.18	0.57
Total	99.83	100.17	99.19	99.64	99.45
Trace elements (ppm)					
Cr	<5	<5	38	16	5
Ni	8	5	26	10	11
Sc	11.5	5.6	17.1	16.6	30
V	45	6	93	93	254
Cu	4	4	4	5	6
Pb	5	6	5	5	3
Zn	16	5	21	30	25
Rb	8.4	11.2	15.2	56	6
Ba	226	281	95	391	317
Sr	691	391	495	407	577
Ga	17	13	17	19	18
Nb	5.3	9.2	5.1	6.5	5.4
Zr	194	139	142	181	112
Y	12.6	30	13	19.5	17.5
Th	5.2	17	3.1	5.7	4.7
U	2.8	5.1	1.9	3.8	3.1
La	26	55	13	31	28
Ce	52	95	36	72	56
Nd	23	51	19	24	26

Appendix-3B: Major and trace element analytical data for the AOT

	88008A	88031	88043	88044	88045	88084	88105
Major element (wt%)							
SiO2	61.51	64.01	64.60	64.71	62.07	67.24	65.30
TiO2	0.67	0.54	0.55	0.48	0.61	0.43	0.48
Al2O3	16.27	15.79	15.88	16.18	16.16	16.30	15.90
Fe2O3tot	6.15	4.88	5.32	4.67	5.89	3.63	4.96
MnO	0.10	0.08	0.09	0.11	0.12	0.05	0.06
MgO	2.68	2.60	2.44	2.85	3.33	1.15	1.48
CaO	4.17	3.12	3.21	3.07	3.94	3.56	2.77
Na2O	4.25	4.31	3.70	3.14	3.97	4.33	4.35
K2O	1.22	1.71	2.38	3.80	1.74	2.01	1.98
P2O5	0.22	0.18	0.19	0.16	0.20	0.12	0.17
L.O.I.	0.98	1.12	0.92	1.12	1.42	0.60	1.28
Total	98.22	98.34	99.28	100.29	99.45	99.42	98.73
Trace element (ppm)							
Cr	35	35	37	28	40	<5	<5
Ni	14	14	15	12	15	4	n.d.
Sc	15.4	14.2	14.3	11.7	16	5.8	12.8
V	106	94	91	81	102	34	49
Cu	10	8	9	7	9	10	62
Pb	9	9	14	14	12	12	4
Zn	46	39	60	52	75	49	26
Rb	31	47	70	88	55	54	62
Ba	471	685	1468	1319	1002	856	864
Sr	376	338	347	325	453	623	311
Ga	20	18	18	18	19	20	17
Nb	13.1	11.4	8.1	9.2	12.1	5	5.8
Zr	187	175	161	169	199	198	210
Y	26	22	19.7	25	33	9.9	24
Th	8.1	30	18	7.8	30	11	11
U	3.9	4.6	5.2	2.7	5.6	5.4	4.1
La	24	76	39	24	35	28	32
Ce	63	142	78	68	80	71	64
Nd	32	53	29	32	39	18	32

Appendix-3C: Major and trace element analytical data for the AOLG. Rock types: 1= coarse-grained AOLG; 2=fine-grained AOLG; 3=aplite; 4=granitic dyke.

Rock Type	1	1	1	1	1	1	1
Name	87106	87131	88032	88034	88037	88040	88041
Major element (wt%)							
SiO2	72.66	71.49	75.41	75.37	74.54	75.07	74.42
TiO2	0.20	0.27	0.30	0.31	0.26	0.29	0.29
Al2O3	13.89	14.05	12.86	12.87	12.62	13.08	12.75
Fe2O3tot	1.99	2.27	2.05	1.87	2.05	2.09	2.27
MnO	0.04	0.02	0.03	0.05	0.03	0.03	0.03
MgO	0.46	1.04	0.53	1.03	1.13	1.17	0.99
CaO	1.78	1.90	0.45	1.39	0.59	1.12	1.54
Na2O	4.56	5.03	5.16	4.11	3.40	4.88	3.65
K2O	2.69	1.33	1.23	1.93	3.88	1.29	2.98
P2O5	0.05	0.08	0.03	0.04	0.05	0.04	0.04
L.O.I.	0.78	1.22	0.95	0.79	1.04	0.73	0.69
Total	99.10	98.70	99.00	99.76	99.62	99.79	99.65
Trace element (ppm)							
Cr	<5	<5	<5	<5	<5	<5	<5
Ni	4	3	4	5	4	3	3
Sc	4.7	6	7.3	5.2	6	5.8	5.9
V	17	27	17	12	15	15	14
Cu	17	9	9	6	4	5	4
Pb	9	7	4	11	6	6	6
Zn	15	16	12	15	13	13	8
Rb	66	31	26	32	55	26	50
Ba	943	695	596	1185	1383	958	1291
Sr	235	234	99	211	154	207	258
Ga	15	15	12	13	13	13	13
Nb	6.6	6.5	11.7	13	9.8	11.6	12.5
Zr	137	145	208	217	186	205	197
Y	12.7	12.8	28	32	15.8	27	27
Th	16	13	17	20	15	20	18
U	3.6	4	3.4	4.8	2.8	3.8	3.3
La	30	28	35	20	23	78	25
Ce	60	52	84	64	60	138	64
Nd	16	18	37	41	21	50	32

Continued

Rock Type	1	1	1	1	1	1	1
Name	88053	88054	88055	88056	88057	88062	88102
Major element (wt%)							
SiO2	74.51	73.60	73.14	72.33	74.48	72.47	71.95
TiO2	0.37	0.31	0.36	0.37	0.23	0.24	0.27
Al2O3	13.18	13.23	13.43	13.49	13.99	14.48	14.12
Fe2O3tot	2.41	1.99	2.47	2.79	1.74	2.28	2.25
MnO	0.03	0.02	0.05	0.04	0.04	0.02	0.04
MgO	0.99	0.67	0.96	0.64	0.75	1.13	0.93
CaO	1.43	0.85	1.75	1.71	1.49	1.25	2.14
Na2O	4.61	4.01	3.71	4.26	4.67	5.29	3.86
K2O	1.17	3.10	2.83	2.10	1.71	1.34	2.44
P2O5	0.08	0.05	0.06	0.05	0.04	0.10	0.07
L.O.I.	0.80	0.94	1.16	0.87	0.92	0.94	1.24
Total	99.58	98.77	99.92	98.65	100.06	99.54	99.31
Trace element (ppm)							
Cr	<5	<5	<5	<5	<5	5	<5
Ni	2	4	4	4	3	3	2
Sc	8.7	6.8	8.1	9	5.9	6.8	6.3
V	20	17	27	23	14	25	25
Cu	4	4	6	5	13	31	3
Pb	4	4	5	7	11	8	7
Zn	14	20	13	12	18	19	19
Rb	21	53	44	39	36	33	41
Ba	1434	1234	1602	1017	587	392	969
Sr	234	178	269	236	211	192	290
Ga	13	13	14	13	15	15	15
Nb	11	12.3	9.2	11.6	7.3	5.2	7.5
Zr	238	204	230	227	158	125	141
Y	24	25	23	24	14.3	12	15.5
Th	15	15	18	16	17	13	13
U	2.5	3.4	3.7	3.9	4.5	3.9	3.6
La	59	31	63	42	33	21	28
Ce	121	63	123	98	63	43	63
Nd	49	35	44	40	23	15	10

Continued

Rock Type	1	1	1	1	1	1	2
Name	88103	88104	88106	88108	88111	88112	87116
Major element (wt%)							
SiO2	73.55	71.66	72.78	73.25	73.27	73.32	76.26
TiO2	0.25	0.25	0.25	0.25	0.19	0.24	0.11
Al2O3	14.02	14.22	14.17	13.90	13.74	13.73	12.72
Fe2O3tot	1.74	2.50	1.47	2.03	1.98	2.33	0.63
MnO	0.02	0.04	0.02	0.04	0.04	0.04	0.02
MgO	0.71	0.89	1.45	0.86	0.79	1.33	0.10
CaO	1.38	2.27	1.08	1.52	1.39	1.34	0.94
Na2O	5.21	4.46	5.03	4.47	4.06	4.60	3.80
K2O	1.12	1.49	1.32	2.02	2.85	1.11	4.11
P2O5	0.06	0.07	0.07	0.05	0.05	0.06	0.02
L.O.I.	0.70	1.13	1.03	1.06	0.96	1.22	0.58
Total	98.76	98.98	98.67	99.45	99.32	99.32	99.29
Trace element (ppm)							
Cr	<5	6	<5	5	<5	<5	<5
Ni	3	5	1	4	3	3	6
Sc	4.7	6.2	6.7	4.1	4.9	6.2	3.2
V	16	28	26	12	20	25	6
Cu	9	10	7	4	3	2	6
Pb	7	11	4	6	8	8	9
Zn	14	23	12	12	16	20	8
Rb	30	32	27	34	50	27	83
Ba	483	994	650	1022	1000	571	871
Sr	218	311	146	211	216	186	135
Ga	15	16	15	14	13	14	13
Nb	5.8	5.5	6.2	5.7	4.7	5.9	8.1
Zr	169	132	129	191	107	118	92
Y	13.1	10.3	10.4	12	7.7	12.4	11.9
Th	14	18	13	13	12	13	20
U	3.2	2.4	3.1	3.8	2.9	3.4	5
La	35	38	31	43	29	29	22
Ce	68	77	65	78	57	58	51
Nd	23	18	19	24	12	20	15

Continued

Rock Type	2	2	2	2	2	2	2
Name	87120	87130	87138	87142	87172	88058	88060
Major element (wt%)							
SiO2	76.22	76.82	72.40	76.54	75.74	76.56	74.51
TiO2	0.11	0.09	0.13	0.12	0.03	0.14	0.07
Al2O3	12.76	12.25	14.75	12.78	13.45	12.60	13.81
Fe2O3tot	1.14	1.03	1.65	0.96	0.44	1.03	0.97
MnO	0.02	0.02	0.05	0.01	0.01	0.00	0.04
MgO	0.14	0.22	0.47	0.10	0.04	0.26	0.53
CaO	0.68	0.40	2.39	0.95	1.10	0.51	1.62
Na2O	4.64	3.77	4.20	4.86	3.88	3.73	3.80
K2O	2.90	4.18	2.13	2.55	4.18	3.93	3.37
P2O5	0.00	0.01	0.04	0.01	0.00	0.01	0.01
L.O.I.	0.68	0.62	1.08	0.64	0.52	0.58	0.70
Total	99.29	99.41	99.29	99.52	99.39	99.35	99.43
Trace element (ppm)							
Cr	<5	<5	<5	<5	<5	<5	<5
Ni	3	4	2	3	2	5	2
Sc	3.1	2.4	3.4	3.1	2.6	2.8	4.5
V	3	3	9	5	4	2	11
Cu	8	10	8	21	8	14	19
Pb	5	11	13	8	17	7	17
Zn	5	8	17	6	4	8	9
Rb	51	58	52	46	92	54	32
Ba	800	895	575	716	323	1320	1348
Sr	97	91	303	133	125	135	266
Ga	13	12	14	12	14	14	14
Nb	7.7	8.4	5	6.4	5.7	6.5	6.5
Zr	109	93	87	104	56	109	69
Y	12.4	13	13.1	11.7	20	7.7	15.6
Th	16	19	10	21	18	16	26
U	3.5	4.2	4	3.3	9.9	2.5	8.1
La	23	25	15	37	7	30	25
Ce	56	67	39	68	19	52	53
Nd	15	18	11	21	10	19	8

Continued

Rock Type	2	2	2	2	2	3	4
Name	88061	88083	88085	88100	88101	88016B	88035
Major element (wt%)							
SiO2	77.21	75.77	77.20	74.35	75.90	76.27	71.04
TiO2	0.10	0.03	0.02	0.05	0.14	0.04	0.13
Al2O3	12.18	13.33	12.51	13.65	12.85	13.50	14.65
Fe2O3tot	0.86	0.41	0.42	0.70	1.18	0.31	1.56
MnO	0.01	0.02	0.02	0.02	0.03	0.02	0.04
MgO	0.33	0.26	0.30	0.35	0.56	0.68	0.39
CaO	0.28	0.93	1.12	1.15	0.48	2.29	1.26
Na2O	3.95	3.99	2.84	3.78	4.35	3.12	3.22
K2O	3.38	4.14	4.88	4.30	2.89	3.50	5.34
P2O5	0.02	0.02	0.00	0.03	0.03	0.04	0.06
L.O.I.	0.71	0.54	0.37	0.56	0.69	0.49	0.79
Total	99.03	99.44	99.68	98.94	99.10	100.26	98.48
Trace element (ppm)							
Cr	<5	<5	<5	<5	<5	<5	<5
Ni	4	3	2	3	3	6	4
Sc	3.1	3.3	2.8	4.7	4.3	3.6	2.9
V	3	4	5	7	6	1	26
Cu	15	33	12	17	8	24	26
Pb	8	25	22	16	7	14	31
Zn	11	6	4	10	12	10	21
Rb	46	93	73	42	40	94	67
Ba	990	693	500	1142	854	1162	3374
Sr	66	138	177	191	97	278	318
Ga	11	16	11	12	14	14	13
Nb	4.6	4.5	0.7	3	6.8	6.6	2.3
Zr	82	43	67	53	114	64	166
Y	8.4	19.5	4.2	16.3	12.4	9.8	12.2
Th	13	13	28	16	14	15	51
U	4.6	2.5	4.7	8.9	5.2	5.2	4.6
La	27	7	8	16	29	15	158
Ce	56	19	17	30	60	28	256
Nd	17	6	5	5	14	9	52

Appendix-3D: Major and trace element analytical data for the AMG

	88089	88090	88091	88092	88093
Mjor element (wt%)					
SiO2	74.64	75.52	76.04	74.50	74.65
TiO2	0.08	0.03	0.02	0.05	0.05
Al2O3	13.89	13.56	13.15	13.71	13.95
Fe2O3tot	0.83	0.34	0.28	0.64	0.70
MnO	0.04	0.02	0.02	0.02	0.04
MgO	0.25	0.28	0.15	0.12	0.63
CaO	0.83	0.77	0.82	1.00	0.92
Na2O	3.67	3.74	4.07	3.91	3.97
K2O	4.47	4.63	4.07	4.14	4.17
P2O5	0.02	0.02	0.03	0.02	0.02
L.O.I.	0.72	0.45	0.43	0.56	0.60
Total	99.44	99.36	99.08	98.67	99.70
Trace element (ppm)					
Cr	<5	<5	<5	<5	<5
Ni	2	4	3	3	3
Sc	3.7	4	1.7	3.3	3.5
V	2	0	1	2	1
Cu	3	6	4	4	5
Pb	30	43	44	32	33
Zn	29	14	13	21	12
Rb	194	178	150	169	171
Ba	479	171	76	535	272
Sr	87	50	45	100	63
Ga	19	17	16	17	19
Nb	13.8	7.7	4.3	8.5	11.4
Zr	66	26	8.9	62	35
Y	21	22	26	17.5	25
Th	16	8.6	7.8	14	10
U	5.6	4.2	4.6	4.7	7.1
La	23	5	3	18	13
Ce	43	16	12	36	23
Nd	16	2	2	7	5

Continued

	88094	88095	88096	88097	88099
Mjor element (wt%)					
SiO2	75.39	75.11	75.31	75.23	74.67
TiO2	0.04	0.05	0.06	0.04	0.07
Al2O3	13.82	14.26	13.81	14.12	13.43
Fe2O3tot	0.56	0.48	0.75	0.54	0.80
MnO	0.02	0.01	0.03	0.04	0.04
MgO	0.13	0.12	0.21	0.16	0.19
CaO	0.86	0.53	0.97	0.62	0.86
Na2O	3.75	3.38	3.74	3.45	3.72
K2O	4.55	4.95	4.39	4.72	4.26
P2O5	0.03	0.02	0.03	0.02	0.02
L.O.I.	0.50	0.67	0.57	0.66	0.58
Total	99.65	99.58	99.87	99.60	98.64
Trace element (ppm)					
Cr	<5	<5	<5	<5	<5
Ni	2	2	3	3	2
Sc	7.3	3.4	3.5	5.8	3.2
V	2	2	2	1	2
Cu	4	4	4	5	4
Pb	31	30	38	31	31
Zn	13	21	26	17	22
Rb	199	172	180	201	181
Ba	73	536	491	194	594
Sr	36	97	92	43	97
Ga	22	17	17	21	16
Nb	16.6	9.3	11	14.5	9
Zr	19.5	65	57	37	79
Y	25	15.8	19.2	27	18.2
Th	5.1	16	13	9.8	21
U	3.6	4.5	3.7	4.9	5.4
La	5	18	19	10	23
Ce	14	39	34	18	48
Nd	1	8	8	5	12

Appendix-3E: Major and trace element analytical data for the ATBS

Type	AYT	AYT	AYT	AYT	AYT	AYT	AYBA
Name	87129	87132	88002	88107	88110	88115	88008B
Major element (wt%)							
SiO2	63.74	64.58	64.32	65.59	64.16	58.84	49.45
TiO2	0.23	0.21	0.23	0.20	0.22	0.31	0.98
Al2O3	17.07	16.46	16.90	16.27	16.83	18.93	14.36
Fe2O3tot	3.42	3.10	3.18	2.87	3.49	3.79	12.62
MnO	0.08	0.08	0.07	0.07	0.08	0.08	0.24
MgO	2.55	2.28	2.58	2.05	2.37	3.55	8.84
CaO	4.71	4.60	4.70	4.10	4.69	6.87	9.63
Na2O	3.73	3.93	3.70	3.56	3.58	4.35	2.58
K2O	2.10	1.97	2.04	2.44	2.05	1.38	0.21
P2O5	0.09	0.08	0.09	0.08	0.10	0.13	0.11
L.O.I.	1.70	1.85	1.50	1.43	1.34	1.37	0.87
Total	99.42	99.14	99.31	98.66	98.91	99.60	99.89
Trace element (ppm)							
Cr	14	14	19	12	13	69	354
Ni	17	17	19	15	17	47	117
Sc	8.6	7.2	8.2	7.8	7.8	11.9	52
V	45	41	44	37	44	60	326
Cu	9	15	16	6	15	4	12
Pb	7	8	10	15	9	9	4
Zn	40	34	42	37	42	52	93
Rb	53	45	51	57	56	60	3.7
Ba	792	893	915	863	862	554	91
Sr	576	541	585	516	584	501	172
Ga	16	16	16	15	17	18	14
Nb	4.4	2.9	3.3	3.5	4.7	3.2	2.5
Zr	84	81	76	71	97	98	64
Y	7.7	6.1	5.6	6.5	10.9	4.7	36
Th	7	8.5	9.7	12	11	5.6	1.1
U	3	3.5	3	3.1	5.6	1.3	1.4
La	22	21	25	27	28	28	31
Ce	40	39	54	44	59	54	57
Nd	14	12	17	22	17	18	23

Appendix-4: REE analytical data for samples from the Atnarpa Igneous Complex

Rock Type	ACAS	ACAS	ACAS	AOT	AOLG
Sample	88016D	88014	87064	88008A	87106
SiO2 (wt%)	51.21	55.48	62.71	61.51	72.66
La	11.11	31.27	23.72	23.65	26.89
Ce	26.01	60.99	47.68	52.16	52.44
Nd	13.66	27.88	20.45	25.61	16.43
Sm	2.55	5.04	3.71	4.69	2.70
Eu	0.66	1.28	1.01	1.08	0.58
Gd	2.03	3.73	3.08	3.70	2.08
Dy	1.36	2.32	2.44	3.14	1.68
Er	0.66	1.08	1.35	1.82	0.98
Yb	0.55	0.91	1.25	1.86	1.04
Total (ppm)	58.60	134.50	104.70	117.70	104.80
(Ce/Yb)n	12.06	17.11	9.74	7.19	12.85
(Eu/Eu*)n	0.86	0.87	0.90	0.78	0.73

Rock Type	AOLG	AMG	AYT	AYT	AYBA
Sample	88032	88090	88002	88115	88008B
SiO2 (wt%)	75.41	75.52	64.32	58.84	49.45
La	30.48	5.79	22.26	23.61	26.02
Ce	66.55	8.86	45.42	39.11	51.77
Nd	29.28	2.92	14.42	15.80	15.80
Sm	5.46	0.74	2.01	2.12	3.50
Eu	1.07	0.22	0.48	0.54	1.03
Gd	4.24	1.03	1.26	1.33	4.12
Dy	3.25	1.83	0.88	0.80	4.40
Er	1.81	1.35	0.49	0.37	2.82
Yb	1.83	1.39	0.49	0.31	2.75
Total (ppm)	144.00	24.10	87.70	84.00	112.20
(Ce/Yb)n	9.90	1.63	23.67	32.05	4.82
(Eu/Eu*)n	0.66	0.77	0.86	0.92	0.84

APPENDIX-5: Major and trace element analytical data for AOT rocks from the Tommy's Gap area (taken from Sando 1987).

	888-20	888-21	888-22	888-25	888-55	888-73	888-82
Major elements (wt%)							
SiO_2	66.04	64.43	64.53	72.48	67.22	63.06	68.09
TiO_2	0.52	0.53	0.57	0.33	0.38	0.63	0.44
Al_2O_3	15.71	16.41	16.44	13.83	16.27	16.33	15.34
Fe_2O_3	4.72	4.95	4.85	2.85	1.34	5.67	3.97
MnO	0.06	0.06	0.08	0.05	0.06	0.07	0.05
MgO	2.00	2.07	1.48	0.74	1.29	2.04	1.18
CaO	4.36	4.58	4.04	2.59	4.61	5.05	3.64
Na_2O	4.06	4.27	4.30	4.03	5.32	3.99	4.23
K_2O	2.33	2.09	2.84	2.62	2.73	2.29	2.36
P_2O_5	0.16	0.16	0.18	0.08	0.12	0.17	0.11
Total	99.96	99.28	99.31	99.60	99.34	99.30	99.41
Trace elements (ppm)							
Rb	76	65	101	85	52	80	66
Sr	412	461	374	241	395	409	360
Ba	616	571	699	405	1146	489	996
Y	13	14.6	15.5	15.5	10.1	14	10
Zr	157	165	171	149	156	145	173
Nb	5.4	5.2	6.6	8	4.1	3.5	5
Sc	7.9	12.6	10.4	5.8	9.5	13.4	8.4
V	84	89	80	36	59	108	62
Ni	15	17	7	5	8	13	12
Cr	<5	<5	<5	<5	<5	<5	<5
La	21	41	40	45	31	39	65
Ce	33	66	56	57	55	55	100
Nd	20	25	19	23	16	21	31
Ga	21	18	20	18	16	20	18
Pb	8	10	11	11	30	8	10
U	2	3	8	5	3	5	4

Fig 1-3

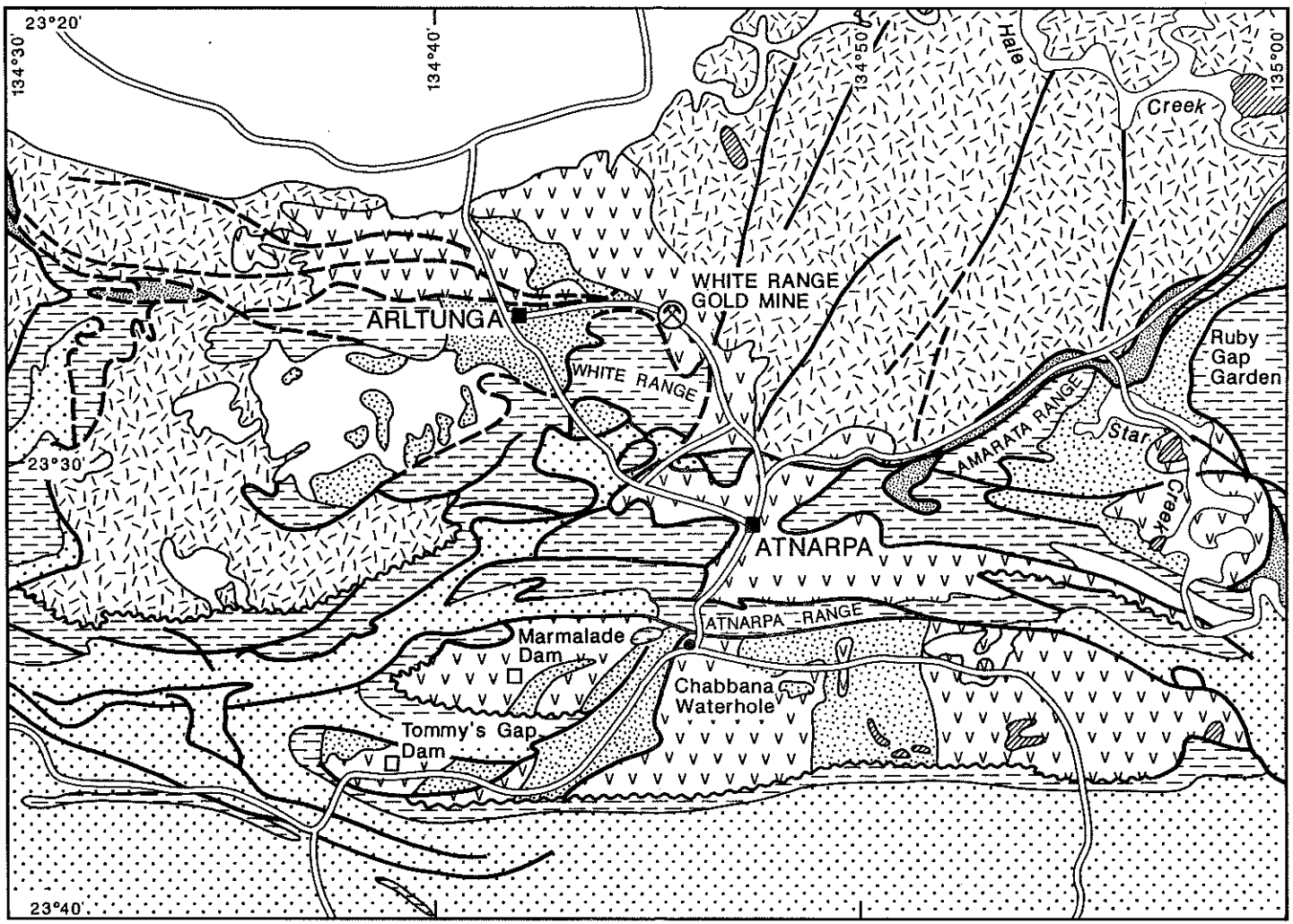
23°20'
134°30'
134°40'
134°50'
135°00'
Hale
Creek
WHITE RANGE
GOLD MINE
ARLTUNGA
WHITE RANGE
Ruby
Gap
Garden
AMARATA RANGE
Star
Creek
23°30
ATNARPA
ATNARPA RANGE
Marmalade
Dam
Chabbana
Waterhole
Tommy's Gap
Dam
23°40
Cainozoic Units
Other members of the
Amadeus Basin
Heavitree Quartzite
Whistleduck Dyke Swarm
Illogwa Schist Zone
Atnarpa Igneous Complex
Division Two,
Tommy's Gap Metamorphics
Division One
Geological boundary
Fault
Unconformity
Road
SCALE: Km
0
5
10
15

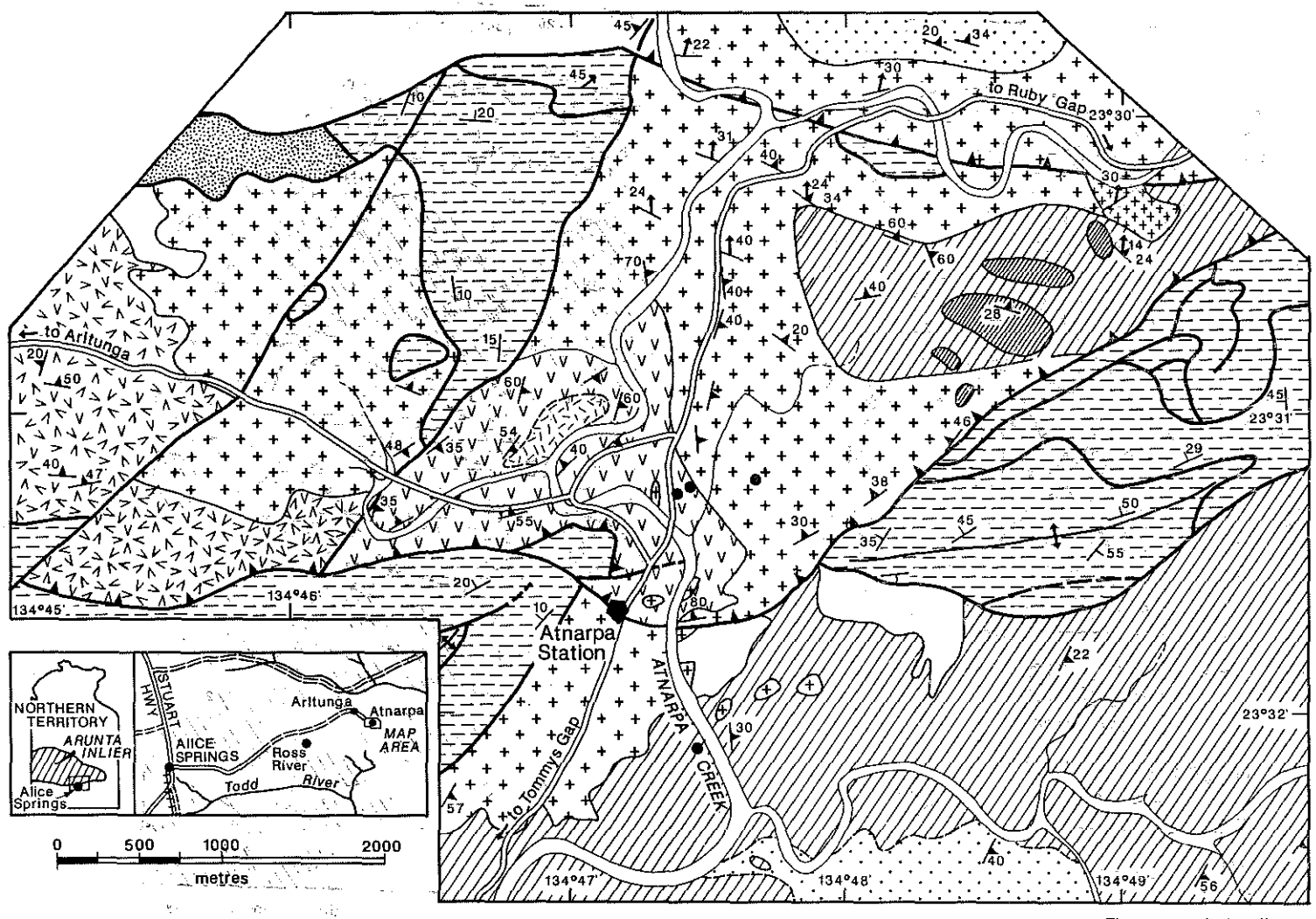
to Ruby Gap
23°30'
to Arltunga
23°31'
23°32'
134°45'
134°46'
134°47'
134°48'
134°49'
Atnarpa Station
ATNARPA CREEK
to Tommys Gap
NORTHERN TERRITORY
ARUNTA INLIER
Alice Springs
STUART HWY
ALICE SPRINGS
Arltunga
Atnarpa
MAP AREA
Ross River
Todd River
0 500 1000 2000
metres
ARUNTA INLIER
Cainozoic Units
AMADEUS BASIN
Bitter Springs Formation
Heavitree Quartzite
Contact metamorphic zone
Atnarpa younger tonalite
Atnarpa Muscovite granite
Atnarpa older leucogranite
Atnarpa older tonalite
Atnarpa Calc-alkaline Suite
Cumulates of the ACAS
Basement supercrustal assemblage
Zircon sample locality
Geological boundary observed, inferred
Fault observed, inferred
Thrust
Fold
Strike & Dip of strata
Strike & Dip of foliation
Dip of lineation
Creek
Track

GEOLOGICAL MAP OF THE ATNARPA AREA, SOUTHEASTERN ARUNTA INLIER, N.T.

SCALE 1:12,500

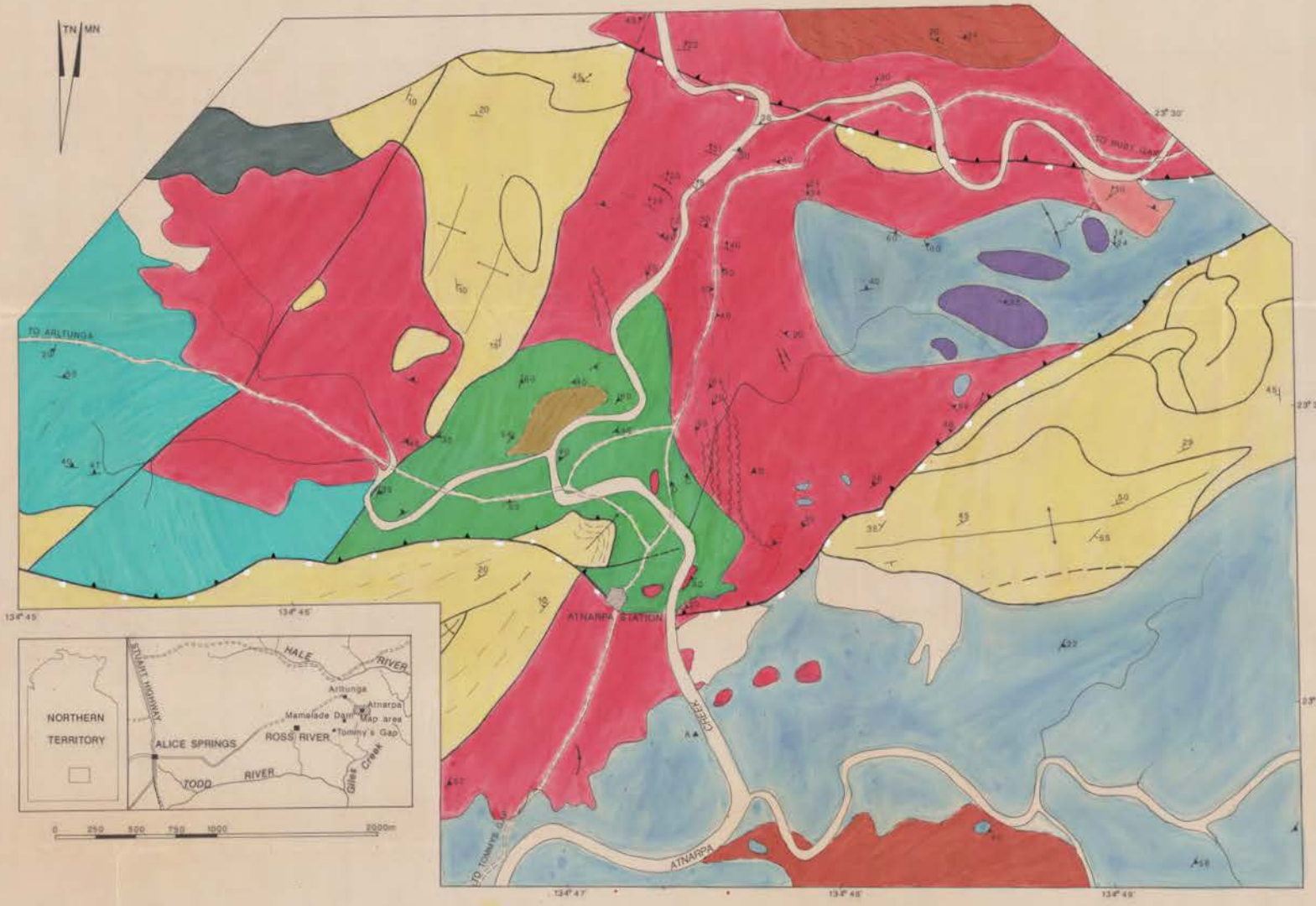

LEGEND

- QUARTERNARY SEDIMENT
- **AMADEUS BASIN**
- LATE PROTEROZOIC
  - BITTER SPRINGS FORMATION
  - HEAVITREE QUARTZITE
- **ARUNTA INLIER**
- MIDDLE PROTEROZOIC
  - ATNARPA YOUNGER TONALITE WITH NUMEROUS BASALTIC AMPHIBOLITE (AYBA) XENOLITHS (AYT)
  - ATNARPA MUSCOVITE GRANITE (AMG)
  - ATNARPA OLDER TONALITE AND GRANODIORITE VARIETY (AOT)
  - ATNARPA OLDER LEUCOGRANITE, GRANITIC MYLONITE AND LOCALLY QUARTZOFELDSPATHIC GNEISS (AOLG)
  - ATNARPA CALC-ALKALINE SUITE, INCLUDING MAFIC CUMULATES, MAFIC DIFFERENTIATES, FELSIC DIFFERENTIATES AND FINE-GRAINED AMPHIBOLITE, INTERLAYERS OF BASEMENT SUPRACRUSTAL ASSEMBLAGE (ACAS)
  - CUMULATES OF THE ATNARPA CALC-ALKALINE SUITE
  - BASEMENT SUPRACRUSTAL ASSEMBLAGE (BSA) INCLUDING QUARTZOFELDSPATHIC GNEISS, CALC-SILICATE, SCHISTOSE AMPHIBOLITE, BIOTITE GNEISS, MUSCOVITE GNEISS, MUSCOVITE SCHIST, CHLORITE SCHIST, ETC
  - CONTACT METAMORPHISM ZONE BETWEEN THE ATNARPA YOUNGER TONALITE AND XENOLITHS
- DYKES OF PEGMITITE, APLITE,QUARTZ
- GEOLOGICAL BOUNDARY
- FAULTS, OBSERVED, INFERRED
- THRUST
- SHEAR ZONE
- STRIKE AND DIP OF STRATA
- STRIKE AND DIP OF FOLIATION
- DIP OF LINEATION
- FOLD AXIS AND PLUNGING DIRECTION
- ROAD
- CREEK

JIANXIN ZHAO, 1989